Engineering particle agglomeration in dry powder inhaler formulations to co- deliver drugs to the lungs

Jaffari, Sara

Awarding institution:
King's College London

ENGINEERING PARTICLE AGGLOMERATION IN DRY POWDER INHALER FORMULATIONS TO CO-DELIVER DRUGS TO THE LUNGS

Sara Jaffari MPharm

A thesis submitted for the degree of Doctor of Philosophy of King's College London

September 2013

Institute of Pharmaceutical Science

King's College London, Franklin-Wilkins Building, 150 Stamford Street, London, SE1 9NH.

ABSTRACT

Dry powder inhalers (DPIs) are well established as a means of delivering inhaled drugs to the lungs. Combination DPIs, containing two or more drugs in a single formulation, may improve patient compliance by simplifying medication regimens. The implications of co-formulation on the aerosolisation behaviour of the component drugs, however, are not fully understood. Using salmeterol xinafoate (SX) and fluticasone propionate (FP) as model drug powders, a systematic approach was undertaken to better understand the consequences of combination formulation on drug dispersion for inhaled delivery. A dry dispersion laser diffraction analysis was developed to characterise the inherent dispersibility of bulk powders as well as de-agglomeration of DPI blends. Eight inhaled drug/excipient powders displayed different dispersibility (represented by the DA_{50}, the dispersing pressure to achieve 50 % de-agglomeration; 0.23-1.45 Bar) and cohesivity (represented by the critical primary pressure (CPP); 1.0-3.5 Bar). Upon co-formulation (in the absence of a carrier) SX deposition in the Next Generation Impactor (NGI) became less efficient as the FP content increased (e.g. fine particle fraction (FPF) 33-18 % recovered dose (RD) for SX:FP ratios 1:0-1:8). However, FP dispersion was generally unaffected when blended with SX (FPF 26-29 % RD, SX:FP ratios 0:1-8:1). This was attributed to the greater adhesivity and cohesivity of SX and FP, respectively, and changes in bulk blend structure and dispersibility. Intra-batch heterogeneity in particle properties within a bulk powder were also studied using solid state, calorimetric and inverse gas chromatographic analysis. The NGI was used to isolate aerodynamic size fractions which displayed distinct physicochemical and aerosolisation properties. For example, FP sub-populations had better dispersibility (FPF 32 vs. 19 % RD, respectively) whereas an SX sub-population had higher bulk and surface disorder and poorer dispersibility (FPF 21 vs. 33 % RD, respectively) compared to the bulk powders. Upon co-formulation (in the absence of a carrier) the fractions responded differently in terms of their aerosolisation behaviour compared to the unfractionated powders, indicating heterogeneity in the response to co-formulation within a bulk powder. When formulated with a carrier, however, there were no modifications to the dispersion (i.e. FPF) of unfractionated SX or FP upon co-formulation at different SX:FP ratios, however, a fraction of SX co-formulated with FP in a DPI blend exhibited changes to SX dispersion that were comparable to those in the absence of a carrier. The effect of co-formulation on SX and FP dispersion, therefore, was found to depend on the drug ratio, properties of the powder/fraction employed and the presence of a carrier.

ACKNOWLEDGEMENTS

First and foremost I would like to thank my PhD supervisors, Dr. Darragh Murnane, Professor Gary P Martin, Dr. Ben Forbes and Dr. Elizabeth Collins. Your expertise and enthusiasm were an inspiration. Throughout this journey, your help, support and advice have been invaluable, and enabled me to grow both academically and personally.

This project was funded by a Biotechnology and Biological Sciences Doctoral Training Award and Pfizer Ltd, which is gratefully acknowledged. I would also like to express my gratitude to Dr. Norman Smith (Analytical & Environmental Sciences Division, King's College London) for access to the high performance liquid chromatography instrument, Drs. Phil Attwool, Majid Naderi and Jiyi Khoo (Surface Measurement Systems Ltd, UK) for collaborating on the project and undertaking the surface energy mapping of the powders, Dr. Kenneth Shankland (Division of Pharmaceutical Chemistry, University of Reading) for access to the powder x-ray diffractometer, Dr. Gema Vizcay-Barrena (Centre for Ultrastructural Imaging, King's College London) for training and assistance with the scanning electron microscopy imaging, Dr. John Murphy and colleagues (Pfizer Ltd., UK) for generation of dispersive surface energy and density measurements, Dr. Darragh Murnane and his MPharm project students (Department of Pharmacy, University of Hertfordshire) for generation of the re-crystallised powders, Ms. Irene Parisini (Department of Pharmacy, University of Hertfordshire) for determining the flow rate and pressure drop measurements for the inhaler devices used in this project, and Dr. David Barlow (Pharmaceutical Biophysics Research Group, King's College London) for assistance with the empirical data modelling. To my colleagues, and the friends made, both within and outside the Drug Delivery Research Group at King's College London, thank you for being a part of my PhD journey.

Finally, I would like to thank the most important people in my life, my parents and sister Roya (a newlywed to my new brother-in-law, Richard) for your generous and unconditional love, support, guidance and encouragement not only over the last four years, but throughout my life. There are no words that can express my gratitude and I am very lucky to call you family. Thanks for always making me smile.

PUBLICATIONS AND PRESENTATIONS

PUBLICATIONS

Jaffari S, Forbes B, Collins E, Barlow DJ, Martin GP, Murnane D. Rapid Characterisation of the Inherent Dispersibility of Respirable Powders using Dry Dispersion Laser Diffraction. International Journal of Pharmaceutics 447 (2013) 124–131.

Jaffari S, Forbes B, Collins E, Khoo J, Martin GP, Murnane D. Agglomeration behaviour of aerodynamically size-fractionated salmeterol xinafoate and fluticasone propionate powders. Manuscript in preparation.

PRESENTATIONS

Jaffari S, Collins E, Khoo J, Forbes B, Martin GP, Murnane D. Aerodynamic Size-fractionated Sub-populations of Salmeterol xinafoate and Fluticasone propionate Powders Possess Distinct Properties and Aerosolisability. Oral presentation; Drug Delivery to the Lungs 23, December 2012, Edinburgh, United Kingdom.

Jaffari S, Collins E, Murphy J, Barlow D, Forbes B, Martin GP, Murnane D. Dry Dispersion Laser Diffraction as a Generic Screening Tool for Powder De-agglomeration. Poster presentation; Drug Delivery to the Lungs 23, December 2012, Edinburgh, United Kingdom.

Jaffari S, Collins E, Murphy J, Khoo J, Forbes B, Martin GP, Murnane D. Probing Powder De-agglomeration using Dry Dispersion Laser Diffraction. Oral presentation; Drug Delivery Australia (hosted by the Australian Chapter of the Controlled Release Society), November 2012, Melbourne, Australia.

Jaffari S, Sandhu G, Martin GP, Forbes B, Collins E, Murnane D. The Effect of Aerodynamic Particle Size and Solid State Disorder on Salmeterol xinafoate Deposition from Pressurised Metered Dose and Dry Powder Inhaler Formulations. Poster presentation; Drug Delivery to the Lungs 22, December 2011, Edinburgh, United Kingdom.

Jaffari S, Martin GP, Forbes B, Harding L, Collins E, Murnane D. *In vitro* Deposition of Combination Drug-only Formulations Delivered via a Dry Powder Inhaler. Poster presentation; UKPharmSci, August - September 2011, Nottingham, United Kingdom.

Jaffari S, Martin GP, Forbes B, Harding L, Collins E, Murnane D. Exploring the Effect of Fine Particle Interactions on the *in vitro* Deposition of Dry Powders for Inhalation. Oral presentation; APS Inhalation Conference, July 2011, Bath, United Kingdom.

TABLE OF CONTENTS

LIST OF FIGURES

LIST OF TABLES

α	Fraction of SX-I re-crystallised from the SX melt
a	Cross-sectional area of an adsorbate probe molecule (for IGC)
A	Actual concentration
ACI	Anderson cascade impactor
AFM	Atomic force microscopy
a_m	Cross sectional area of a solute molecule (for IGC)
ANOVA	Analysis of variance
AUC	Area under the curve
β	Heating rate
β_2	Beta 2 (referring to the receptor or agonist)
B	Mobility of a particle (i.e. velocity per unit force)
BDP	Beclometasone dipropionate
BET	Brunauer-Emmett-Teller
BN.	Batch number
BP	British Pharmacopeia
Bud	Budesonide
C	Concentration
C:A ratio	Cohesive to adhesive ratio
C_C	Cunningham correction factor
CFC	Chlorofluorocarbon
CFP	Crystallised fluticasone propionate
CL	Coarse lactose
COPD	Chronic obstructive pulmonary disease
C_{opt}	Optical concentration
CPP	Critical primary pressure
CSX	Crystallised salmeterol xinafoate
Cu	Copper
CV	Coefficient of variance
ΔP	Pressure drop (across an inhaler device)
ΔH_f	Enthalpy of fusion of SX-II
$\Delta H_f^{\beta exp}$	Enthalpy of fusion of SX-II at an experimental heating rate
$\Delta H_f^{\beta 0.1}$	Enthalpy of fusion of SX-II at 0.1 $^oC.min^{-1}$
d’	A characteristic dimension of an object (i.e. particle)

$D_{4,3}$	Volume weighted mean particle size (equivalent to the VMD)
d	Diameter (of a particle)
D	Detected concentration
d_{ae}	Aerodynamic particle size
DA	Degree of de-agglomeration
DA_{50}	Ease of dispersion; primary pressure to achieve 50 % de-agglomeration
DA_{max}	Maximum degree of de-agglomeration
d_g	Geometric particle size
DNA	Deoxyribonucleic acid
DPF	Dry powder feeder
DPI	Dry powder inhaler
d_r	Difference ratio
DSC	Differential scanning calorimetry
DUSA	Dose uniformity sampling apparatus
D_{v10}	Particle size below which 10 % of the particles, by volume, is found
D_{v50}	Particle size below which 50 % of the particles, by volume, is found
D_{v90}	Particle size below which 90 % of the particles, by volume, is found
D_H	Particle size at the highest pressure employed in dry dispersion sizing
D_L	Particle size from liquid dispersion sizing
D_x	Particle size at the primary pressure of interest in dry dispersion laser diffraction particle sizing
η	Dynamic viscosity of a gas
η	Air viscosity
ED	Emitted dose
EMEA	European Medicines Agency
F	Flow rate
f2	Similarity factor
FDA	Food and Drug Administration
FEV_1	Forced expiratory volume
FF	Fine fraction

FID	Flame ionisation detector
FP	Fluticasone propionate
FPD	Fine particle dose
FPM	Fine particle mass
FPF	Fine particle fraction
γ	Density of air
γ^+	Acidic component of the surface energy
γ^-	Basic component of the surface energy
γ_D	Dispersive surface energy
γ^D_L	Dispersive surface tension of the adsorbate
γ_{SP}	Specific surface energy
γ_T	Total surface energy
g	Acceleration due to gravity
ΔG_P	Specific free energy of adsorption
GR	Glucocorticoid receptor
GSD	Geometric standard deviation
HELOS	Helium neon laser optical system
HFA	Hydrofluoroalkane
HPLC	High performance liquid chromatography
IC	Inhaled corticosteroid
IF	Intermediate fraction
IGC	Inverse gas chromatography
j	James-Martin pressure drop correction factor
k	Integrated rate constant for the re-crystallisation of SX-II
K_L	Langmuir adsorption/equilibrium constant
K_F	Adsorptive capacity
LABA	Long acting beta agonist
LH300	Lactohale 300
LOD	Limit of detection
LOQ	Limit of quantification
m	Particle mass
m	Sample mass (packed into an IGC column)
MFP (or SX)	Micronised fluticasone propionate (or salmeterol xinafoate)
MMAD	Mass median aerodynamic diameter
MOC	Micro-orifice collector

MSLI	Multistage liquid impinger
mRNA	Messenger ribonucleic acid
n	Avrami exponent of the Avrami-Erofe'ev-type equation
n	Amount adsorbed
N	Number of time points (in the dissolution profile)
N_A	Avagadro's number
n_m	Number of moles of solute adsorbed for monolayer coverage
NGI	Next generation impactor
P_D	Molar deformation polarisation of the IGC probes
PEG	Polyethyleneglycol
pMDI	Pressurised metered dose inhaler
p	Equilibrium partial pressure
p_o	Saturation pressure (of a liquid)
PIF	Peak inspiratory flow rate
PP	Primary pressure
PPG	Polypropylene glycol
PR	Percentage recovery
PS	Pre-separator
PSD	Particle size distribution
PTFE	Polytetrafluoroethylene
PXRD	Powder x-ray diffraction
Q	Flow rate corresponding to a pressure drop of 4 kPa across an inhaler device
ρ	Particle density
ρ_g	Gas density
R	Gas constant
R^2	Coefficient of determination
R_D	Specific resistance (of an inhaler device)
R*e*	Reynolds number
RD	Recovered dose
RH	Relative humidity
RODOS	Rotating dosing and dispersing system
Rpm	Rotations per minute
R_t	Mean percentage of drug dissolved of a reference product at a specific time point in a dissolution curve

S	Stopping distance (of a particle)
S1-7	Stage 1 – 7
SA100 (or 500)	Seretide Accuhaler 100 (or 500)
S_B	Standard error of the y estimate (i.e. y intercept)
SB	Salbutamol base
SD	Standard deviation
Sccm	Standard cubic centimetres per minute
SEA	Surface energy analyser
SEM	Scanning electron microscopy
Span 80 (or 85)	Sorbitan monooleate 80 (or 85)
SS	Salbutamol sulphate
SSA	Specific surface area
Stk	Stokes number
SX	Salmeterol xinafoate
SX-I	Salmeterol xinafoate polymorph form I
SX-II	Salmeterol xinafoate polymorph form II
t_o	Dead volume of the IGC probes
T	Temperature
Tof	Tofimilast
t_R	Gross retention time of the IGC probes
T_{ref}	Reference temperature
T_s	Column temperature
T_t	Mean percentage of drug dissolved of a test product at a specific time point in the dissolution curve
TSI	Twin Stage Impinger
U	Initial velocity of a particle
U	Air velocity
USP	United States Pharmacopeia
V	Gas velocity
V_N	Net retention volume
VDW	Van der Waals forces
VMD	Volume mean diameter
WHO	World Health Organisation
Y_B	y intercept (from the regression equation)
Φ	Packing fraction

1 GENERAL INTRODUCTION

1.1 BACKGROUND

Respiratory disease, such as asthma and chronic obstructive pulmonary disease (COPD), is a major, global, public health problem. The World Health Organisation (WHO) estimates that asthma and COPD affects 235 million (WHO, 2011) and 65 million individuals, respectively, worldwide (WHO, 2012). Many patients with these diseases require treatment with more than one inhaled drug, specifically inhaled corticosteroids (ICs) and long acting beta agonists (LABAs). Inhalers containing both classes of drug in a single formulation are commercially available, and include Seretide, Symbicort, Flutiform and Fostair (BNF, 2013).

In combination dry powder inhaler (DPI) formulations, two micron-sized drug powders are present in a physical mixture, which may also contain a carrier and ternary agent. A major challenge in DPI development is achieving efficient de-agglomeration of the small, inherently cohesive, drug particles. The particulate interactions that exist within each powder component, and between the drug and any excipient particles, are an important factor in dictating the dispersion and aerodynamic deposition profile of the drug. The incorporation of a second drug powder therefore introduces a further level of complexity in combination formulations. The physicochemical properties of the two drug powders may be different, which will not only influence the inter-particulate interactions within the blend, but also the resulting powder structure. This could lead to differences in the dispersibility of the drugs upon co-formulation, and may ultimately manifest as altered drug bioavailability. Micronised powders show variability in their properties, and therefore a distribution in the magnitude of drug interactions and powder microstructure may also occur. In order to gain a fundamental understanding of the effects of co-formulation on aerosolisation performance in these complex systems, investigations into the influence of physicochemical interactions using model drug powders are required. In introducing the importance of this research, it is pertinent to review the structure and function of the lungs, the role of inhaled delivery in the treatment of respiratory disease, and the most common delivery devices employed for inhaled drugs. This will be followed by considering the fate of particles in the lungs, including particle deposition and dissolution, and finally, combination therapy, focusing on the two most extensively used drugs: salmeterol xinafoate (SX) and fluticasone propionate (FP), and outlining the rationale for formulating two drugs in a single inhaler product.

1.2 THE STRUCTURE AND FUNCTION OF THE LUNGS

The lung is a complex, heterogeneous organ occupying the majority of the volume of the thoracic cavity. Each lung is divided into several lobes consisting of a series of dichotomously branching airways (Martonen, 1993; Sherwood, 2001). The lung is the site of gas exchange between oxygen and carbon dioxide, and therefore has the main role of respiration in the body (Sherwood, 2001). The lungs consist of two main functional areas, the conducting zone (i.e. trachea, bronchi, bronchioles and terminal bronchioles) and the respiratory zone (i.e. respiratory bronchioles, alveolar ducts and alveolar sacs), the latter of which represents the site of gas exchange (Martonen, 1993). The airways are often characterised into generations, starting from the trachea (I = 0), the bronchi, bronchioles and terminal bronchioles (I = 1 - 16), the partially alveolated respiratory bronchioles (I = 17 – 19), the alveolar ducts (I = 20 – 22) and finally the alveolar sacs/alveoli (I = 23) (Martonen, 1993).

The respiratory tract is considered to consist of three main regions. The nasopharynx which comprises the airways of the head and are often referred to as the extrathoracic airways. The tracheobronchial region which comprises the bronchial airways and includes the trachea and terminal bronchioles; these airways are lined with smooth muscle thus maintaining the physical integrity of the lungs, and have ciliated epithelium which is covered in mucus. Finally, the pulmonary region, which comprises the respiratory bronchioles and alveolar ducts, and is the site of gas exchange. The epithelium of these airways is non-ciliated and covered in surfactant (Martonen, 1993). The large number of densely packed alveoli in the lungs (approximately 300 million, Weibel and Gomez, 1962) results in a very large surface area for gas exchange of approximately 143 m^2 (Gehr et al., 1978). The air-blood tissue barrier and the epithelium are also very thin, exhibiting mean values of 2.2 µm and 0.61 µm, respectively, in the human lung (Gehr et al., 1978). The cellular composition of this organ is also heterogeneous, and is often described in terms of the main tissue compartments i.e. the endothelium, epithelium and interstitium. The endothelium is composed of a layer of squamous cells, whereas the epithelium comprises two main cell types. Type I epithelial cells are similar to those of the endothelium (i.e. large, squamous) whereas Type II epithelial cells are round or cuboidal, have microvilli and secrete pulmonary surfactant (Gehr et al., 1978; Sherwood, 2001). The interstitium on

the other hand contains a range of cell types such as fibroblasts, lymphocytes and mast cells (Gehr et al., 1978).

1.3 INHALED THERAPY

The inhalation of medicinal agents dates back over 4000 years to smoking of the leaves of the *Atropa belladonna* plant to supress coughing, and inhalation of sea mists, hot vapours and aerosols to ease airway obstruction. Over the years, the direct delivery of drugs to the lungs to treat respiratory diseases has grown into a multi-billion dollar market. Not only have formulation and device technologies generated convenient and portable delivery systems, but the inhaled route has provided an alternative, non-invasive means to deliver pharmaceuticals, particularly including biologics such as insulin. With research in this area proceeding at a fast rate, not only will it be possible to improve the efficiency and reproducibility of delivery via this route, but also greater exploit the favourable features of the lungs for the delivery of systemic therapies (Gonda, 2000; Weers et al., 2010).

1.3.1 RESPIRATORY DISEASES

Inhaled therapy is widely accepted as the optimal route of drug administration for local diseases such as asthma, chronic obstructive pulmonary disease (COPD), cystic fibrosis and chronic bronchitis. By delivering high doses of drug directly to the site of action, a rapid clinical response is elicited and systemic side effects are minimised. Furthermore, by bypassing processes such as first-pass metabolism and gastro-intestinal absorption, a similar or superior therapeutic response is achievable using much lower doses than would be required following systemic delivery, for example, an oral dose of 2 – 4 mg of salbutamol is equivalent to an inhaled dose of 100 – 200 µg of the drug (Labiris and Dolovich, 2003b).

1.3.1.1 ASTHMA

Asthma is a common respiratory condition affecting people of all ages. It is estimated that there are 300 million individuals with asthma worldwide, and therefore the condition poses a serious public health problem (GINA, 2012). Asthma is a chronic inflammatory disorder of the airways, which is associated with airway hyper-

responsiveness. This leads to symptoms of wheezing, breathlessness, chest tightness and coughing, particularly in the early morning or night. There may also be airway obstruction which although reversible, may require treatment (GINA, 2012). There is currently no standard definition of asthma pathogenesis, and diagnosis is therefore clinical and relates to the presence of symptoms and variable airflow obstruction (BTS/SIGN, 2008 (revised 2012); GINA, 2012). With appropriate treatment, using inhaled therapies in the first instance, it is possible to attain good asthma control such that the occurrence of symptoms is minimal and severe exacerbations should be rare (GINA, 2012).

1.3.1.2 CHRONIC OBSTRUCTIVE PULMONARY DISEASE

COPD is estimated to affect three million people in the UK. Of these individuals, approximately 900,000 are diagnosed but two million are thought to be undiagnosed (Healthcare Commission, 2006). COPD is the fourth leading cause of death in the world, despite being both preventable and treatable (GOLD, 2013). The condition is characterised by persistent airflow limitation that may be stable over several months but which deteriorates progressively in the longer term. There is also an enhanced chronic inflammatory response to noxious particles/gases (NICE, 2010; GOLD, 2013). Airflow obstruction arises from a combination of small airways disease (obstructive bronchiolitis) and parenchymal damage (emphysema), as a result of chronic inflammation (GOLD, 2013). Tobacco smoke is a major risk factor for COPD, along with other occupational exposures. There may be significant airflow obstruction prior to the patient becoming aware of it, therefore diagnosis tends to occur later in life and is based on a combination of patient history, physical examination, spirometry and the presence of symptoms (e.g. exertional breathlessness, chronic cough, regular sputum production and wheeze) (NICE, 2010). Exacerbations can also occur in COPD patients, triggered by bacterial/viral infections, environmental pollutants, or unknown factors, in which there is rapid worsening of symptoms (GOLD, 2013). Smoking cessation and inhaled therapy are the first steps in the management of stable COPD, in order to improve lung function, provide symptomatic relief, minimise exacerbations and improve quality of life (NICE, 2010).

1.4 DELIVERY DEVICES

Aerosol drug delivery systems consist of a drug formulation, metering system and device technology (Hickey, 2013), and must fulfil a number of key requirements. Primarily, the system must generate an aerosol in which the majority of the particles have an aerodynamic particle size (d_{ae}) less than 10 µm, but ideally in the size range 0.5 – 5.0 µm, in order to attain deposition in the peripheral regions of the lungs (Zeng et al, 2001). The delivery system must provide reproducible dosing, drug physicochemical stability, ease of use, portability, and must also be economically viable (Zeng et al, 2001). There are three major categories of dosage forms used to deliver therapeutic aerosols to the lungs; these are nebulisers, pressurised metered dose inhalers (pMDIs) and dry powder inhalers (DPIs).

1.4.1 NEBULISERS

The first nebulisers (initially called atomisers) were developed in the mid-19th century in France. By the 1930s, early electric and compressor nebulisers had been developed, and with further technological advancements, nebulisers still remain in routine use for aerosol delivery today (Anderson, 2005). Despite a low delivery efficiency of approximately 10 % and high variability between formulations, they afford better stability for sensitive drugs such as antibiotics, mucolytics and other high dose drugs (Watts et al., 2008). Drug particles are formulated as aqueous solutions or suspensions contained within nebules. The nebule contents are dispensed into the reservoir chamber via an air-jet, ultrasonic or vibrating mesh nebuliser device (Hickey, 2013). Air-jet nebulisers operate under a venturi principle using compressed oxygen/air, and are generally used in acute and home care settings to deliver aerosolised drugs to nonambulatory patients. Despite being generally large and cumbersome, design improvements have increased delivery efficiency and allowed for breath actuated delivery. Ultrasonic devices have a piezoelectric crystal which vibrates at a high frequency (1 – 3 MHz) to generate respirable droplets, described by the capillary wave and cavitation theory. Although they have higher delivery efficiencies, they exhibit a number of limitations compared to air-jet nebulisers such as settling of suspensions and the degradation of heat sensitive drugs. Modifications to ultrasonic devices led to the development of the vibrating mesh devices, which retain the piezoelectric crystal but instead utilise mesh oscillation to drive aerosol production (Watts et al., 2008). These

latter devices benefit from low velocity aerosols, high respirable fractions and high fine particle fractions (FPFs) due to narrow droplet size distributions and low aerosol losses, as well as high output rates leading to shortening of treatment times (Lass et al., 2006; Watts et al., 2008).

1.4.2 PRESSURISED METERED DOSE INHALERS

The first pMDI was developed in the 1950s. The formulations consist of drug particles either dissolved and in solution or micronised and in suspension (Lewis, 2007). Hydrofluoroalkanes (HFAs) are typically used as the suspending media, and these were preceded by the chlorofluorocarbons (CFCs). Both HFAs and CFCs also function as propellants (Michael et al., 2001). Generation of the respirable dose for inhalation requires atomisation of the liquid formulation. Upon exiting the metering chamber, the formulation expands and this is followed by rapid evaporation of the highly volatile propellant as the dose is emitted from the inhaler mouthpiece. Although pMDIs show cost-effectiveness, portability and apparent simplicity, they are not without their drawbacks (Lewis, 2007). These include patient difficulty in co-ordinating breathing with pMDI actuation, and poor stability either due to creaming (i.e. phase separation) and coalescence (i.e. aggregation) particularly in suspension formulations, and reduced drug chemical stability and drug loss due to partitioning to container walls/values for solution based formulations (Smyth, 2003; Lewis, 2007). Additionally there is high plume velocity and high oropharyngeal deposition, which can limit the efficiency of these inhalers to deliver drug particles to the lungs (Lewis, 2007). For example, the CFC containing suspension-based beclometasone dipropionate pMDI produced 90 – 94 % deposition of the *ex*-actuator dose in the oropharynx and only 4 – 7 % in the lungs. When formulated as a solution based HFA formulation, the extra-fine particles (mass median aerodynamic diameter (MMAD) of 1.1 µm compared to 3.5 µm for the suspension formulation) were able to lower deposition in the oropharynx to 55 – 60 % and increase lung deposition to 29 – 30 % compared to the CFC formulation (Leach et al., 1998).

1.4.3 DRY POWDER INHALERS

The initial development of DPIs was guided by the limitations of previously available portable inhalation devices; solution nebulisers were limited by the physicochemical

properties of drug solubility and solution viscosity, whereas for pMDIs only small quantities of inhalant (approx. maximum 5 mg) could be delivered before problems, such as mechanical obstruction of the valves, occurred (Bell et al., 1971; Labiris and Dolovich, 2003b). Over the years, interest in DPI devices has grown for a number of reasons. DPIs do not require co-ordination between the breath and actuation, thus improving ease of use for patients. Furthermore, they do not require propellant gases hence providing a 'greener' alternative to pMDIs. A range of DPI devices are available on the market and are generally characterised as single-unit devices which require each individual dose to be loaded by the patient prior to use (e.g. Aerolizer, Rotahaler), multi-unit devices which contain multiple doses that are either provided as a blister pack (e.g. Diskhaler) or a sealed blister strip that moves within the device (e.g. Diskus) or reservoir type, bulk powder systems (e.g. Turbuhaler). The majority of DPI devices are passive, and depend on the patient's inspiratory effort in order to generate an aerosol within the respirable particle size range. Active DPIs conversely do not depend on patient inspiration, and instead utilise an energy source for powder entrainment and de-agglomeration (Labiris and Dolovich, 2003b). Examples of active dispersion include the use of compressed air e.g. Aspirair™ (Tobyn et al., 2004), battery-powered propellers e.g. Spiros (Nelson et al., 1999) and the use of high frequency piezoelectric vibrators e.g. Microdose DPI (Crowder, 2005; Fleming, 2007), although currently these devices are not available on the market in the UK.

1.4.3.1 PARTICLE PRODUCTION FOR INHALATION

Particles for inhalation are typically produced by batch crystallisation of the drug from solution, followed by a filtering and drying step. During crystallisation, the particle size of the drug is not well controlled and is often large, thus requiring a comminution step such as micronisation/milling to reduce the size to within the respirable size range (i.e. < 5 µm) (Telko and Hickey, 2005; Chow et al., 2007). A jet or ball mill is usually employed. In the jet mill, high pressure nitrogen gas is fed into the mill and causes particle acceleration. Particle attrition occurs as a result of high velocity particle-particle collisions, whereby it is possible to obtain a particle size as small as 1 µm by controlling the milling conditions. A ball mill conversely consists of a cylinder containing the powder and milling balls. As the cylinder is rotated, particle attrition occurs as the balls tumble within the vessel. Ball milling is much slower and less scalable than jet milling, which is therefore generally favoured (Telko and Hickey, 2005).

Following micronisation, the particle size distribution (PSD) is broad and poorly controlled (Steckel et al., 2003a; Steckel et al., 2003b). Subjecting particles to such a high energy process results in disorder, defects, and/or amorphous regions on crystal surfaces (Ward and Schultz, 1995; Brodka-Pfeiffer et al., 2003b; Gaisford et al., 2010). Amorphous regions are metastable, and at a higher energy state than crystalline regions. Depending on the environmental conditions, water adsorption and re-conversion to the more stable crystalline form can occur and often coincides with particle growth (Brodka-Pfeiffer et al., 2003b). Even low levels of amorphous content can have marked effects on the physical and chemical stability of the powder. For example, micronisation can increase surface energy (Feeley et al., 1998; Newell et al., 2001; Gamble et al., 2012) and surface energy heterogeneity (Thielmann et al., 2007), affect powder flow (Feeley et al., 1998), alter inter-facial chemistry and thus the cohesive-adhesive balance (Kubavat et al., 2012) and induce agglomeration (Zhou et al., 2010b; Le et al., 2012b; Han et al., 2013). The inability to control the changes in particle properties both within and between powder batches (Feeley et al., 1998; Ticehurst et al., 2000; Marek et al., 2011; Le et al., 2012b) also has implications for the reproducibility of formulation performance. For example, different batches of powder can exhibit different tendencies for agglomeration and thus agglomerate sizes upon dispersion (Le et al., 2012b), may respond differently to processing stresses which may impair the flowability and dispersion of the formulation (Marek et al., 2011), and have different powder stabilities dictated by the rate of re-crystallisation of amorphous regions induced during micronisation (Brodka-Pfeiffer et al., 2003a).

1.4.3.2 DRY POWDER INHALER FORMULATIONS AND THE ROLE OF EXCIPIENTS

DPI formulations in their simplest form consist of agglomerated micron-sized drug particles. By their nature, small particles have a large surface area and high cohesive/adhesive forces, therefore not only do they form agglomerates, they are highly adhesive towards surfaces such as inhaler walls, and exhibit poor flow, entrainment and dispersion. Depending on the drug, the dose required can vary from a few micrograms (e.g. formoterol fumarate) to 10s or 100s of milligrams (e.g. tobramycin). Particularly when the dose is low, the handling, dispensing and metering of drug particles, in addition to achieving dose reproducibility, is difficult. A well-established strategy is to

formulate drug particles with larger carrier particles, which play a number of key roles in the formulation (Frijlink and De Boer, 2004; Telko and Hickey, 2005).

1.4.3.2.1 THE ROLE OF THE CARRIER

The coarse excipient in a DPI formulation is generally an inert material that is at least one order of magnitude larger (i.e. 50 – 100 μm) than the drug particles in the formulation. The excipient is generally referred to as a carrier as drug particles associate with the surface of these particles. Consequently, there is a reduction in cohesivity and improvement in the flow and fluidisation properties of the powder formulation. The coarse excipient forms the major component of the formulation, thus further having a role as a diluent to improve powder handling and dose reproducibility (Pilcer et al., 2012). During aerosolisation, drug particles must be liberated from the surface of the carrier in order to penetrate into the lungs, and therefore drug-carrier adhesion needs to be carefully considered. The choice of carrier is critical, and depends on the nature, quality and source, as well as size distribution, morphology and surface properties of the particles. All these factors need to be considered with a view to maintaining an adequate balance between drug-carrier adhesion and drug-drug cohesion (Ho et al., 2010; Pilcer et al., 2012).

Although lactose is most commonly employed as a carrier, alternative sugars such as mannitol, erythritol, trehalose and sorbitol have been investigated (Tee et al., 2000; Jones et al., 2008a). A great deal of research has focussed on determining the optimal carrier properties for drug dispersibility, including carrier particle size (Larhrib et al., 2003; Donovan and Smyth, 2010; Ooi et al., 2011), shape e.g. elongation ratio (Larhrib et al., 2003; Kaialy et al., 2011), surface roughness (Adi et al., 2008b; Donovan and Smyth, 2010), pseudopolymorphic form (Traini et al., 2008), cohesive-adhesive balance (Jones et al., 2008a; Jones et al., 2008b) and fines concentration (Ho et al., 2010; Le et al., 2012a). These properties, however, have complex and interacting effects on dispersion which are thought to be drug-specific (Jones et al., 2008b) and therefore the selection and optimisation of a carrier needs to occur in tandem with a knowledge of the physicochemical properties of the drug.

1.4.3.2.2 THE ROLE OF TERNARY AGENTS/FINES

The addition of ternary agents (or fines) to DPI formulations is well established as a means of improving de-agglomeration efficiency (e.g. Lucas et al., 1998; Zeng et al., 1998). A small quantity of fine excipient particles with a similar particle size to the drug in the formulation is either added extrinsically or may be generated *in situ* during processing of the excipient and/or formulation (Shur et al., 2008). Lactose particles are most commonly used however alternative sugars such as mannitol, sorbitol and glucose have been investigated for their use as ternary agents (Tee et al., 2000; Louey and Stewart, 2002), as well as amino acids such as leucine, although a fine particle (rather than coarse) lactose was included in the formulation as the 'carrier' (Lucas et al., 1999). The ability of lactose, mannitol and sorbital fines, for example, to improve the FPF, suggests that it may be the presence of the fine particle, and not its chemical entity, which is important in order to improve formulation performance. For example, there may be changes in the work of cohesion/adhesion between the particles which may affect the powder structure and thus powder dispersibility. The exact mechanism by which 'fines' exert their performance modifying effects are still unclear. Two mechanisms are currently suggested. The first is the 'active sites' mechanism, which arises from the interactions which occur between coarse and fine particles during ordered mixing (Hersey, 1975). It is proposed that active binding sites exist on the surface of large carrier particles, which are unevenly distributed across the surface (Hersey, 1975). During formulation with a fine excipient, the 'fines' preferentially associate with the most energetic active sites on the carrier surface such that the drug particles associate with less energetic regions. Upon inhalation, the drug particles are therefore more readily liberated from the carrier (Jones and Price, 2006). The second proposed mechanism is called the 'agglomerates' mechanism, in which during mixing agglomerates form comprising particles of both the drug and fines particles. Improvements in performance are considered to arise due to lower adhesive forces between particles in the drug-fines agglomerates leading to more efficient dispersal, as well as the direct liberation and deposition of these agglomerates due to their small aerodynamic particle size (d_{ae}) (Lucas et al., 1998).

A further component that may be involved is a change in the powder structure that may arise from the introduction of fine particles to the bulk powder. With increasing drug loadings in carrier based blends, it is suggested that upon saturation of active sites on the carrier surface, multiple agglomerate systems will be present due to the carrier

surface reaching monolayer (and even multilayer) coverage. At very high drug loadings, there will be drug particle agglomeration and drug carrier segregation, which may result in changes in aerosol performance and blend uniformity (Young et al., 2011). The presence of fines may also alter the bulk properties of a powder; high fines contents can increase the cohesive inter-particulate interactions within a powder bed and thus increase the tensile strength. This has been associated with a change in the fluidisation and dispersion mechanism of the powder, from an erosion mechanism typical of powders with low cohesivity, to the entrainment of powder plugs due to fracture of the powder bed, which is typical of the fluidisation behaviour of highly cohesive powders (Shur et al., 2008). This increase in cohesive strength of the powder bed has been shown to increase the DPI performance of budesonide particles when formulated with a lactose carrier and lactose fines (Kinnunen, 2010), whereby the entrainment of large powder plugs increases the number of particle-particle and particle-device collisions and can enhance the detachment of drug from a carrier (Shur et al., 2008; Kinnunen, 2010). A more subtle improvement in performance by the addition of milled compared to micronised lactose fines (both having D_{v50} values < ~ 5 µm) was attributed to stronger interactions between the milled lactose and drug particles compared to the micronised lactose (Kinnunen, 2010), further highlighting the complex inter-play between inter-particulate forces and bulk powder properties in determining aerosolisation behaviour. Furthermore, in addition to each powder constituent having its own PSD, work of cohesion, and density which contribute towards its powder strength, there will also be a distribution in powder strengths within the bulk powder due to micro-areas which exhibit different powder structures (Das et al., 2012). This non-homogeneity in powder bed microstructure is likely to be greater in powder mixtures, which would exhibit broader distributions in particle size, surface energy (and hence work of cohesion) and packing fraction across the bulk powder.

1.4.3.3 INTER-PARTICULATE FORCES

The particles in any powdered dosage form will interact with each other via cohesive and/or adhesive interactions (Zeng et al, 2001). The attractive physical forces in DPI formulations are classified into three major categories: van der Waals, electrostatic, and capillary forces. Other forces, such as frictional forces, exist and are important, but are generally less frequently studied (Xu et al., 2010b). The particle-particle interactions within powders have implications not only in handling processes such as comminution, blending and storage, but also affect bulk powder properties such as flowability, de-

agglomeration and dissolution (Zeng et al, 2001). Furthermore, particle-capsule and particle-device interactions will also arise in the final formulated product, and affect the overall efficiency of aerosolisation.

1.4.3.3.1 VAN DER WAALS FORCES

Of the major categories of inter-particulate force, van der Waals (VDW) forces are generally dominant in uncharged dry powders, particularly where the magnitude of the particle size (i.e. < 10 μm) and separation distance (< 100 nm) are both small. VDW forces are typically two orders of magnitude greater than electrostatic and capillary forces, however, they decay rapidly with separation distance (Xu et al., 2010b). VDW forces are also sensitive to particle shape and surface roughness, as surface asperities can limit how close particles are able to come (Pilcer et al., 2012). Depending on particle shape, particles in close contact may experience very strong VDW forces, resulting in possible mechanical inter-locking (Pilcer et al., 2012).

1.4.3.3.2 ELECTROSTATIC FORCES

Electrostatic charges arise within a powder bulk when an uncharged particle makes contact with a charged particle, upon which a transfer of electrons/ions occurs between them. Positively or negatively charged particles will experience electrostatic attractive/repulsive forces with neighbouring particles depending on their charge. Powder processing steps such as mixing, handling and filling can induce electrical charges, as can the fluidisation and de-agglomeration process itself, therefore the term triboelectrification is generally used to describe this effect (Zeng et al, 2001; Pilcer et al., 2012).

1.4.3.3.3 CAPILLARY FORCES

Capillary forces can arise as a result of water adsorption onto particle surfaces leading to the formation of liquid bridges which can greatly increase the attractive forces between particles. Capillary forces prevail at high relative humidity (RH), usually in excess of 60 %, where liquid capture can also increase the surface energy and surface conductivity of the particle (Zeng et al, 2001; Xu et al., 2010b). However, even storage at relatively low RHs in the range 15 – 75 % for short periods of time (12 h) can have detrimental effects on the achievable FPF, and was attributed to the increasing dominance of capillary forces of increasing magnitude as the RH increased (Young et

al., 2003, Young et al., 2004). Not all drugs however exhibit this change in FPF, and the generation of higher FPFs has been postulated to occur due to the dissipation of surface charges induced by triboelectrifcation due to electron mobilisation. Therefore, even at high RHs aerosolisation behaviour is dependent on the balance of inter-particulate forces, which are related to the physical and chemical properties of the powder (Young et al., 2003).

1.4.3.4 AEROSOL GENERATION TO DELIVER PARTICLES TO THE LUNGS

The aerosolisation process in DPI systems comprises four phases during which a powder, which is initially at rest in a static bed, must undergo dilation, fluidisation and drug re-suspension/de-agglomeration. These phases are considered to occur concurrently rather than in sequence (Xu et al., 2010b). Inter-particulate forces and aerosolisation must be considered in tandem, as it is attractive forces that cause particles to agglomerate, and it is these attractive forces that must be overcome in order to generate an aerosol for particle delivery to the lungs (Xu et al., 2010b). In passive DPI systems, detachment forces arise from the airflow generated by patient inspiration, and include aerodynamic forces (drag and lift), inertial forces (vibration, rotation, centrifugal and collision) and shear and frictional forces (Louey et al., 2006; Xu et al., 2010b). As the patient inhales through the device, the flow rate continually changes, increasing to a maximum peak inspiratory flow rate (PIF) before reducing back down to a baseline. Consequently, the flow rate through a DPI is not static and varies according to the time from the start of inhalation. Although perhaps paradoxically, *in vitro* inhaler testing is generally carried out at a constant flow rate. The metered dose is typically released prior to the patient achieving their PIF, as the patient vital capacity exceeds the internal volume of the inhaler; faster initial flow rates may therefore promote the entrainment and de-agglomeration of the initially static dose within the device (Martin et al., 2007). The efficiency of de-agglomeration determines the fine particle delivery of the drug, and is dependent on device, patient and particle factors.

1.4.3.4.1 DEVICE FACTORS

When a patient inhales through a passive DPI device, the airflow transfers kinetic energy into the powder bed as a result of the continuous bombardment of air molecules, and therefore provides detachment forces to overcome the inter-particulate interactions within the powder (Louey et al., 2006; Xu et al., 2010b). The airflow within a device

can be laminar or turbulent, and is described by the Reynolds number (R*e*), Equation 1.1, where ρ_g is the gas density, V is the gas velocity, d' is a characteristic dimension of the object, and η is the dynamic viscosity of the gas (Zeng et al, 2001).

Equation 1.1 $$R_e = \frac{\rho_g V d'}{\eta}$$

DPI devices are often designed to generate turbulent air flows (i.e. R*e* > 4000), using design features such as tortuous airflow paths, grids or impactor plates in order to optimise de-agglomeration efficiency (Louey et al., 2006; Xu et al., 2010). The internal dimensions and geometry also influence the specific resistance (R_D) of the device, and is related to the pressure drop (ΔP) and the flow rate (Q), according to Equation 1.2 (Louey et al., 2006). A high R_D is generally considered to generate greater turbulence and higher FPFs at a given flow rate compared to devices with a lower R_D. However, devices with high R_D values require a greater respiratory effort by the patient in order to achieve the required flow rate (Labiris and Dolovich, 2003b; Louey et al., 2006), and this might pose difficulties to respiratory compromised patients.

Equation 1.2 $$\sqrt{\Delta P} = R_D . Q$$

1.4.3.4.2 PATIENT FACTORS

A number of patient factors influence the efficiency of aerosol generation from DPIs. The inhalation flow rate generated by the patient is critical. Although high flow rates may promote de-agglomeration, there may also be a reduction in the amount of drug reaching the lungs due to impaction of rapidly moving aerosol particles in the oropharyngeal region and the larynx (Dolovich, 1993; Labiris and Dolovich, 2003a). The flow rate also varies with time during a single inhalation, between inhalations, and between patients. In an attempt to account for this, the electronic lung was developed for use during *in vitro* cascade impactor testing which utilises simulated or replicated inhalation profiles with varying flow rates and flow accelerations (Burnell et al., 1998). The inhalation manoeuvre adopted by the patient can, however, further modify deposition, for example increasing the breath holding time allows greater time for particles to deposit by sedimentation (Burnell et al., 1998).

Airway calibre and anatomy also differs between individuals, and in the diseased lung. Bronchoconstriction, inflammation and airway narrowing can alter drug deposition, and may require the inhalation of more drug in order to achieve an optimal clinical response (Dolovich, 1993; Labiris and Dolovich, 2003a). Airway disease can alter the architecture of the lungs and thus the deposition and distribution pattern of aerosols. For example, changes to bifurcation angles and airway obstruction can occur, which in the latter case causes higher air velocities and higher turbulence due a reduced cross-sectional area in areas of the lung where air flow is usually laminar (Labiris and Dolovich, 2003a).

1.4.3.4.3 PARTICLE FACTORS

The particle properties that influence dry powder aerosol generation are numerous. Particle engineering is therefore well established as a means of obtaining particles with controlled physicochemical attributes. The aerodynamic particle size (d_{ae}) is a critical factor in both the dispersion and site of deposition in the lungs. The aerodynamic diameter relates the particle to the diameter of a sphere which has unit density and the same settling velocity as the particle of interest (Labiris and Dolovich, 2003a). The aerodynamic particle size is linked to the geometric particle size according to Equation 1.3 (Louey et al., 2004a), where d_g in the geometric particle size and ρ is particle density. A small aerodynamic diameter can therefore be attained by reducing particle density whilst maintaining a large geometric particle size. Geometrically large, low density porous particles have hence been prepared which exhibit superior dispersion compared to non-porous particles with the same aerodynamic diameter, which further exhibit smaller surface area-to-volume ratios and a lower tendency for particle agglomeration (Edwards et al., 1997). This approach has been used to prepare drug particles (e.g. Steckel and Brandes, 2004), as well carriers for therapeutic agents such as insulin (e.g. Ungaro et al., 2009).

Equation 1.3 $$d_{ae} = d_g . \sqrt{\rho}$$

In DPI formulations, particles exist as agglomerates. The particle size affects the tensile strength of agglomerates which is directly related to the packing fraction (ϕ) i.e. the volume of particles/volume of the agglomerate, and inversely related to particle diameter (Kendall and Stainton, 2001). Whilst airborne, larger agglomerates experience

higher aerodynamic drag forces and kinetic energy, as these are proportional to the square and cube of agglomerate diameter, respectively, and thus would be expected to de-agglomerate more efficiently (Begat et al., 2004b). The shape of the drug particle is also important, and can be modified either in an uncontrolled way due to micronisation or using controlled crystallisation methods. Needle-like particles, for example, although displaying poorer homogeneity when blended with lactose have better dispersibility than micronised particles due to a greater propensity for needle-like particles to remain airborne and disperse (Larhrib et al., 2003; Kaialy et al., 2011). The degree of surface corrugation/roughness can alter the contact area of particles for example with a carrier and therefore affect dispersion. The reduction in adhesive forces as a result of a rougher surface generates higher FPFs following aerosolisation (Adi et al., 2008b).

Particle surface energy can influence dispersibility, as it affects the magnitude of interactive forces and therefore the cohesivity and adhesivity of the particles. Changes to particle surface energy can occur during processing, particularly micronisation, during which particle fracture occurs along the weakest attachment energy facet of the crystal. This subsequently becomes the dominant facet and generally causes higher surface energy, in addition to changes to the surface chemistry of the particle (Heng et al., 2006b). The resulting changes to the crystal shape/aspect ratio can cause secondary fractures to occur along a different facet, inducing further alterations to the surface energy/chemistry of the final milled product (Heng et al., 2006b). In the absence of a carrier, higher surface energy has increased the FPF of salbutamol sulphate (Shariare et al., 2011) but had the opposite effect on the FPF of salmeterol xinafoate samples (Tong et al., 2006; Das et al., 2009b). Conflicting trends have also been observed in carrier formulations, in which surface energies were used to calculate the work of adhesion between the drug and carrier particles. Higher drug-carrier adhesion was associated with both higher (Cline and Dalby, 2002) and lower FPFs (Traini et al., 2008) for dry powder formulations. This highlights the complexity in terms of the range of factors that affect the aerosolisation process, and indicates that any correlation between surface energy and FPF may be drug and/or carrier specific. Furthermore, it is necessary to consider changes in the dispersive, specific and total surface energy (Das et al., 2009b) and the non-homogeneity in particle properties within a bulk powder (Das et al., 2012), as the surface energy, and balance of interactions, can change with for example drug

polymorphic form (Tong et al., 2006; Traini et al., 2008) and particle crystallinity (Tong et al., 2001; Rehman et al., 2003; Shekunov et al., 2003).

1.5 THE FATE OF PARTICLES IN THE LUNGS

1.5.1 DEPOSITION

The process of deposition in the lungs involves inhaled particles separating from the air flow and contacting a surface without any rebound or re-suspension (Zeng et al, 2001). Particle deposition in the airways is complex, and can occur by any one of five mechanisms; these are inertial impaction, sedimentation, diffusion, interception and electrostatic precipitation. The first three are considered to be the principal mechanisms (Newman et al., 1982). Any particles that remain airborne during the respiratory cycle are exhaled, and this occurs most frequently with very small particles (< 0.5 μm) (Zeng et al, 2001).

1.5.1.1 INTERTIAL IMPACTION

Inertial impaction is the most important mechanism of deposition, particularly for particles larger than 1 μm. Deposition by impaction is predominant in the extrathoracic (nose, mouth, larynx) and large, more central, conducting airways of the lungs where air flow velocities are high and there are rapid changes in airflow direction (Newman et al., 1982; Schulz, 1998). When an airstream changes direction, an airborne particle will continue to move along its original trajectory for a stopping distance (S) according to Equation 1.4, where B is the mobility of the particle (i.e. velocity per unit force), m is particle mass and U is the initial velocity of the particle (De Boer et al., 2002a).

Equation 1.4 $$S = m.B.U$$

If the stopping distance is greater than the diameter of the airway, the particle will deposit by impaction (De Boer et al., 2002a). Large, heavy particles travelling at high velocities, and therefore possessing high momentum, are less able to follow gas airstreams as they change direction in the respiratory tract, and instead undergo deposition by impaction (Newman et al., 1982; Zeng et al, 2001). The probability that a particle will deposit by impaction is therefore dependent on its size, density and

travelling velocity (Schulz, 1998), and is represented by the dimensionless Stokes Number (Stk) described in Equation 1.5, where ρ is particle density, d is particle diameter, U is air velocity, η is air viscosity, R is airway radius and C_c is the Cunningham correction factor for slip flow for particles in the size range 0.1 – 3.0 μm (Zeng et al, 2001; De Boer et al., 2002a).

Equation 1.5 $$Stk = \frac{C_C.\rho.d.U}{18.\eta.R}$$

The higher the value of Stk the more readily a particle will deposit by impaction. Although any particle > 1 μm can deposit by impaction, this mechanism is particularly relevant in the case of large particles i.e. those with an aerodynamic particle size greater than 3 μm, and when air flow rates are high (Zeng et al, 2001; De Boer et al., 2002a; Scheuch et al., 2006).

1.5.1.2 SEDIMENTATION

Deposition by sedimentation occurs when a particle travelling through the airways settles under the influence of gravity, and is therefore a time-dependent process (Newman et al., 1982). When airborne, initially a particle will accelerate before reaching a terminal velocity, at which the gravitational force is equal to the frictional, drag forces experienced as the particle travels through the air. The probability of sedimentation is proportional to the settling distance of the particle within the airways, which depends on the particle residence time and terminal settling velocity (Schulz, 1998). The latter is proportional to the square of particle diameter, as shown in Equation 1.6, where γ and η are the density and viscosity of the air, respectively, ρ and d are the density and diameter of the particle, respectively, and g is the acceleration due to gravity.

Equation 1.6 $$\frac{(\rho-\eta).g.d^2}{\gamma}$$

Deposition by sedimentation is therefore supported by a relatively large size (0.5 – 5.0 μm), and when particle residence time is increased such as during breath holding, low frequency steady breathing, and in the small conducting airways and alveolar regions of

the lung. In the latter regions, air flow velocities are low and the airway dimensions are small, further favouring deposition by sedimentation (Newman et al., 1982; Schulz, 1998).

1.5.1.3 DIFFUSION

Diffusion (sometimes referred to as Brownian diffusion) is the most important mechanism of deposition for ultrafine particles (i.e. < 1 μm). As these particles travel through the airways, they undergo random bombardment with gas molecules causing them to collide with airway walls and deposit (Newman et al., 1982). This random displacement of particles from the airstream increases with particle residence time and decreasing particle diameter, thus occurs with the highest probability for very small particles in the lung periphery, where the airway dimensions are small (Schulz, 1998).

1.5.1.4 INTERCEPTION AND ELECTROSTATIC PRECIPITATION

Two, more minor, deposition mechanisms are interception and electrostatic precipitation. Deposition by interception will occur when a particle's centre of gravity is within the gas streamline, however, a distal part of the particle has made contact with and therefore deposits on a respiratory surface. Interception is likely to occur when a particle has dimensions that are comparable with the airway radius. As therapeutic particles generally have a particle size that is much smaller than the airways, deposition by interception should not be important, but may play a role for irregularly shaped particles such as those with elongated shapes (Zeng et al, 2001). Electrostatic precipitation occurs as a result of electrostatic charges imparted on a particle as it is inhaled. Subsequently, a charge can be induced on a respiratory surface and thus deposition can occur as a result of mutual charge attraction (Zeng et al, 2001).

1.5.2 DISSOLUTION

The efficiency and clinical safety of an inhaled drug will depend on the dose delivered, the site of deposition, and the physicochemical properties of the drug, including the aerodynamic particle size distribution (Davies and Feddah, 2003; Riley et al., 2012). The latter are important in determining the rate of drug dissolution and subsequent systemic absorption, metabolism and elimination. Standardised, pharmacopoeial dissolution test methods exist for solid and semi-solid dosage forms as a quality control

tool to assess batch to batch variability, and to predict *in vivo* release, however, there is currently no such method to assess the dissolution behaviour of inhaled powders (Davies and Feddah, 2003; May et al., 2012; Riley et al., 2012).

Following deposition, undissolved particles may be cleared by the mucociliary escalator in the upper airways or by uptake into macrophages in the lower airways (May et al., 2012; Riley et al., 2012). The bioavailability and therapeutic action of the drug will therefore depend on the dissolution of the particles in the fluid lining of the lungs (Riley et al., 2012). Dissolution is defined as the process in which a solid enters a solvent to generate a solution, and is controlled by the affinity between the solid and the solvent (Davies and Feddah, 2003). Furthermore, the small volume of the lung lining fluid, approximately 10 – 20 mL/100 m^2, might also be expected to limit the dissolution process (May et al., 2012).

A range of dissolution methodologies have been employed to date to study inhaled dosage forms. These include the compendial USP 2 paddle apparatus (Son and McConville, 2009; Son et al., 2010), a modified USP 4 flow-through apparatus which is custom made (Davies and Feddah, 2003) and diffusion-controlled systems using the Franz cell (Salama et al., 2008; Salama et al., 2009) or Transwell® systems (Arora et al., 2010). In the latter system, the inclusion of a respiratory cell monolayer further provides a more realistic *in vitro* model (e.g. Grainger et al., 2009; Ong et al., 2012; Haghi et al., 2013). In addition to the dissolution apparatus, other factors such as particle presentation and dissolution media are important considerations. It is likely to be advantageous to test aerosolised particles in the respirable particle size range, and using representative dissolution media (e.g. simulated lung fluids) at the correct temperature and pH in order to mimic the *in vivo* environment as closely as possible (Riley et al., 2012). Dissolution profiling of inhaled products has indicated that drug solubility (Davies and Feddah, 2003; Arora et al., 2010), particle size/mass (Son and McConville, 2009; Arora et al., 2010; Son et al., 2010), and aerosol delivery (e.g. inhaler device, Arora et al., 2010, and single vs. co-delivery, Haghi et al., 2013) are important factors that may influence the dissolution rate of an inhaled drug.

1.6 COMBINATION THERAPY

The National Heart, Lung and Blood Institute expert panel classifies asthma into four levels of severity depending upon the symptoms and lung function prior to the initiation of treatment. These are: (1) mild intermittent asthma, (2) mild persistent asthma, (3) moderate persistent asthma and (4) persistent asthma (Nelson et al., 2003; NHLBI, 2007). Long acting beta agonists (LABAs) are used in combination with inhaled corticosteroids (ICs) for long term control and prevention of symptoms in moderate or severe persistent asthma. Due to the heterogeneous nature of COPD, the severity of the disease is assessed based on the individual patient. Combination therapy is therefore advocated in stable disease where the patient has breathlessness or exacerbations despite the use of short-acting bronchodilators (NICE, 2010). Combination DPIs currently available on the market contain salmeterol xinafoate (SX) and fluticasone propionate (FP; Seretide Accuhaler) or formoterol fumarate and budesonide (Symbicort) (BNF, 2013). SX and FP were therefore selected as model drug powders in order to assess the influence of co-formulation on drug dispersion.

1.6.1 SALMETEROL XINAFOATE

1.6.1.1 PHARMACOLOGICAL AND PHYSICOCHEMICAL PROPERTIES

Salmeterol xinafoate ((4-hydroxy-a1-[[[6-(4-phenylbutoxy)hexyl]amino]methyl]-1,3-benzenedimethanol,1-hydroxy-2-naphthalenecarboxylate; SX) was developed as a long acting bronchodilator to provide control for nocturnal asthma symptoms and therefore a more convenient maintenance therapy for patients with asthma (NICE, 2010). SX is a LABA with a chemical structure as shown in Figure 1.1. SX consists of a racemic form of the 1-hydroxy-2-naphthoic acid salt of salmeterol, possessing a long carbon side chain which contributes towards its high lipophilicity (Michael et al., 2000).

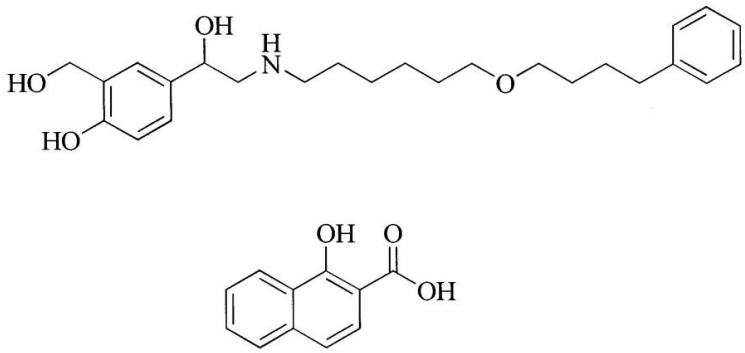

Figure 1.1 Chemical structure of salmeterol xinafoate (SX) taken from Michael et al. (2000).

SX is highly selective towards the β_2 receptor, and primarily causes bronchial smooth muscle relaxation (Lofdahl, 1990; Dransfield and Bailey, 2004). SX has a higher affinity for the β_2 receptor than salbutamol, and is over 10,000 times more lipophilic. The lipophilic nature of SX causes it to partition into the cell membrane, before diffusing to the active site of the β_2 receptor. Although having a slower onset of action than other β_2 agonists such as salbutamol and formoterol, SX has a much longer duration of action of up to 12 h (Lofdahl, 1990; Johnson et al., 1993).

The physical appearance of SX is a white powder, which is freely soluble in methanol, slightly soluble in ethanol, chloroform and isopropanol, and sparingly soluble in water (Kim et al., 2009). SX exists in two crystalline polymorphic forms, Form I (SXI) and Form II (SXII), which are enantiotropically related (Tong et al., 2002). SXI is the thermodynamically stable form at ambient temperature and pressure, compared to the metastable SXII form. Polymorphs display different properties, for example surface energy and solubility, and may therefore have consequences for the performance of the final formulated product (Tong et al., 2001, Tong et al., 2006).

1.6.1.2 ROLE IN ASTHMA AND COPD TREATMENT

LABAs (e.g. SX) are indicated as the first choice add on therapy for asthma patients not adequately controlled with short acting bronchodilators (treatment step 1) and regular preventer therapy using inhaled steroids (treatment step 2) (BTS/SIGN, 2008 (revised 2012)). Due to safety concerns regarding the use of LABAs, including the increased risk of severe exacerbations and even death, the FDA now recommends that LABAs should only be used in conjunction with a steroid and never alone in the treatment of asthma

(FDA, 2010). In COPD, LABAs are indicated as maintenance therapy in patients remaining symptomatic whilst using short acting bronchodilators, either alone or in combination with an inhaled steroid and depending on patient force expiratory volume (FEV_1) (NICE, 2010).

1.6.2 FLUTICASONE PROPIONATE

1.6.2.1 PHARMACOLOGICAL AND PHYSICOCHEMICAL PROPERTIES

Fluticasone propionate (FP) is a synthetic corticosteroid having the chemical structure shown in Figure 1.2, that was developed to obtain a more potent corticosteroid that exhibited improved airway selectivity (Johnson, 1998; Kim et al., 2009). FP is used both intra-nasally and via the inhaled route as a topical anti-inflammatory agent (Shaw et al., 1994; Kim et al., 2009).

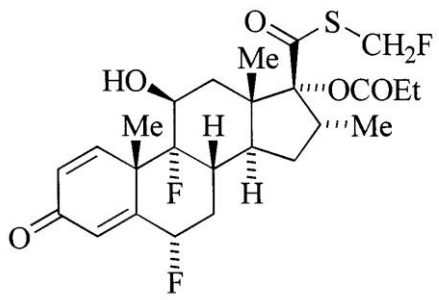

Figure 1.2 Chemical structure of fluticasone propionate (FP) taken from Michael et al. (2000).

FP is a potent agonist at the cytosolic glucocorticoid receptor (GR) and has little activity at the progesterone receptor (Shaw et al., 1994). FP is highly selective for the GR and has a long duration of action, with a half-life greater than 10 h (Shaw et al., 1994; Johnson, 1998). Following binding, the corticosteroid-GR complex is internalised into the nucleus of the cell where it binds to DNA sequences, altering the mRNA for the production of anti-inflammatory cytokines, mediators and proteins in order to elicit its anti-inflammatory effect (Shaw et al., 1994). FP has low oral bioavailability, and undergoes efficient hepatic first pass metabolism to the inactive 17β-carboxylic acid derivative, which is rapidly excreted from the body (Harding, 1990; Shaw et al., 1994).

FP has the physical appearance of a white powder, and is extremely lipophilic, being 3 and 300 times more lipophilic than beclomethasone dipropionate and budesonide,

respectively (Johnson, 1998). As a result, FP is practically insoluble in water, but has varying solubility in dimethyl sulfoxide, dimethylformamide, methanol and 95 % ethanol (Shaw et al., 1994; Kim et al., 2009). When inhaled, this degree of lipophilicity limits the dissolution of FP in the lung lining fluids, slows release from the lung lipid compartment, and therefore prolongs the retention time in the lungs (Shaw et al., 1994; Johnson, 1998).

1.6.2.2 ROLE IN ASTHMA AND COPD TREATMENT

Inhaled steroids, such as FP, are indicated for asthma patients not adequately controlled with short acting bronchodilators (treatment step 1), and are considered if the patient uses their inhaled β_2 agonists more than three times a week, are symptomatic more than three times a week, wake one night a week and/or have experienced exacerbations within the last two years (BTS/SIGN, 2008 (revised 2012)). In COPD, inhaled steroids are added to treatment as maintenance therapy in combination with a LABA, for patients in which symptoms persist with short acting bronchodilators and having an FEV_1 less than 50 % predicted (NICE, 2010).

1.6.3 RATIONALE FOR COMBINATION THERAPY

Many patients with asthma and COPD require the concurrent administration of an anti-inflammatory agent and bronchodilator. Combination inhalers containing both drugs in a single formulation are therefore more convenient and simpler to use (NICE, 2010). Adherence may be improved due to the simplification of complicated medication regimens, thus encouraging the refill persistence of the SX and FP combination inhaler compared to separate inhalers. There is also greater chance of the patient inhaling both drugs (Stoloff et al., 2004; Stempel et al., 2005).

1.6.3.1 PHARMACOLOGICAL RATIONALE

When more than one drug is administered simultaneously there is the potential for additive, complementary and/or synergistic effects between the drugs which may improve the clinical outcome (Johnson, 2004). Synergy between SX and FP has been suggested at the cellular level, however, this remains controversial. Various mechanisms have been proposed. At the receptor level, LABAs may 'prime' GR receptors such that they are more sensitive to activation (Johnson, 2004; Caramori et al.,

2006) and increase translocation of the GR receptor into the nucleus and increase DNA binding (Johnson, 2004; Akabane et al., 2006), whereas the corticosteroid may reduce the down-regulation of β_2 receptors which can occur with long term treatment (Caramori et al., 2006). A reduction in the release of inflammatory mediators has also been suggested (e.g. Pang and Knox, 2000; Akabane et al., 2006). It has been suggested that both drugs should be present on the same airway target cell, at adequate concentrations, and simultaneously, in order to aid in a pharmacologically synergistic effect, and that the likelihood of this occurring may be increased by combination inhalers (Theophilus et al., 2006).

1.6.3.2 EVIDENCE FOR PHYSICOCHEMICAL INTERACTIONS

By formulating two drugs in a single product, there is the potential for physicochemical interactions between the particles, and this may result in altered drug dispersibility and deposition in the lungs. Physicochemical interactions between SX and FP have been reported in solution and suspension (CFC and HFA) environments. The altered behaviour of SX and FP in combination was suggested to arise from heterofloc formation in which the drug components had interacted, and was found to be dependent on the chemical and physical properties of the drugs, as well as the solvent environment (Michael et al., 2000; Michael et al., 2001). In such systems, SX and FP may be inextricably bound, potentially being chemical in nature, however, further studies are required to confirm this (Michael et al., 2001; Rogueda et al., 2011). Association between SX and FP has also been identified following co-delivery using the Raman microscope for pMDI formulations (Theophilus et al., 2006; Rogueda et al., 2011) in which greater co-association was identified for the combination product (Theophilus et al., 2006). These interactions in pMDIs have also reported implications for the deposition of both drugs to pMDI canister walls (Michael et al., 2000). However, combination delivery has been shown to produce no change in the FPF of FP compared to single-drug pMDI delivery (Hoe et al., 2009).

DPI systems differ from pMDIs in that they lack a solvent in the formulation, therefore the mechanism for any altered dispersibility/deposition is likely to be different. A second fine drug particle may function as a performance modifying agent or fine, and will depend on the interactive affinities between SX and FP particles as well as with any excipients in the formulation. When measured using the atomic force microscope

(AFM), SX-SX cohesive forces were found to be stronger than SX-lactose adhesive forces, whereas the converse trend was true for FP in terms of its adhesivity with lactose. Overall, SX-FP interactions were found to be the strongest of all the interactions (Young, 2004a). The physicochemical properties of the drugs (Kubavat et al., 2012) including heterogeneity in properties (Das et al., 2012), as well as the storage/processing history (Das et al., 2009b), will also influence the magnitude and distribution of the interactive forces adding a further level of complexity in studying particulate interactions, especially in combination formulations.

Following assessment of the aerodynamic deposition performance of commercial single-active and combination DPI formulations, differences between single and co-delivery was observed for SX and FP (Taki et al., 2011). Regardless of the inhaler device used, combination delivery generated comparable MMADs but lower and higher FPFs for SX and FP, respectively, compared to single delivery. There were also significant differences between the mass deposited across the stages, in which combination delivery resulted in a lower total fine particle dose (FPD) in the deeper stages of the Next Generation Impactor (NGI), i.e. at and beyond stage 4 (Taki et al., 2011). This suggests altered dispersibility/deposition when formulated in combination, however, it is not only the presence of the second drug that may be important but also the physicochemical properties of the drug particle. For example, changes in the FPF of FP and SX varied depending on the mechanical properties and interfacial chemistry of the FP particles (Kubavat et al., 2012). As physicochemical properties affect the interactive inter-particulate forces between particles, it is important to take these into consideration when studying the formulation performance of combination DPI products. Associations between SX and FP that are suggested to occur in combination formulations are thought to play a role in the improved patient outcomes from combination delivery, as a result of increasing the chances of the proposed pharmacological requirement of simultaneous deposition of both drugs on the same site in the airways for a potential synergistic effect (Theophilus et al., 2006). Combination delivery may however alter the dispersion of one or both drugs from the formulation, leading to optimised deposition profiles in the lungs. It may therefore be these effects, rather than the co-association and ‘co-deposition’ of the particles in the airways that promote improved outcomes and long term management of the disease by combination delivery.

1.7 OVERALL AIM OF THE THESIS

The overall aim of this thesis is to study the factors affecting drug particle interactions, the de-agglomeration of particles and deposition from dry powder systems at a particulate level and in formulations with a view to attempting to understand some of the factors affecting aerosolisation performance. This will enable drug co-delivery from combination formulations to be studied systematically in order to gain insight into the influence of inter-particulate interactions on fine particle delivery to the lungs.

The objectives of this thesis are to:

1. Develop a dry dispersion laser diffraction analysis method to characterise powder de-agglomeration.
2. Determine the influence of particle interactions on drug dispersibility in fine particle blends.
3. Characterise the physicochemical properties of aerodynamically size-fractionated and re-crystallised drug particles, and the influence on particle agglomeration and aerosolisation.
4. Trace the potential dispersion modifying effects and co-association of drug particles in co-formulated pre-blends and DPI formulations.
5. Determine the ability to engineer drug aerosolisation and dissolution upon co-formulation based on drug particle and agglomeration properties.

2 CHARACTERISATION OF THE INHERENT DISPERSIBILITY OF RESPIRABLE POWDERS USING DRY DISPERSION LASER DIFFRACTION AND A PRESSURE TITRATION APPROACH

2.1 INTRODUCTION

Achieving drug deposition within the respiratory tract is dependent foremost on attaining an appropriate particle size during aerosol delivery. It is generally accepted that an aerodynamic size of 3 – 5 μm is required in order for particles to reach the central airways and peripheral regions of the lung (Shekunov et al., 2003). The intrinsic cohesivity of such fine and often irregularly shaped particles means that there is a tendency for agglomeration to occur (Adi et al., 2011). The interactive cohesive forces involved in the agglomeration of drug particles include van der Waals, electrostatic, capillary and frictional forces, and mechanical interlocking (Louey et al., 2006). The magnitude and type of such interactive forces is further dependent on particle properties (Podczeck et al., 1994) including intrinsic physicochemical properties, particle size, shape, morphology and surface area (Telko and Hickey, 2005). Heterogeneity in particle properties can lead to mixed populations of agglomerates with different dispersion behaviours (Behara et al., 2011b) thus rendering the situation highly complex.

During delivery it is essential that attractive interparticulate forces are overcome in order to restore drug particles to their primary de-agglomerated state. In passive DPIs, detachment forces arise from the turbulent airflow generated as a patient inhales through the inhaler device. The efficiency of de-agglomeration is therefore dependent on the patient's inhalation profile and device characteristics such as geometry and resistance, as these factors determine the level of turbulence, shear and impaction events that the powder is subjected to (Louey et al., 2006; Islam and Cleary, 2012). The inherent dispersibility of the powder is also important (Louey et al., 2006). The balance of cohesive and adhesive forces between drug and carrier particles can dictate the ease with which de-agglomeration occurs; an excess of either may prevent de-agglomeration resulting in poor aerosolisation and increased deposition in the upper airways (Begat et al., 2004b). DPI efficiency is generally very low, with drug dispersion from commercial devices and formulations varying from 12 – 40 % of the load dose. This is also complicated by variability between the delivered dose between uses (i.e. intra-patient) and between patients (i.e. inter-patient) (Islam and Cleary, 2012). It is therefore clear that there is a need to improve DPI performance, with knowledge of the dispersibility of powders being an important factor for consideration.

A number of approaches are available to study powder dispersibility/de-agglomeration, each of which has advantages and limitations (Table 2.1). Dry dispersion laser diffraction is more frequently being adopted and provides a fast, reproducible approach to characterising inhalation aerosols, allowing automated data recording and processing (De Boer et al., 2002a; Marriott et al., 2006). As well as being easy to use, the absence of liquids and high optical contrast between sample particles and the gas phase make the technique ideal in the study of dry powders (Calvert et al., 2009). A drawback of laser diffraction is that an assumption is made that particles are spherical; however, the difference in the measured size may not be critical, demonstrated by De Boer et al. (2002b) where a difference of only 3 % was observed between the calculated laser diffraction diameter and equivalent volume diameter of wedge shaped lactose monohydrate particles. Laser diffraction may therefore provide a useful tool in characterising DPI formulations under well-controlled conditions, allowing powder de-agglomeration efficiency to be assessed as a function of air flow rate, inhaler design or formulation (De Boer et al., 2002a).

Laser diffraction systems used by researchers to study de-agglomeration have included the Malvern Spraytec (Adi et al., 2006, Adi et al., 2008a), Malvern Mastersizer 2000 (Das et al., 2009a) and Sympatec HELOS (Shekunov et al., 2003). The particle size distributions (PSDs) generated under controlled dispersing conditions have been used to provide a qualitative indication of de-agglomeration where the numbers of modes and their location have been used to describe the composition of powders at differing stages of de-agglomeration. These findings were developed further by Behara et al. (2011b), where the Malvern Spraytec was used to quantitatively characterise the de-agglomeration of cohesive pharmaceutical powders and a number of de-agglomeration parameters were derived. However, although these studies provided useful information regarding the de-agglomeration characteristics of the samples, the powders were filled into gelatine capsules and aerosolised from a Rotahaler resulting in both device and capsule-specific effects contributing to the dispersion of the powders. It therefore remains desirable to develop methods to assess the fundamental de-agglomeration properties of dry powders which are not influenced by device/capsule characteristics.

Sympatec GmbH (Clausthal-Zellerfeld, Germany) have developed and produced an in-line Helium Neon Laser Optical System (HELOS) laser diffractometer for particle size analysis. This instrument has been used alongside the dry dispersion RODOS unit by a

number of researchers to analyse the dispersibility of pharmaceutical powders (Shekunov et al., 2003; Kaye et al., 2009; Ghoroi et al., 2013). The RODOS unit disperses particles using pressurised air that accelerates particles once they reach a dispersing line. Control over dispersing conditions can be achieved by varying the pressure of the air feed to the unit from 0.1 – 6 Bar with the potential to disperse particles down to 0.1 μm (Calvert et al., 2009). The dosing method is selected based on the sample; the vibratory feeder is used for large, free flowing samples requiring quantities of material in the order of magnitude of grams. However, for smaller sample sizes consisting of fine cohesive particles as is the case for inhaled powders, the ASPIROS or rotary feeder are more appropriate. The evaluation of particle size as a function of dispersion pressure in a system such as Sympatec HELOS/RODOS is generally accepted to provide a semi-quantitative assessment of the degree of agglomeration/de-agglomeration (Ghoroi et al., 2013). The gradient of the D_{v90}, for example, over a dispersion pressure range can be used to assess the extent of dispersibility, where shallower gradients would imply better dispersibility (Shekunov et al., 2003; Kaye et al., 2009). It was therefore proposed that the Sympatec HELOS/RODOS could form the basis of a quantitative tool to analyse the de-agglomeration of inhalation powders.

Table 2.1 A summary of current methods used to study powder de-agglomeration and the associated advantages and limitations of each technique.

Technique	**Output**	**Advantages**	**Limitations**	**References**
Atomic force microscopy (AFM)	Interactive force Cohesive-adhesive balance ratio	1. Direct force measurement of colloid size particles	1. Time consuming and labour intensive sample preparation 2. Small number of particles 3. Unknown particle orientation 4. Measures only a single interaction 5. Contact area/nature unknown 6. Requires highly crystalline substrates of controlled geometry	Begat et al. (2004a); Tsukada et al. (2004); Bunker et al. (2005); Jones et al. (2008b)
Inverse gas chromatography (IGC)	Surface energy arising from dispersive and specific interactions	1. Derivation of cohesive and adhesive forces from the surface energy 2. Uses bulk powder rather than individual powder particles	1. Large sample quantity 2. Long analysis time 3. Different probes/data analysis approaches limit data comparison between research groups 4. Infinite dilution unable to reveal surface heterogeneity	Das et al. (2011a); Jones et al. (2012)
Centrifugation	Interactive force	1. Direct measurement of autoadhesion (i.e. cohesive) forces 2. Uses larger numbers of particles than AFM	1. Specialist equipment 2. Long experimental time 3. Contact surface (e.g. roughness) needs to be quantified 4. Centrifugal and adhesion force is sensitive to small variations in particle size	Podczeck et al. (1994); Nguyen et al. (2010)

Table 2.1 A summary of current methods used to study powder de-agglomeration and the associated advantages and limitations of each technique (continued).

Technique	Output	Advantages	Limitations	References
Time of flight aerosol beam spectrometry e.g. Aerosizer	Particle size following the application of a known level of shear and de-agglomeration	1. Aerodynamic particle size (range 0.2 – 700 µm) 2. Sample delivery via a dry dispersion unit or inhaler cell attachment	1. Particle detection on a one at a time basis 2. Measurement discrepancies at high particle densities 3. Assumes spherical particles 4. Cannot distinguish between particles e.g. drug and excipient	Holzner and Müller (1997); Begat et al. (2004b); Adi et al. (2006); Das et al. (2011b)
Dry dispersion laser diffraction 1. Malvern Spraytec 2. Malvern Mastersizer 3. Sympatec HELOS/RODOS	Particle size following controlled dispersion conditions of: Airflow rate Shear Pressure	1. Rapid 2. Reproducible 3. Sample delivery via a dry dispersion unit or inhaler cell attachment 4. Controlled dispersion conditions	1. Not an aerodynamic particle size 2. Scirocco feeder (for Malvern Mastersizer) vibrates powder prior to dispersion 3. Inhaler dosing attachments (Malvern Spraytec/Sympatec) limit determination of fundamental dispersibility 4. Limited approaches to quantify dispersion	Shekunov et al. (2003); Adi et al. (2006); Marriott et al. (2006); Adi et al. (2008a); Behara et al. (2011b)
Specific de-agglomeration apparatus e.g. de-agglomeration rigs, standard entrainment tubes	Outcome dependent on the apparatus/experimental set-up	1. Precise control and characterisation of airflow conditions 2. Can be used in conjunction with established methods e.g. cascade impactors	1. Specialist equipment therefore difficult to reproduce between research labs 2. Complex designs 3. Also requires lengthy impactor analysis	Voss and Finlay (2002); Louey et al. (2006); Kurkela et al. (2008)
Impactors and impingers	Fine particle fraction, mass median aerodynamic diameter, emitted dose	1. Widely accepted ‘gold standard’ for product development and quality control	1. Laborious and time consuming 2. Classifies particles into a small number of class sizes	Marriott et al. (2006)

2.2 AIM AND OBJECTIVES

The aim of this study was to develop a laser diffraction technique to quantify powder de-agglomeration through studying powder dispersion in the dry state. The specific objectives were to:

a) Establish the geometric primary particle size of beclometasone dipropionate (BDP), budesonide (Bud), fluticasone propionate (FP), lactose monohydrate (Lactohale 300, LH300), PF-00613322 (PF), salbutamol base (SB), salmeterol xinafoate (SX) and tofimilast (Tof) powders when fully dispersed in a liquid medium.

b) Generate geometric size measurements for each powder using dry dispersion laser diffraction under different dispersion conditions, achieved by varying the dispersing pressure used to aerosolise the powder.

c) Analyse the particle size of each powder as a function of the primary pressure (PP) imposed during the dry dispersion laser diffraction sizing method with a view to generating relevant parameter(s) to describe the resultant de-agglomeration profile.

d) Compare the de-agglomeration parameter(s) with the cohesivity of each powder, derived from surface energy measured using inverse gas chromatography (IGC) at infinite dilution.

2.3 MATERIALS

The materials and equipment used in this chapter are summarised in Table 2.2.

Table 2.2 Suppliers of materials and equipment (Chapter 2).

Material / Equipment	**Supplier**
Beclometasone dipropionate (BDP; BN. WC60329)	Pharm Dev Europe, GWRD, UK
Budsonide (Bud; BN. U0015/1V040)	LGM Pharma, USA
Tofimilast (Tof; BN. CP-325366)	Pfizer Ltd, PGRD Sandwich Laboratories, UK
Fluticasone propionate (FP; BN. 458763)	LGM Pharma, USA
PF-00613322 (PF; BN. PF-00613322)	Pfizer Ltd, PGRD Sandwich Laboratories, UK
Lactohale 300 (LH300; BN. 6125224/S)	Frieslands Foods, Domo, The Netherlands
Salbutamol base (SB; BN. WC46269)	Pharm Dev Europe, GWRD, UK
Salmeterol xinafoate (SX; BN. SX-0081010)	Vamsi Labs, India
Cyclohexane (BN. 10D120503)	VWR international Ltd, UK
Methanol (HPLC Grade)	Sigma Aldrich Ltd, UK
Hexane	Fisher Scientific, UK
Sorbitan monooleate 80 (Span 80)	Sigma Aldrich Ltd, UK
Sorbitan monooleate 85 (Span 85)	Merck, Germany
Tween 80	Merck, Germany
Malvern Mastersizer X	Malvern Instruments Ltd, UK
Ultrasonic water bath	Sonorex, Bandelin Electronic, Germany
Cellulose acetate syringe filters (pore size 0.2 µm)	Gema Medical S.L., Spain
Aluminium pin stubs (0.5 inches) and double-sided adhesive carbon tabs	Agar Scientific Ltd, England
K550X sputter coater	Emitech, Quorum Technologies Limited, England
Quanta 200F field emission scanning electron microscope	FEI UK Ltd, England
Sympatec HELOS BF and RODOS dispersing unit	Sympatec GmbH, Clausthal-Zellerfeld, Germany
SMS Inverse Gas Chromatograph (Serial No. 031112-01) and silanised glass columns	Surface Measurement Systems Ltd, UK

2.4 METHODS

2.4.1 PARTICLE SIZE ANALYSIS BY LIQUID DISPERSION LASER DIFFRACTION

Laser diffraction particle sizing was carried out using the Malvern Mastersizer X fitted with a 100 mm focal length lens (0.5 – 180 µm) and an MS7 magnetically stirred cell. Dispersant was prepared by saturating an appropriate solvent (containing surfactant to aid dispersion) with sample and sonicating in an ultrasonic water bath for 30 min. The dispersant was visually checked for saturation and stirred overnight using a magnetic flea. Prior to sizing, the laser was switched on for 30 min. The sample cell was cleaned with methanol, allowed to air dry and filled with dispersant filtered through a 0.2 µm cellulose acetate syringe filter. Approximately 1 mg of powder was added to 2 mL filtered dispersant in a 7 mL glass vial and sonicated (Sonicleaner, DAWE, Ultrasonics Ltd, USA) for the required time. The presentation was selected, laser aligned and a background reading taken. The suspension was added drop wise to the sample cell until the obscuration was within range (~ 10 – 30 %) with the appropriate stirrer speed setting. The sample was allowed to equilibrate in the cell for 30 – 60 s prior to initiating the sizing sequence. Ten individual measurements were taken for n = 3 samples to obtain particle size measurements calculated using Fraunhofer theory. The D_{v10}, D_{v50} and D_{v90} which correspond to the particle size below which 10 %, 50 % and 90 % of the particles by volume are smaller than and the $D_{4,3}$ were recorded. The $D_{4,3}$ or volume mean diameter (VMD), is the volume weighted mean particle size of the sample and is sometimes referred to as the volume moment mean diameter, as it represents the central point of the frequency in terms of volume from which the distribution would rotate, Equation 2.1, where d is particle diameter (Rawle, 1993). The mean values of each parameter were averaged to obtain the final particle size result. A summary of the dispersant, sonication time, stir setting, sweeps, and equilibration time used to size each powder are summarised in Table 2.3. For PF and Tof, the sizing parameters were validated according to ISO 13320-1 (1990) (data not shown).

Equation 2.1 $$d_{4,3} = \frac{\sum d^4}{\sum d^3}$$

Table 2.3 A summary of the liquid dispersion laser diffraction parameters used to size beclometasone dipropionate (BDP), budesonide (Bud), fluticasone propionate (FP), lactohale 300 (LH300), PF-00613322 (PF), salbutamol base (SB), salmeterol xinafoate (SX) and tofimilast (Tof).

Powder	**Dispersant (% w/v)**	**Sonication time (min)[1]**	**Stir Setting[2]**	**Sweeps[3]**	**Equilibration time (s)[4]**
BDP[a]	1 % Span 80 in cyclohexane[a]	5[a]	3	3500	60
Bud[b]	0.1 % Span 80 in cyclohexane[b]	15[b]	3	3500[b]	60
FP[c]	0.1 % Span 80 in cyclohexane[c]	2.5[c]	3[c]	3500[c]	60[c]
LH300[d]	0.1 % Span 80 in cyclohexane[d]	1[d]	3[d]	3500[d]	30[d]
PF	0.1 % Span 80 in cyclohexane	1	5	2500	60
SB	1.0 % Span 85 in hexane	1	3	3500	30
SX[c]	0.5 % Span 80 in cyclohexane[c]	5[c]	3[c]	2500[c]	60[c]
Tof	0.05 % Tween 80 in 5 % v/v methanol in water	5	5	2500	60

[1]Sonication time required to ensure dispersion of powder particles in the dispersant prior to the size measurement. [2]Setting corresponding to the speed of rotation of a magnetic flea in the bottom of the measurement cell. [3]Measurement sweeps corresponding to the measurement time in s, where 2500 sweeps is equivalent to 5 s and 3500 sweeps equivalent to 7.5 s. [4]Sample equilibration time within the cell prior to the size measurement. [a]Zeng et al. (2000), [b]Buttini et al. (2008), [c] Murnane (2007), [d]Tang (2008).

2.4.2 SCANNING ELECTRON MICROSCOPY

Aluminium pin stubs were cleaned with acetone, labelled and a double-sided adhesive carbon tab mounted onto each. Circular coverslips (10 mm diameter) were cut roughly in half using a diamond cutter and compressed air used to remove any glass particles. The coverslip was placed onto the carbon tab in order to cover approximately half of the stub. A small spatula was loaded with powder (5 – 10 mg) and held above the stub. The spatula was gently tapped so that the powder fell onto the stub; excess powder was removed by tilting and gently tapping to ensure an even coverage of powder over the stub surface. The samples were sputter coated with gold (approx. 15 – 20 nm) for 2 min

using a K550X sputter coater. The samples were viewed, using the glass mounted half of the stub where possible, using a Quanta 200F field emission scanning electron microscope operated at 10 kV in low vacuum mode and using a working distance of approximately 10 mm. Images were taken at a high and low magnification using the highest possible resolution (3584 x 3094).

2.4.3 DRY DISPERSION LASER DIFFRACTION METHOD DEVELOPMENT

Method development was carried out using the Sympatec HELOS and RODOS dispersing unit, using SX as a model powder, in order to ensure selection of the optimal experimental parameters for determining particle size as a function of primary pressure (PP) using the rotary feeder.

2.4.3.1 CHOICE OF LENS, TRIGGER CONDITIONS, MEASUREMENT TIME AND TIMEBASE

The choice of lens, trigger conditions, measurement time and timebase were investigated. The lenses available were the R3 and R5 lens which are employed to determine particles within a size range of 0.9 – 175 µm and 4.5 - 875 µm, respectively. Particle size measurements (n = 1) were carried out for SX at 0.5 and 4.0 Bar PP using both lenses. The trigger conditions refer to the optical concentration of powder (C_{opt}, %) detected on the detector channels in order to initiate (start C_{opt}) and end (end C_{opt}) a particle size measurement. The start C_{opt} was investigated in the range 0.1 – 5 % and the end C_{opt} in the range 0.1 – 2 % for SX particle size measurements (n = 1) taken at 2.0 Bar PP. The detector channel on which the C_{opt} was detected was also investigated in the Channel range 10 – 31, corresponding to trigger sizes of 3.99 to 160.39 µm. The measurement time i.e. the duration of time that particle size data is collected whilst the C_{opt} was within the trigger condition range was investigated, within the time range of 1 – 20 s for SX particle size measurements (n = 1) taken at 2.0 Bar PP. The timebase was investigated in the range 0.001 – 0.500 s, representing the frequency at which the software collects data during a measurement, for SX measurements taken at 0.3 Bar PP.

2.4.4 PARTICLE SIZE-PRIMARY PRESSURE PROFILES

Pressure titration curves were generated using the Sympatec HELOS/RODOS using the rotary feeder with protruding aspiration tube (Figure 2.1). Powder sample was hand-filled into the u-shaped groove of a rotating table to cover a length of approximately 1 cm. The sample passed under a plough scraper and roller to remove any excess and was subsequently drawn up into the dispersing line via the protruding aspiration tube from a static bed. During sample delivery the rotating table was maintained at a constant rotation setting of 20 %.

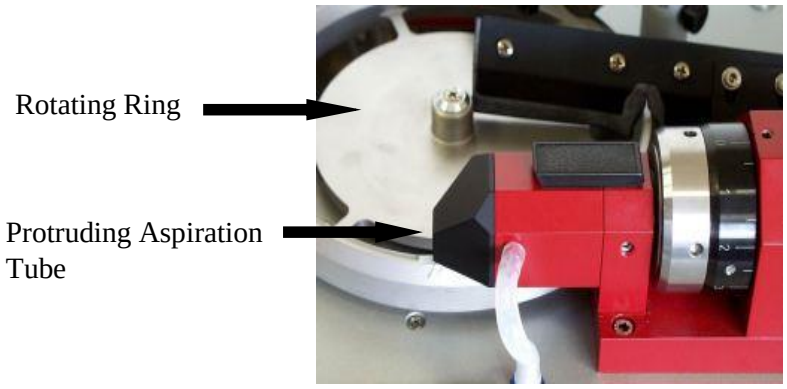

Figure 2.1 The Sympatec HELOS/RODOS rotary feeder comprising a rotating ring and protruding aspiration tube (image taken from www.sympatec.com/EN/LaserDiffraction/RODOS.html, accessed on 27.08.13).

The PP was manually set using the adjustment valve to values in the range 0.2 to 4.5 Bar. Three measurements were taken at each pressure setting using freshly loaded powder. All measurements for a single powder were generated on a single day. PSDs were calculated using Fraunhofer theory and analysed in WINDOX 4.0 software (Sympatec GmbH, Clausthal-Zellerfeld, Germany). Each measurement generated a PSD and the D_{v10}, D_{v50} and D_{v90} were measured and recorded. The volume mean diameter (VMD) was also recorded. A summary of the operational parameters used are summarised in Table 2.4.

Table 2.4 A summary of the dry dispersion laser diffraction parameters used to size the powders using the Sympatec HELOS/RODOS laser diffractometer.

Parameter	
Feeder	Rotary
Lens	R3 (0.9 – 175 µm)
Start optical concentration (C_{opt}, %)	1.1
Trigger channel	None specified
End optical concentration (C_{opt}, %)	1
Measurement time (s)	5 or 60 s real time
Time base (ms)	100
Forced stability	4

2.4.4.1 CRITICAL PRIMARY PRESSURE DERIVATION

The PP at which the particle size-primary pressure profile reached a plateau size was considered to represent the pressure required to overcome the interactive forces holding agglomerates together and therefore provide a measure of the cohesivity of the powder. The parameter was called the critical primary pressure (CPP) and derived as follows. The mean particle size (D_{v50}, D_{v90} and VMD) at each PP was calculated, followed by the difference between the mean size and the preceding mean size. A difference ratio (d_r) was calculated by expressing the mean particle size in question as a proportion of the difference between the sizes, as shown in Equation 2.2, where PP1 and PP2 are two consecutive PPs, where PP2 > PP1.

Equation 2.2 $$d_r = \frac{{D_{v50}}^{PP1} - {D_{v50}}^{PP2}}{{D_{v50}}^{PP1}}$$

If the difference ratio was within the range $-0.06 < d_r < 0.06$ for the D_{v50} and VMD, or $-0.10 < d_r < 0.10$ for the D_{v90} then the particle size was considered to be the same (ISO 13320:1990). When no difference was observed for three consecutive increases in the PP, this was taken to represent the plateau. The PP at which the particle size was first observed to be the same as that recorded at the preceding PP (i.e. difference ratio within the above range) was taken to represent the CPP.

2.4.5 NORMALISATION OF PARTICLE SIZING DATA AND DE-AGGLOMERATION ANALYSIS

The particle size data were normalised to account for differences in the primary particle size of each powder. The particle size at each PP (D_x) was expressed as a proportion of the fully dispersed particle size as shown in Equation 2.3. The fully dispersed size was represented by both the dry dispersion particle size at the highest PP employed (D_H) and the liquid dispersion size (D_L). The parameter was termed the degree of de-agglomeration (DA) and represented the extent of de-agglomeration achieved at a particular PP. When DA = 1 complete dispersion of the powder to primary particles would have occurred.

Equation 2.3 $$DA = \frac{D_H \text{ or } D_L}{D_x}$$

DA was plotted as a function of PP in order to generate de-agglomeration profiles. The de-agglomeration data exhibited rectangular hyperbolas therefore equations describing the same trend were selected with a view to empirically modelling the data. These were the Langmuir (Equation 2.4), Frendlich (Equation 2.5) and Michaelis Menten (Equation 2.6) equations where DA is the degree of de-agglomeration, DA_{max} is the asymptote degree of de-agglomeration and PP is the primary pressure. K_L is the Langmuir adsorption/equilibrium constant and K_F is a measure of adsorptive capacity. The term 1/n in the Freundlich equation is a measure of the intensity of adsorption. The DA_{50} in the modified Michaelis Menten equation (Equation 2.6) represents the PP required to achieve 50 % de-agglomeration and is derived from the intercept and slope of the trendline fitted to the linearised data.

Equation 2.4 Langmuir Equation: $$DA = \frac{DA_{max} \cdot K_L \cdot PP}{1 + K_l \cdot PP}$$

Equation 2.5 Freundlich Equation: $$DA = K_F \cdot PP^{\frac{1}{n}}$$

Equation 2.6 Michaelis Menten Equation: $$DA = \frac{DA_{max} \cdot PP}{DA_{50} + PP}$$

The de-agglomeration profiles were linearised in order to undertake data fitting. For the Langmuir and Michaelis Menten equation the Hanes Woolf method was used in order to prevent bias towards data points in the low PP region (Equation 2.7 and Equation 2.8, respectively) and for the Freundlich equation this involved $\log_{10}$ transformation (Equation 2.9). The goodness of fit of each model to the data was deduced by comparison of the R^2 values.

Equation 2.7 $$\frac{PP}{DA} = \frac{1}{DA_{max}}.PP + \frac{1}{K_L.DA_{max}}$$

Equation 2.8 $$\frac{PP}{DA} = \frac{1}{DA_{max}}.PP + \frac{DA_{50}}{DA_{max}}$$

Equation 2.9 $$log\, DA = log\, K_F + \left(\frac{1}{n}\right) log\, PP$$

2.4.6 INVERSE GAS CHROMATOGRAPHY AT INFINITE DILUTION

A 30 cm silanised glass column with an internal diameter of 3 mm was filled with 200 – 300 mg of sample and sealed at each end with silanised glass wool. Columns were packed by placing a small funnel in the top of the column, transferring sample into the funnel and gently tapping and rotating the column. Samples were analysed using an SMS Inverse Gas Chromatograph. The columns were conditioned under dry nitrogen for 12 h at 0 % relative humidity (RH), total flow of 10 standard cubic centimetres per min (sccm) and eluent temperature of 303 K. A flame ionisation detector (FID) was used with a data saving interval of 2 s. Infinite dilution analysis was conducted using fixed probe volume injections at a partial pressure of 0.03 p/p_o, where p is the partial pressure of the vapour and p_o is the saturation pressure of the liquid (Newell and Buckton, 2004). The probe and column temperature were set at 303 K, and analysis was conducted at 0 % RH using a total flow of 10 sccm and nitrogen as the carrier gas. The non-polar probes employed were nonane, octane, heptane and hexane with run times of 40, 20, 10 and 10 min, respectively. The polar probes were acetone, acetonitrile and ethanol and were injected with a run time of 20 min each. The dead time was calculated using methane. A single column was analysed in triplicate using each probe with a 60 min delay between each analysis in order to allow the column to be purged of residual solvent between replicates.

2.5 RESULTS

2.5.1 SCANNING ELECTRON MICROSCOPY

SEM imaging revealed differences in the morphology of the powders (Figure 2.2 and Figure 2.3). All the powders were agglomerated and displayed a range of agglomerate sizes. Upon visual assessment, the agglomerates of all the powders appeared to be densely packed. The agglomerates were also observed to be in association with each other, suggesting that inter-agglomerate interactions occurred leading to the formation of larger agglomerated structures within the powder. Considering particle morphology, all the powders showed a variety of irregular particle shapes. Overall the particles of each powder appeared flat/plate-like and SB had the smallest particle size. Tof and SX had smooth particle surfaces whereas the remaining powders seemed to have rougher surfaces. There was little uniformity in particle morphology within and between powders.

2.5.2 DRY DISPERSION LASER DIFFRACTION METHOD DEVELOPMENT

The particle size of the powders was generally within the low micron size range, therefore the R3 lens (0.9 – 175 µm) was considered more suitable than the R5 lens (4.5 – 875 µm). Nevertheless, it was important to determine whether larger agglomerates were present. Measurements were taken at low and high PPs using both lenses for confirmation (Figure 2.4). Use of the R5 led to a loss in part of the PSD at the fine particle size range for SX at both PPs. Furthermore, the lowest limit of the R5 lens (4.5 µm) was larger than the D_{v50} of all the powders (Table 2.5). For these reasons, the R3 lens was selected for use in the study.

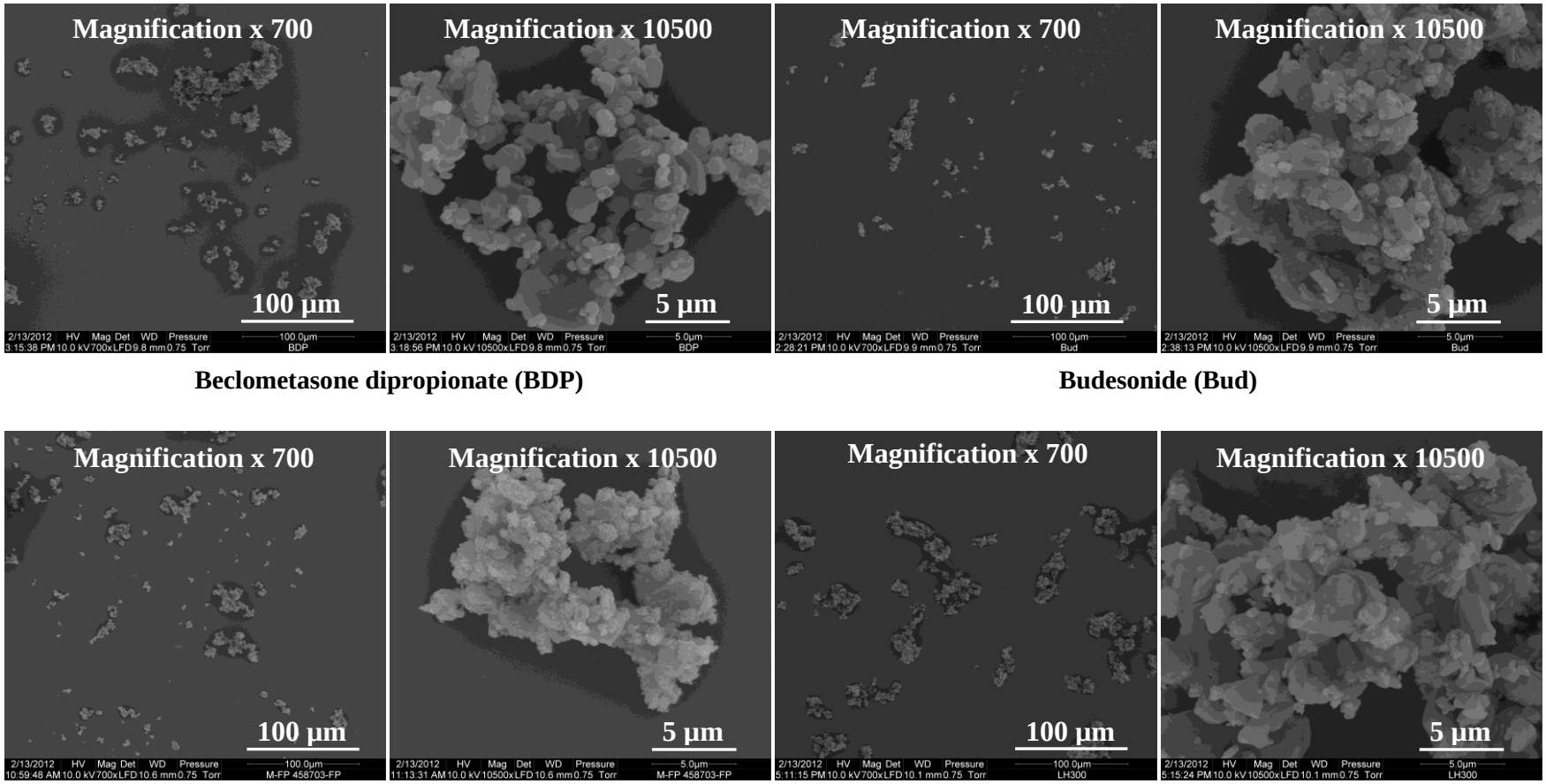

Figure 2.2 Morphology of beclometasone dipropionate (BDP), budesonide (Bud), fluticasone propionate (FP) and lactohale 300 (LH300) imaged by scanning electron microscopy at x 700 and x 10500 magnification.

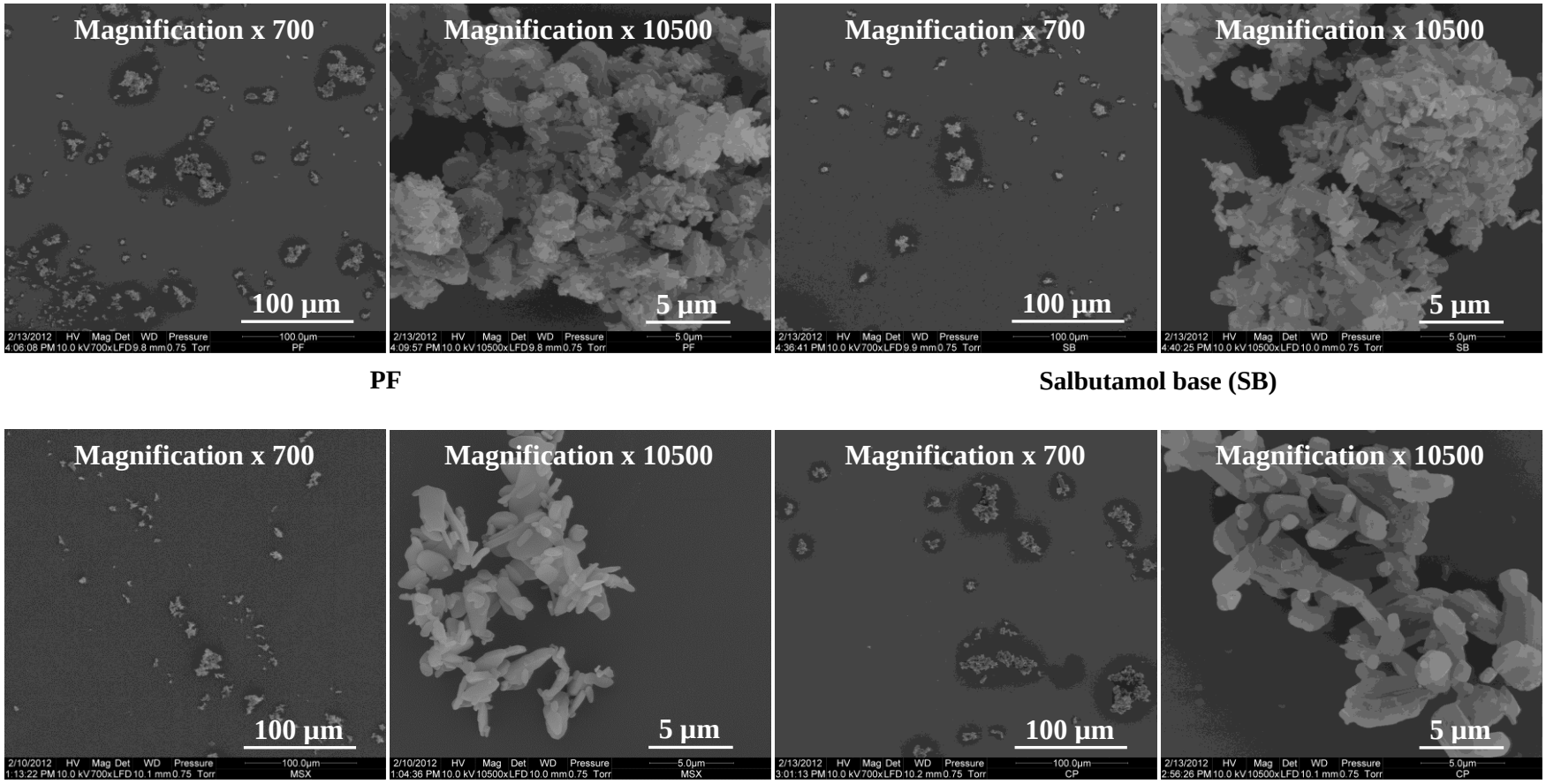

Figure 2.3 Morphology of PF, salbutamol base (SB), salmeterol xinafoate (SX) and tofimilast (Tof) imaged by scanning electron microscopy at x 700 and x 10500 magnification.

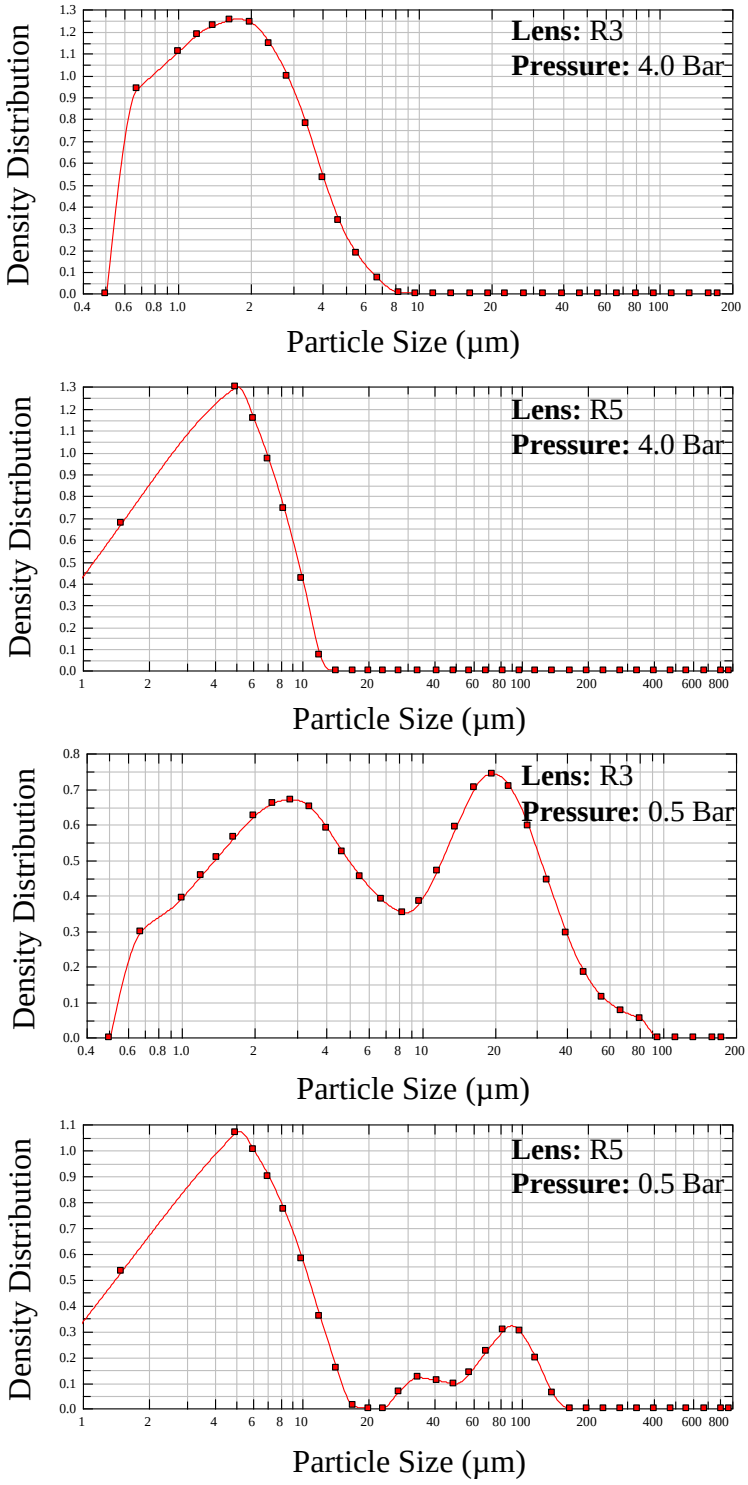

Figure 2.4 The particle size distribution of salmeterol xinafoate (SX) sized by Sympatec HELOS/RODOS laser diffraction (using the rotary feeder) at 4.0 Bar and 0.5 Bar primary pressure using the R3 (0.9 – 175 µm) and R5 (4.5 – 875 µm) lens (*n* = 1 measurement shown).

The trigger conditions were found to have little effect on the particle size data. Altering the start (0.1 – 5 %) and end (0.1 – 2 %) C_{opt} and measurement time (1 – 20 s) had no effect on the D_{v10} ($p > 0.05$), D_{v50} ($p > 0.05$) and D_{v90} ($p > 0.05$) values of SX (one-way ANOVA with post-hoc Tukey's test, GraphPad Prism 5), when sized at 2.0 Bar PP, which was selected as an intermediate dispersal pressure (Figure 2.5). The timebase i.e. the frequency at which the software collects data during a measurement was varied in the range 0.001 – 0.500 s at 0.3 Bar pressure. At low dispersal pressures, fewer particles are likely to be present due to less efficient powder de-agglomeration. The timebase at low pressures was therefore considered to be critical, as the combination of fewer particles and a low sampling rate may have reduced the sensitivity of the measurement and led to the misinterpretation of large particles as noise. However, altering the time base had no effect on the measured particle size of SX (D_{v50} = 3.68 ± 0.17 µm, mean of n = 1 measurement taken at n = 11 different timebases). When the trigger channel was altered to cover the Channel range 10 – 31, corresponding to trigger sizes of 3.99 to 160.39 µm, there was also no change in the measured particle size of SX at 0.3 Bar pressure (D_{v50} = 3.70 ± 0.13 µm, mean of n = 1 measurements taken using n = 4 different trigger channels), where again due to the presence of larger agglomerates at the low pressures, the trigger condition was considered to be critical.

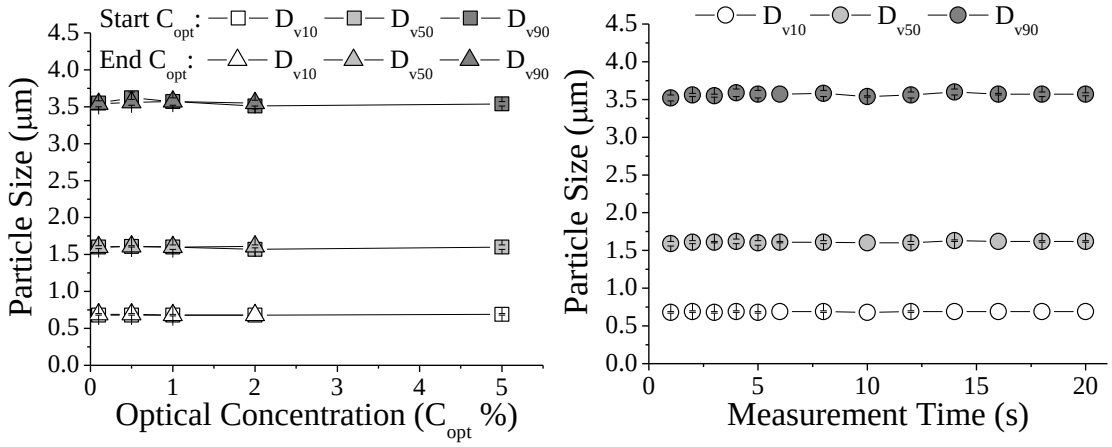

Figure 2.5 The particle size, represented by the D_{v10}, D_{v50} and D_{v90}, of salmeterol xinafoate (SX) sized by Sympatec HELOS/RODOS laser diffraction (using the rotary feeder) at 2.0 Bar primary pressure (mean ± SD, $n \geq 2$) using different trigger conditions (i.e. optical concentration (C_{opt})) to start and end a measurement, and measurement times.

While measuring the PSDs, a particle size mode was observed in some replicate measurements suggesting the presence of large particles (Figure 2.6). This was confirmed to be a measurement artefact as there was a lack of particles/agglomerates greater than 100 µm when viewed by SEM (Figure 2.2 and Figure 2.3). Forced stability was therefore incorporated into the method in order to eliminate this peak from calculations and to enable accurate data analysis to be conducted. The minimum number of channels was excluded from the size measurement in order to remove this peak and was found to be a forced stability of '4' corresponding to exclusion of channels measuring particles larger than ~ 100 µm.

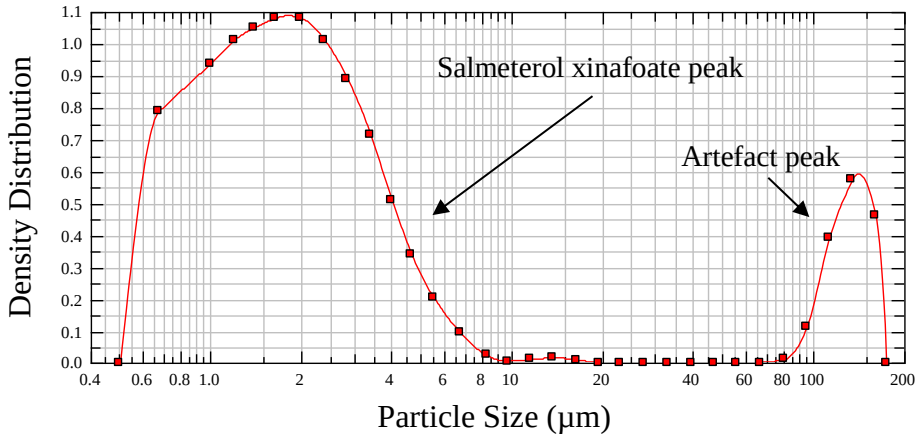

Figure 2.6 The particle size distribution of salmeterol xinafoate (SX) sized by Sympatec HELOS/RODOS laser diffraction (using the rotary feeder) at 3.0 Bar primary pressure (n = 1 measurement shown).

2.5.3 DRY DISPERSION LASER DIFFRACTION TO STUDY POWDER AGGLOMERATION STATE

2.5.3.1 VALIDATION OF PARTICLE SIZE DISTRIBUTION MEASUREMENTS BY LASER DIFFRACTION

The geometric particle size results (D_{v10}, D_{v50}, D_{v90}, and VMD) obtained using liquid and dry dispersion laser diffraction are presented in Table 2.5. All the powders were found to possess a PSD within the micron size range with D_{v50} values less than 4 µm. The liquid dispersion particle size results enabled the primary, fully dispersed particle size in a liquid medium to be determined. BDP, Bud, FP, PF, SB and SX showed significant differences between liquid and dry dispersion particle sizes whereas Tof and LH300 did not.

Table 2.5 The measured particle size (represented by the D_{v10}, D_{v50}, D_{v90} and volume mean diameter, VMD) and span of beclometasone dipropionate (BDP), budesonide (Bud), fluticasone propionate (FP), lactohale 300 (LH300), PF-00613322 (PF), salbutamol base (SB), salmeterol xinafoate (SX), and tofimilast (Tof) by dry dispersion laser diffraction (at 5.0 Bar pressure) and liquid dispersion laser diffraction (mean ± SD, $n \geq 3$).

Powder	Dispersion	D_{v10} (µm)	D_{v50} (µm)	D_{v90} (µm)	VMD (µm)	Span
BDP	Dry	0.70 ± 0.00	1.65 ± 0.00	3.50 ± 0.00	1.90 ± 0.01	1.70
	Liquid	1.20 ± 0.02	2.62 ± 0.24	4.75 ± 0.71	2.87 ± 0.32	1.36
Bud	Dry	0.70 ± 0.00	1.74 ± 0.00	4.08 ± 0.01	2.12 ± 0.00	1.94
	Liquid	1.02 ± 0.02	2.17 ± 0.03	4.39 ± 0.03	2.49 ± 0.02	1.55
FP	Dry	0.88 ± 0.03	2.44 ± 0.12	5.75 ± 0.23	3.01 ± 0.13	1.90
	Liquid	1.25 ± 0.01	2.81 ± 0.03	5.18 ± 0.13	3.06 ± 0.05	1.40
LH300	Dry	0.91 ± 0.01	3.32 ± 0.01	8.26 ± 0.02	4.06 ± 0.01	2.22
	Liquid	1.78 ± 0.08	3.74 ± 0.41	6.57 ± 1.14	4.02 ± 0.52	1.28
PF	Dry	0.68 ± 0.00	1.59 ± 0.01	3.90 ± 0.01	2.00 ± 0.01	2.02
	Liquid	0.92 ± 0.00	2.05 ± 0.01	4.34 ± 0.04	2.43 ± 0.02	1.67
SB	Dry	0.60 ± 0.01	1.07 ± 0.01	2.17 ± 0.01	1.25 ± 0.01	1.46
	Liquid	0.78 ± 0.08	1.44 ± 0.16	2.51 ± 0.29	1.57 ± 0.17	1.19
SX	Dry	0.67 ± 0.00	1.51 ± 0.03	3.47 ± 0.03	1.84 ± 0.01	1.83
	Liquid	0.81 ± 0.01	2.05 ± 0.12	4.33 ± 0.25	2.39 ± 0.18	1.71
Tof	Dry	1.13 ± 0.02	2.78 ± 0.02	5.48 ± 0.01	3.08 ± 0.01	1.56
	Liquid	0.87 ± 0.01	2.62 ± 0.02	4.98 ± 0.06	2.81 ± 0.02	1.57

2.5.3.2 EFFECT OF PRIMARY PRESSURE ON THE PARTICLE SIZE DISTRIBUTION

Changes in the PSD were seen for all the powders when the PP was increased, and the powders became more fully dispersed. Using the rotary feeder, BDP, Bud, PF, LH300 and Tof showed a shift in the distribution towards the smaller particle size range with increasing PP, along with the appearance of a small shoulder in the curve due to very fine particles. This shoulder may arise as a result of particle fracture occurring at high pressures leading to the production of fine particles. SB conversely showed no shift and only a narrowing in the PSD. FP and SX demonstrated bimodal distributions at low PPs attributed to fine particles and agglomerate formation. Both showed a shift of the peak corresponding to the fine particle fraction towards smaller particle sizes and a tendency to eliminate agglomerates. Representative PSDs for Bud, SB and SX at 0.5, 1.0, 2.0 and 4.0 Bar generated using the rotary feeder are shown in Figure 2.7. Considering the PSDs numerically, a gradual reduction in the D_{v10}, D_{v50}, D_{v90} and VMD was observed for all the powders with increasing PP. For all the powders the particle size reduced until a

plateau size was reached, which was comparable to the particle size from liquid dispersion measurements. The pre-plateau region differed between the powders indicative of powder-specific de-agglomeration behaviour (Figure 2.8).

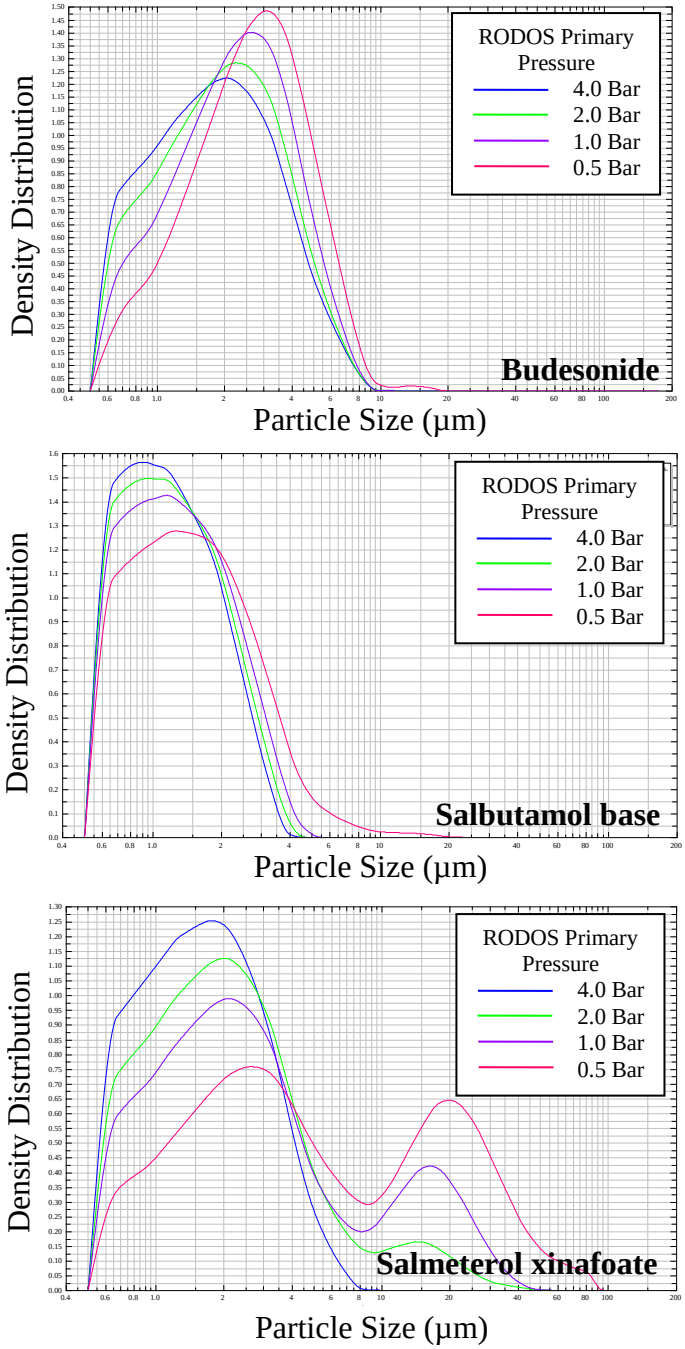

Figure 2.7 The particle size distribution of budesonide, salbutamol base and salmeterol xinafoate at 0.5, 1.0, 2.0 and 4.0 Bar primary pressure sized by Sympatec HELOS/RODOS laser diffraction (using the rotary feeder) (n = 1 measurement shown).

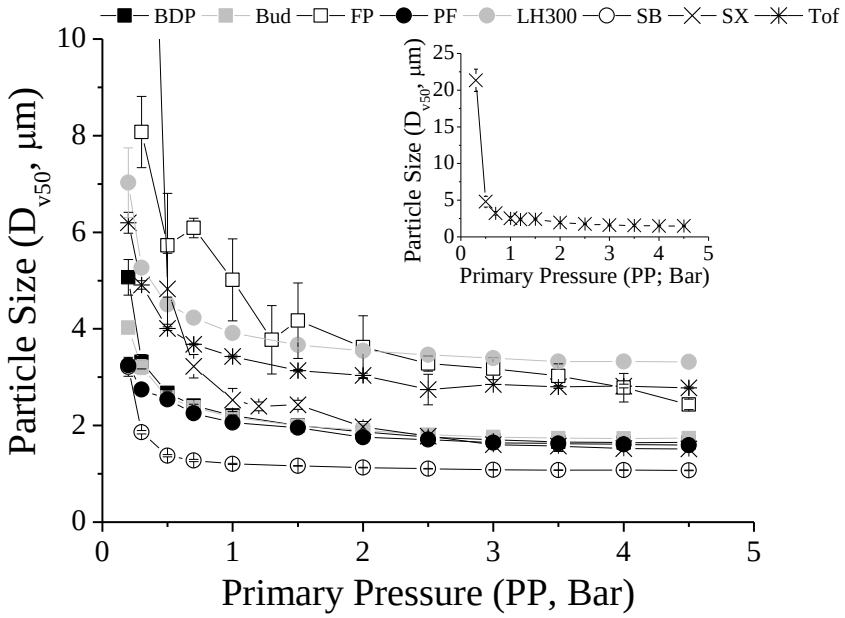

Figure 2.8 Particle size-primary pressure profiles of beclometasone dipropionate (BDP), budesonide (Bud), fluticasone propionate (FP), lactohale 300 (LH300), PF-00613322 (PF), salbutamol base (SB), salmeterol xinafoate (SX) and tofimilast (Tof) sized by Sympatec HELOS/RODOS laser diffraction (using the rotary feeder) (mean ± SD, n = 3). SX had a large D_{v50} at the lowest pressure employed; this value was omitted from the main graph but is shown in the inset graph.

2.5.3.3 CRITICAL PRIMARY PRESSURE DERIVATION

The CPP of all the powders when sized using the rotary feeder are summarised in Table 2.6. In all instances (except for BDP and LH300) the CPP determined from the D_{v50} and VMD was identical and varied from 1.0 Bar for SB to 3.5 Bar for SX, representing the least and most cohesive powders respectively. For FP, the particle size only remained consistent for two increases in the PP, 3.0 and 3.5 Bar, therefore 3.0 Bar was taken to represent the CPP. In some instances the D_{v50} and D_{v90} predicted the same CPP value; this occurred for PF and SB. For the remaining powders (except FP and SX), the CPP calculated from the D_{v90} was smaller than for the D_{v50}. Again, FP only showed particle size consistency at two increases in the PP (3.0 and 3.5 Bar) using the D_{v90}. For SX, it was only at 4.5 Bar that the d_r indicated no difference between the particle sizes for the Dv_{90} thus it was not possible to assign a CPP value. Although the CPP of the D_{v90} may allow comparison between the powders, it would represent a population of powder comprising both fully disrupted and partially disrupted agglomerates. As the contribution of each of these to the size measurements is not known, the CPP generated using the D_{v90} was considered to be of less value than the CPP generated using D_{v50} values.

Table 2.6 A summary of the critical primary pressure (CPP) values of the powders determined from Sympatec HELOS/RODOS dry dispersion laser diffraction (using the rotary feeder). The CPP value was derived using the mean D_{v50}, D_{v90} and volume mean diameter (VMD) values.

Powder	**Critical Primary Pressure (CPP, Bar)**		
Particle Size	**D_{v50}**	**D_{v90}**	**VMD**
BDP	2.5	2.0	2.0
Bud	2.0	1.0	2.0
FP	3.0*	3.0*	3.0*
LH300	2.0	0.7	1.5
PF	2.5	2.5	2.5
SB	1.0	1.0	1.0
SX	3.5	-	3.5
Tof	3.0	2.0	3.0

***** Measured size unchanged for 2 consecutive dispersing pressures only, 3.0 and 3.5 Bar.

2.5.4 CHARACTERISATION OF DE-AGGLOMERATION BEHAVIOUR OF MICRONISED POWDERS BY LASER DIFFRACTION

Figure 2.9 shows the de-agglomeration profiles of the powders generated using dry dispersion laser diffraction and the D_H/D_x approach. The profiles exhibited rectangular hyperbolas with subtle differences in the shape of the curve suggestive of different de-agglomeration behaviours. When the de-agglomeration data (calculated from the D_{v50} values) were fitted to the linearised forms of the Langmuir, Freundlich and Michealis Menten equations, the Freundlich equation exhibited poorer linearity (R^2 = 0.69 – 0.92 and 0.73 – 0.94 for the D_L/Dx and D_H/Dx de-agglomeration data, respectively) compared to the Langmuir or Michaelis Menten equation (R^2 = 0.92 – 1.00 and 0.91 – 1.00 for the D_L/Dx and D_H/Dx de-agglomeration data, respectively) and on this basis it was not considered further as a potential model. The linearised plot for the Langmuir and Michealis Menten equations were identical and hence the fit of the data was also identical. As neither of the original equation derivations can be directly compared to de-agglomeration, the choice of model was arbitrary. Whereas in the Langmuir adsorption isotherm k represents an equilibrium constant, in Michelis Menten it is the substrate concentration required to reach 50 % of the limiting rate of the reaction. The Michealis-Menten equation was therefore selected, where k would represent the PP required to achieve 50 % de-agglomeration and called DA_{50}.

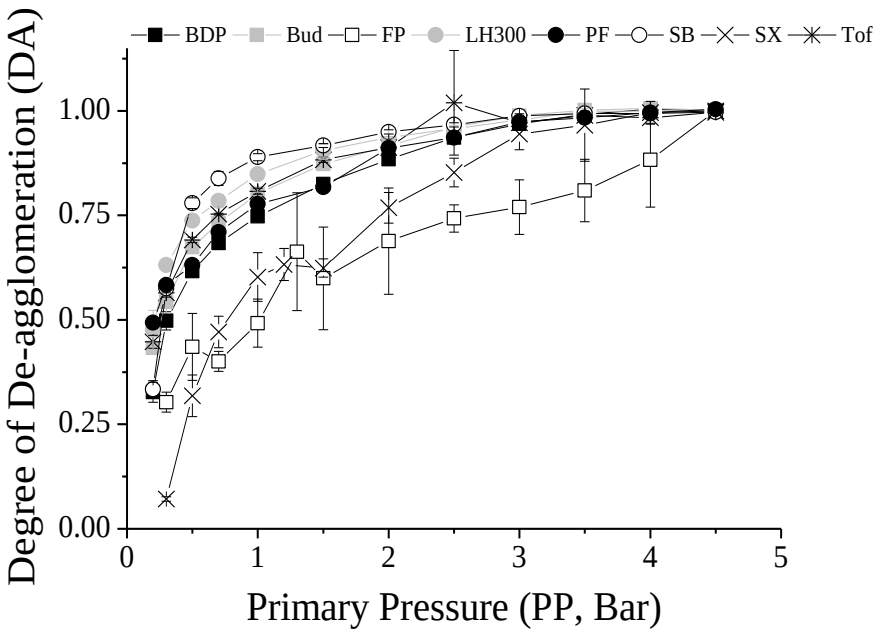

Figure 2.9 De-agglomeration profiles derived from particle size data generated by Sympatec HELOS/RODOS laser diffraction (using the rotary feeder) at primary pressures in the range 0.2 – 4.5 Bar. Particle size data (i.e. D_{v50} values) were normalised using the D_H/D_x approach for the powders beclometasone dipropionate (BDP), budesonide (Bud), fluticasone propionate (FP), lactohale 300 (LH300), PF-00613322 (PF), salbutamol base (SB), salmeterol xinafoate (SX) and tofimilast (Tof) (mean ± SD, n = 3).

The derived DA_{50} and DA_{max} from D_L/Dx and D_H/Dx de-agglomeration plots (using the D_{v50}) are shown in Table 2.7. Considering the D_{v50} data, both the D_L/Dx and D_H/Dx de-agglomeration data showed excellent linearity ($R^2 > 0.91$) and the derived DA_{50} values were similar. The DA_{max} values, however, differed. The values were generally higher for D_L/Dx rather than D_H/Dx de-agglomeration data. When assuming D_L to represent the fully dispersed particle size in liquid medium, higher DA_{max} values (generally > 1) could indicate that particles were fractured at high pressures in the dispersing line of the Sympatec laser diffractometer. As different instruments were used, differences in the numerical algorithms used to calculate the particle sizes may also have contributed to this effect. Using the D_H approach, the theoretical DA_{max} is 1, and in most instances the derived values were ≤ 1.20 with the exception of SX where $DA_{max} = 1.35$, where slight deviations are likely from the goodness of fit of the model. When considering the R^2 values, DA_{max}, and the fact that all particle size measurements were derived from a single instrument, the D_H/D_x approach was deemed to be the most appropriate for data analysis.

Table 2.7 The R^2, primary pressure required for 50 % de-agglomeration (DA_{50}) and maximum degree of de-agglomeration (DA_{max}) of the powders derived from de-agglomeration data obtained by dry dispersion laser diffraction. The values correspond to the D_L/D_x and D_H/D_x data analysis approach, determined from the mean D_{v50} values of the powders.

Approach: D_L/D_x			
Powder	**R^2**	**DA_{50}**	**DA_{max}**
BDP	0.9990	0.44	1.70
Bud	0.9979	0.38	1.33
FP	0.9169	1.15	1.28
LH300	0.9997	0.23	1.18
PF	0.9981	0.33	1.31
SB	0.9976	0.23	1.29
SX*	0.9742	1.45	1.63
Tof	0.9962	0.28	0.96
Approach: D_H/D_x			
Powder	**R^2**	**DA_{50}**	**DA_{max}**
BDP	0.9990	0.44	1.11
Bud	0.9995	0.32	1.08
FP	0.9049	1.15	1.13
LH300	0.9997	0.23	1.06
PF	0.9980	0.33	0.94
SB	0.9979	0.25	1.06
SX*	0.9711	1.45	1.35
Tof	0.9964	0.28	1.07

*Particle size data generated at the lowest PP (i.e. 0.3 Bar) were removed from data fitting due to poor linearity with these data included (D_L/D_x R^2 = 0.4548, D_H/D_x R^2 = 0.4532)

De-agglomeration data generated using the D_{v90} and VMD overall showed good linearity, although it was generally poorer than for the D_{v50} data (Table 2.8). SX, however, showed very poor linearity (R^2 = 0.17 – 0.20) and therefore it was not possible to derive de-agglomeration parameters for this powder. The de-agglomeration parameters (DA_{max} and DA_{50}) were higher for BDP, Bud, FP and SB using the D_{v90} and VMD compared to the D_{v50} data. For Tof they were comparable, and for LH300 they were lower. For PF, they were lower and higher for the D_{v90} and VMD, respectively. These differences may reflect heterogeniety in particulate properties and agglomerate strength/structures within the powder bulk. Furthermore, when using the D_{v90}, D_H may comprise agglomerates as well as individual particles, such that LH300 for example

may have weaker inter-agglomerate interactions compared to intra-agglomerate interactions. However, due to the uncertainty in the powder structure for the D_{v90}, such interpretations must be made with caution. The D_{v50} was therefore selected for further analysis, as it represents the median particle size of the powder, enabled parameters to be derived for SX, and the D_H would be less likely to include agglomerates.

Table 2.8 The R^2, primary pressure required for 50 % de-agglomeration (DA_{50}) and maximum degree of de-agglomeration (DA_{max}) of the powders derived from de-agglomeration data obtained by dry dispersion laser diffraction. The values were determined using the D_H/D_x approach, calculated from the mean D_{v90} or volume mean diameter (VMD) of the powders.

Approach: D_H/D_x

Particle Size Data used: D_{v90}

Powder	**R^2**	**DA_{50}**	**DA_{max}**
BDP	0.9608	0.58	1.16
Bud	0.8679	0.88	1.26
FP	0.8838	2.27	1.40
LH300	0.9991	0.12	1.03
PF	0.9951	0.30	0.93
SB*	0.9767	0.60	1.16
SX	0.1737	-	-
Tof	0.9989	0.24	1.06

Approach: D_H/D_x

Particle Size Data used: VMD

Powder	**R^2**	**DA_{50}**	**DA_{max}**
BDP	0.9870	0.60	1.16
Bud	0.9588	0.72	1.21
FP	0.9092	1.76	1.28
LH300	0.9994	0.19	1.05
PF	0.9956	0.38	0.92
SB	0.8872	0.96	1.28
SX	0.1957	-	-
Tof	0.9974	0.27	1.06

* Particle size data generated at the lowest (i.e. 0.2 Bar) PP removed from data fitting due to poor linearity with these data included (R^2 = 0.4073).

2.5.5 INVERSE GAS CHROMATOGRAPHY AT INFINITE DILUTION

The dispersive surface energy was determined from IGC analysis at infinite dilution for a selection of powders displaying varying behaviour; BDP, SX, FP and LH300. The gross retention time of each probe (t_R), determined from the peak maximum, was used to calculate the retention volume (V_N) according to Equation 2.10, and was corrected for the dead volume (t_o) i.e. the time a probe molecule would take to travel through the column without interacting with the sample. In Equation 2.10, F is the carrier gas flow rate at standard temperature and pressure, T_s is the column temperature in Kelvin, T_{ref} is the reference temperature for flow rate determination, *m* is the sample mass packed into the column and j is the James-Martin pressure drop correction factor which corrects the retention time for the pressure drop along the packed column (Thielmann, 2004; Jones et al., 2012).

Equation 2.10 $$V_n = \frac{j}{m} . F . (t_R - t_o) . \frac{T_s}{T_{ref}}$$

Equation 2.11 $$Work\ of\ cohesion = 2 . (\gamma_D . \gamma_D)^{\frac{1}{2}}$$

The dispersive surface energy was calculated by the Schultz method (Schultz et al., 1987). Four non-polar probes were injected onto the column and a plot of RT(ln V_N) against $a(\gamma^D_L)^{1/2}$ constructed where R is the gas constant, T is the column temperature, V_N is the net retention volume, a is the cross-sectional area of the adsorbate probe molecule and γ^D_L is the dispersive surface tension of the adsorbate. The plot yields a straight line with gradient $2N_A(\gamma_D)^{1/2}$ where N_A is Avagadro's number and from which the dispersive surface energy of the solid (γ_D) can be determined. A representative plot used to determine the dispersive surface energy of SX is shown in Figure 2.10. The polar probe data were added to the plot and the vertical distance of the data points from the alkane line is equal to the specific free energy of adsorption (ΔG_P) arising due to polar interactions with the sample material. The dispersive surface energy of the powders differed and ranged from 36.2 ± 0.14 $mJ.m^{-2}$ for SX to 49.9 ± 0.08 $mJ.m^{-2}$ for FP. The work of cohesion arising from the dispersive interactions was calculated using Equation 2.11 (Azioune et al., 2002; Voelkel et al., 2009) where γ_D is the dispersive surface energy of the sample. A summary of the dispersive surface energies (γ_D), specific free energy of adsorption (ΔG_P) and work of cohesion of BDP, FP, LH300 and

SX are shown in Table 2.9. As well as having the highest dispersive surface energy, FP also had the highest work of cohesion. This was followed by LH300, BDP and SX, representing a rank order of reducing cohesivity. For FP, the run time of the polar probes was not sufficiently long enough for complete elution of the acetone and ethanol peaks therefore it was not possible to calculate the ΔG_P for these probes. Considering the other three powders, overall LH300 had the greatest polar component, followed by BDP and finally SX.

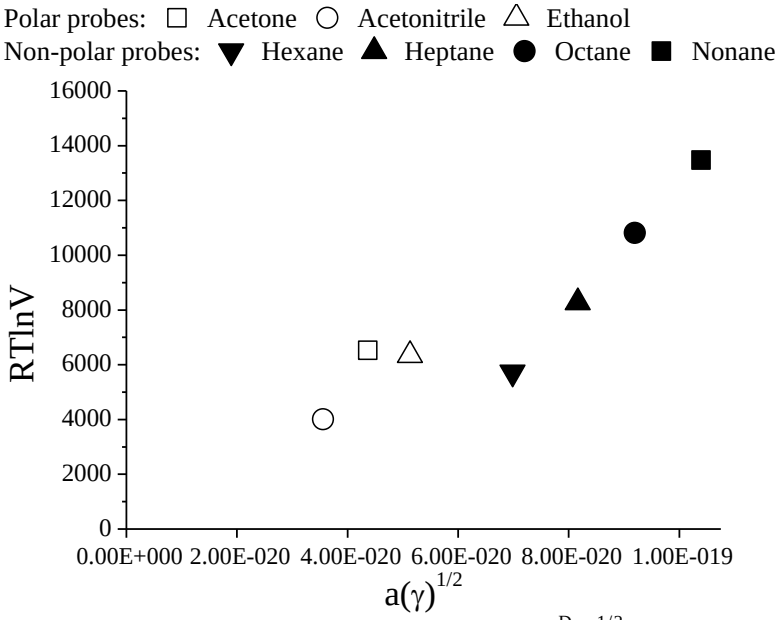

Figure 2.10 Representative plot of $RT(\ln V_N)$ against $a(\gamma^D_L)^{1/2}$ for the determination of the dispersive surface energy using the Schultz method. The data presented are for salmeterol xinafoate (SX).

Table 2.9 The dispersive surface energy, free energy of adsorption (generated from acetone, acetonitrile and ethanol probes) and work of cohesion of beclometasone dipropionate (BDP), fluticasone propionate (FP), lactohale 300 (LH300) and salmeterol xinafoate (SX) (mean ± SD, *n* = 3 injections onto a single column).

Sample	**Dispersive Surface Energy ($mJ.m^{-2}$)**	**Work of Cohesion ($mJ.m^{-2}$)**	**Free Energy of Adsorption ($kJ.Mol^{-1}$)**		
			Acetone	**Acetonitrile**	**Ethanol**
BDP	40.6 ± 1.22	81.3 ± 2.44	7.9 ± 0.21	7.9 ± 0.26	8.0 ± 0.12
FP	49.9 ± 0.08	99.9 ± 0.16	-	14 ± 0.09	-
LH300	44.9 ± 0.92	89.8 ± 1.85	9.5 ± 0.16	11 ± 0.16	13 ± 0.19
SX	36.2 ± 0.14	72.5 ± 0.29	7.0 ± 0.11	6.2 ± 0.07	5.0 ± 0.04

2.6 DISCUSSION AND CONCLUSIONS

The difficulty in achieving efficient delivery of drug particles to the lungs has resulted in extensive efforts to engineer DPI device and formulation characteristics. Consistent performance of a DPI product depends on the properties of the formulation and the interaction of the formulation with the commercial device. Specifically, each of the components are required to work together to provide efficient de-agglomeration of the drug from the carrier system. Complex variables are involved including PSD, particle shape, surface energy and environmental conditions all of which affect powder behaviour (Wong et al., 2011). Furthermore such properties are not straightforward to quantify in relation to de-agglomeration. Production and processing steps such as micronisation result in different surface energy distributions and potential heterogeneity in powder properties. However, approaches to determine the dispersibility of a powder can not only aid in rational formulation and device design, but also allow the influence of drug/formulation properties on dispersibilty to be ascertained. Of particular importance is an understanding of the cohesivity/adhesivity of agglomerated systems, as it is such interactive forces that need to be overcome in order to achieve aerosol dispersion. The balance of cohesive forces with adhesive interactions within a formulation e.g. with a second drug or carrier, can be used to predict the blending, segregation and de-agglomeration characteristics of DPI formulations (Begat et al., 2004a, Begat et al., 2004b). The aim of this chapter was to seek to develop a methodology which provided a realistic characterisation of powder dispersion using readily available equipment through the use of dry dispersion laser diffraction.

The liquid dispersed particle size (D_L) confirmed that the powders were micronised and of a size suitable for inhaled delivery to the conducting airways, each having a D_{v50} less than 4 μm. The SEM images further supported this finding, showing micron-sized particles (i.e. approximately 1 – 10 μm) that formed agglomerates which in most cases were also agglomerated with each other. The median particle size (D_{v50}) obtained at the highest PP using the dry dispersion laser diffraction method (D_H) where complete dispersion is assumed was in good agreement with the liquid dispersed size. In most instances (except for Tof and LH300) there were significant differences in the dry and liquid dispersed size (D_{v50}) however the order of magnitude of the differences was small. For example, SX was found to have a D_{v50} of 1.51 ± 0.03 μm and 2.05 ± 0.12 μm in the dry and liquid dispersed state, respectively. Differences between the liquid and

dry dispersed particle sizes would not be unexpected due to the use of different laser diffraction apparatus and dispersing media.

2.6.1 DEVELOPMENT OF THE LASER DIFFRACTION DATA ANALYSIS TECHNIQUE

Method development for the Sympatec HELOS/RODOS was conducted to investigate the influence of parameters such as the trigger conditions (comprising start and end optical concentration, C_{opt}), measurement time, trigger channel and timebase on the particle size measurement. These parameters were found to have negligible effects on the measured particle size. Each paramater was varied univariantly rather that using a multivariate design of experiment approach, which would have involved validation at each PP, which was not the objective of the study. The objective was to develop rather than validate a method of dry dispersion laser diffraction for de-agglomeration analysis. The reported findings were therefore deemed sufficient to proceed with the study. Based on these objectives, it was not overly critical to generate a 'true' particle size measurement at each PP, instead it was necessary to ensure that the parameters employed provided a true and reproducible reflection of the sample performance under a specfic dispersion condition. This would therefore allow de-agglomeration to be assessed over a range of dispersing conditions (Marriott et al., 2006).

When calculating the degree of de-agglomeration (DA) both the D_L and D_H were considered. Incorporating either parameter in subsequent calculations resulted in similar linearity and powder dispersibility (represented by DA_{50}) for the powders. The maximum degree of de-agglomeration (DA_{max}) however was generally larger when using D_L than $D_{H.}$ In the first instance, the choice of approach is important in order to retain consistency in data analysis between powders/studies, as it is influenced by the assumptions made with regards to complete dispersion to primary particles. The use of either D_H or D_L each has limitations. Powders subjected to high PPs in the Sympatec may undergo a degree of particle attrition/erosion due to high gas velocities and impactions in the dispersing line (Leschonski et al., 1984; Ghoroi et al., 2013) such that D_H may be smaller than the true particle size. The use of D_L on the other hand requires the use of validated methods to ensure that primary particles are sized. The method also accommodates the potential for interactions with liquid media which may alter properties such a particle shape, size and volume; the orientation of the particles within

the liquid sample cell may also affect the measured size (Berthold et al., 2000). Furthermore, in the current study, D_L was generated using a different laser diffraction apparatus whereas ideally particle size data should be generated from the same instrument (e.g. Sympatec SUCELL wet dispersing unit), to maintain consistency in particle size calculations, although in both instruments Fraunhofer theory was used. Overall, the use of D_H was considered most appropriate in subsequent analysis.

2.6.2 CHARACTERISATION OF DE-AGGLOMERATION BEHAVIOUR

The dry dispersion particle size results at low PPs indicated that under low shear conditions the powders were agglomerated, a finding corroborated by SEM images. Following the application of a low level of shear the powders showed some de-agglomeration. The dispersing line of the Sympatec HELOS/RODOS is optimised for dispersion, with the release of compressed air into the dispersing line generating a primary/driving air flow which initiates particle acceleration and subsequent dispersion. As the air is released into the dispersing line, its path is contoured to generate a high shear zone to further promote powder break-up. As the sample passes along the dispersing line it is subjected to frictional, shear and centrifugal forces that result in collisions beween gas and powder particles, and particle-particle and particle-wall collisions (Röthele, 1990). At the end of the dispersing line the powder is subjected to an impact cascade to aid dispersion (Leschonski et al., 1984). Due to the dispersion promoting features of the dispersing line, it is likely that the powders exhibited de-agglomeration even under very low PP/shear conditions. These geometric effects however would be consistant between all the powders allowing differences in cohesion and de-agglomeration to be studied.

Dry dispersion sizing showed differing degrees of agglomeration and therefore powder structures between the samples. At low PPs e.g. 0.3 Bar, SX and FP had the largest agglomerate size (D_{v50} = 21.35 ± 1.52 and 8.08 ± 0.74 µm, respectively). LH300 and Tof had intermediate sizes (D_{v50} = 5.26 ± 0.08 and 4.91 ± 0.09 µm, respectively), and BDP and Bud had small sizes (D_{v50} = 3.32 ± 0.15 and 3.88 ± 0.75 µm, respectively). SB had the smallest size (D_{v50} = 1.86 ± 0.03 µm). Therefore, it is likely that under these conditions SB, for example, would have a powder structure mainly comprising individual particles and small SB–SB agglomerates, whereas SX would consist of large SX–SX agglomerates. Differences in powder structure arise due to the propensity for,

and extent of, agglomeration, which is determined by the magnitude, type and heterogeneity in interactive forces between powder particles. Such forces are dependent on particle size, shape, rugosity, hardness, press-on forces exerted during handling and relative humidity (De Boer et al., 2003) which will ultimately affect the dispersibility of the powders. The agglomeration state at low PPs cannot in isolation be used as an indicator of dispersion, but allows for a qualitative distinction between powders of different cohesivity and structure.

Increasing the PP and therefore the initial driving airflow resulted in a change in the PSD of the powders. Upon increasing the dispersing pressure, there was a gradual shift towards smaller particle sizes suggesting that powder dispersion was better effected. Higher flow rates are associated with greater viscous shear stress in the Sympatec HELOS/RODOS (Shekunov et al., 2003) and the increased turbulent forces leads to improved de-agglomeration (Voss and Finlay, 2002; Louey et al., 2006; Kurkela et al., 2008). Turbulence alone, however, is not the only mechanism involved in de-agglomeration (Voss and Finlay, 2002). Increasing air flow rates increase the velocity gradient between the gas and powder thus promoting greater dispersion through acceleration of powder agglomerates (Calvert et al., 2009) and also increases wall impactions (Wong et al., 2011), and it is therefore likely that a combination of factors were involved.

2.6.2.1 DETERMINATION OF DE-AGGLOMERATION PARAMETERS

It was proposed that the developed laser diffraction method would enable parameterisation of the de-agglomeration behaviour of inhaled powders. De-agglomeration is related to powder flowability. The FT4 powder rheometer is traditionally used to study flow by measuring the behaviour of powders under the application of stress, and can provide insight into the relative cohesivity of powders (Shur et al., 2008). Rheometer testing however involves a conditioning step, where the powder is gently disturbed by a blade (Freeman, 2007). By removing the packing history and generating a homogenised, uniform powder with a low packing stress (Shur et al., 2008) it can be argued that the measurements do not represent the intrinsic flowability/compressability of the powders. Outcomes will also be of little relevance in understanding inhaled formulation performance due to the absence of conditioning steps during powder delivery. Technologies such as entrainment tubes which are used in tandem with cascade impactors provide an aerodynamic assessment of powder de-

agglomeration and deposition, and show greater relevance to inhalation delivery (Louey et al., 2006). Dispersion is achieved under airflow conditions which can be controlled by the user, and characterised in terms of for example the pressure drop, R*e*, and shear stress (τ_S) (Louey et al., 2006). This is however at the expense of the tubes needing to be engineered and manufactured in-house for the required application, and involves lengthy, labour intensive, impactor testing. Dry dispersion laser diffraction removes the need for the latter thus providing a more rapid tool for assessing de-agglomeration under different shear conditions. Single particle techniques such as AFM can also provide useful insights e.g. Bud has demonstrated stronger cohesive interactive forces than lactose (Begat et al., 2004a), whereas those of SX and FP were indicated to be of comparable magnitude (Young, 2004a). However, as AFM only employs a small number of isolated particles then extrapolation of the results to the aerosolisation behaviour of a powder bed should only be effected with caution, particularly as a distribution of particles is likely due to inter- and intra-batch variability in properties (Feeley et al., 1998; Price, 2011), which could lead to an overestimation of the cohesive force of a bulk powder. Being a bulk measurement technique, laser diffraction, if conducted within a controlled environment, is able to account for every factor which may influence de-agglomeration, including particulate, bulk, and external factors. As there is little powder manipulation prior to analysis, there is minimal disturbance to the powder structure/packing. These advantages provide a convenient, accessible and highly relevant tool in powder characterisation and the necessary preceding step in formulation development.

The particle size-primary pressure profiles were distinctive, undergoing an initial reduction in size until a plateau was reached, and provided a mechanistic insight into the de-agglomeration process. For example, the rapid drop in the D_{v50} of SB under the application of a dispersing pressure, and rapid attainment of the plateau particle size, indicated efficient de-agglomeration to near complete agglomerate dispersal occurring very readily under the application of shear. However, for FP, the drop in the D_{v50} was more progressive suggesting a more gradual de-agglomeration process, in which a flatter gradient may have initially been considered to indicate better dispersibility (Begat et al., 2004b; Adi et al., 2006; Kaye et al., 2009; Ghoroi et al., 2013). Unlike previous studies, by using multiple dispersing pressures over a wide titration range, it is clear that that it is necessary to consider the entire particle size-primary pressure curve when evaluating powder de-agglomeration. For example, when SB and FP were

empirically modelled, FP was found to have poorer dispersibility than SB. It was also possible to obtain information regarding powder structure, for example, high standard deviations were obtained in the measured agglomerate size at each dispersing pressure for FP, and highlighted agglomerate size heterogeneity during dispersion, leading to mixed populations of agglomerate and/or particle sizes.

2.6.2.1.1 POWDER COHESIVITY

The plateau region of the curve was investigated as a measure of powder cohesivity. The PP at which the plateau occurred (CPP), was derived and varied between the powders in the range 1.0 to 3.5 Bar. The absence of further changes in the particle size was considered to reflect the particles in their dispersed state, and therefore the PP required to achieve 100 % de-agglomeration to primary particles. The parameter therefore provided a measure of interparticulate cohesive interactions, and in particular the most cohesive particle populations. Comparing the CPP derived from the D_{v50} and D_{v90} provided an indication of the heterogeniety in interactive forces within the powder. For example Bud, CP, and PF had identical CPPs to achieve the dispersed D_{v50} and D_{v90}, however, for the remaining powders, the values were different. In the case of BDP and LH300 the CPP value was lower, and for SB and SX the CPP was higher, using the D_{v90}. However, by utilising the D_{v90} i.e. the particle size below which 90 % of the particles, by volume, are smaller than, the plateau region may consist of mixtures of agglomerates and dispersed particles. Therefore, comparisons must be made with caution, as the composition of the D_{v90} powder structure is not known and may differ between powders.

2.6.2.1.2 DEGREE OF DE-AGGLOMERATION

In order to characterise de-agglomeration behaviour, the degree of de-agglomeration (DA) representing the extent to which a powder has de-agglomerated at a specific PP was plotted as a function of PP. The de-agglomeration profiles were empirically modelled to derive de-agglomeration parameters. The linearised Langmuir and Michealis Menten equations had excellent linearity (e.g. using the D_H/D_x approach and D_{v50} values, $R^2 = 0.91 – 1.0$), and was superior to the Freundlich equation ($R^2 = 0.73 – 0.94$) which was subsequently not considered further. Linearisation of the Langmuir and MM equation was conducted using the Hanes Woolf method rather a double reciprocal/Lineweaver-burk plot as there is less bias in the data points towards low PPs

and it provides a more faithful representation of experimental errors (Cornish-Bowden, 2004). The fits were empirical as it is not applicable to draw analogies between adsorption theory or enzyme kinetics respectively and powder de-agglomeration. The median particle size (i.e. D_{v50}) was selected for use in the study, as there was marginally improved linearity compared to the D_{v90} or VMD, and it was not possible to derive de-agglomeration parameters for SX. Furthermore, by using the D_{v50} and not the D_{v90}, or a fixed particle size e.g. 5.4 µm (Behara et al., 2011b), the DA would represent the degree of de-agglomeration to primary particles rather than a size which may also comprise a proportion of small agglomerates. Using this analysis, the DA indicated that under low shear, the proportion of de-agglomerated particles would be low (e.g. DA = 0.30 ± 0.02 for FP and DA = 0.07 ± 0.01 for SX).

Two parameters were obtained following empirical modelling. Considering the DA_{max}, all the powders attained a value close to 1.0 under the dispersing conditions employed, as would be expected based on the normalisation data analysis approach adopted. The DA_{max} also provided a further measure of the degree of fit of each data set to the model, as powders showing the greatest deviation in this parameter from the theoretical value of 1.0 (i.e. SX and FP) also had the poorest linearity owing to them possessing the largest variability (i.e. highest standard deviations) for replicate particle size measurements particularly at low dispersing pressures. The DA_{50} values described the PP required to achieve 50 % de-agglomeration. The DA_{50} provided an indication of how readily a powder disperses to its primary particles, with smaller DA_{50} values suggesting more ready dispersal. The derived values were in the correct region when compared to the raw de-agglomeration data and the powders showed a range of behaviours. Being directly determined from linear regression parameters (i.e. gradient and intercept), the use of the DA_{50} avoided any errors of interpolation which may occur with other indices (e.g. 10th percentile). Based on the DA_{50}, the powders could be characterised into those that were poor (SX and FP, DA_{50} = 1.45 and 1.15 Bar, respectively), intermediate (BDP, DA_{50} = 0.44 Bar) and good (Bud, LH300, SB, Tof, DA_{50} = 0.32, 0.23, 0.25, 0.28 Bar, respectively) dispersers.

The shape of the particle size-primary pressure profile, CPP and DA_{50} values further allowed the de-agglomeration mechanisms of the powders to be postulated. The difference between the DA_{50} and the CPP value can be used to estimate the degree of heterogeneity in cohesive forces of the sample powder. A low CPP and DA_{50} were

obtained for LH300, SB and Bud, and resulted in a powder that dispersed very readily, and de-agglomerated completely, under a range of shear stresses. The PSDs of these powders were monomodal, consistent with low cohesive forces between the particles and fluidisation via an erosion mechanism, where a stream of de-agglomerated particles is continually entrained into the airflow (Shur et al., 2008; Tuley et al., 2008). In contrast, when the CPP and DA_{50} values were both large, e.g. SX and FP, an explosive de-agglomeration is indicated. At low shear the powders would undergo very little dispersion, due to the entrainment of large agglomerates (Shur et al., 2008; Tuley et al., 2008), some of which are so tightly associated that a bimodal PSD is observed indicative of a distinct population of fine particles/small agglomerates and tightly associated large agglomerates within the powder structure. As the level of shear increased, the size of the fine mode increased, and the agglomerate mode reduced, until it was eliminated, suggesting a step-wise de-agglomeration with progressive break-up of powder agglomerates under increasing shear (Behara et al., 2011b). Upon the application of levels of shear equal to or greater than the CPP, instantaneous de-agglomeration to primary particles would occur as the inter-particulate forces are overcome. The CPP values suggested that both SX and FP had high cohesive inter-particulate interactions and therefore potentially high agglomerate tensile strength, which is directly related to the work of cohesion of the interacting particles, their size, and packing fraction (Kendall and Stainton, 2001). Therefore, a high level of shear and/or impaction events would be required for complete dispersion; this would be provided by the faster flow rates, induced by higher PPs in the Sympatec, providing greater energy for dispersion (Shekunov et al., 2003; Behara et al., 2011b). Complete agglomerate break-up would therefore not occur unless high PPs were employed, and consequently it was only at high PPs that the PSDs of these powders became monomodal. One of the powders, Tof, had a high CPP but a low DA_{50}. This may suggest heterogeneity in the magnitude of inter-particulate forces as some powder agglomerates will break-up readily (hence a low DA_{50}) but others will require a much higher dispersing pressure (hence a high CPP) for de-agglomeration. Powders with inter-particulate force homogeneity would conversely have similar DA_{50} and CPP values, with complete dispersion of agglomerates occurring upon the application of the appropriate level of shear.

By means of comparison with a well establised technique, the dispersive surface energies of BDP, FP, LH300 and SX were assessed by IGC analysis at infinite dilution

(Table 2.10). Surface energy is directly proportional to adhesive/cohesive forces (Traini et al., 2008; Das et al., 2011b) and has been used by researchers to investigate aerosol performance and efficiency (e.g. Cline and Dalby, 2002; Traini et al., 2008). The dispersive surface energy, and corresponding work of cohesion, ranked the powders in the order: SX < BDP < LH300 < FP in terms of increasing cohesivity. The CPP values from laser diffraction predicted a different rank: LH300 < BDP < FP < SX. There are a number of possible reasons for the discrepancies in the ranks. Firstly, dispersive surface energy represents the contribution of van der Waals forces only towards the interaction, and therefore does not account for polar (and other) interactions. By adopting infinite dilution, where probes are injected at very low concentrations, solute molecules cover only a small proportion of the surface, often less than 0.1 % (Ylä-Mäihäniemi et al., 2008). Subsequently, there is preferential adsorption of the probes to high energy sites on the particle surface resulting in an overestimation of the surface energy (Ylä-Mäihäniemi et al., 2008) and therefore it may not represent true powder cohesivity. Micronised particles for inhalation are also heterogenous as a result of the varying and uncontrolled degree of disruption to the crystal structure during the micronisation process (Feeley et al., 1998). Differences in surface functional groups, irregular surface crevices and impurities can result in a range of surface energies on the particle surface; therefore a single value of surface energy may not represent the entire surface characteristics of the powder (Das et al., 2011a). By adopting a technique such as the laser diffraction methodology described in this study, it is possible to account for powder heterogeneity, and in doing so provide a more accurate representation of powder properties compared to existing techniques.

2.6.3 CONCLUSIONS

In conclusion, an approach to analyse powder de-agglomeration using dry dispersion laser diffraction was successfully developed. A method of data analysis was applied which enabled parameters to be generated to describe de-agglomeration. The parameters were able to differentiate de-agglomeration behaviour in a range of inhaled powders. The relationship between the cohesivity (represented by the CPP) and ease of dispersion (represented by the DA_{50}) revealed inter-particulate force heterogeneity and potential de-agglomeration mechanisms. The method could also be considered more representative of powder cohesivity compared to the work of cohesion derived from dispersive surface energy measurements at infinite dilution. The method has the

potential for use in powder characterisation and the design of DPI formulations and devices. The derived parameters would provide an initial screen of intrinsic powder dispersibility to enable the rational engineering of formulation and device characteristics in order to obtain efficient dispersion of drug particles for lung delivery.

3 EVALUATION OF DISPERSION MODIFICATION IN COMBINATION DRUG-DRUG POWDER MIXTURES CONTAINING SALMETEROL XINAFOATE AND FLUTICASONE PROPIONATE

3.1 INTRODUCTION

Combination DPI formulations contain two different types of drug particles either blended together in the absence e.g. Symbicort or presence e.g. Seretide®/Advair® of a coarse fraction of lactose which functions as a carrier particle and having an aerodynamic size usually greater than 60 μm. The carrier excipient often contains intrinsic fine lactose particles (less than 5 μm) termed 'fines' (Taki et al., 2011a) or these can be added extrinsically at a known concentration as a means of improving aerosolisation efficiency (Jones et al., 2008b). In the case of Symbicort, the drug particles are tumbled with micronised lactose particles to form larger agglomerates which have improved flowability and ease of handling (Borgstrom, 2002). There is therefore the potential for a range of physicochemical interactions between particles in a formulation. Interactions involving the drug include drug-drug (occurring both within and between drug powders in a co-formulation), drug-coarse excipient and drug-fine excipient. Furthermore fine-fine, coarse-coarse and coarse-fine excipient interactions may occur. The relative magnitude of the interactions will be specific to the formulation, and will contribute towards the dispersibility and bioavailability of the delivered drugs (Taki et al., 2011a). The multitude of interactions between different particle types, both in terms of the origin of the interaction forces e.g. van der Waals, electrostatic etc., and their relative magnitude renders studies involving multi-component formulations such as combinations highly complex. A common rationale in studying DPI performance has therefore involved sequential analysis of drug particle interactions with different components of a formulation (Young et al., 2004a; Adi et al., 2008a). Therefore, in this study, the implications of blending two fine particle drug powders in combination in the absence of a carrier particle was determined using the model powders salmeterol xinafoate (SX) and fluticasone propionate (FP); both of these powders were found to be poorly dispersible and highly cohesive (represented by the high DA_{50} and CPP values) according to dry dispersion laser diffraction analysis in Chapter 2.

The commercially available combination inhalation product, Seretide®/Advair®, contains the drugs SX and FP as the long acting beta agonist and corticosteroid, respectively. Aggregation of SX and FP in pMDI propellants has been reported, including the formation of hetero-flocs in 1,1,2-trichlorotrifloroethane (CFC-113), leading the authors to suggest that the two drugs interact inter-molecularly (Michael et

al., 2000; Michael et al., 2001). The aggregation behaviour was found to be dependent on the physical and chemical properties of the drug particles, and also the solvent environment (Michael et al., 2001) such that it is not possible to translate these findings directly to dry powder inhaler formulations. In powder formulations, the second fine particle drug has the potential to function as a performance modifier for the other drug in the system. SX-FP interactions have been reported to be stronger than SX-SX and FP-FP cohesive interactions when measured by AFM indicating that when blended in combination there are likely to be implications for the aerosolisation performance of the drugs (Young et al., 2004a). If cohesive drug-drug interactions dominate, the aerosolisation of each drug is likely to be independent of each other, however, when adhesive forces dominate as is reported to be the case for SX-FP interactions, aerosolisation of the drugs may differ compared to mono-delivery (Jetmalani et al., 2012). Studies have suggested that SX has a small but significant positive effect on the aerosolisation of FP from commercial Seretide Accuhaler devices, however, the inability to control the grade and concentration of coarse and fine lactose in the formulation, along with any differences in the blending/manufacturing process between the single drug and combination inhalers, hindered any firm conclusions to be drawn (Taki et al., 2011). The deposition profile of SX was also found to change when aerosolised from the inhaler containing the highest FP concentration, however, again it was not possible to deduce whether this was due to the increased FP content, reduced lactose content or an increasing FP to lactose ratio (Taki et al., 2011). Furthermore, the adhesive affinity of FP towards lactose and SX can change following processing, therefore requiring the manufacturing process and history of the powders to also be considered (Kubavat et al., 2012).

The balance of SX, FP and lactose (coarse and fine) interactions, particularly in terms of the cohesivity and adhesivity of each component, will play a major role in the aerosolisation of the drugs in the formulation. Atomic force microscopy and centrifuge investigations have revealed that SX-lactose interactions are weaker than SX-SX interactions (Podczeck et al., 1994; Young et al, 2004a), which increases emission (Adi et al., 2006), and may arise in part due to improved release of SX from a carrier surface. Conversely, FP-lactose interactions are stronger than FP-FP interactions (Young et al, 2004a), however, formulating with a carrier has also improved the emission and FPF of FP compared to drug-only formations (Louey et al., 2004b) indicating that the cohesive-adhesive balance is not the only factor important in dictating aerosolisation. Bulk

powder properties such as flowability, fluidisation, air permeability and powder strength distribution play an important role in the entrainability and de-agglomeration of powder particles (Le et al., 2010; Zhou et al., 2010a; Das et al., 2012). Furthermore, heterogeneity in particle properties such as surface energy and surface roughness, may alter the adhesive tendencies of individual particles within the bulk, and have implications for the bulk powder dispersibility (Podczeck et al., 1994; Das et al., 2012; Das and Stewart, 2012). Studies to determine the implication of inter-particulate drug-drug interactions on dispersibility in combination systems must therefore be undertaken systematically to determine the influence of each individual formulation component, take into account the inherent heterogeneity in particulate properties, as well as the influence of bulk powder properties on aerosol performance.

3.2 AIM AND OBJECTIVES

The aim of this study was to prepare fine particle blends consisting of two drugs with comparable particle sizes and evaluate the cohesive and adhesive tendencies in order to investigate the performance modifying effects on drug dispersibility. The objectives were therefore to:

a) Prepare homogenous fine particle blends containing micronised SX and FP.

b) Assess the de-agglomeration of the blends using a novel dry dispersion laser diffraction methodology (developed as described in Chapter 2), to determine whether it can be used as a predictive tool to assess blend performance.

c) Measure the dispersibility (in terms of ED and FPF) and deposition profiles (in terms of MMAD and GSD) of micronised SX and FP particles using Next Generation Impactor (NGI) analysis and assess the effect of blending each of these drugs with a second fine particle on dispersion and deposition.

d) Calculate the cohesivity and adhesivity of micronised SX and FP particles using surface energy measurements generated by inverse gas chromatography (IGC) in order to evaluate the effect of cohesivity/adhesivity on particle dispersion and deposition when in combination.

3.3 MATERIALS

The materials and equipment used in Chapter 3, not listed in Section 2.3, are shown in Table 3.1.

Table 3.1 Suppliers of materials and equipment (Chapter 3).

Material / Equipment	**Supplier**
Methanol; HPLC grade	Fisher Scientific Ltd, UK
Ammonium acetate; HPLC grade	Chromanorm Hipersolv for HPLC, BDH Prolabo, VWR International Ltd, UK
Nylon filters; pore size 0.45 µm, diameter 47 mm	Whatman™ (now part of GE Healthcare, purchased from Fisher Scientific Ltd, UK)
Next Generation Impactor	MSP Corporation, USA (supplied by Copley Scientific, UK)
Polypropylene glycol; PPG, 975 – 1075 $g.mol^{-1}$	Riedel-de Haen AG, Germany (now part of the Sigma-Aldrich group, UK)
Polypropylene glycol; average Mn approx. 1000	Aldrich Chemistry, Sigma-Aldrich Company Ltd, UK
Monodose Inhaler	Miat S.p.A, Italy (supplied by Pfizer Ltd, UK)
Capsules; gelatin, size 3	Capsugel, France
Flow meter; model 4040	TSI Inc, UK
Hexane	Fisher Scientific Ltd, UK
Phenomenex Luna 3u C_{18} column, 150 x 4.60 mm, 3 µm	Phenomenex UK Ltd, UK
PureLab Ultra system; for type I, resistivity 18 MΩ-cm, (water for HPLC, referred to as ultrapure water)	Elga LabWater, UK (part of Veolia Water Solutions and Technologies)
Whirlimixer	Fisons, UK
Turbula mixer; Type 2C	Willy A. Bachofen AG Machinenfabrik, Switzerland
IGC Surface Energy Analyser; SEA	Surface Measurement Systems Ltd, UK

3.4 METHODS

3.4.1 HIGH PERFORMANCE LIQUID CHROMATOGRAPHY VALIDATION

3.4.1.1 ASSAY CONDITIONS

High performance liquid chromatography (HPLC) analysis was conducted as previously described (Murnane et al., 2006). The column was a Phenomenex Luna 3u C_{18} column (150 x 4.60 mm, 3 µm) maintained at a temperature of 40 ^{o}C. The mobile phase flow rate was 1 mL.min^{-1}, injection volume 20 µL, run time 6 min and triplicate injections were made per sample. The detection wavelength was 228 nm. The mobile phase consisted of 0.6 % w/v ammonium acetate dissolved in ultrapure water, which was then mixed with methanol in the ratio 25:75 v/v. The solution was filtered through a 0.45 µm nylon filter using a Milipore filter unit. The HPLC system consisted of a Waters Alliance HT 2795 separations module, a Waters 2996 photodiode array detector and Waters column heater. Due to an in-built degasser, the mobile phase was not de-gassed prior to use. Samples were maintained at 10.0 ± 1.0 ^{o}C in the autosampler chamber. Peak integration was conducted using Empower Pro software (Empower 2 software, Build 2154, Waters Corporation, USA).

3.4.1.1.1 LINEARITY

Calibration standards were prepared in the range 0.5 - 50 µg.mL^{-1} containing SX and FP in co-solution. To prepare the standards, 2 mg of drug was accurately weighed and dissolved in mobile phase with sonication for approximately 10 min. Upon visual inspection to check for complete drug dissolution, the solutions were made to final volume (50 mL) to prepare a 50 µg.mL^{-1} stock solution. Six standards were prepared (0.5, 1, 2, 5, 12.5, and 25 µg.mL^{-1}), each involving a direct dilution of the stock solution with mobile phase. Three replicate injections of each sample were performed. Linearity was assessed by plotting the individual data points (i.e. the peak areas of the salmeterol base peak and fluticasone propionate peak, integrated from the chromatograms using the Empower Pro software, plotted against the concentration), and using the LINEST function in Microsoft Excel.

3.4.1.1.2 PRECISION

To assess intra-day precision, a single set of standards was analysed in duplicate on the same day, with three replicate injections of each standard. The peak areas were

normalised by dividing the detected peak area by the concentration of the standard. The normalised data for each standard were pooled (n = 6) and the percentage coefficient of variance (% CV) calculated. To assess inter-day precision, three sets of standards were freshly prepared and analysed on three separate days. The peak areas were normalised, the data for each standard pooled (n = 9) and the % CV calculated.

3.4.1.1.3 LIMIT OF DETECTION AND QUANTIFICATION

The limit of detection (LOD) and limit of quantification (LOQ) were calculated using Equation 3.1 and Equation 3.2 for each calibration curve, where Y_B is the y intercept from the regression equation and S_B the standard error of the y estimate (i.e. y intercept) calculated using the LINEST function in Microsoft Excel. The peak areas for the calibration curves prepared on three separate days were pooled to establish the LOD and LOQ of the method.

Equation 3.1 $$LOD = Y_B + 3S_B$$

Equation 3.2 $$LOQ = Y_B + 10S_B$$

3.4.1.1.4 ACCURACY AND THE INTERFERENCE OF CO-SOLUTES

The accuracy of the assay was assessed by injecting six co-solutions onto the column. Each sample consisted of 1.50 mg of each drug, accurately weighed and dissolved in 50 mL mobile phase. The detected concentration (D) of each sample was calculated from the standard calibration curve and expressed as a percentage of the actual concentration (A) (calculated based on the sample mass) using Equation 3.3 .

Equation 3.3 $$\text{Accuracy (\%)} = \left(\frac{D}{A}\right) x\ 100$$

3.4.2 BLEND PREPARATION

Drug-drug blends (1:8, 1:4, 4:1, 8:1) were prepared in 5 g batches. Blend preparation involved geometric mixing, where additions approximately equal in volume (i.e. 1 spatula full) of each drug were sequentially made into a 100 mL Duran bottle. Following each addition the blending vessel was placed on a Whirlimixer and subjected

to agitation for 60 s, followed by 60 s of stirring with a spatula to break up any large agglomerates. Three ceramic beads (approx. 10 mm diameter) were added to the vessel and the blend was tumbled using a Turbula mixer at 62 rpm for 40 min. Blends were stored at room temperature in a desiccator over dry silica and allowed to rest for 7 d prior to testing.

3.4.3 BLEND HOMOGENEITY

To assess blend homogeneity, approximately 2 mg of blend was accurately weighed and dissolved in mobile phase with the aid of sonication (≥ 10 min). The sample was visually checked for complete drug dissolution prior to being made to final volume (50 mL) and an aliquot removed for HPLC analysis. The detected concentration (D) was compared to the concentration of each sample (C), calculated from the sample mass, and expressed as a percentage recovery (PR, %) according to Equation 3.4. The blend was considered homogenous when the CV of the PR values of $n \geq 6$ samples was less than or equal to 6 %. The SX and FP content was calculated by converting the detected drug concentration into a drug mass, which was then expressed as a proportion of the weighed sample mass (in $\mu g.mg^{-1}$) for each content uniformity sample. The mean drug content of the samples was then used to calculate the actual SX:FP ratio in the product blend.

Equation 3.4 $$\text{Percentage Recovery } (PR; \%) = \left(\frac{D}{C}\right) x\ 100$$

3.4.4 PARTICLE SIZE ANALYSIS BY LIQUID DISPERSION LASER DIFFRACTION

The particle size of the blends was measured by liquid dispersion laser diffraction (n = 4) using the Malvern Mastersizer X as described in Chapter 2, Section 2.4.1 using Fraunhofer theory. A summary of the sizing parameters used is given in Table 3.2.

Table 3.2 A summary of the liquid dispersion laser diffraction parameters used to size combination salmeterol xinafoate (SX) and fluticasone propionate (FP) blends.

Dispersant (% w/v)	Sonication time (min)	Stir Setting	Sweeps	Equilibration time (min)
0.5 % span 80 in cyclohexane	5	3	3500	1

3.4.5 DISPERSIBILITY BY DRY DISPERSION LASER DIFFRACTION

The dispersibility of the blends was assessed using the Sympatec HELOS/RODOS and rotary feeder with protruding aspiration tube. Particle size/primary pressure profiles were constructed over the PP range 0.2 – 5.0 Bar (n = 3) as described in Chapter 2 from which the CPP was deduced. The liquid dispersion D_{v50} was used as the reference size to determine whether 'complete' dispersion of the powder or blend had occurred at the highest PP. The D_{v50} at each PP was expressed as a proportion of the D_{v50} at the highest PP (D_H) in order to calculate the DA, and de-agglomeration profiles constructed. The profiles were empirically modelled to derive the DA_{50} and the DA_{max} as described in Chapter 2 using Equation 2.8.

3.4.6 NEXT GENERATION IMPACTOR ANALYSIS

3.4.6.1 CAPSULE FILLING

Size 3 gelatin capsules were hand-filled with sample. The cap was removed, the base placed in a holder and 'tared' on a balance. Powdered sample was transferred into the capsule to obtain a fill weight of 15.00 ± 2.00 mg and the cap replaced. All capsules were analysed within 24 h of filling. One capsule was filled and actuated into the NGI per analysis.

3.4.6.2 AEROSOLISATION INTO THE NEXT GENERATION IMPACTOR

The impactor plates were first coated with 10 mL of coating solution per plate in order to minimise particle bounce and re-entrainment. The coating solution consisted of 11 % w/v PPG dissolved in hexane, prepared by accurately weighing 11.00 g of PPG into a 100 mL volumetric flask, making to volume with hexane, and shaking thoroughly. The solution was swirled in the plate to ensure complete and uniform coverage of coating solution on the entire surface of the plate. Excess solution was tipped out and the plates left to air dry in a fume hood for 10 – 15 min. The NGI was assembled with 15 mL of mobile phase accurately pipetted into the pre-separator. A vacuum pump was attached to the airflow outlet of the NGI and a flow meter attached to the throat via a tightly–fitting mouthpiece. The flow control value was adjusted to attain a flow rate of 60 $L.min^{-1}$ ± 5 % (corresponding to a pressure drop of 1.4 kPa), the vacuum pump was then switched off and the flow meter removed. A single capsule was loaded into the Monodose inhaler device and the side buttons depressed so that the capsule was pierced

at each end by a single needle. The device was attached to the throat using an appropriate mouthpiece ensuring a tight seal. The vacuum pump was switched on and after a period of 4 s switched off corresponding to the amount of time required for 4 L of air to be drawn through the device and NGI. The empty capsule was removed from the device and set aside. The device was carefully rinsed with mobile phase (20 – 50 mL) to collect the drug deposited. The capsule was taken apart and both the cap and bottom portion were thoroughly rinsed with mobile phase (20 mL). The NGI was then sequentially taken apart, starting with the throat and pre-separator which were rinsed with 50 and 100 mL mobile phase, respectively. The four samples (device, capsules, throat and pre-separator) were sonicated for ≥ 5 min and visually checked to ensure complete drug dissolution prior to being made to final volume. A sample was removed from each for HPLC analysis. In order to assess drug deposition on the impactor plates, 10 mL mobile phase was accurately pipetted into plates corresponding to stages 1 – 5 and 5 mL pipetted into plates corresponding to stages 6 – 8. The solution was swirled in the plate to ensure coverage of the entire surface and each plate sonicated for ≥ 1 min. The solutions were visually inspected for dissolution and a sample removed for HPLC analysis. Following quantification of the amount of drug deposited in the device, capsules and component parts of the NGI, the following parameters were calculated:

- *Recovered dose (RD)* – the total recovered dose of drug (including the device, capsules, throat, pre-separator and stages) expressed as a percentage of the total actuated dose (i.e. mass weighed into capsule),
- *Emission (or emitted dose, ED)* – the recovered dose, excluding drug deposited in the device and capsules, expressed as a percentage of the RD,
- *Fine particle fraction (FPF)* – the percentage of the RD or ED with a particle size < 5 µm, determined from a log normal-probability plot of the cumulative mass percent of drug deposited on the stages versus the stage cut sizes,
- *Fine particle mass (FPM)* – the mass of deposited drug with a particle size < 5 µm, calculated by converting the FPF (% RD) into a mass,
- *Mass median aerodynamic diameter (MMAD) and geometric standard deviation (GSD)* – the median aerodynamic diameter (50^{th} percentile) and standard deviation (ratio of the 84.1 and 15.9^{th} percentile) of the drug obtained from interpolation of the log normal-probability plot of the cumulative undersize distribution of the impactor sizing stages.

3.4.7 QUANTIFICATION OF DRUG RECOVERY BY HIGH PERFORMANCE LIQUID CHROMATOGRAPHY

Content uniformity and NGI samples were quantified using pooled calibration curves consisting of mixed SX and FP standards in the range 0.5 – 50 μg.mL^{-1}. Each curve was prepared and analysed on the same day (n = 5). The linearity, LOD and LOQ of SX were R^2 = 0.9991, 0.24 μg.mL^{-1} and 0.80 μg.mL^{-1}, respectively. For FP they were R^2 = 0.9996, 0.16 μg.mL^{-1} and 0.54 μg.mL^{-1}, respectively. Where individual NGI samples were outside this range, quantification was using pooled curves in the range 20 – 400 μg.mL^{-1}. SX had linearity, LOD and LOQ of R^2 = 0.9982, 3.12 μg.mL^{-1} and 10.4 μg.mL^{-1}, respectively. For FP, they were R^2 = 0.9967, 4.25 μg.mL^{-1} and 10.2 μg.mL^{-1}, respectively.

3.4.8 INVERSE GAS CHROMATOGRAPHY

3.4.8.1 FINITE DILUTION

Surface energy mapping was conducted using an IGC Surface Energy Analyser (SEA). Approximately 200 mg of sample was packed into a 300 mm silanised glass column with an internal diameter of 3 mm. Columns were pre-conditioned for 2 h at 30 ^{o}C and 0 % RH using helium carrier gas to remove adsorbed water. A series of non-polar (nonane, octane, heptane and hexane) and polar probes (ethanol, acetone, ethyl acetate, acetonitrile and dichloromethane) were injected onto the columns at a range of surface coverages. The experiments were carried out at 30 ^{o}C using helium carrier gas at 10 sccm. Methane gas was used for dead volume corrections.

3.4.8.2 SURFACE COVERAGE

The surface coverage was calculated by first determining the Brunauer-Emmett-Teller (BET) specific surface area (SSA) of the sample using the octane isotherm data, and was obtained directly from the SEA. This enabled calculation of the monolayer capacity (n_m, the number of moles of solute adsorbed for monolayer coverage) using Equation 3.5, where a_m is the cross sectional area of a solute molecule and N_A is the Avagadro's number. The surface coverage (n/n_m) at each injection concentration could then be calculated from the amount adsorbed (n) obtained from integration of the net retention volume (V_N) versus the equilibrium partial pressure (p) of each injection (Ho et al., 2010).

Equation 3.5 $$SSA = a_m . N_A . n_m$$

3.4.8.3 SURFACE ENERGY AND WORK OF ADHESION AND COHESION

The dispersive surface energy (γ_D) was obtained by first measuring the V_N of the alkane probes (nonane, octane, heptane and hexane) using the peak centre of mass approach. The Dorris and Gray method (Dorris and Gray, 1980) was then used, whereby a plot of $RTln(V_N)$ versus the carbon number of the alkanes was generated and the slope of the linear regression used to obtain the dispersive surface energy. The construction of a plot for each surface coverage enabled the surface energy distribution of the sample to be determined.

To determine the specific surface energy (γ_{SP}), the van Oss approach (Traini et al., 2008) and Della Volpe scale (Della Volpe and Siboni, 1997) was adopted. This involved injecting two monopolar probes onto the column of material, these were dichloromethane (γ+ 124.58 $mJ.m^{-2}$) and ethyl acetate (γ- 475.67 $mJ.m^{-2}$), and measuring the retention volume. Using the polarisation approach (Dong et al., 1989), a plot of $RTln(V_N)$ versus the molar deformation polarisation of the probes (P_D) was generated from the alkane data to generate a straight line, above which the polar probe data points were located. The vertical distance between the polar probe data points and the straight line was equal to the specific component of the free energy of adsorption (ΔG_P) (Dong et al., 1989), from which the specific surface energy (γ_{SP}) was determined.

The total surface energy (γ_T) was determined from summing the dispersive and specific surface energies. The work of cohesion and adhesion was calculated from Equation 2.11, using either the dispersive, specific or total surface energy.

3.5 RESULTS

3.5.1 HIGH PERFORMANCE LIQUID CHROMATOGRAPHY VALIDATION

Calibration standards containing SX and FP in co-solution in the concentration range 0.5 - 50 µg.mL^{-1} showed good linearity, with R^2 values of 0.9995 and 0.9993 for SX and FP, respectively (Figure 3.1 and Table 3.3). The intra-day precision of the standards indicated good reproducibility with % CV values < 4 % (Table 3.3). The inter-day precision was poorer than the intra-day precision, but the % CV was < 8 % for both drugs (Table 3.3). The LOD and LOQ calculated from pooled data generated over three days were 0.19 µg.mL^{-1} and 0.62 µg.mL^{-1} for SX and 0.21 µg.mL^{-1} and 0.69 µg.mL^{-1} for FP, respectively. The accuracy of drug recovery from co-solutions of known concentration was 97.05 ± 1.11 % and 98.04 ± 1.12 % for SX and FP, respectively (*n* = 6).

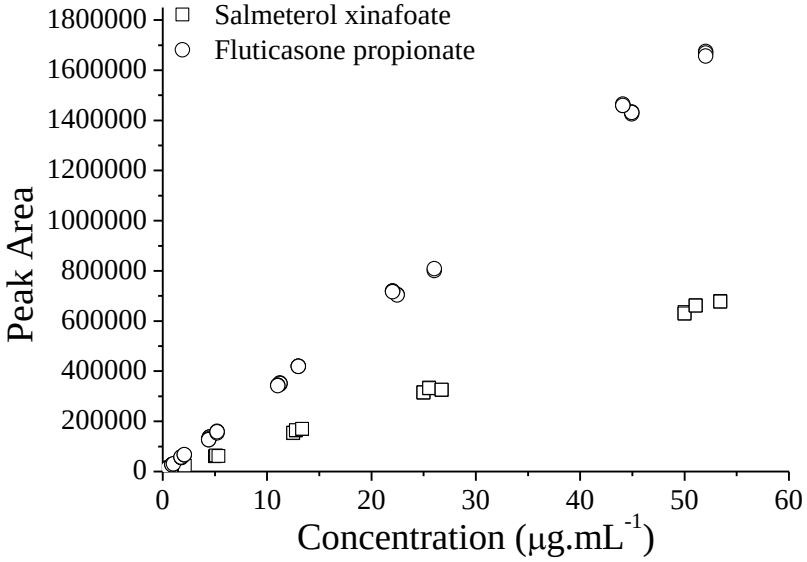

Figure 3.1 Salmeterol xinafoate and fluticasone propionate calibration curves comprising standards containing both drugs in co-solution in the concentration range 0.5 – 50 µg.mL^{-1}. The standards were freshly prepared on three separate days and the data plotted are the individual peak areas for triplicate injections made on the three separate days.

Table 3.3 The intra- and inter-day precision of salmeterol xinafoate (SX) and fluticasone propionate (FP) calibration standards in co-solution (0.5 – 50 µg.mL^{-1}) according to high performance liquid chromatography analysis.

Precision (% CV)	**Drug**	**Concentration (µg.mL^{-1})**						
		0.5	1.0	2.0	5.0	12.5	25	50
Intra-day	SX	1.21	2.48	0.78	0.21	0.71	0.32	0.40
	FP	3.21	1.38	0.63	1.05	0.61	0.21	0.38
Inter-day	SX	7.75	6.80	3.53	3.35	3.00	2.85	1.21
	FP	3.53	2.63	1.68	2.60	1.76	2.33	1.95

3.5.2 BLEND HOMOGENEITY AND DRUG CONTENT

The blend homogeneity of the drug-drug blends is shown in Table 3.4. The blend with the lowest SX content (i.e. SX:FP 1:8) was subjected to two 40 min tumbling sessions in the Turbula at 62 rpm however the CV value of SX still remained high at 5.51 %. Overall FP displayed optimal homogeneity at high FP concentrations. Although the homogeneity of the blends in some instances was poor it was deemed appropriate for the study.

Table 3.4 The blend homogeneity expressed as the coefficient of variance (% CV) and drug content (µg.mg^{-1}) of salmeterol xinafoate (SX) and fluticasone propionate (FP) co-formulated in fine particle blends.

	Homogeneity (% CV)		**Drug Content (µg.mg^{-1})**		**Detected Ratio**
SX:FP Ratio	**SX**	**FP**	**SX**	**FP**	
1:8	5.51	1.37	92.6	836.0	1.0:9.0
1:4	2.15	0.84	183.9	750.8	1.0:4.1
4:1	3.98	5.28	750.1	178.5	4.2:1.0
8:1	4.31	5.61	875.0	92.8	9.4:1.0

3.5.3 PARTICLE SIZE ANALYSIS BY LIQUID DISPERSION LASER DIFFRACTION

Table 3.5 shows the PSD of the blends measured by liquid dispersion laser diffraction. The measured particle size was comparable between the blends indicating that the particles were physically mixed and thus could be re-dispersed in a liquid medium.

Table 3.5 The particle size distribution (represented by the D_{v10}, D_{v50}, D_{v90}, and volume mean diameter, VMD) and span of salmeterol xinafoate (SX) and fluticasone propionate (FP) combination fine particle blends assessed by liquid dispersion laser diffraction (mean ± SD, n = 4).

SX:FP Ratio	D_{v10}	D_{v50}	D_{v90}	VMD	Span
1:8	0.94 ± 0.02	2.00 ± 0.06	3.85 ± 0.19	2.24 ± 0.09	1.46
1:4	0.95 ± 0.04	2.03 ± 0.12	3.79 ± 0.20	2.23 ± 0.13	1.40
4:1	0.80 ± 0.02	2.12 ± 0.06	4.45 ± 0.15	2.44 ± 0.08	1.72
8:1	0.77 ± 0.01	2.06 ± 0.08	4.52 ± 0.25	2.56 ± 0.27	1.82

3.5.4 DISPERSIBILITY BY DRY DISPERSION LASER DIFFRACTION

The particle size-primary pressure profiles of the blends exhibited the characteristic reduction in measured size until a plateau size was reached. The D_{v50} at the highest primary pressure employed was smaller compared to that measured by liquid dispersion (Table 3.5); the fully dispersed D_{v50} in the dry state was 1.63 ± 0.01 µm, 1.52 ± 0.03 µm, 1.55 ± 0.01 µm and 1.66 ± 0.01 µm for the 1:8, 1:4, 4:1 and 8:1 blends, respectively. Table 3.6 shows the de-agglomeration parameters for the blends. The DA_{50} values suggested that the dispersibility of the blend improved when FP was present, compared to SX alone. However, when the amount of FP was greater than the amount of SX in a combination blend, the DA_{50} increased beyond that of SX alone indicating poorer dispersibility. For FP, the converse was true, where a small amount of SX worsened the dispersibiliy of the blend compared to FP alone. However, when the amount of SX exceeded the amount of FP, dispersibility improved beyond that of FP alone. When considering only the combination blends, as the amount of FP in the blend increased, the bulk dispersibility of the powder became worse (i.e. higher DA_{50} values).

The CPP values indicated that FP was more cohesive than SX. In combination, the cohesivity of the blend reduced at every SX:FP ratio compared to FP alone, but there were only small/no differences compared to SX alone. Although there was no precise trend, generally the FP-rich blends were more cohesive (i.e. CPP = 1.20 – 1.70 Bar) than the SX-rich blends (CPP = 1.0 – 1.20 Bar). There were also differences in the relative magnitude of the DA_{50} and CPP values, which indicated differences in bulk powder structure. Although a lower DA_{50} is indicative of a powder that disperses well, due to proportions of weakly associated agglomerates, if the powder also had a high CPP value then there would also be populations of particles within the bulk that

exhibited very strong agglomeration. There would therefore be high heterogeniety in agglomerate strengths, as was the case for the FP powder when compared to the SX powder. In the combination blends, generally as the amount of FP in the blend increased, the heterogeniety in agglomerate strengths reduced.

Table 3.6 The primary pressure for 50 % de-agglomeration (DA_{50}), maximum degree of de-agglomeration (DA_{max}) and critical primary pressure (CPP) of salmeterol xinafoate (SX) and fluticasone propionate (FP) co-formulated in fine particle blends. The values were derived from de-agglomeration data obtained by dry dispersion laser diffraction using the mean D_{v50} values.

SX:FP Ratio	R^2	DA_{50} (Bar)	DA_{max}	CPP (Bar)
0.0:1.0	0.9832	0.48	1.04	4.00
1.0:9.0	0.9890	0.89	1.13	1.20
1.0:4.1	0.9906	0.57	1.17	1.70
4.2:1.0	0.9980	0.30	1.08	1.00
9.4:1.0	0.9981	0.20	1.02	1.20
1.0:0.0	0.9968	0.36	1.10	1.20

3.5.5 NEXT GENERATION IMPACTOR ANALYSIS

Figure 3.2, Figure 3.3 and Table 3.7 show the NGI analysis of SX:FP blends with various drug ratios. Considering the aerosolisation of SX, when blended with FP, there was an increase in the MMAD ($p < 0.05$, one-way ANOVA with post-hoc Tukey's test, GraphPad Prism 5), but no change in the GSD at all drug ratios. The MMAD progressively increased as the amount of FP in the blend increased. This could indicate the presence of SX agglomerates that were more difficult to disperse; interactions between SX and FP may have led to the formation of mixed agglomerates in which the presence of FP was detrimental to the dispersibility of SX from agglomerates. The FPF (ED and RD) of SX reduced by almost half when blended with the largest quantity of FP (i.e. 1.0:9.0, $p < 0.05$). For example, the FPF ED was 54.2 ± 5.28 % for SX alone compared to 25.5 ± 10.1 % when in combination with FP in the ratio 1.0:9.0. Comparing between the ratios, the FPF (ED and RD) from the 1.0:9.0 blend was also lower when compared to the 1.0:4.1, 4.2:1.0 and 9.4:1.0 blends ($p < 0.05$). Overall, SX emission was unchanged across the ratios ($p > 0.05$), except for an increase in SX emission when blended in the ratio 1.0:4.1 ($p < 0.05$) compared to SX alone.

Considering the aerosolisation of FP when blended with SX, different trends were observed compared to those seen for SX following co-formulation. The MMAD of FP reduced in the presence of SX at all SX:FP ratios ($p < 0.05$), and there was no change in the GSD (Table 3.7). This indicates that the presence of SX may have weakened FP agglomerates rendering them more readily dispersed compared to those of FP alone. Overall, however, there was no change in the FPF RD or ED of FP when blended with SX compared to FP aerosolised alone ($p > 0.05$, Figure 3.3). There were differences between the drug ratios; the FPF ED of FP was lower when aerosolised from the 1.0:9.0 ratio compared to the 1.0:4.1 ratio ($p < 0.05$), and the FPF RD was lower from the 1.0:9.0 ratio compared to the 1.0:4.1 and 4.2:1.0 ratio. This suggests that the relative amount of SX present in a co-formulation may affect FP dispersion, with higher FPFs being generated in the presence of larger amounts of SX. In terms of the emission, larger amounts of SX resulted in lower FP emission compared to smaller amounts of SX when in combination (i.e. 9.4:1.0 vs. 1.0:4.1 and 1.0:9.0, 4.2:1.0 vs. 1.0:4.1, $p < 0.05$).

Table 3.7 The recovery (% of the actuated dose), mass median aerodynamic diameter (MMAD) and geometric standard deviation (GSD) of salmeterol xinafoate (SX) and fluticasone propionate (FP) aerosolised at different SX:FP ratios into the Next Generation Impactor (mean ± SD, n = 4 - 6).

SX:FP Ratio	Recovery (%)	MMAD (µm)	GSD
Salmeterol xinafoate			
1.0:0.0	82.6 ± 5.46	2.45 ± 0.12	1.92 ± 0.04
9.4:1.0	95.4 ± 5.70	2.88 ± 0.07	1.86 ± 0.01
4.2:1.0	91.0 ± 4.52	3.13 ± 0.24	1.85 ± 0.03
1.0:4.1	106 ± 2.92	3.63 ± 0.30	1.77 ± 0.05
1.0:9.0	106 ± 5.99	3.89 ± 0.15	1.84 ± 0.06
Fluticasone propionate			
0.0:1.0	81.9 ± 6.76	4.52 ± 0.14	2.09 ± 0.09
1.0:9.0	94.6 ± 1.85	3.75 ± 0.08	1.80 ± 0.05
1.0:4.1	109 ± 9.97	3.87 ± 0.30	1.72 ± 0.05
4.2:1.0	93.5 ± 12.7	3.77 ± 0.24	1.73 ± 0.03
9.0:1.0	104 ± 10.5	3.80 ± 0.27	1.95 ± 0.07

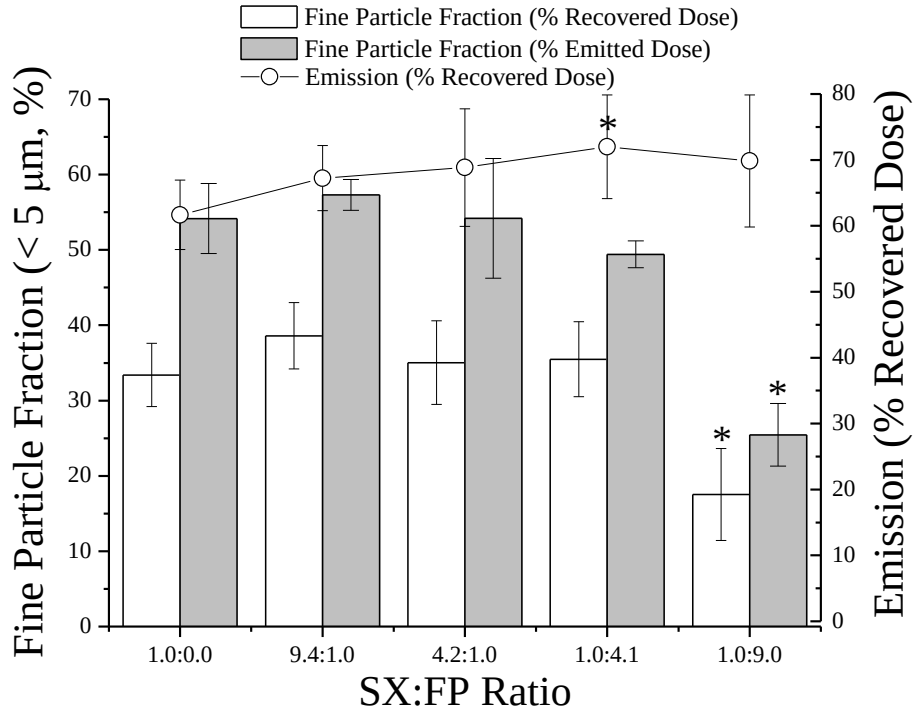

Figure 3.2 The fine particle fraction (FPF < 5 µm, expressed as a percentage of the emitted dose, ED, and recovered dose, RD) and emission (% RD) of salmeterol xinafoate (SX) when blended in combination with fluticasone propionate (FP) at different SX:FP ratios assessed by Next Generation Impactor analysis (mean ± SD, *n* = 4 - 6); * = $p < 0.05$ for single drug vs. combination blends using a one-way ANOVA with post-hoc Tukey's test.

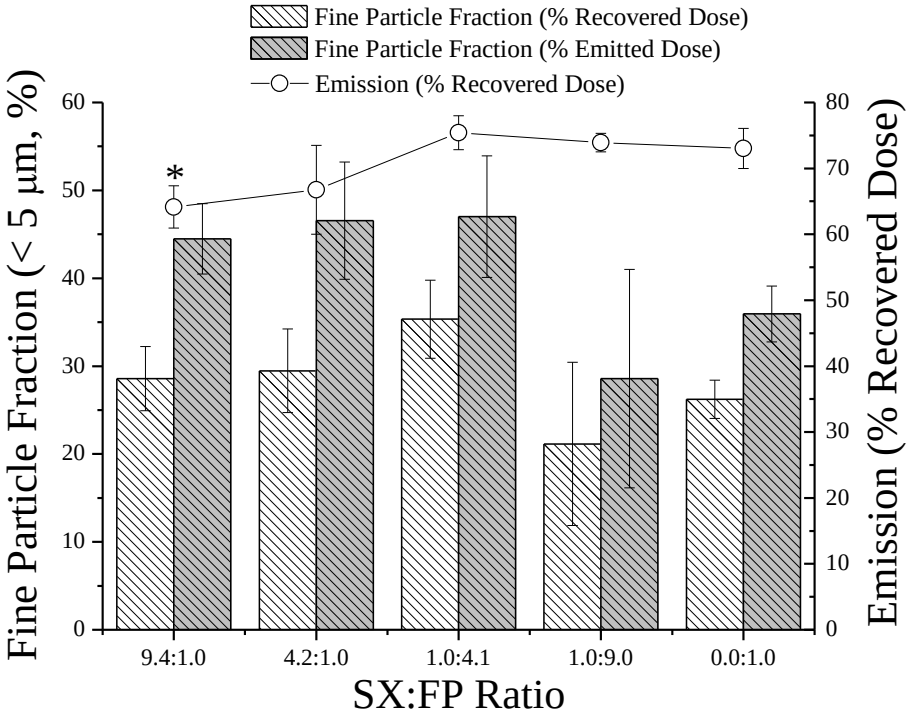

Figure 3.3 The fine particle fraction (FPF < 5 µm, expressed as a percentage of the emitted dose, ED, and recovered dose, RD) and emission (% RD) of fluticasone propionate (FP) when blended with salmeterol xinafoate (SX) at different SX:FP ratios assessed by Next Generation Impactor analysis (mean ± SD, *n* = 4 - 6); * = $p < 0.05$ for single drug vs. combination blends using a one-way ANOVA with post-hoc Tukey's test.

3.5.6 INVERSE GAS CHROMATOGRAPHY

3.5.6.1 WORK OF COHESION AND ADHESION FROM INFINITE DILUTION

In Chapter 2, the gross retention times of the probes (t_R) were obtained from IGC analysis at infinite dilution and used to calculate the net retention volume (V_N) and dispersive surface energy (γ_D) of both SX (36.23 ± 0.14 $mJ.m^{-2}$) and FP (49.92 ± 0.08 $mJ.m^{-2}$). Using Equation 2.11, these values were used to calculate the work of cohesion and adhesion, shown in Table 3.8. FP was found to be more cohesive than SX. SX-FP interactions were stronger that SX-SX interactions and weaker than FP-FP interactions.

Table 3.8 The work of cohesion and work of adhesion of salmeterol xinafoate (SX) and fluticasone propionate (FP) from inverse gas chromatography at infinite dilution (mean ± SD, triplicate injections of the probes were made onto a single column).

	Salmeterol xinafoate	**Fluticasone propionate**
Work of Cohesion ($mJ.m^{-2}$)	72.45 ± 0.29	99.85 ± 0.16
Work of Adhesion ($mJ.m^{-2}$)	85.05 ± 0.23	

3.5.6.2 SURFACE ENERGY AND WORK OF COHESION/ADHESION FROM FINITE DILUTION

Finite dilution IGC enabled surface energy heterogeneity maps to be constructed, and confirmed that FP had higher surface energy than SX (Figure 3.4). The results indicated that dispersive interactions formed the major contribution towards the total surface energy of both powders. Surface energy mapping further revealed that FP had much higher surface energy heterogeneity compared to SX. For example, the dispersive surface energy ranged from 40.18 to 48.33 $mJ.m^{-2}$ for FP compared to 36.9 to 38.5 $mJ.m^{-2}$ for SX. The surface energy values were lower compared to those generated from infinite dilution, particularly for FP. This difference is likely to arise from the overestimation of surface energy using the latter method due to low solute concentrations probing only the most energetic surface sites (Ylä-Mäihäniemi et al., 2008). The total surface energy was calculated by summing the dispersive and specific surface energy contributions.

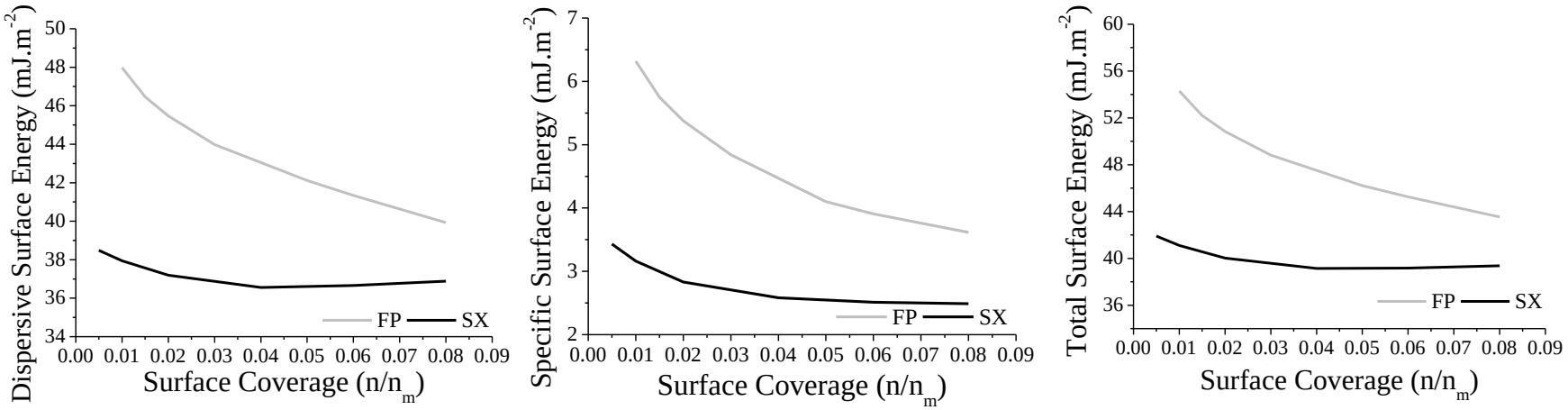

Figure 3.4 The dispersive, specific and total surface energy distributions of salmeterol xinafoate (SX) and fluticasone propionate (FP) assessed by finite dilution inverse gas chromatography.

The work of cohesion, determined from the total surface energy, also showed heterogeneity for both drugs ranging from 87.66 – 109.43 $mJ.m^{-2}$ for FP and 78.74 – 83.83 $mJ.m^{-2}$ for SX (Figure 3.5). The work of adhesion between SX and FP was larger than the work of cohesion of SX but smaller than the work of cohesion of FP. The work of cohesion or adhesion was calculated according to Equation 2.11 by matching the surface energy at equivalent surface coverages. However, due to the random orientation of particles within a bulk powder, situations may arise where for example an FP surface with high surface energy is adjacent to an FP surface with low surface energy. There will therefore be a complex distribution in the magnitude of interactive forces within the bulk, bracketed by the largest and smallest interactive forces shown in Figure 3.5 arising from interactions between the most energetic and least energetic surfaces on the particles. This will result in a complex blend structure and heterogeneity in agglomerate properties.

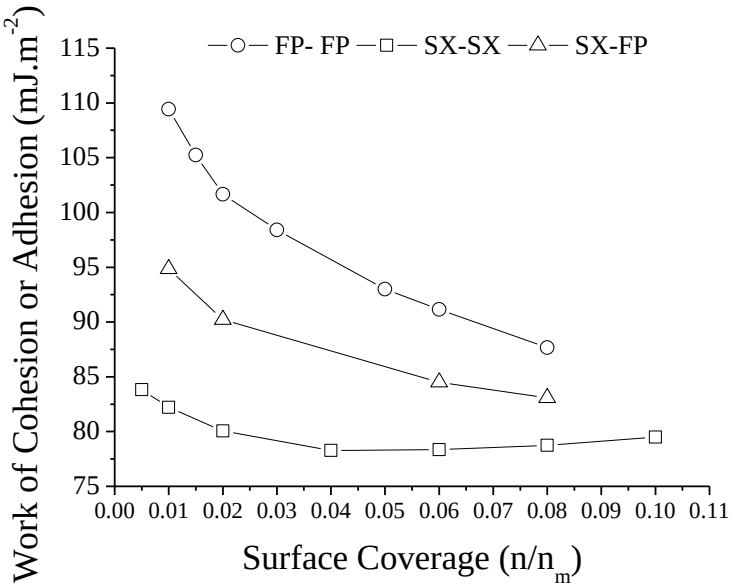

Figure 3.5 The work of cohesion and work of adhesion of salmeterol xinafoate (SX) and fluticasone propionate (FP) determined from the total surface energy distributions of the drug powders obtained by finite dilution inverse gas chromatography.

3.6 DISCUSSION AND CONCLUSIONS

Combination DPIs can contain up to four distinct particulate powders; two drugs, a coarse carrier and a fine/ternary agent. Inter-particulate interactions govern the efficiency of drug aerosolisation from such formulations and it is clear that a number of interactions are possible. It is well established that fine particles can improve the aerosolisation of a drug in the presence of carrier. This improvement is postulated to arise through the 'active sites' and/or 'agglomerates' mechanisms, both of which involve carrier particles (Shur et al., 2008). According to the 'agglomerates' mechanism, the drug and fines form mixed agglomerates which associate with the carrier. Fine particles however have the potential to alter the aerosolisation of drugs in the absence of carrier. For example, mixed SX and fine lactose agglomerates have been observed in carrier-free blends by SEM which exhibited reduced agglomerate strength compared to SX agglomerates (Adi et al., 2008a). In the current study, the ability of fine particles to alter the aerosolisation of the inhaled drugs SX and FP was investigated; these drugs are found in commercial combination DPIs and have demonstrated different deposition patterns compared to single-drug DPIs (Taki et al., 2011). In order to probe the origin of the altered deposition patterns, a systematic approach was taken to investigate the agglomerate behaviour of the drugs in the absence of a carrier to ascertain the performance modifying capabilities and any changes in dispersibility that might arise due to interactions between the drug particles. The implications of these interactions on the performance of DPI blends will be studied in a later chapter.

3.6.1 DISPERSION BEHAVIOUR OF SALMETEROL XINAFOATE AND FLUTICASONE PROPIONATE

An awareness of the dispersion modifying effects of drugs in combination formulations is important in order to optimise drug delivery. SX and FP have been found to have contrasting effects on each other's aerosolisation when formulated in combination (Taki et al., 2011). Interactions between SX and FP particles have been proposed (Michael et al., 2000; Michael et al., 2001; Taki et al., 2011) and the formation and deposition of the drugs as mixed agglomerates in the NGI has been suggested (Theophilus et al., 2006; Vernall et al, 2012). Comparing the aerosolisation of each drug separately, SX was found to have a lower emission (61.7 ± 4.65 % RD) than FP (73.3 ± 3.05 % RD). This may arise from high levels of adhesion between SX and the device and capsule walls

(Podczeck et al., 1996; Adi et al., 2008a). The FPF (% RD) of the drugs was comparable (33.4 ± 4.19 and 26.2 ± 2.17 %, respectively) however the FPF (% ED) of SX was much higher (54.2 ± 5.28 %) than FP (35.9 ± 3.17 %) indicating a greater de-agglomeration efficiency for SX. Less cohesive SX-SX agglomerates were therefore less well entrained but de-agglomerated in the turbulent airflow more readily than the more cohesive FP-FP agglomerates when the drugs were aerosolised into the NGI. The higher cohesivity and poorer dispersibility of FP compared to SX was supported by dispersibility assessment by dry dispersion laser diffraction. The CPP (4.0 Bar and 1.20 Bar, respectively) and DA_{50} values (0.48 Bar and 0.36 Bar, respectively) were both higher for FP than SX. The magnitude of the difference in these parameters was also larger for FP, indicating that although there was a proportion of FP agglomerates that dispersed readily (i.e. at 0.48 Bar for dispersion of 50 % of the bulk powder), there was also a proportion of very poorly dispersible agglomerates which required a much higher dispersing pressure for agglomerate break-up (i.e. 4.0 Bar). FP therefore had greater heterogeneity in agglomerate strengths within the bulk compared to SX, and this was further supported by the surface energy measurements from IGC. FP had higher surface energy and a higher work of cohesion than SX, and also showed higher surface energy heterogeneity across the particle surface as observed in the surface energy distributions.

The aerosolisation characteristics of SX and FP, in terms of their emission and FPF when aerosolised into the NGI may also be explained by their agglomerate sizes and the formation of metastable agglomerates, determined by their cohesivity. Micronised FP has previously demonstrated a high emission but low FPF when aerosolised alone into an impactor (Louey et al., 2004b). It was proposed that highly cohesive FP particles formed large agglomerates, which owing to their size provided good flow and entrainment properties, but poorer de-agglomeration (Louey et al., 2004b). It is also important to consider the powder emission process from a Monodose inhaler which is highly complex. Upon the introduction of an airflow through the device, the capsule begins to rotate. Powder within the capsule is then entrained and exits the holes at either end of the capsule, however, it may also undergo a degree of de-agglomeration as a result of mechanical impaction as the capsule rattles, and due to the complex airflows that arise. The mass of powder exiting the device therefore depends both on a combination of how well the powder entrains and de-agglomerates (Coates et al., 2005; Zhou et al., 2010a).

The distribution of agglomerates of different sizes and strengths comprising the powder structure will also be different between the powders. The theoretical tensile strength of an agglomerate is directly proportional to its work of cohesion, inversely proportional to its particle size, and is also related to the packing fraction and structure of the agglomerate (Kendall and Stainton, 2001). Begat et al. (2004b) describe a situation in which during dispersion the intra-agglomerate forces are equal to the forces available for agglomerate dispersion, resulting in metastable agglomerates; these metastable agglomerates will not disperse under the specific set of de-agglomeration conditions and will remain agglomerated in the airstream. The higher heterogeneity in the work of cohesion of FP would lead to the formation of a wider range of agglomerate sizes/strengths compared to SX, and therefore a higher propensity for metastable agglomerate formation. These agglomerates would deposit on stages of the NGI corresponding to larger aerodynamic particle sizes compared to individual FP particles, and may have contributed towards the lower FPF of FP. The greater heterogeneity in agglomerate strengths for FP was also apparent from dry dispersion laser diffraction analysis. The large difference between the DA_{50} and CPP parameters indicated that for complete dispersion of FP to individual particles high dispersal forces are required; if these high dispersal forces are not available then there will remain populations of tightly associated FP agglomerates in the airstream which would not disperse and therefore would deposit on the higher stages of the NGI.

3.6.2 DISPERSION MODIFICATION IN CO-FORMULATED POWDER BLENDS

In drug-only fine particle combination blends, the aerosolisation of SX became poorer in the presence of FP. The MMAD showed a gradual increase from 2.45 ± 0.12 µm for SX alone to 3.89 ± 0.15 µm in the presence of the largest amount of FP. The emission and FPF (% RD) were unchanged compared to SX alone except for when FP was incorporated in the highest ratio, whereupon the FPF RD and ED was reduced ($p < 0.05$) and the emission was higher, although not significantly, compared to SX alone. This was an important finding considering that commercial DPI formulations contain a small amount of SX (50 µg) and a larger amount of FP (100 – 500 µg). A comparison of single-active versus combination DPI inhalers also reported significantly altered deposition profiles for SX in the presence of FP, where the presence of FP caused a reduction in the FPD in the deeper stages of the NGI (Taki et al., 2011). It was

postulated by the authors that increasing FP concentration might be a factor in reducing the FPD. However, due to the presence of a carrier and the maintenance of a constant SX content whilst the FP content per 12.5 mg powder dose increased, it was not possible to deduce whether increasing FP content, reduced lactose content, or increased FP-to-lactose ratio were responsible for the changes observed. The results in the current study suggest that SX dispersion can be modified by FP only at high FP concentrations, at which point de-agglomeration efficiency becomes worse. These findings may not however be directly translatable to SX dispersion upon co-formulation in carrier-based DPI blends, and therefore would require the preparation and testing of co-formulated SX and FP in the presence of a carrier in order to confirm these effects on aerosolisation behaviour.

Considering FP, the alteration in aerosolisation was different compared to SX, when blended in combination. The MMAD of FP reduced ($p < 0.05$) from 4.52 ± 0.14 µm for FP alone to 3.75 ± 0.08 µm – 3.87 ± 0.30 µm in the presence of SX. The reduction in MMAD of FP was independent of the amount of SX in the blend. This suggested that there was weaker agglomeration of FP in the presence of SX, however, there was no change ($p > 0.05$) in the FPF (% RD) or FPF (% ED) of FP from the drug combinations compared to micronised FP alone, and there was a trend towards lower emission in higher SX content blends, significant only at the SX:FP ratio 9.4:1.0 compared to FP alone. Higher FPFs have been reported for FP in combination compared to single-active DPI products, where it was suggested that SX might have a small but significantly positive performance modifying effect on FP (Taki et al., 2011). However, once more in the latter study it was not possible to further determine whether this was due to SX content, the grade and/or content of coarse and fine lactose, or SX-FP agglomerates that had different dispersibility compared to FP-FP or FP-FL agglomerates between the single drug and combination inhaler products. It is also possible that all these factors may have contributed to the overall net improvement in the deposition of FP. Nevertheless, the results suggest that SX and FP particles may interact in combination, as the aerosolisation profiles of each drug were modified compared to those obtained after the aersolisation of each drug alone. Such a finding has also been reported for salbutamol sulphate (SS) and beclometasone dipropionate (BDP) when blended in combination in the absence of carrier (Jetmalani et al., 2012). These drugs were both predominantly adhesive, undergoing a physical interaction which resulted in lower aerosolisation efficiency (i.e. emission) for both drugs and lower FPF for BDP only

compared to drug alone. When comparing the FPF of SS and BDP between different drug ratios there was no significant change, indicating that the presence of a second drug, but not the quantity of that second drug, altered aerosol performance in this instance (Jetmalani et al., 2012).

In the current work, the presence of a second drug resulted in significant differences in the FPF of SX and the emission of FP in an SX-rich blend, when compared to the aerosol performance of the drug on its own. IGC analysis revealed that FP-FP interactions were the strongest, followed by SX-FP and SX-SX interactions (Figure 3.5). This explained the poorer homogeneity of SX in FP-rich compared to SX-rich blends (Table 3.4), due to poor SX interaction with FP leading to inadequate mixing. Therefore, in an FP-rich blend, FP-FP forces would dominate but in an SX-rich blend SX-FP forces would dominate. When cohesive FP forces dominate, the aerosolisation of FP would be unchanged in the presence of a small amount of SX due to little interaction between SX and FP particles; the excess amount of FP and strong FP-FP interactions would result in FP aerosolisation that was generally unchanged compared to that of FP alone. Any interactions between SX and FP which may arise for example due to the energy input during blending and the adhesive tendency of SX, would result in the formation of mixed agglomerates that were more tightly associated than SX-SX agglomerates but more weakly associated than FP-FP agglomerates. It is therefore not unexpected that the de-agglomeration efficiency of SX was generally reduced in the presence of FP whereas FP was unaffected due to more strongly and more weakly associated mixed agglomerates, if present, compared to the cohesive drug agglomerates of each powder, respectively.

Conversely, in SX-rich blends, a dominance of SX-FP interactions due to the adhesive tendency of SX would aid in the disruption of cohesive FP agglomerates. Although when in combination with SX, FP exhibited a smaller MMAD regardless of the amount of SX in the blend, this was insufficient to improve the emission or FPF. Any SX-FP agglomerates that formed would be weaker than FP-FP agglomerates and therefore be expected to entrain and disperse more readily. The fact that the FPF did not improve, and the emission was lower, was therefore unusual. This may have arisen from FP becoming ‘trapped’ in SX agglomerates which were retained in the device and/or capsules prior to agglomerate dispersion due to high SX adhesivity towards these surfaces. FP deposition in the device and capsules was observed to increase from 25.1 ±

2.35 % RD to 35.9 ± 3.22 % RD between the 1.0:9.0 and 9.4:1.0 SX:FP ratios, respectively. Alternatively, greater FP dispersion to individual particles due to weaker FP agglomeration may have increased FP retention in the device and capsules; individual FP particles, due to their smaller particle size and larger surface area, would be more likely to remain in the device/capsule compared to larger FP agglomerates which would exhibit better flow and entrainability. It is also necessary to consider the heterogeneity in the work of cohesion and adhesion, particularly for FP. For example, SX may have only been able to interact with the less cohesive FP particles within the bulk to form mixed agglomerates. There may have remained proportions of FP particles that were agglomerated by very cohesive interactions and thus their dispersion was not altered by the presence of SX, and these particles may have dictated the dispersion behaviour of FP, particularly in terms of the FPF, from the blends. For SX in an SX-rich blend, SX-FP forces would dominate and support the formation of mixed SX-FP agglomerates, however, due to the smaller amount of FP in the blend relative to SX, the proportion of these would be low such that the dispersion of SX was affected to a lesser extent in the presence of a small amount of FP compared to a large amount of FP.

The particle size-primary pressure profiles of the blends retained the distinctive shape seen for the micronised powders in Chapter 2. The particle size measured at the highest dispersing pressure in the dry state (D_{v50} = 2.00 ± 0.06 µm, 2.03 ± 0.12 µm, 2.12 ± 0.06 µm, 2.06 ± 0.08 µm) was comparable with the liquid dispersion size, however, the dry dispersed D_{v50} was always smaller (1.63 ± 0.01 µm, 1.52 ± 0.03 µm, 1.55 ± 0.01 µm and 1.66 ± 0.01 µm for the 1:8, 1:4, 4:1 and 8:1 ratios, respectively; $p < 0.05$, unpaired t-test). Differences may arise due to the use of different dispersing media, different laser diffractometers, incomplete dispersion in liquid media or particle attrition at high dispersing pressures in the air stream. Following empirical data modelling, the linearity of the data was good ($R^2 > 0.98$). The DA_{50}, a measure of the ease of dispersion, indicated that as the amount of FP in the co-formulated blend increased, the dispersibility of the blend became worse. The CPP (i.e. cohesivity) of the FP-rich blends was also higher (1.20 – 1.70 Bar) than the SX-rich blends (1.00 – 1.20 Bar). FP was more cohesive than SX (CPP 4.00 Bar and 1.20 Bar, respectively), therefore in the presence of SX the cohesivity of the blend reduced compared to FP alone, and suggested modifications in particulate interactions and agglomerate break-up within the blend. This may explain the smaller MMAD obtained for FP when in combination with

SX (regardless of the amount of SX) and the increasing MMAD of SX in the more cohesive, FP-rich blends.

Compared to both SX alone and FP alone, the bulk dispersibility of the blend improved in SX-rich blends, and became worse in FP-rich blends. This showed some agreement with the aerosol characteristics of the drugs when aerosolised in the NGI. For SX, the lowest FPF and largest MMAD were obtained in the highest FP-content blend when comparing SX aerosolisation between single drug and co-delivery, and between the ratios. Conversely for FP, although the MMAD was lower, the FPF across the ratios was unchanged compared to single drug delivery and the emission worsened in the highest SX content blend. This method could therefore be used as a pre-formulation screening tool to assess the influence of fine particles on bulk blend aerosolisability. Although this information does not in isolation allow the aerosolisation behaviour of the drugs to be predicted following cascade impaction, it will help guide the formulation and device characteristics that may be required to optimise aerosolisation. Further development of the method to discriminate between the different de-agglomeration behaviours of individual powders within mixtures could further strengthen the method for use in dispersibility screening.

3.6.3 CONCLUSIONS

In conclusion, the study completed in this chapter has demonstrated that the dispersibility of SX and FP drug particles was modified by the presence of a second fine drug particle in the absence of a carrier. The fine particles investigated are components of combination dry powder inhaler formulations, and therefore determining their influence on drug aerosolisation might assist optimal formulation design. FP had a lower MMAD in the presence of SX regardless of SX concentration however the FPF was generally unchanged but the emission reduced in high SX content blends. The aerosolisation of SX was poorest at high FP concentrations, where the FPF reduced, and the MMAD sequentially increased as the amount of FP in the blend increased. Dry dispersion laser diffraction de-agglomeration analysis was able to detect differences in the bulk dispersibility/de-agglomeration of the blends, but differences in the dispersion mechanisms (i.e. those attained in the feeding/dispersing line of the Sympatec versus those imparted by the device/capsule after aerosolisation for impactor analysis) resulted in some discrepancies between the trends seen in the laser diffractometer and impactor.

The different adhesive and cohesive tendencies of the drugs were able to explain the changes in agglomeration that in turn affected the overall aerosolisation behaviour. This work has indicated that SX and FP particles have the potential to interact resulting in a range of agglomerate populations with different dispersibilities. The implications of these interactions when formulated with a carrier therefore warrants further investigation.

4 PHYSICOCHEMICAL CHARACTERISATION, AGGLOMERATION BEHAVIOUR AND DISPERSION OF BULK, AERODYNAMICALLY SIZE-FRACTIONATED AND RE-CRYSTALLISED DRUG POWDERS

4.1 INTRODUCTION

Micron-sized particles for delivery to the lungs can be produced using a number of different methods. Crystallisation is the most common process employed, however, drug particles are rarely crystallised directly to the required or optimum particle size. Therefore, a comminution step such as micronisation/milling is required (Ward and Schultz, 1995). Traditionally particles are placed in a fluid-energy, often an air jet mill, and undergo comminution as a result of mechanical fracture from particle collisions at high speeds (Malcolmson and Embleton, 1998). There is, however, poor control over the physicochemical properties of the particles, including the particle size and size distribution, shape, morphology, electrostatic charge and surface properties (Steckel et al., 2003b; Steckel et al., 2006; Perkins et al., 2009). The high energy input and mechanical stress that particles experience can introduce disorder onto surfaces as a result of disruptions to the crystal structure beyond that of an occasional molecular dislocation, such as extensive crystal fracture and lattice rearrangement (Ward and Schultz, 1995). This can result in the conversion of crystalline surfaces into partially amorphous surfaces (Brodka-Pfeiffer et al., 2003b; Steckel et al., 2003b; Gaisford et al., 2010). Thermodynamically, amorphous regions are at a higher energy state and metastable, and in time may revert back to their crystalline form (Ward and Schultz, 1995). The amorphisation of micronised particles can lead to the creation of more energetic surfaces possessing higher surface energy (Perkins et al., 2009; Das and Stewart, 2012; Gamble et al., 2012), which can increase inter-particulate attractive forces resulting in greater adhesion and cohesion to other materials (Cline and Dalby, 2002; Perkins et al., 2009).

The process induced changes resulting from the micronisation process can lead to batch-to-batch variability between powders in terms of their surface energy (Ticehurst et al., 1994; Feeley et al., 1998), flow (Feeley et al., 1998), cohesive properties/agglomeration (Kubavat et al., 2012; Le et al., 2012b) and physical stability (Ward and Schultz, 1995). This has important implications in the performance characteristics of inhaled drugs, where the cohesive-adhesive balance of the formulation is a major determinant of the efficiency at which a drug is delivered from a DPI and deposits in the lungs. For example, FP has demonstrated a shift from an initial cohesive FP-FP led system to a more adhesive FP-SX led system with increasing numbers of milling cycles (Kubavat et al., 2012). Furthermore, intra-batch variability may also arise. Differing levels of

processing stress experienced across various sites within a bulk powder may lead to micro-areas of powder which possess different properties (Marek et al., 2011). This may manifest as altered flowability and aerosol dispersion/de-agglomeration behaviour (Marek et al., 2011; Das et al., 2012) and have implications following formulation. In Chapter 3, it was observed that the aerosolisation behaviour of salmeterol xinafoate (SX) and fluticasone propionate (FP) powders altered following co-formulation in the absence of a carrier, and there were changes in powder structure. These effects may have been specific to the batches of powder tested, and the specific powder micro-structures arising from intra-batch variability in powder properties within the bulk powder. There is therefore merit in attempting to characterise bulk micronised powders for their variability in particle, agglomeration and dispersion properties.

Particle engineering approaches have been developed as alternatives to micronisation. The direct crystallisation of particles to the appropriate size can be achieved by anti-solvent precipitation from conventional or supercritical fluids. This has the potential to overcome problems associated with the introduction of amorphous content whilst allowing for a degree of control in surface solid state (Murnane et al., 2008a). By controlling the experimental parameters, specifically the stirring speed and addition rate of the anti-solvent, it was possible to produce particles with a size suitable for inhalation (Murnane et al., 2008a; Murnane et al., 2008b). Furthermore, both SX and FP were found to crystallise into their most stable polymorphic form and display either similar, in the case of FP (Murnane et al., 2008b), or higher (for SX) crystalline content (Murnane et al., 2008d) than micronised material. Particles which are directly crystallised to their required particle size have exhibited lower surface energy than particles which are micronised after crystallisation (e.g. Rehman et al., 2003; Shekunov et al., 2003) and have displayed more favourable aerosolisation, for example higher FPFs following cascade impaction (e.g. Steckel et al., 2003a; Steckel et al., 2003b).

Although particle engineering technologies enable particle production in the micron-size range, there remains an inability to control the aerodynamic particle size. It is the aerodynamic size which is generally accepted as a key parameter in determining lung deposition (Usmani et al., 2005), and takes into consideration the geometric size, shape and density of the particle (De Boer et al., 2002a). Impactors such as the NGI fractionate aerosolised particles on the basis of aerodynamic particle size. They are typically used for the assessment of inhaler performance; however, the NGI has recently

been used to isolate SX, FP and fine lactose particles with a controlled aerodynamic particle size (Taki et al., 2011b). Powder depositing on stages 1 to 6 demonstrated sequentially smaller aerodynamic diameters, along with a statistically significant linear relationship with the geometric particle size of each fraction. The deposits also showed lower span values compared to the unfractionated powder, indicating a reduction in the polydispersity of the deposited powder (Taki et al., 2011b). The technique has therefore been proposed as a useful research tool to investigate drug-drug interactions because operation of the impactor is not affected by powder physicochemical properties. Hence, differences in the performance of aerosols of fractionated powders may be attributed to differences in the physicochemical properties or processing of particles within the bulk powder rather than the aerodynamic particle size (Taki et al., 2011b).

4.2 AIM AND OBJECTIVES

The aim of this study was to isolate SX and FP fractions of known aerodynamic particle size from the bulk starting powder, and then characterise the particles within each fraction with regard to their physicochemical properties and dispersibility. The objectives were to:

a) Determine the geometric particle size of commercial micronised SX and FP powders.

b) Crystallise SX and FP with a view to generating powders of equivalent size but with altered solid state properties compared to the micronised powders.

c) Fractionate the commercial micronised SX and FP powders to isolate fractions with different aerodynamic particle sizes.

d) Characterise unfractionated, fractionated and recrystallised SX and FP powders so as to determine the following:
    a. Geometric particle size,
    b. Morphology,
    c. Crystalline/amorphous content,
    d. Surface energy distribution,
    e. Dispersibility.

4.3 MATERIALS

The materials and equipment used in Chapter 4, not listed in Section 2.3 and 3.3, are shown in Table 4.1.

Table 4.1 Suppliers of materials and equipment (Chapter 4).

Material / Equipment	**Supplier**
Fluticasone propionate (FP); BN. 5501-B-11030	LGM Pharma, USA
Polypropylene glycol 400 (PEG400)	Sigma Aldrich Ltd, UK
Malvern QSpec dry powder feeder (DPF)	Malvern Instruments Ltd, UK
High shear mixer (Model L4RT laboratory homogeniser)	Silverson Machines, USA
Hydrophobic PTFE syringe filters (pore size 0.2 µm)	Whatman™ (now part of GE Healthcare, supplied by Fisher Scientific Ltd, UK)
Heidolph overhead stirrer (RZR 2051 2051)	Heidolph, UK
Brucker D8 Advance X-ray diffractometer system	Brucker AXS Ltd, USA
Q Series differential scanning calorimeter; Q20-5023 for SX samples, Q200-1934 for FP samples	TA Instruments, UK
Aluminum DSC pans and lids	TA Instruments, UK
Hermetic Press for SX samples and Tzero press for FP samples	TA Instruments, UK
IGC Surface Energy Analyser (SEA)	Surface Measurement Systems Ltd, UK
Helium penta-pycnometer	Quantachrome Instruments, USA

4.4 METHODS

4.4.1 AERODYNAMIC FRACTIONATION OF DRUG POWDERS

Aerodynamic fractionation was conducted using an NGI in preparative mode as described previously (Taki et al., 2011b). The NGI was assembled and connected to a vacuum pump (Twin Impinger Model, TI2). The flow rate through the NGI was measured at the air inlet i.e. throat using a flow meter with a tightly fitting seal. The

flow was adjusted to 60 L.min^{-1} using the flow control valve on the pump. The NGI plates were used uncoated and the drug was aerosolised into the NGI using a Malvern QSpec dry powder feeder. The DPF was placed on a lab jack and the height adjusted so that the outlet of the DPF was in line with the centre of the NGI throat. The DPF was connected to a supply of compressed air and vacuum using the appropriate ports on the feeder via vacuum tubing. The jet pressure was set between dial marks 2 and 3 and the feed rate was set between dials 4 and 7 depending on the amount of powder that was visualised leaving the feeder and depositing on the stages in order to ensure a sufficient amount of powder was aerosolised per fractionation cycle but not too much as to overload the NGI. Approximately 1- 2 g of powder was loaded into the DPF feeding tray, the DPF switched on and the airflow dial set to 'airflow'. The vacuum pump connected to the NGI was then switched on, followed a few seconds later by the airflow dial being set to 'feed' for a period of 2 min. The airflow dial was then switched back to 'airflow' and after 10 – 15 s the vacuum pump switched off. The NGI was disassembled and the powder deposits recovered. The deposits were carefully removed using a plastic scraper and transferred into clean, dry pre-weighed glass vials. Each vial was labelled with the stage and the mass of recovered powder recorded. As the quantity of powder in the DPF reduced, it was necessary to run each cycle for up to 4 min at the highest feed rate in order for sufficient material to be deposited for recovery. The fractionation cycles were repeated until a yield of approximately 1 g was obtained on any two of the stages.

4.4.2 RE-CRYSTALLISATION OF DRUG POWDERS

Precipitation by anti-solvent crystallisation was undertaken as previously described (Murnane et al., 2008a-d) to generate re-crystallised control particles. PEG400 solutions were prepared containing 4.5 % w/w SX or 0.65 % w/w FP by weighing approximately 1 g of each drug into a glass beaker and making to final weight with PEG. SX solutions were subjected to high shear mixing (Silverson model L4RT laboratory homogeniser) at 2100 rpm for SX and according to the following protocol for FP: 2000 rpm for 10 min, 3000 rpm for 10 min, and 1000 rpm for 5 min until the powder dissolved. This was followed by ultrasound sonication for 5 min to degas the solutions. The solutions were then filtered through a 0.2 µm hydrophobic PTFE syringe filter prior to anti-solvent addition. The addition of anti-solvent (water) was carried out until a ratio of 1:11 (solution:water) for SX and 1:7 for FP was obtained, and occurred at a rate of 20 g.min^{-}

$^{1}.g^{-1}$ of solution, whilst the mixture was stirred using an Heidolph overhead stirrer. During addition, water was passed through a funnel which was positioned such that the water entered along the inside wall of the vessel. Stir speeds were 1000 rpm for SX solutions and ramped from 700 to 1430 rpm during the period of water addition for FP solutions. The crystals were then harvested by vacuum filtration (0.2 µm nylon filter) and dried overnight at 50 °C in a vacuum oven. The following day the dried powder was washed with 200 mL cold water (pre-cooled to 4 °C) with the aid of stirring at 1470 rpm for 5 min. The crystals were again harvested by filtration and dried overnight. Finally, the crystals were de-caked by sonicating (5 – 6 min) with 15 mL cyclohexane and vacuum drying at 50 °C for 3 h. The crystals were transferred into glass vials and stored in a desiccator until required.

4.4.3 PARTICLE SIZE ANALYSIS BY LASER DIFFRACTION

Laser diffraction particle sizing of SX (n = 4) and FP samples (n = 6) was carried out using the Malvern Mastersizer X as described in Section 2.4.1. Particle size calculations were based on Mie theory, using the presentations 2OHD and 2NHE for SX and FP, respectively.

4.4.4 SCANNING ELECTRON MICROSCOPY

The morphology of crystallised and fractionated SX and FP powders was viewed using an FEI Quanta 200F field emission scanning electron microscope. The samples were mounted and images generated as described in Section 2.4.2.

4.4.5 DISPERSIBILITY ASSESSMENT BY LASER DIFFRACTION

The dispersibility of the SX and FP samples was assessed using the dry dispersion laser diffraction methodology developed in Chapter 2. The Sympatec HELOS/RODOS was used with the rotary feeder and protruding aspiration tube as described in Section 2.4.4, using a timebase of 100 ms, and trigger conditions of $C_{opt} \geq 1.1$ % to start a measurement and $C_{opt} \leq 1.0$ % for 5 s (or 60 s real time) to end a measurement. Particle size measurements (preceded each time by a reference measurement) were taken at PPs in the range 0.3 – 5.0 Bar (n = 1) for each sample. The data were analysed as described

in Section 2.4.4.1 and Section 2.4.5, using the D_H/D_x approach calculated using D_{V50} measurements, and empirically modelled according to Equation 2.8.

4.4.6 CRYSTALLINE/AMORPHOUS CONTENT DETERMINATION

4.4.6.1 DIFFERENTIAL SCANNING CALORIMETRY

DSC thermographs for SX samples were produced using a Q20 – 5023 Q Series differential scanning calorimeter. Approximately 1 mg of sample was accurately weighed into an aluminium pan and the latter hermetically sealed using a press. An empty pan was weighed and sealed for use as the reference. Prior to analysis the instrument was calibrated by heating an indium standard at the required heating rate to 170 – 200 ^oC. SX samples were equilibrated at 30 ^oC and maintained isothermal for 10 min. The sample was then heated to 160 ^oC at heating rates of 0.1, 0.5, 1, 2, 5, 10, 20 and 40 $^oC.min^{-1}$ under a nitrogen purge at 50 $mL.min^{-1}$ (n = 3). The onset and peak melting temperatures, and the enthalpies of fusion were derived from integration of the relevant peaks using TA Universal Analysis 2000 software (version 4.5.2, TA Instruments, UK).

DSC thermographs for FP were generated using a Q200 – 1934 Q series differential scanning calorimeter. FP samples (including the reference sample) were prepared as for SX except a pinhole was made in the lid prior to sample preparation (using a BD microlance 3, 21G x 2" 0.8 x 50 mm needle) and pans were sealed using a Tzero press. The same indium sample was used to calibrate the instrument at 20 $^oC.min^{-1}$. FP samples were equilibrated at 30 ^oC, held isothermal for 5 min and ramped to 320 ^oC at a heating rate of 20 $^oC.min^{-1}$. Analysis was conducted in triplicate (n = 3) under a nitrogen purge of 50 $mL.min^{-1}$. Analysis of the thermographs was conducted using TA Universal Analysis 2000 software, version 4.5.2 (TA Instruments, UK).

4.4.6.2 POWDER X-RAY DIFFRACTION

Powder x-ray diffraction (PXRD) was conducted using a Brucker D8 Advance x-ray diffractometer system. X-rays were generated by a copper (Cu) source operated at a 40 kV tension and 40 mA current. Powder samples were mounted onto a zero background sample holder and scanned from $2\theta = 4 – 30^o$ for SX samples and $2\theta = 4 – 35^o$ for FP samples, with a step size of 0.039^o and count time of 0.5 s per step.

4.4.7 INVERSE GAS CHROMATOGRAPHY AT FINITE DILUTION

Surface energy analysis of the crystallised and fractionated samples was conducted using an IGC Surface Energy Analyser as described in Section 3.4.8.1 to determine the surface energy distributions of the samples.

4.4.8 HELIUM PENTAPYCNOMETRY

A helium penta-pycnometer was used to measure the true density of micronised (i.e. unfractionated) SX and FP powders. Each sample was weighed directly into a sample cell (1.0 – 1.5 g) and placed in the instrument which was operated using flow purge mode. The maximum number of runs and run deviation were set at 3 and 0.005 % respectively, such that measurements would continue until three that were within 0.005 % of each other were obtained. The maximum purge time was 60 min.

4.4.9 NEXT GENERATION IMPACTOR ANALYSIS

NGI analysis was conducted as described in Section 3.4.6, using a reduced fill weight of 10.00 ± 1.00 mg for each capsule due to the more limited quantity of each sample that was available. Powder was aerosolised into the NGI at 60 $L.min^{-1}$ for 4 s from a Monodose inhaler device (ΔP = 1.4 kPa). Drug recovery quantification was effected using the HPLC method described in Section 3.4.1.1. Pooled mixed standard calibration curves (n = 5) in the range 1 – 25 $\mu g.mL^{-1}$ (R^2; SX = 0.999, FP = 0.998) and 40 – 400 $\mu g.mL^{-1}$ (R^2; SX = 0.998, FP = 0.997) in which each curve was freshly prepared on separate days, were used to quantify drug recovery. The LOD and LOQ values were 0.2 $\mu g.mL^{-1}$ and 0.7 $\mu g.mL^{-1}$, and 4.0 $\mu g.mL^{-1}$ and 13.5 $\mu g.mL^{-1}$ for the lower and upper concentration ranges of SX, respectively. The LOD and LOQ values were 0.3 $\mu g.mL^{-1}$ and 0.8 $\mu g.mL^{-1}$, and 5.1 $\mu g.mL^{-1}$ and 16.9 $\mu g.mL^{-1}$, for the lower and upper concentration ranges of FP, respectively. Quantification of individual samples was routinely made using the lower concentration range curve, except where samples were outside this range in which case the upper range curve was used.

4.5 RESULTS

4.5.1 AERODYNAMIC FRACTIONATION

Both SX and FP were fractionated at 60 $L.min^{-1}$ and required approximately 12 – 15 g of material to be fed through the NGI to achieve a sufficient yield (approx. 1 g) on the individual stages for further analysis. The fractionation process was therefore labour-intensive and inefficient in terms of material and operator time. For both powders losses occurred in the DPF, via deposition in the throat and during powder recovery from the stages. SX was more difficult to recover from the stages due to the powder being highly electrostatic, leading to greater losses compared to FP. For SX the largest recovery was on stage 4 (d_{ae} = 1.66 – 2.82 µm) followed by stage 5 (d_{ae} = 0.94 – 1.66 µm). Recoveries on the remaining stages were much lower, and this was attributed to the narrow particle size distribution of the original micronised material. During fractionation, it was noticed that a large proportion of SX deposited in the pre-separator (d_{ae} > 12.8 µm) therefore this material was collected as an additional fraction. For FP, maximum deposition occurred on stage 4 followed by stage 3 (d_{ae} = 2.82 – 4.46 µm). Once more, powder recovery from the remaining stages was much lower and there was negligible deposition on stage 7 (d_{ae} = 0.34 – 0.55 µm) and the micro-orifice collector (MOC). The shift in yield towards stages corresponding to larger aerodynamic particle sizes for FP compared to SX was attributed to the larger particle size of the original micronised FP material. Like SX, a large proportion of material deposited in the pre-separator and this was therefore collected as an additional fraction (Table 4.2).

4.5.2 POWDER PRODUCTION BY RE-CRYSTALLISATION

Ampiphilic crystallisation was successfully employed to produce SX and FP crystals. The differing concentrations of SX and FP in the drug-PEG400 solutions reflected the different solubility values of the drugs in PEG400, where FP has poorer solubility. Two batches of re-crystallised SX were produced; the first employed a drug to anti-solvent ratio of 1:11 and the second a ratio of 1:7 in an attempt to reduce the particle size of the crystals. However, both batches of particles were found to have comparable particle sizes. The batches were therefore combined and washed as described in Section 4.4.2 to generate the final batch of crystals for testing.

4.5.3 PARTICLE SIZE ANALYSIS BY LASER DIFFRACTION

The PSDs of unfractionated, crystallised, pre-separator and stage fractionated SX sized using liquid dispersion laser diffraction are shown in Figure 4.1 and Table 4.2. Crystallised SX (CSX) was larger in size than unfractionated SX however both had a D_{v50} smaller than 5 µm and therefore may be deemed as suitable (in terms of appropriate particle size) for inhaled delivery. Material depositing in the pre-separator and stages 1 – 4 was comparable in particle size and these samples also were similar in size to the unfractionated material following dispersal in liquid, despite the aerodynamic particle sizes of the stages being markedly different. It is postulated that powder depositing on these stages remained agglomerated, and that agglomerates with an equivalent aerodynamic size to the stage in question deposited rather than discrete particles. Hence, following dispersion in liquid to individual particles, the measured particle size between the samples was comparable. Material depositing on stages 5, 6 and 7 showed a gradual shift towards a smaller particle size, and displayed geometric particle sizes that were comparable with the aerodynamic size of the respective stage. Therefore, powder depositing on these stages may have comprised fully dispersed particles.

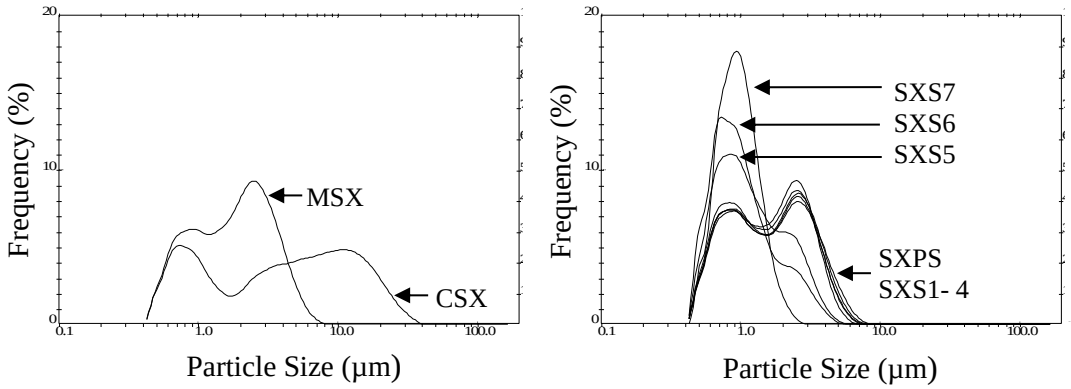

Figure 4.1 The particle size distribution of micronised (i.e. unfractionated) salmeterol xinafoate (MSX), crystallised salmeterol xinafoate (CSX), pre-separator salmeterol xinafoate (SXPS) and stage fractionated salmeterol xinafoate (SXS1-7) samples sized by liquid dispersion laser diffraction (*n* = 1 measurement shown).

Table 4.2 The particle size distribution (represented by the D_{v10}, D_{v50} and D_{v90}) of unfractionated, crystallised, and fractionated salmeterol xinafoate (SX) and fluticasone propionate (FP) sized by liquid dispersion laser diffraction (mean ± SD, *n* = 4 and 6, respectively) and the aerodynamic cut sizes across the Next Generation Impactor when operated at 60 $L.min^{-1}$, representing the minimum size of particles depositing on the corresponding stage.

		Salmeterol xinafoate				**Fluticasone propionate**			
Sample	**Stage d_{ae} (Minimum, µm)**	**Yield (mg)**	**D_{v10} (µm)**	**D_{v50} (µm)**	**D_{v90} (µm)**	**Yield (mg)**	**D_{v10} (µm)**	**D_{v50} (µm)**	**D_{v90} (µm)**
Unfractionated	n.a	n.a.	0.62 ± 0.00	1.42 ± 0.08	3.78 ± 0.23	n.a.	1.04 ± 0.40	2.94 ± 1.22	6.10 ± 2.65
Crystallised	n.a	840.1	0.72 ± 0.01	4.93 ± 0.37	17.4 ± 1.07	1157.0	1.09 ± 0.42	3.62 ± 1.43	10.8 ± 4.67
Pre-separator*	12.8	704.2	0.64 ± 0.00	1.51 ± 0.05	3.65 ± 0.23	2887.5	0.97 ± 0.01	2.39 ± 0.09	4.83 ± 0.49
Stage 1	8.06	20.0	0.65 ± 0.01	1.51 ± 0.06	3.32 ± 0.10	87.5	0.99 ± 0.03	2.41 ± 0.13	5.07 ± 0.58
Stage 2	4.46	100.1	0.65 ± 0.00	1.54 ± 0.06	3.54 ± 0.12	464.5	1.00 ± 0.03	2.48 ± 0.22	5.03 ± 0.66
Stage 3	2.82	423.2	0.66 ± 0.01	1.72 ± 0.11	3.86 ± 0.29	1029.6	0.95 ± 0.02	2.14 ± 0.18	3.93 ± 0.54
Stage 4	1.66	1704.2	0.64 ± 0.01	1.51 ± 0.06	3.51 ± 0.18	1362.5	0.88 ± 0.01	1.91 ± 0.09	3.56 ± 0.35
Stage 5	0.94	1158.7	0.61 ± 0.00	1.12 ± 0.04	2.78 ± 0.23	318.7	0.71 ± 0.02	1.59 ± 0.12	3.28 ± 0.29
Stage 6	0.55	162.8	0.59 ± 0.03	0.93 ± 0.02	2.10 ± 0.42	44.8	0.65 ± 0.02	1.46 ± 0.23	3.50 ± 0.61
Stage 7	0.34	35.9	0.55 ± 0.01	0.87 ± 0.05	1.92 ± 0.33	-	-	-	-

*The pre-separator SX fraction was not collected throughout the whole fractionation process and hence does not reflect the total yield of the fraction isolated from the unfractionated powder.

The PSDs of unfractionated, crystallised, pre-separator and stage deposits of FP sized using liquid dispersion laser diffraction are shown in Figure 4.2 and Table 4.2. As for SX, the particle size of the crystallised FP (CFP) material was larger than the micronised (i.e. unfractionated) material but once more the D_{v50} was smaller than 5 µm. The particle size of deposits in the pre-separator and stages 1 – 4 were comparable in magnitude both to each other and to that of the unfractionated material, indicating that powder may have deposited in an agglomerated state. There was however also a slight shift towards smaller particle sizes, which was not seen with SX. Samples of powder depositing on stages 5 and 6 had a smaller geometric size and therefore may indicate the deposition of fully dispersed powder particles on these stages.

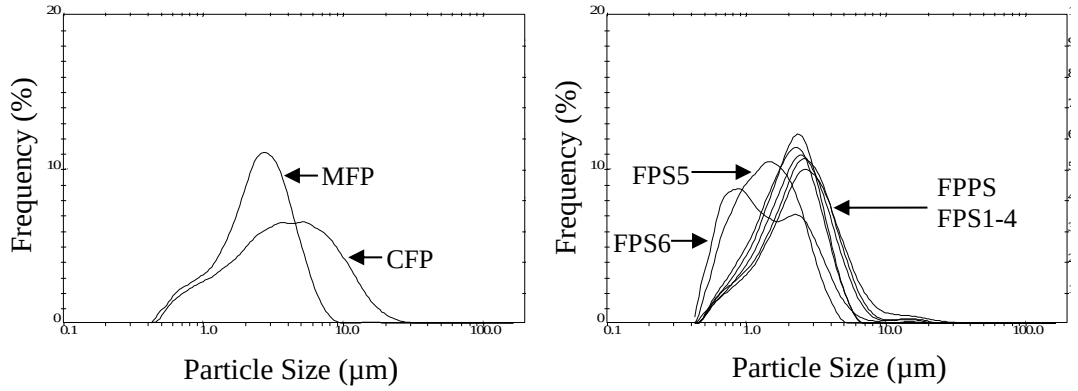

Figure 4.2 The particle size distribution of micronised (i.e. unfractionated) fluticasone propionate (MFP), crystallised fluticasone propionate (CFP), pre-separator fluticasone propionate (FPPS) and stage fractionated fluticasone propionate (FPS1-6) samples sized by liquid dispersion laser diffraction (n = 1 measurement shown).

4.5.4 SCANNING ELECTRON MICROSCOPY

The morphology of unfractionated and crystallised SX is shown in Figure 4.4. The unfractionated material displayed agglomerates of variable size with individual particles that were irregular in shape. The crystallised material comprised larger agglomerates and individual particles that were flatter than the unfractionated particles. The morphology of the fractionated SX powders is shown in Figure 4.5. Once more agglomeration was observed in all the samples. There was negligible difference between the agglomeration and particle morphology of the fractionated and unfractionated SX material. The morphology of unfractionated and crystallised FP is also shown in Figure 4.4. FP particles had a more regular, rounded morphology than SX and formed tightly packed agglomerates. The crystallised material showed a distinct change in

morphology, the particles were needle-like and the powder appeared to form smaller agglomerates. The morphology of the fractionated FP powders is shown in Figure 4.6. The pre-separator fraction appeared to form larger agglomerates compared to the unfractionated and stage deposited powder. Visually, there was no apparent change in agglomerate and particle morphology between the fractionated and unfractionated FP material.

4.5.5 CRYSTALLINE/AMORPHOUS ASSESSMENT

4.5.5.1 DIFFERENTIAL SCANNING CALORIMETRY

DSC thermographs revealed differences in the melting behaviour of unfractionated, crystallised and fractionated SX (Figure 4.3). Each sample displayed an initial melting peak corresponding to the melting of SX-I followed by an exotherm corresponding to the re-crystallisation of SX-II from the melt. This was followed by a second melting peak corresponding to the melting of SX-II. Unfractionated and crystallised SX showed a much smaller SX-II melting peak compared to the fractionated samples. Increasing the heating rate inhibited the crystallisation and subsequent melting of the SX-II polymorph in all the samples. For unfractionated and crystallised SX this occurred at 1 and 5 $^{o}C.min^{-1}$ respectively, however, for the fractionated samples a higher heating rate of 40 $^{o}C.min^{-1}$ was required.

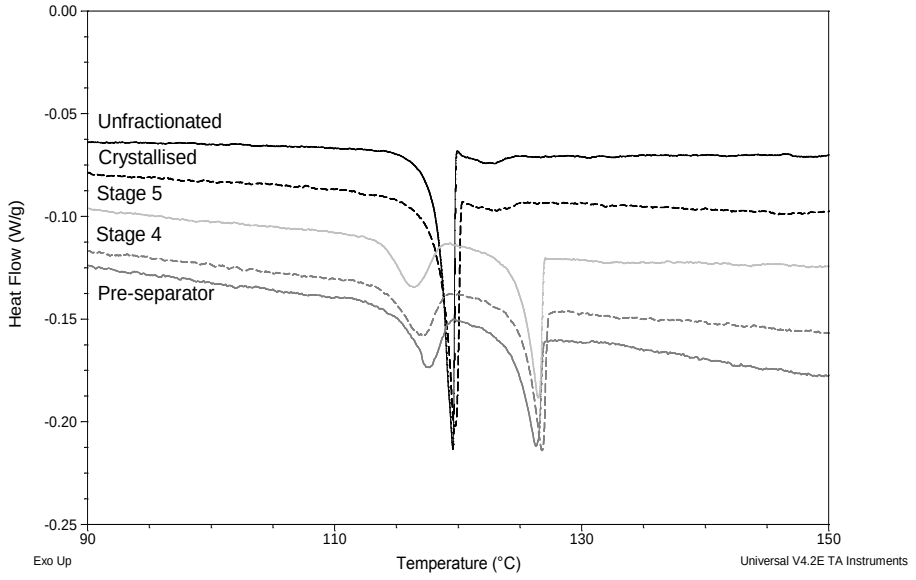

Figure 4.3 Differential scanning calorimetry thermographs of unfractionated, crystallised and fractionated salmeterol xinafoate at a heating rate of 0.1 $^{o}C.min^{-1}$ (n = 1 measurement shown).

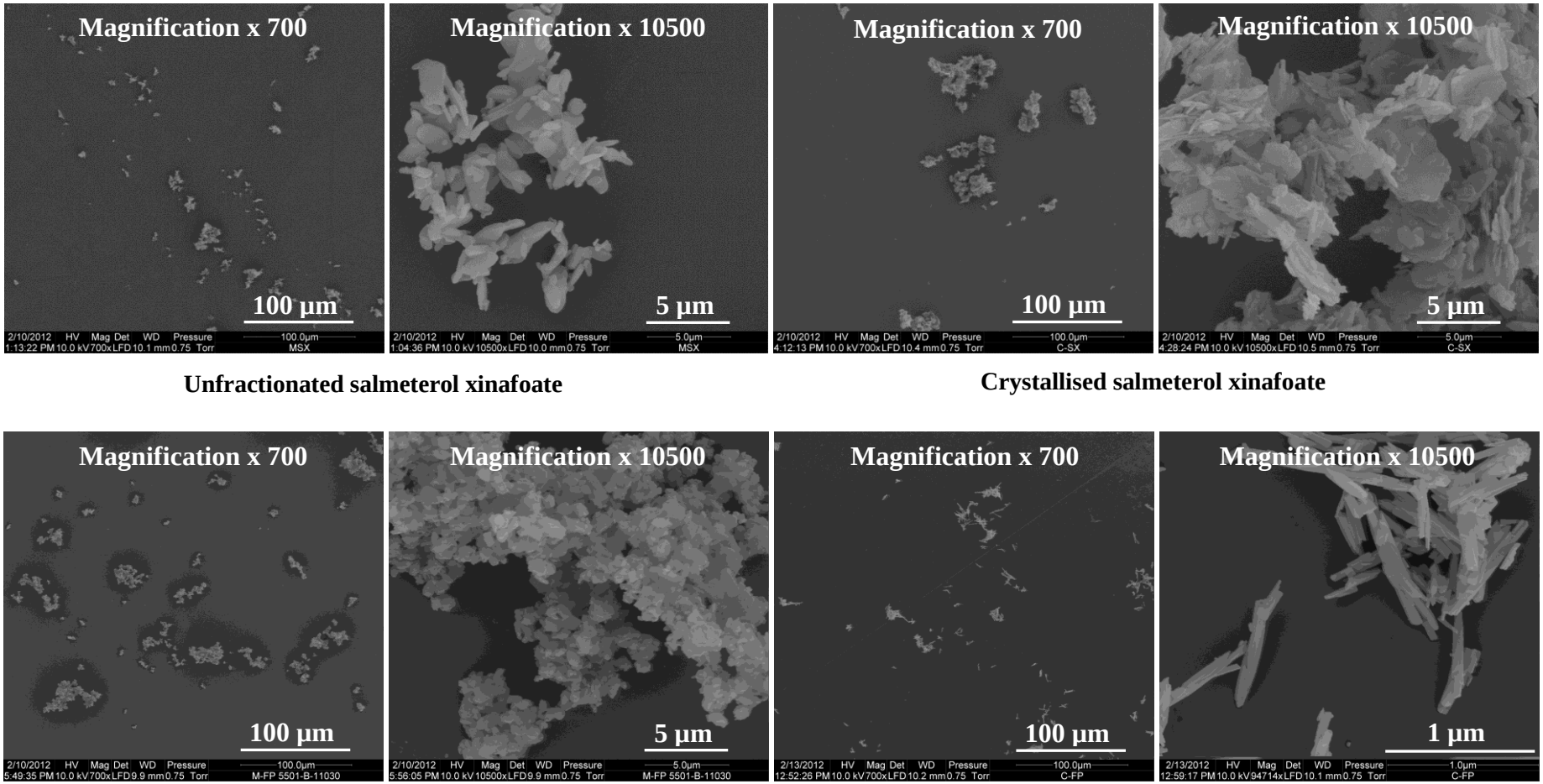

Figure 4.4 Morphology of unfractionated and crystallised salmeterol xinafoate and fluticasone propionate viewed by scanning electron microscopy at x 700 and x 10500 magnification.

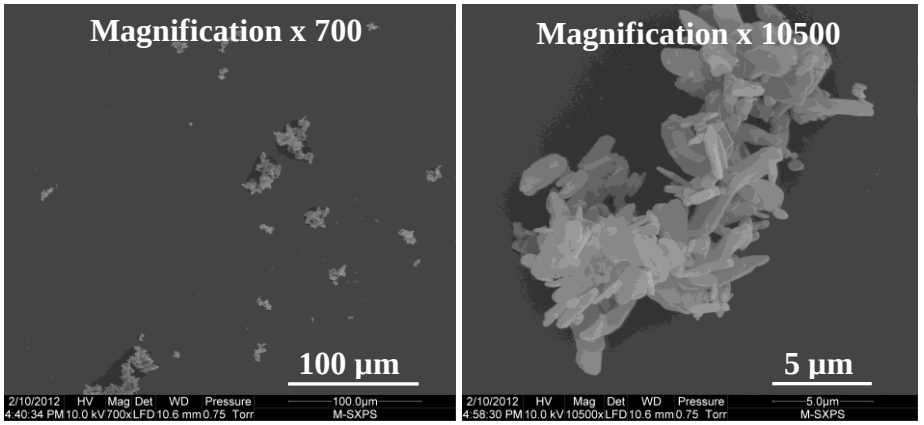

Pre-separator salmeterol xinafoate

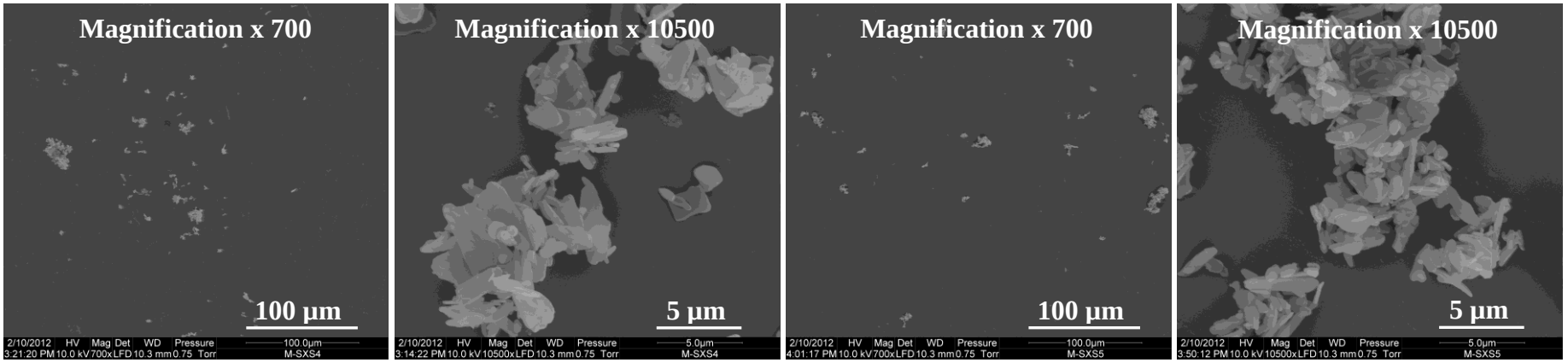

Stage 4 salmeterol xinafoate **Stage 5 salmeterol xinafoate**

Figure 4.5 Morphology of fractionated salmeterol xinafoate viewed by scanning electron microscopy at x 700 and x 10500 magnification.

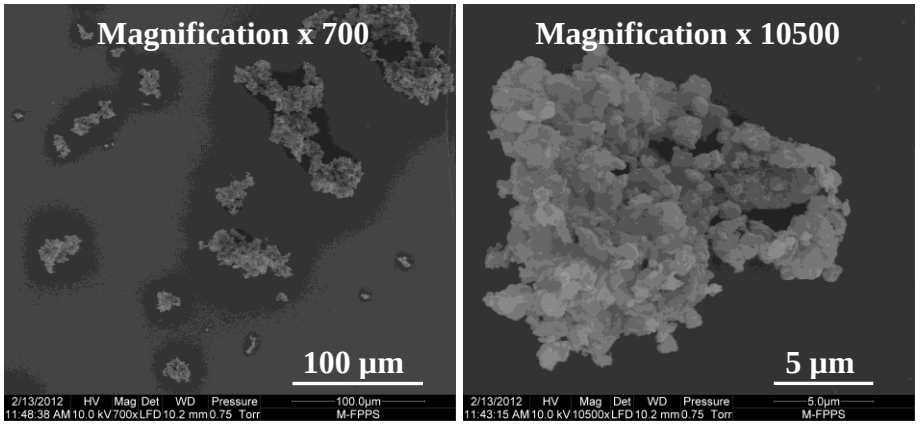

Pre-separator fluticasone propionate

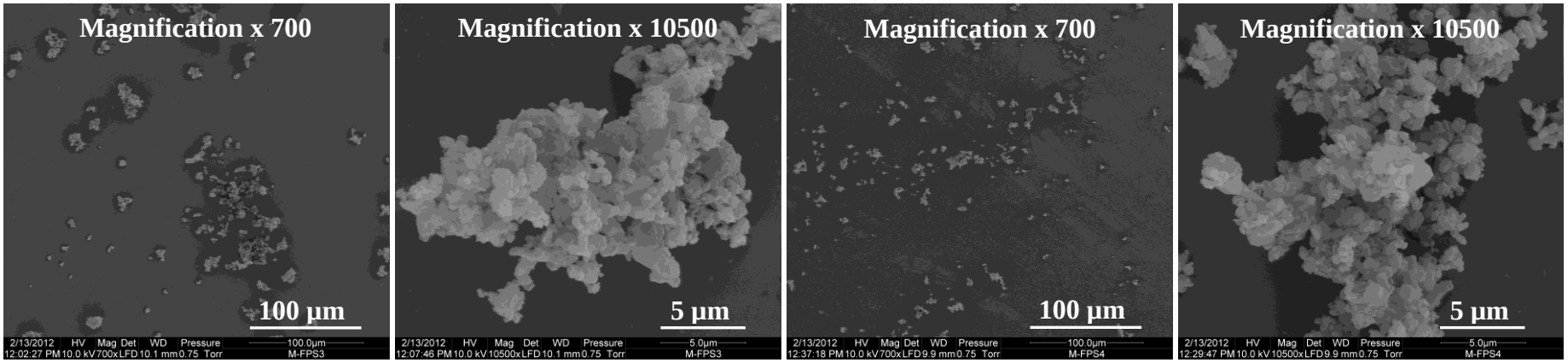

Stage 3 fluticasone propionate **Stage 4 fluticasone propionate**

Figure 4.6 Morphology of fractionated fluticasone propionate viewed by scanning electron microscopy at x 700 and x 10500 magnification.

Thermo-kinetic analysis of the re-crystallisation process was undertaken by constructing α-heating rate (β, $^{o}C.min^{-1}$) curves for the fractionated samples, where α is the fraction of SX-II re-crystallised from the melt. This enabled data fitting to an Avrami-Erofe'ev-type equation (Equation 4.1) to determine the kinetic parameters k and n, representing the integrated rate constant for the re-crystallisation of SX-II and the Avrami exponent of the model, respectively (Murnane et al., 2008d).

Equation 4.1 $$\propto = 1 - exp^{-(k\beta^{-1})^{n}}$$

The α-heating rate curves of the SX samples are shown in Figure 4.7. Initially α was calculated by expressing the experimentally determined enthalpy of fusion (ΔH_f) of SX-II as a proportion of the standard literature value as previously described (Murnane et al., 2008d), but this generated poor fits to the data (R^2 = 0.64 – 0.79). The data were therefore normalised as follows. The enthalpy of fusion at the lowest heating rate was used to represent complete conversion of SX-I to SX-II. The degree of conversion at each heating rate was calculating by expressing the enthalpy of fusion at each heating rate employed ($\Delta H_f^{\beta exp}$) as a proportion of the enthalpy of fusion at the lowest heating rate ($\Delta H_f^{\beta 0.1}$), as shown in Equation 4.2.

Equation 4.2 $$\alpha = \frac{\Delta H_f^{\beta exp}}{\Delta H_f^{\beta 0.1}}$$

Following normalisation, the fit improved (R^2 = 0.96 – 0.98) and allowed the kinetic parameters k and n to be determined (Table 4.3). The Avrami exponent was close to 2 for each sample, which is expected as SX particles have a platelet shape and therefore predominantly grow in two directions (Tong et al., 2003). The k values revealed a different degree (or rate) of re-crystallisation between the fractionated samples. Stage 4 and 5 particles had comparable k values whereas pre-separator particles had a much higher k value, indicating a higher degree of crystalline disorder.

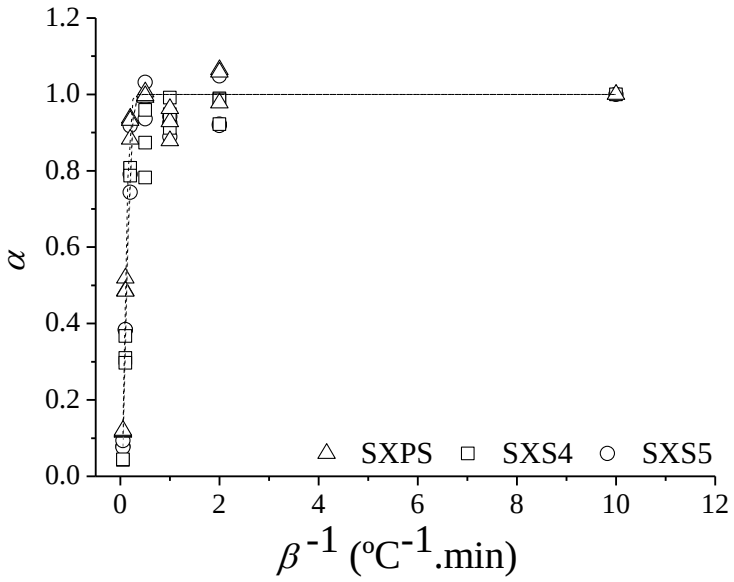

Figure 4.7 α-heating rate curves of salmeterol xinafoate fractions recovered from the pre-separator (SXPS), Stage 4 (SXS4) and Stage 5 (SXS5) of the Next Generation Impactor assessed by differential scanning calorimetry, where α is the fraction of the SX-II polymorph that re-crystallises after melting of the SX-I polymorph, and β^{-1} is the heating rate expressed in min per ^{o}C (*n* = 3 data points per heating rate).

Table 4.3 The degree of re-crystallisation (k) and Avrami exponent (n) of pre-separator, Stage 4 and Stage 5 salmeterol xinafoate (SX) samples determined from thermo-kinetic analysis of the differential scanning calorimetry thermographs of the samples.

Particle Type	**Degree of Re-crystallisation (k, $^{o}C^{-1}$.min)**	**Avrami Component (n)**
Pre-separator SX	8.12 ± 0.26	2.08 ± 0.17
Stage 4 SX	6.29 ± 0.28	2.18 ± 0.25
Stage 5 SX	6.66 ± 0.27	1.96 ± 0.18

DSC thermographs for FP were typical for this compound, which indicated melting followed by degradation (Figure 4.8) and agreed with results reported previously (Westmeier and Steckel, 2008; Xu et al., 2010a). Therefore, it was not possible to model the crystallisation kinetics as described for SX. Integration of the onset temperature of the melting peaks indicated negligible differences in the melting point between the samples (Table 4.4).

Table 4.4 The melting point of unfractionated, crystallised and fractionated fluticasone propionate obtained by differential scanning calorimetry at a heating rate of 20 ^{o}C.min^{-1} (mean ± SD, *n* = 3).

Particle Type	**Melting Point (^{o}C)**
Unfractionated FP	293.4 ± 2.44
Crystallised FP	294.2 ± 3.10
Pre-separator FP	293.8 ± 0.92
Stage 3 FP	295.5 ± 1.24
Stage 4 FP	297.3 ± 2.25

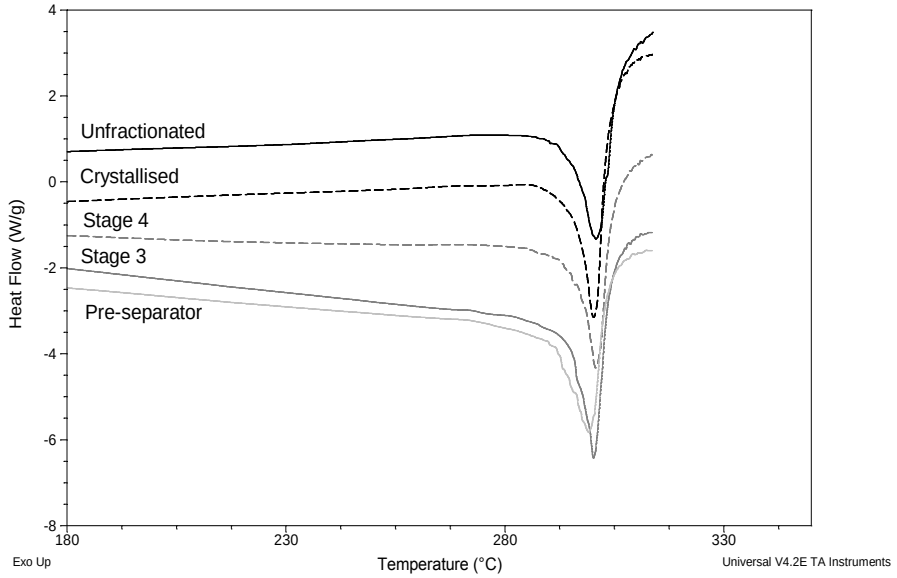

Figure 4.8 Differential scanning calorimetry thermographs of unfractionated, crystallised and fractionated fluticasone propionate at a heating rate of 20 ^{o}C.min^{-1} (*n* = 1 measurement shown).

4.5.5.2 POWDER X-RAY DIFFRACTION

The PXRD traces of the SX and FP samples are shown in Figure 4.9. Changes to the diffraction patterns, including peak widening and worsened resolution, are indicative of changes to the crystal structure of the material (Steckel et al., 2003b) and a very broad peak generally referred to as a 'halo' would indicate an amorphous material. As no changes were observed between the different isolated samples of either SX or FP, this indicated that there was no change in the polymorphic form between the different samples of either drug.

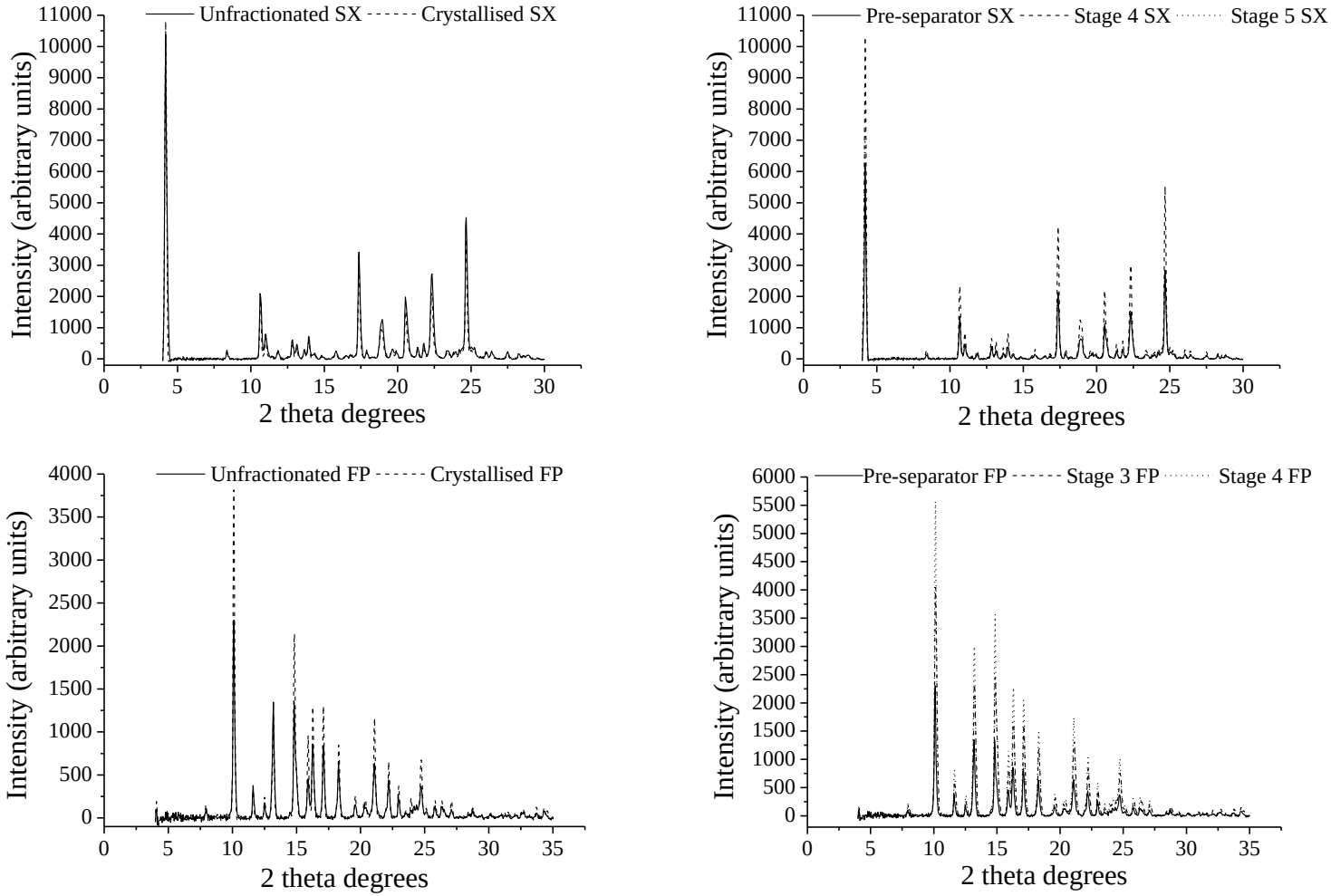

Figure 4.9 Powder x-ray diffraction traces of unfractionated, crystallised and fractionated salmeterol xinafoate (SX) and fluticasone propionate (FP) samples (n = 1).

4.5.6 INVERSE GAS CHROMATOGRAPHY AT FINITE DILUTION

4.5.6.1 BRUNAUER-EMMETT-TELLER SURFACE AREA

The BET SSA of the samples were determined from the octane sorption isotherm (at 303.15 K) and obtained directly from the IGC SEA (Table 4.5). Differences between the SSA of the SX samples generally reflected the different particle sizes of the samples. For example, unfractionated (D_{v50} = 1.42 ± 0.08 µm) and Stage 5 SX powders (D_{v50} = 1.12 ± 0.04 µm) had BET SSA values of 8.34 $m^2.g^{-1}$ and 12.75 $m^2.g^{-1}$, respectively. The FP samples also followed the trend of increasing SSA with a smaller particle size. However, when comparing the fractionated samples, pre-separator particles displayed a larger SSA than the stage fractions, despite also having a larger particle size (Table 4.2). Such differences may arise from different particle shape/surface properties between the powders.

Table 4.5 The Brunauer-Emmett-Teller (BET) specific surface area of salmeterol xinafoate and fluticasone propionate samples obtained from the octane sorption isotherm of the inverse gas chromatography surface energy analyser.

Sample	**BET specific surface area ($m^2.g^{-1}$)**	
	Salmeterol xinafoate	**Fluticasone propionate**
Unfractionated	8.37	7.50
Crystallised	9.74	5.00
Pre-separator	7.01	10.67
Stage 3	7.10	8.02
Stage 4	7.88	8.56
Stage 5	12.75	8.12

4.5.6.2 DISPERSIVE SURFACE ENERGY

Table 4.6 shows the dispersive surface energy measurements of the samples at the lowest surface coverage from finite dilution, and is equivalent to an infinite dilution measurement. Overall FP was found to have higher surface energy than SX. For both drugs, the crystallised material displayed the lowest surface energy. Whereas for FP the dispersive surface energy was comparable between the fractionated samples, for SX there was an increase in surface energy as the aerodynamic size reduced.

Table 4.6 The dispersive surface energy of salmeterol xinafoate and fluticasone propionate samples by inverse gas chromatograpgy at infinite dilution (i.e. 0.01 n/nm surface coverage of the probes).

Sample	**Dispersive surface energy ($mJ.m^{-2}$)**	
	Salmeterol xinafoate	**Fluticasone propionate**
Unfractionated	37.94	43.08
Crystallised	34.13	38.12
Pre-separator	37.04	43.16
Stage 3	38.87	43.48
Stage 4	38.78	42.74
Stage 5	40.14	43.05

Figure 4.10 shows the dispersive surface energy distributions of the different SX and FP powder fractions and crystals from finite dilution. The results indicated that for every powder, dispersive interactions formed the major component of the surface energy. The dispersive surface energy of unfractionated FP was higher than unfractionated SX. Both powders showed heterogeneity in the dispersive surface energy values, but the difference in heterogeneity of the two drugs was negligible. The dispersive surface energy of the crystallised particles of FP was lower, and less heterogeneous, compared to the respective micronised (i.e. unfractionated) powders. When the fractionated powders are considered there were found to be different trends in the surface energy between the SX and FP samples. In the case of FP, there was little difference in the surface energy and heterogeneity between the powders; the fractionated samples appeared to have marginally lower surface energy than the unfractionated powders. For SX, the differences between the surface energies of the unfractionated, pre-separator, Stage 3, and Stage 4 SX samples were also small. However, the surface energy of the Stage 5 SX powder, particularly at low surface coverage, was found to be higher, and displayed greater surface energy heterogeneity compared to the other SX powders.

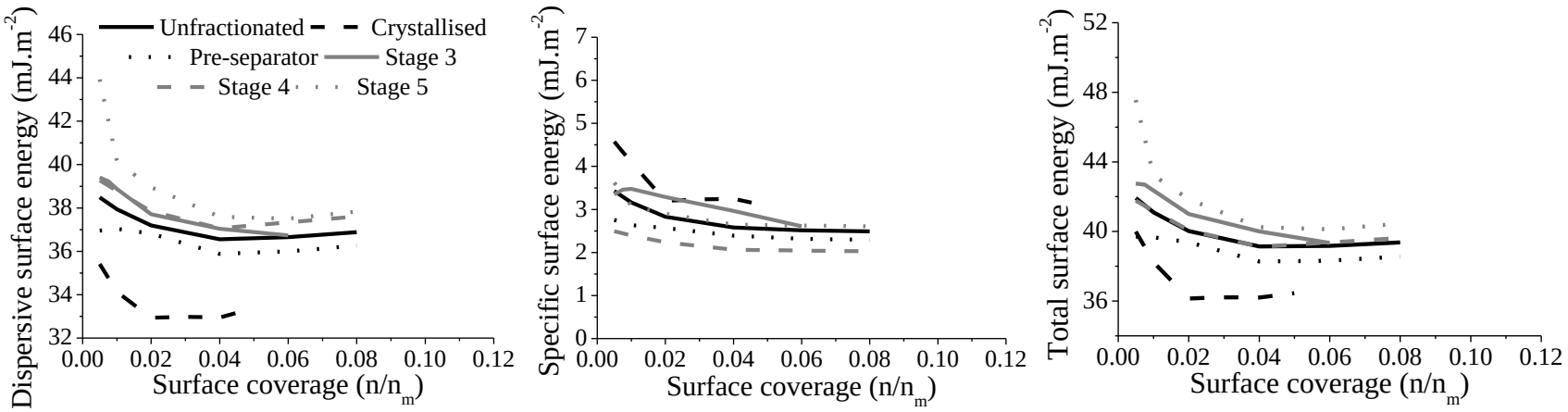

(a) Surface energy distributions of unfractionated, fractionated and crystallised salmeterol xinafoate

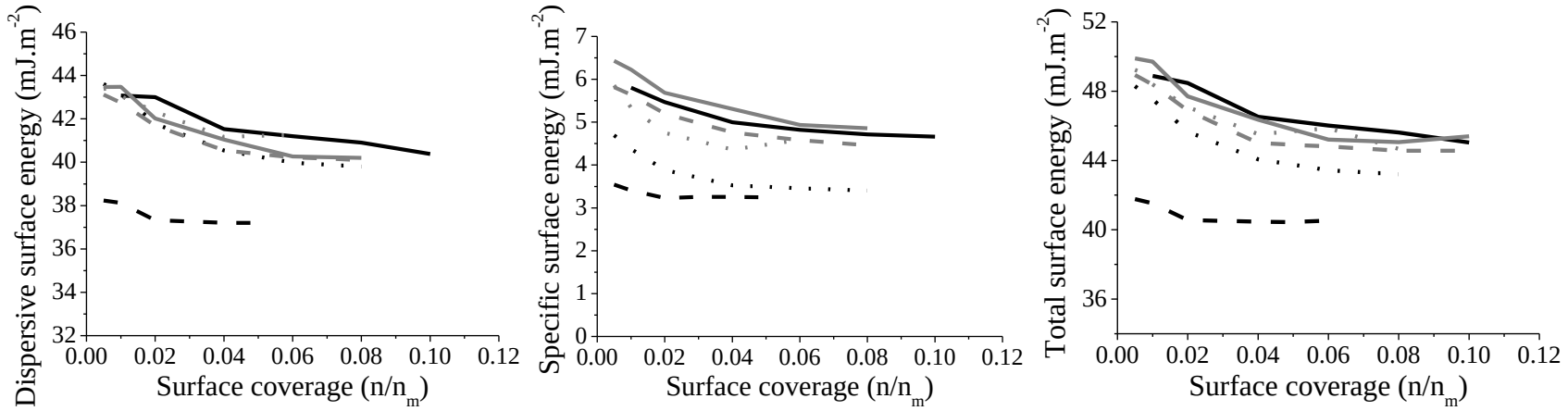

(b) Surface energy distributions of unfractionated, fractionated and crystallised fluticasone propionate

Figure 4.10 The dispersive, specific and total surface energy distributions of unfractionated, crystallised, and fractionated (a) salmeterol xinafoate and (b) fluticasone propionate powders by inverse gas chromatography at finite dilution. Note that the same legend is used for each graph.

4.5.6.3 SPECIFIC SURFACE ENERGY

The specific surface energies of SX and FP were much lower than their dispersive surface energies (Figure 4.10). The specific surface energy component of FP was larger than that of SX, indicating the different surface chemistry between the powders, with a larger proportion of polar surface groups for FP which facilitated polar inter-particulate interactions. The specific surface energy of crystallised particles of FP was lower, with decreased surface energy heterogeneity, compared to unfractionated FP, whereas the converse occurred for SX. Between the fractionated powders, there was little difference in the specific surface energy for unfractionated, Stage 3, Stage 4 and Stage 5 FP samples, but pre-separator particles were found to have the lowest surface energy. Differences between unfractionated and fractioned SX samples were also small, with Stage 4 particles having the lowest specific surface energy.

4.5.6.4 TOTAL SURFACE ENERGY

When considering the total surface energy, i.e. the sum of the dispersive and specific surface energies, for both SX and FP, then the crystallised particles were found to have the lowest surface energy of all the powders. For FP, all the fractionated samples had a lower surface energy than that obtained for unfractionated samples, although these differences were small, and the pre-separator sample had the lowest surface energy. Unfractionated SX was found to have an identical surface energy to the sample isolated from Stage 4, whereas Stage 3 particles had a slightly higher and more heterogeneous surface energy and the fraction obtained from Stage 5 had the highest and most heterogeneous surface energy of all the samples. Pre-separator SX particles again had the lowest surface energy of the fractionated particles.

4.5.7 TRUE DENSITY AND AERODYNAMIC PARTICLE SIZE

The true density of unfractionated SX was 1.2103 $g.cc^{-1}$ and 1.4885 $g.cc^{-1}$ for unfractionated FP. This enabled the aerodynamic particle size to be calculated using Equation 4.3, where d_{ae} is the aerodynamic diameter, d is the geometric diameter and ρ is the particle density (Louey et al., 2004a). The calculated aerodynamic sizes in terms of the D_{v10}, D_{v50}, D_{v90} and VMD are shown in Table 4.7.

.

Equation 4.3 $$d_{ae} = d \cdot \sqrt{\rho}$$

Table 4.7 The geometric and calculated aerodynamic particle sizes (represented by the D_{v10}, D_{v50}, D_{v90} and volume mean diameter, VMD) of micronised (i.e. unfractionated) salmeterol xinafoate and fluticasone propionate.

Particle Size (μm)	**Geometric**	**Aerodynamic**	**Geometric**	**Aerodynamic**
	Salmeterol xinafoate		**Fluticasone propionate**	
D_{v10}	0.62	0.68	1.04	1.27
D_{v50}	1.42	1.56	2.94	3.59
D_{v90}	3.78	4.16	6.10	7.44
VMD	1.94	2.13	3.41	4.16

4.5.8 DISPERSIBILITY ASSESSMENT BY LASER DIFFRACTION

Dry dispersion laser diffraction revealed differences in dispersibility between the powders (Table 4.8). The cohesive strength, CPP, was derived from the particle size-primary pressure profiles. For SX, only pre-separator particles showed a lower CPP compared to unfractionated SX; the CPPs of Stage 4 and Stage 5 particles were comparable and similar also to the CPP of the unfractionated powder. For some of the powders, including the majority of the FP samples, it was not possible to deduce a CPP due to the D_{v50} fluctuating in the 'plateau' region. This could arise as a result of high heterogeneity in particle properties, incomplete de-agglomeration even at the highest dispersing pressure employed, or conversely occur due to particle fracture/attrition. It was therefore not possible to compare the CPP values of all the FP samples. For SX, only pre-separator particles showed a reduction in cohesive strength compared to the unfractionated particles.

Following data normalisation and linearisation, the linearity of each data set was good and the DA_{max} was close to 1.0. Once more, the powders that showed the greatest deviation from the theoretical value of DA_{max} = 1.0 had the poorest linearity. Considering SX, in all instances the DA_{50}, a measure of the ease of dispersion, improved except for Stage 5 SX in which the ease of dispersion was comparable to unfractionated SX. Pre-separator and Stage 4 SX showed the largest improvement in dispersibility compared to unfractionated powder, and the former samples were found to

have similar DA_{50} values. For crystallised SX any improvement was less marked. FP particles showed a different behaviour, with pre-separator particles displaying a much poorer dispersibility (by almost 2-fold) compared to unfractionated particles. The remaining powder fractions showed improved ease of dispersion compared to unfractionated FP with the following rank: FPS3 > CFP > FPS4.

Table 4.8 The primary pressure for 50 % de-agglomeration (DA_{50}), maximum degree of de-agglomeration (DA_{max}) and critical primary pressure (CPP) of unfractionated, crystallised, pre-separator and stage fractionated salmeterol xinafoate and fluticasone propionate determined from dry dispersion laser diffraction analysis.

Salmeterol xinafoate	**R^2**	**DA_{50} (Bar)**	**DA_{max}**	**CPP (Bar)**
Unfractionated	0.9711	1.45	1.35	3.50
Crystallised	0.9823	1.21	1.18	n.a
Pre-separator	0.9984	0.54	1.11	1.20
Stage 4	0.9931	0.51	1.10	3.50
Stage 5*	0.8921	1.40	1.40	3.00
Fluticasone propionate	**R^2**	**DA_{50} (Bar)**	**DA_{max}**	**CPP (Bar)**
Unfractionated	0.9338	1.72	1.34	n.a.
Crystallised	0.9680	1.05	1.13	3.50
Pre-separator	0.9462	2.36	1.45	n.a
Stage 3	0.9545	0.85	1.07	n.a.
Stage 4	0.9057	1.50	1.27	n.a.

*Data modelled in the PP range 0.3 – 5.0 Bar (due to poor linearity when the data for 0.2 Bar was included); for all other samples PPs were in the range 0.2 – 5.0 Bar; n.a. = not possible to assign a CPP.

4.5.9 NEXT GENERATION IMPACTOR ANALYSIS

Cascade impactor analysis of the SX powder samples revealed differences in the aerosolisation of the particles (Figure 4.11 and Table 4.9). The FPF RD, FPF ED, and emission of unfractionated SX were 33.2 ± 2.18 %, 61.2 ± 2.51 %, and 54.4 ± 5.17 %, respectively. Despite a larger particle size, crystallised SX was emitted in higher amounts (91.0 ± 2.07 %, $p < 0.05$, one-way ANOVA with post-hoc Tukey's test, GraphPad Prism 5) than the unfractionated material, potentially as a result of reduced adhesion to device/capsule walls, reduced cohesivity, and the larger particle size which would act to improve flow and increase entrainment. The FPF RD of CSX did not change ($p > 0.05$) but the FPF ED was reduced ($p < 0.05$) compared to that obtained using unfractionated SX. This was due to greater deposition (~ 3-fold) in the throat and

pre-separator, reflecting a reduced retention in the device/capsules for crystallised particles. The SX obtained from the pre-separator sample also exhibited higher emission than unfractionated SX, although the increase was smaller than for the crystallised particles and not significant ($p > 0.05$). The similarity of the FPF (RD and ED) for unfractionated and pre-separator SX indicated that although the particles within the pre-separator sample were entrained more readily, the de-agglomeration efficiency of this material to primary particles was worsened. The emission of unfractionated, Stage 4 and Stage 5 SX did not differ significantly. There was no difference between the FPF RD of Stage 4 and unfractionated SX ($p > 0.05$), but an increase in the FPF ED ($p < 0.05$) suggesting that this powder may have improved de-agglomeration efficiency compared to the unfractionated material. For Stage 5 SX, the FPF RD and ED reduced significantly compared to unfractionated SX, reflecting the worsened de-agglomeration efficiency compared to unfractionated SX. The MMAD of the majority of SX samples was unchanged compared to unfractionated SX ($p > 0.05$), apart from the crystallised material for which the MMAD was bigger ($p < 0.05$). The FPM was also unchanged for all the samples compared to unfractionated SX ($p > 0.05$) except for Stage 5 SX, when the FPM was found to be markedly lower than for the other SX samples ($p < 0.05$).

The different FP samples also displayed altered aerosolisation behaviour (Figure 4.12 and Table 4.9). The emission of micronised FP (62.2 ± 7.60 % RD) was unchanged compared to the crystallised, pre-separator, Stage 3 and Stage 4 material ($p > 0.05$), although there was a reduction in the variability (i.e. SD) between replicate analyses. The latter could potentially be a consequence of a narrower distribution in particle properties, which might be expected to improve the reproducibility of entrainment and the emitted dose. The FPF ED and RD of pre-separator FP did not change compared to unfractionated FP. However, crystallised, Stage 3 and Stage 4 FP produced higher FPFs ($p < 0.05$) than the unfractionated sample, indicating improved de-agglomeration efficiency. There was no significant difference in the FPF between Stage 3 and Stage 4 FP indicating equivalent de-agglomeration efficiency between the two sub-populations. The MMAD of the FP samples did not change compared to unfractionated FP ($p > 0.05$), except for the Stage 4 FP for which the MMAD was smaller. The FPM of crystallised, Stage 3 and Stage 4 FP was higher than the FPM generated by unfractionated FP ($p < 0.05$) whereas the FPM of pre-separator FP was unchanged compared to the unfractionated FP powder ($p > 0.05$).

Table 4.9 The recovery (% of the actuated dose), fine particle mass (FPM), mass median aerodynamic diameter (MMAD) and geometric standard deviation (GSD) of unfractionated, crystallised and fractionated salmeterol xinafoate and fluticasone propionate aerosolised into the Next Generation Impactor (mean ± SD, n = 3 - 4).

Salmeterol xinafoate	**Recovery (%)**	**FPM (mg)**	**MMAD (µm)**	**GSD**
Unfractionated	77.8 ± 6.5	2.7 ± 0.2	2.7 ± 0.1	1.8 ± 0.0
Crystallised	87.1 ± 1.3	2.4 ± 0.2	3.5 ± 0.2	2.1 ± 0.0
Pre-separator	79.5 ± 1.9	3.0 ± 0.4	2.6 ± 0.1	1.8 ± 0.0
Stage 4	78.9 ± 6.7	2.7 ± 0.5	2.5 ± 0.1	1.8 ± 0.0
Stage 5	71.5 ± 2.6	1.4 ± 0.0	2.7 ± 0.1	2.0 ± 0.0
Fluticasone propionate	**Recovery (%)**	**FPM (mg)**	**MMAD (µm)**	**GSD**
Unfractionated	78.0 ± 3.1	1.5 ± 0.1	4.1 ± 0.3	2.0 ± 0.1
Crystallised	89.5 ± 2.0	2.2 ± 0.3	4.1 ± 0.2	2.0 ± 0.1
Pre-separator	78.9 ± 3.8	1.8 ± 0.1	4.1 ± 0.1	2.1 ± 0.2
Stage 3	78.6 ± 3.5	2.5 ± 0.1	3.7 ± 0.1	1.9 ± 0.0
Stage 4	77.7 ± 1.7	2.5 ± 0.1	3.5 ± 0.1	1.9 ± 0.0

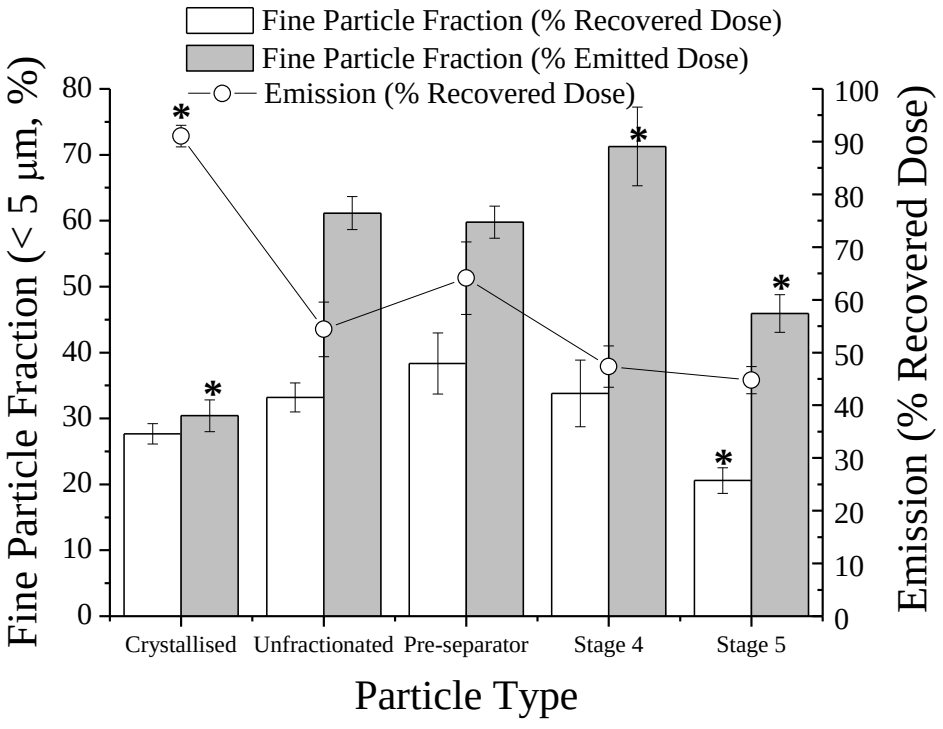

Figure 4.11 The fine particle fraction (FPF < 5 µm, expressed as a percentage of the emitted dose, ED, and recovered dose, RD) and emission (% RD) of salmeterol xinafoate samples (crystallised, unfractionated, pre-separator, stage 4 and stage 5) assessed by Next Generation Impactor analysis (mean ± SD, n = 3 - 4); * = $p < 0.05$ for crystallised or fractionated powders vs. unfractionated powder using a one-way ANOVA with post-hoc Tukey's test.

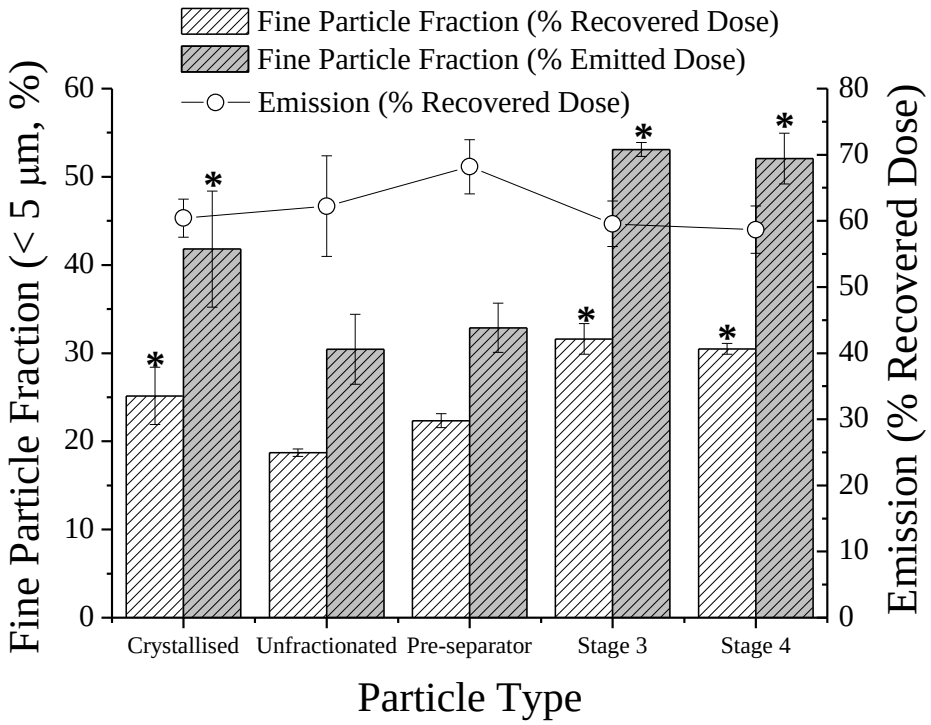

Figure 4.12 The fine particle fraction (FPF < 5 µm, expressed as a percentage of the emitted dose, ED, and recovered dose, RD) and emission (% RD) of fluticasone propionate samples (crystallised, unfractionated, pre-separator, stage 3 and stage 4) assessed by Next Generation Impactor analysis (mean ± SD, n = 3 - 4); * = $p < 0.05$ for crystallised or fractionated powders vs. unfractionated powder using a one-way ANOVA with post-hoc Tukey's test.

4.6 DISCUSSION AND CONCLUSIONS

Particles produced with the intent of efficient delivery to the lungs are derived most commonly by crystallisation. These are then subjected to a comminution step such as micronisation, in order to achieve an appropriate particle size for deposition. Such a highly energetic micronisation process can result in poor control over the physicochemical properties of the particles, with the potential for both intra- and inter-batch variability (Feeley et al., 1998). A consequence of this could be the formation of sub-populations of particles which display different aerosolisation behaviour compared to the bulk of the powder. For example, amorphous regions may be introduced onto crystalline drug surfaces, which can increase surface energy and adhesive/cohesive forces (Steckel et al., 2003b; Perkins et al., 2009) such that the particles are more difficult to fluidise and/or de-agglomerate. In addition, the processing may create a proportion of particles that are so tightly agglomerated that they do not disperse during dry powder delivery. A recently developed aerodynamic technique which enables powders to be separated based on their aerodynamic particle size has therefore provided the possibility of isolating discrete powder fractions (Taki et al., 2011b). The latter study identified differences in the formulation performance when particles of drug and excipient with a different particle size were incorporated into carrier-based blends (Taki, 2008). This use of the fractionation methodology should provide a means of characterising the physicochemical properties of aerodynamically differentiated material, and therefore allow the effect of intra-batch variability in particle properties present within bulk powders to be better determined.

4.6.1 POWDER PREPARATION BY AERODYNAMIC FRACTIONATION AND ANTI-SOLVENT CRYSTALLISATION

Aerodynamic fractionation using the NGI was successfully conducted to isolate powder samples with a known aerodynamic size, however, it was found to be an inefficient process leading to the loss of large quantities of material. The stages upon which the largest yields were obtained were therefore selected for further analysis. For both SX and FP this included the pre-separator fraction comprising the coarsest particles (aerodynamic size > 12.8 µm). Deposition across the NGI stages differed between the powders, and was found to be the largest on stages 4 and 5 for SX and stages 3 and 4 for FP. This was attributed to the smaller particle size of SX (d_{ae}; D_{v50} 1.56 µm, span 2.23)

compared to FP (d_{ae}; D_{v50} 3.59 µm, span 1.72). For both powders, the geometric particle size measured by liquid dispersion laser diffraction (Table 4.2), which measures the fully dispersed particle size, revealed that the powders were depositing as agglomerates within the NGI.

During DPI delivery, powder agglomerates need to disperse within an airstream in order to attain a particle size which is able to enter and deposit in the lungs. The geometric D_{v50} of the pre-separator and stage 1 – 4 fractions following dispersion in liquid media were comparable for SX powders. When operated at 60 $L.min^{-1}$, powder depositing in the pre-separator and on stages 1 - 4 of the NGI comprises particles with an aerodynamic size > 12.8 µm and 1.66 – 12.80 µm, respectively. Therefore, the particles remained agglomerated during fractionation and when depositing in the NGI. The aerodynamic particle cut size therefore represented the aerodynamic size of the agglomerate rather than the individual particles. The agglomerates therefore possessed an aerodynamic diameter equivalent to a single particle with a similar size, shape and density (Taki et al., 2011b). The geometric D_{v50} of SX particles depositing on stages 5, 6 and 7 (1.12 ± 0.04 µm – 0.87 ± 0.05 µm) were smaller than the unfractionated material (1.42 ± 0.08 µm) and more closely matched the aerodynamic particle size of the stages (1.66 - 0.34 µm) suggesting that these particles may have deposited in a dispersed state. A similar finding was observed for FP samples; powder depositing in the pre-separator and stages 1 – 3 had comparable geometric D_{v50} values after liquid dispersion indicating agglomeration of deposited particles on these stages. Beyond stage 3 the particles became increasingly smaller, and may have been more fully dispersed before depositing. Although efficient fractionation was achieved by Taki et al. (2011b), the deposition of powder agglomerates was not discounted. This was postulated to be the cause of a degree of overlap in the geometric PSDs of fractionated samples, and the presence of tailing/secondary modes in the distributions following dispersion in liquid.

As a comparator for the unfractionated and fractionated particles, ampiphilic crystallisation was undertaken to produce crystallised particles which would have been expected to comprise a molecular lattice in the lowest energy state. Although the re-crystallised particles were larger than the micronised material (D_{v50} 4.93 ± 0.37 µm and 3.62 ± 1.43 µm for SX and FP, respectively) they each had a D_{v50} that was below 5 µm and therefore within the required particle size range for pulmonary aerosol delivery. Achieving an appropriate particle size is one of the major challenges of controlled

crystallisation methods, as small molecules tend to form relatively large crystals (10 – 100 µm) (Chow et al., 2007). The crystal size distribution is dependent on the crystallisation conditions such as the mixing regimen (Chow et al., 2007), as well as the solvent (Murnane et al., 2008a; Murnane et al., 2008c) and anti-solvent (Kubavat et al., 2012) employed. As the purpose of the study was to obtain particles which had not been subjected to secondary processing in order to function as a control, rather than obtain the smallest possible crystal size, the crystallisation method was not further optimised in order to attain optimum sizing.

4.6.2 PHYSICOCHEMICAL CHARACTERISATION OF BULK, FRACTIONATED AND RE-CRYSTALLISED DRUG POWDERS

There were negligible changes in the morphology and agglomeration, following a visual assessment, of the unfractionated and fractionated powders of both drugs. Pre-separator FP appeared to form the largest agglomerates of the FP samples, which would not be unexpected as this sample was the coarsest fraction with an aerodynamic particle size greater than 12.8 µm. The crystallised particles showed different particle morphology to the unfractionated and fractionated particles. Crystallised SX particles were flatter and more plate-like and formed larger more densely packed agglomerates compared to the unfractionated material. Crystallised FP particles were needle-like, formed smaller agglomerates and appeared to be less agglomerated than the unfractionated material. These changes in morphology were consistent with those observed by Murnane et al. (2008c) following ampiphilic crystallisation from PEG solutions.

Differences in crystallinity and surface energy were observed between the samples. The PXRD traces of SX and FP were typical of those reported for each of the two drugs (Steckel et al., 2003b; Westmeier and Steckel, 2008; Kumon et al., 2010). Qualitatively, there were no changes in the traces between the respective SX and FP samples, indicating no change in polymorphic form and that all the samples were crystalline. The crystallinity (subsequently referred to as bulk disorder) of SX was further assessed using DSC. The DSC traces were characteristic for SX, attributable to the two crystalline polymorphs of the drug, form I (SX-I) which is the more stable form and form II (SX-II) which is the metastable polymorph under ambient conditions (Tong et al., 2001). Unfractionated and crystallised SX displayed smaller SX-II endotherms than those derived from powder fractions depositing in the pre-separator or on Stages 4 and

5, when obtained at low heating rates, indicating that a smaller degree of conversion between the SX-I to SX-II form was occurring. Upon increasing the heating rate, the SX-II melting peak was eliminated at much lower heating rates for these two samples (i.e. unfractionated and crystalline) compared to the fractionated samples. Differences in polymorphic conversion rates between SX samples have been attributed to the presence of SX-II seeds that can arise from particle damage during powder processing such as micronisation (Tong et al., 2001). Following manual trituration, a pure SX-I polymorph which would have been initially absent of any seeds, generated a DSC trace that resembled that of micronised SX (Tong et al., 2001). This suggests that the fractionated particles contained greater crystal damage in comparison to the unfractionated and crystallised samples.

Thermokinetic analysis using a modified Avrami Erofe'ev equation enabled quantification of a re-crystallisation rate constant (k) for the samples (Murnane et al., 2008d). Whereas the k values of Stage 4 and 5 particles were comparable, pre-separator particles had a much higher k value, indicating greater bulk disorder in these particles. Differences in bulk disorder arise due to uncontrolled and variable amorphisation of particles during micronisation. The levels of amorphous content detected in micronised particles increases with the amount of energy imparted during size reduction, including the micronisation grind pressure (Ticehurst et al., 2000; Brodka-Pfeiffer et al., 2003b) and milling time (Young et al., 2007; Gaisford et al., 2010). Such processing leads to a distribution in the degree of damage/disorder within a single batch of powder. The crystal damage observed for fractionated SX particles may not have been detected in the unfractionated material due to the more severely damaged particles, as represented by the pre-separator and stage fraction samples, being present in a much smaller proportion in the bulk material. The most damaged particles in terms of bulk disorder, i.e. the pre-separator sample, was found to have the lowest propensity for de-agglomeration during fractionation, as pre-separator particles formed larger agglomerates (d_{ae} > 12.8 µm) compared to Stage 4 and 5 particles (d_{ae} 0.55 – 1.66 µm).

Changes to the crystal structure of a particle leading to disordered or amorphous regions on particle surfaces are also known to manifest as higher surface energy (Feeley et al., 1998; Tong et al., 2001). These changes rarely distribute uniformly throughout the powder and can affect the powder's processing and formulation characteristics (Feeley et al., 1998). IGC employed using the traditional method of infinite dilution, in which

very low solute concentrations are injected, probes only the highest energy sites and results in an overestimation of the surface energy. It also provides no indication of the heterogeneity of the particle surface (Ylä-Mäihäniemi et al., 2008). Finite dilution IGC enables an understanding of the surface energy across the particle surface to be attained. Although the dispersive surface energy values at low surface coverage revealed some differences between the samples, examining the surface energy distributions using finite dilution provided greater insight.

Pre-separator SX particles had the lowest dispersive and total surface energy of the unfractionated and fractionated SX samples, despite having the highest bulk disorder when assessed by DSC. Stage 4 particles also exhibited comparable dispersive and total surface energy to the unfractionated material. Whereas the material isolated from Stage 5 possessed the highest and most heterogeneous dispersive and total surface energy of all the samples. Surface energy arising from specific interactions provided a small contribution to the total surface energy for all the SX samples. There was little difference in the specific surface energy between the SX samples, with Stage 4 particles displaying the lowest and least heterogeneous specific surface energy. High dispersive and total surface energy for the Stage 5 particles, i.e. those with the smallest net individual mean particle size and largest surface area, may have arisen due to these particles having been subjected to the highest degree of particle attrition during comminution. These particles would therefore display a high degree of particle damage (Ticehurst et al., 2000; Brodka-Pfeiffer et al., 2003b; Young et al., 2007; Gaisford et al., 2010) both to the bulk (represented by the k value) and surface (represented by the surface energy) of the particle. Higher dispersive surface energies have been reported with increasing milling energy and grinding pressures, and these exhibited an inverse relationship with reducing geometric particle size. It was suggested that greater forces experienced during micronisation leads to greater crystal disruption, and the formation of new highly energetic interaction sites and/or exposure of more energetic crystal faces (Shariare et al., 2011; Gamble et al., 2012). Furthermore, size reduction of the particles may have occurred by different particle size reduction mechanisms (e.g. brittle fracture or attrition) and/or at different cleavage planes resulting in altered exposure of functional groups at the crystal surface, as the balance of dispersive and specific interactions differed for the particles. For example, Stage 4 SX exhibited higher dispersive and lower specific surface energy compared to unfractionated SX, whereas

pre-separator particles displayed lower dispersive and lower specific surface energy compared to unfractionated particles.

In contrast to SX, the differences in surface energy between FP samples were less marked. There were only small differences in the surface energies between the unfractionated and fractionated samples; however, the fractionated samples appeared to possess lower dispersive and specific surface energy than unfractionated FP. Of these, the pre-separator particles displayed the lowest surface energy. Like SX, differences in the relative contributions of the dispersive and specific surface energies were observed, indicating that the fractionated materials consisted of particles with differing electron donating and accepting functional groups at the exposed crystal surface (Shariare et al., 2011).

The re-crystallised particles of both SX and FP displayed the lowest dispersive and total surface energy, as a consequence of the lack of process-induced damage (Rehman et al., 2003; Shariare et al., 2011). For SX, the specific surface energy of the re-crystallised sample was higher and more heterogeneous than the unfractionated powder. This indicated an altered surface chemistry of particles within this sample. It has been suggested that this is due to greater exposure of proton donor and acceptor groups e.g. OH or COOH, and NH, respectively, compared to bulky non-polar groups such as benzene and naphthalene at the SX crystal surface, although molecular modeling would be required for confirmation (Tong et al., 2001).

4.6.3 DISPERSIBILITY OF BULK, FRACTIONATED AND RE-CRYSTALLISED DRUG POWDERS

Each powder fraction displayed distinct aerosolisation behaviours when the fraction was considered as a bulk powder and re-aerosolised. A powder composed of pre-separator material would be likely to have a structure that comprised large agglomerates (> 12.8 µm) exhibiting good flow (Hickey et al., 2007). Low inter-agglomerate cohesive forces are likely due to the relatively large agglomerate sizes, however, poor dispersal during fractionation would suggest that intra-agglomerate cohesive forces between the individual component particles was high. Both SX and FP pre-separator particles demonstrated a higher emission and a higher FPF than the respective unfractionated particles, although the differences were not significant ($p > 0.05$). Low inter-

agglomerate cohesive forces would assist the efficient entrainment of powder agglomerates into the airstream during aerosolisation. High inter-particulate forces between individual particles may have restricted the efficiency of the fractionation, but during re-aerosolisation of the smaller powder mass into the NGI then the powder structure would be altered compared to the unfractionated starting material. The efficiency of de-agglomeration hence depends on the balance between high inter-particulate cohesive forces, which is related to the powder structure, and the high aerodynamic drag forces and kinetic energy experienced by large agglomerates (compared to smaller agglomerates). The latter of which may increase de-agglomeration efficiency, for example through a greater number of collisions/impaction within the device (Begat et al., 2004).

Changes in the intrinsic dispersibility of the pre-separator fractions as assessed by dry dispersion laser diffraction, however, differed between the two drugs. Whereas SX pre-separator particles showed an improvement in the ease of de-agglomeration (DA_{50}), for FP the DA_{50} of this fraction was worse compared to the respective unfractionated powder. The CPP also revealed a difference in the cohesive strength of the fractionated SX particles; there were negligible differences between the CPP of the stage fractions, but the CPP of the pre-separator SX particles was lower than that of the unfractionated material. These results correlated well with those relating to the total surface energy of the pre-separator sample which displayed the lowest energy in comparison to the powder derived from the stage fractions and the unfractionated material. Whereas cascade impactor analysis considers powder entrainability (i.e. emission) and de-agglomeration efficiency (i.e. FPF) as separate parameters, the ease of dispersibility (i.e. DA_{50}) as determined using the laser diffraction technique incorporates the flow, entrainment and de-agglomeration of the powder, independent of the method of delivery (i.e. device and flow rate), into a single, powerful parameter for assessing powder dispersion. Measurements also take into account every type of interactive force present, as well as powder structure and history. The structural characteristics of a powder play an important role in dictating de-agglomeration patterns (Behara et al., 2011a; Behara et al., 2011b), and are influenced by the physicochemical properties of the individual particles. The work of cohesion (dependent on factors including the surface energy distribution of the particles), agglomerate structures resulting from the magnitude and distribution of interactive forces, packing fraction (i.e. volume of particles/volume of the agglomerate), and the size of the individual particles, dictate powder structure, and

can result in a lack of structure homogeneity across the powder bed (Kendall and Stainton, 2001; Behara et al., 2011b). It is therefore necessary to consider both the fundamental dispersibility of the powder and the powder delivery system, including the device, formulation and flow rate, when assessing powders for their de-agglomeration efficiency and developing delivery systems for optimised fine particle delivery to the lungs.

The aerosol performance of the stage fractions differed between the drugs. The Stage 4 SX powdered sample, despite having an improved DA_{50}, showed no change in emission or FPF RD, but a higher FPF ED suggesting a degree of improved dispersibility, compared to unfractionated SX. Stage 5 deposited SX powder when re-aerosolised, however, displayed a comparable, poor, DA_{50} and a reduced FPF ED and RD ($p < 0.05$ compared to unfractionated SX). When combined with the absence of change in the emission, the high DA_{50} and reduced FPF indicated a poorer de-agglomeration efficiency of Stage 5 SX particles. In this instance, a combination of a small particle size, high bulk disorder, and high surface energy resulted in a reduction in aerosol performance, where it is likely that strong cohesive forces (CPP = 3.0 Bar, Table 4.8) between the particles led to the formation of stable agglomerates that were difficult to disperse (Louey et al., 2004a). Conversely, stage fractionated FP (i.e. both Stage 3 and 4 particles) showed an improvement in the DA_{50} and an increase in the FPF ED and RD ($p < 0.05$) in comparison to unfractionated material. Since there was no change in emission of the two fractions this indicated an improvement in de-agglomeration efficiency compared to unfractionated material. This improvement could not be attributed to changes in crystallanity or surface energy between the unfractionated and stage fractionated FP particles, and highlights the complexity in the factors that influence the de-agglomeration process. It was also not possible to deduce a CPP for the unfractionated or fractionated FP samples, despite a change in the DA_{50}. The particle size-primary pressure profiles flattened as the dispersing pressure increased, however, examination of this region of the curve indicated that the particle size continued to reduce up to 5.0 Bar. The magnitude of the reduction was small in comparison to the early region of the curve (e.g. for Stage 3 FP, D_{v50} = 12.29 µm at 0.2 Bar, D_{v50} = 2.75 µm at 1.5 Bar and D_{v50} = 1.80 µm at 5.0 Bar). It is likely that a combination of particle heterogeneity and particle fracture/attrition (as a result of high dispersing pressures) resulted in the lack of a plateau region in the profile.

The lower surface energy and larger size of the re-crystallised control particles resulted in improved dispersibility in terms of the DA_{50} for both drugs, as well as the entrainability of SX and the de-agglomeration efficiency (i.e. FPF) of FP compared to the unfractionated powders. Although the FPF of SX was lower than for the unfractionated particles, there was higher retention in the throat and pre-separator, which was attributed to the larger particle size of the re-crystallised material resulting in greater impaction. Had the PSD been reduced by modifying and optimising the crystallisation conditions, it can be postulated that the FPF may have been improved compared to that achieved using unfractionated particles. The FPFs of precipitated drug crystals have been shown to be higher than jet-milled particles for both disodium chromoglycate (Steckel et al., 2003a), and salbutamol sulphate (Shariare et al., 2011), and equivalent for SX (Murnane et al., 2009). FP crystals have demonstrated improved (Steckel et al., 2003b), or similar (Murnane et al., 2009) FPFs depending on the crystallisation conditions employed. In addition to the omission of the high energy micronisation step, other factors such as altered surface chemistry, and changes to particle shape, particularly for FP, would also have contributed to the difference in aerosolisation behaviour that occurred.

4.6.4 CONCLUSIONS

This study has shown that SX and FP powders fractionated into distinct aerodynamic size classes comprised sub-populations of the bulk micronised powder. These sub-populations consisted of individual particles agglomerated to varying extents and displaying distinct physicochemical properties of crystallinity and surface energy. The sub-populations showed differences in both their intrinsic dispersibility and aerosol performance when aerosolised into the NGI. This may have implications for the performance of the drug powders when co-formulated, and will be studied in later chapters. This study has highlighted the importance of considering powders as collections of particle populations with their own distinct properties, the need to consider powder properties as distributions, and on an individual basis according to the drug. By gaining better control over the generation and properties of sub-populations of particles, this can lead to the optimisation of powder properties for the efficient delivery of drug particles to the lungs.

5 PROBING DRUG PARTICLE CO-ASSOCIATION AND DISPERSION MODIFYING EFFECTS IN COMBINATION DRY POWDER INHALER FORMULATIONS

5.1 INTRODUCTION

Asthma and COPD are characterised by airway inflammation, smooth muscle dysfunction and airway limitation (Nelson et al., 2003; ATS/ERS Task Force, 2004). In order to target the different components of the disease, corticosteroids and bronchodilators are often administered together (Aubier et al., 1999). In Europe, there are currently four commercially available combination LABA/ICS products containing fluticasone propionate (FP) and salmeterol xinafaote (SX), FP and formoterol fumarate, budesonide (Bud) and formoterol fumarate, and beclometasone dipropionate (BDP) and formoterol fumarate (Tamm et al., 2012). The use of combination inhalers has been shown to be at least as effective as separate delivery of each drug (Bateman et al., 1998; Aubier et al., 1999; Chapman, 1999; Hagedorn et al., 2013). Improved patient outcomes (Kavuru et al., 2000; Nelson et al., 2003), steroid sparing effects (Busse et al., 2003; Jarjour et al., 2006) and improved patient adherence due to the simplification of medication regimens (BTS/SIGN, 2008 (revised 2012)) are also likely. By delivering two drugs from a single inhaler rather than separate devices, differences in deposition patterns arising from natural variations in inspiratory manoeuvres (both intra- and inter-patient) may also be avoided (Theophilus et al., 2006).

A physicochemical interaction between the two drugs during manufacture/delivery may alter the aerosolisation of drugs from combination formulations. This has the potential to enhance patient outcomes if there is an altered deposition profile leading to improved fine particle delivery of the drug/s to the target regions of the lungs (Taki et al., 2011). In Chapter 3, SX and FP aerosolisation performance, in terms of the FPF for SX, and the MMAD for FP, were altered upon co-formulation. However, these blends did not contain a carrier. In a carrier-based formulation, the range of physicochemical interactions that may occur between the different components in a combination DPI is numerous, resulting in a complicated multi-factorial scenario (Taki et al., 2011a). The role of carriers and fines as dispersion aids is well established, although the exact mechanism of action of fines is still not fully understood. The addition of a second drug to a formulation therefore adds an extra level of complexity in attempting to determine any potential performance modifying effects of the drug/s. For example, alterations in the aerosolisation profiles of SX and FP when delivered in combination have been reported, but it was not possible to attribute these to SX/FP interactions, as the grade and concentration of the coarse and fine lactose in the formulation, and the

manufacturing history of the inhaler products were not known (Taki et al., 2011). As identified in Chapter 4, intra-batch variability in properties within a bulk micronised powder can also occur, and may alter the aerosolisability of powder sub-populations when compared to the bulk powder. This may further influence the aerosolisation performance of drug powders following co-formulation, and the implications of this will be studied in a later chapter.

Drug co-association in combination formulations has been studied using the Raman microscope for both pMDI (Steele et al., 2004; Theophilus et al., 2006; Rogueda et al., 2011) and DPI formulations (Jetmalani et al., 2012; Traini et al., 2012; Vernall et al, 2012) containing the drug combinations SX and FP, Bud and formoterol fumarate, and salbutamol base and BDP. This technique is useful in multicomponent formulations as it enables individual drugs to be chemically identified. Imaging of NGI plates following aerosol delivery of combination DPIs and pMDIs has suggested that drug particles may deposit as mixed agglomerates. In these studies, co-association was assessed through qualitative interpretation of Raman images and spectra, using the PSD/particle and agglomerate counts, and novel statistical analysis. Single particle techniques such as aerosol time of flight mass spectroscopy also allows the chemical identity of particles to be determined, and has also identified co-association between SX and FP particles in combination DPI and pMDI formulations (New et al., 2008). Another approach has been to consider the stage deposition across an impactor for formulations containing particles of each drug in a physical powder mix, or combination particles which contain both drug entities in a single particle (Kumon et al., 2010). Whereas parameters such as the emission and FPF provide an indication of powder entrainability and de-agglomeration efficiency, the stage-by-stage deposition provides an indication of how uniformly each drug is delivered across the impactor (Pitchayajittipong et al., 2009). Where both drugs in a formulation have demonstrated concomitant *in vitro* deposition patterns, this has been attributed to co-deposition of the drugs (Westmeier and Steckel, 2008; Pitchayajittipong et al., 2009; Kumon et al., 2010; Adi et al., 2012; Traini et al., 2012).

Although studies have investigated the presence of co-association, the cause of particle association is still not clear. Whereas SX and FP interactions and co-aggregation to form hetero-flocs have been identified in pMDI formulations (Michael et al., 2000; Michael et al., 2001), DPI formulations differ greatly in their composition. For example,

a 30 % increase in co-associated SX and FP particles from the Seretide DPI has been reported compared to the pMDI (New et al., 2008). An interactive affinity between SX and FP powder particles has been reported (Young et al, 2004a; Kubavat et al., 2012), and this may alter the aerosolisation performance of one or both drugs in combination formulations. To identify this, test formulations need to be prepared that are matched in terms of their manufacturing, storage and drug content, as well as fines and carrier properties and load. Also, to identify the origin of any altered performance, it is necessary to assess the performance of the combination drug-drug powder mixes (subsequently referred to as pre-blends) prior to formulating with lactose, to allow any carrier effects to be discounted. Any drug-drug interactions within DPI formulations which may lead to co-association of the particles can therefore occur at a number of stages during manufacture and delivery. These include processing steps such as blending and capsule filling/device manufacture, upon storage, as well as in the aerosol plume during and following actuation (New et al., 2008). Any property/process which affects agglomeration has the potential to influence particle co-association and mixed agglomerate formation. It is currently not known at what stage co-association of SX and FP particles may occur in powder formulations, however, gaining such understanding would enable formulations to be designed for optimal dispersion performance. For example, the generation of agglomerates consisting of FP nanoparticles and salbutamol sulphate (SS) did not change the dispersion (in terms of FPF) of FP compared to the single drug nanoparticle agglomerates, but changes to the dispersion of SS were attributed to FP agglomerates functioning as a carrier for SS in the mixed agglomerate formulations (El-Gendy et al., 2011). Further complexity also arises as particle co-association may not be a class effect and thus may differ depending on the specific drug combination in the formulation (Rogueda et al., 2011).

Whether or not particle co-association occurs in DPI formulations, the presence of a second drug has the potential to alter bulk powder properties including powder flow, packing, and tensile strength (Shur et al., 2008). The cohesive and adhesive tendencies of the drugs will alter the balance of interactions in the formulation and thus the powder structure. The combination formulation may have a higher fine particle content, which in a similar manner to the presence of *in situ* or *ex situ* lactose fines, may increase the tensile strength of the powder bed. The resulting stabilisation of the powder bed towards disturbance by an airflow may alter the mechanism of powder entrainment and subsequent dispersion (Shur et al., 2008). An increase in cohesive/adhesive forces

between individual particles can increase agglomerate strength, but the latter is also influenced by the packing fraction (i.e. volume of particles/volume of agglomerate), particle size and agglomerate structure (Kendall and Stainton, 2001). A high drug concentration, particularly of inherently cohesive drugs, may also be detrimental to mixing and content uniformity of powder blends, due to powder agglomeration and thus segregation (Le et al., 2012d). An understanding of bulk powder properties is therefore also necessary in the development of combination DPI formulations.

5.2 AIM AND OBJECTIVES

The aim of this study was to probe the occurrence of SX and FP co-association in combination formulations and determine the implications on powder aerosolisation. The objectives were therefore to:

a) Establish benchmark data for the aerodynamic PSD and intrinsic dispersibility of Seretide Accuhalers to determine the effect of drug ratio and flow rate on the aerosolisation of co-formulations.
b) As a measure of co-association, use the SX:FP ratio of the deposited masses across the NGI to determine SX and FP co-association in Seretide Accuhalers as a function of product strength and flow rate.
c) Measure the aerodynamic PSD and intrinsic dispersibility of SX and FP when formulated as representative DPI formulations and SX:FP pre-blends to ascertain:
    a. The dispersion modifying effects of SX and FP when blended in different ratios in the absence and presence of a carrier.
    b. Co-association of the drugs as a function of drug ratio and in the absence and presence of a carrier.

5.3 MATERIALS

The materials and equipment used in Chapter 5, not listed in Section 2.3, 3.3 and 4.3, are shown in Table 5.1.

Table 5.1 Suppliers of materials and equipment (Chapter 5).

Material / Equipment	**Supplier**
Coarse lactose (CL; BN: 120904-25)	Pfizer Ltd, PGRD Sandwich Laboratories, UK
Minisart single use filter unit (0.2 µm pore size)	Sartorius Stedium biotech, UK
Seretide Accuhalers	Allen and Hanburys Ltd, UK (supplied by AAH Pharmaceuticals, UK. See Table 5.2 for BN.)
Sympatec INHALER 2000	Sympatec GmbH, Clausthal-Zellerfeld, Germany
Critical flow controller TPK	Copley Scientific Ltd, UK

5.4 METHODS

5.4.1 BLEND PREPARATION

5.4.1.1 PRE-BLENDS

Pre-blends containing micronised (i.e. unfractionated) SX and FP particles were prepared in the ratios 1:8, 1:1 and 8:1 by geometric mixing. Equal quantities of each drug (27.78 mg for the 1:8 and 8:1 ratios, 31.25 mg for the 1:1 ratio) were weighed directly into the blending vessel (a 4 mL glass HPLC vial) and subjected to whirlimixing for 60 s. The vial was tapped to remove any powder adhered to the inside walls and a second addition of drug was made, in an equal quantity, such that the total powder mass was doubled. The vessel was then whirlimixed and tapped as above. This procedure was repeated until the required amount of each drug had been added to a final total blend mass of 250 mg. A single glass bead (diameter approx. 5 mm) was added to the vessel and the blend was placed in a Turbula blender for 40 min at 62 rpm.

5.4.1.2 DRY POWDER INHALER BLENDS

DPI blends were prepared containing 1.38 % w/w micronised (i.e. unfractionated) SX, FP or SX:FP pre-blend (SX:FP ratio 8:1, 1:1, 1:8). The total blend size was 3 g. First, 41.4 mg of SX, FP or pre-blend was sandwiched between two layers (41.4 mg each) of CL (D_{v10} = 28.5 ± 0.78 µm, D_{v50} = 56.4 ± 0.20 µm, D_{v90} = 88.8 ± 0.43 µm, determined

by Sympatec HELOS/RODOS dry dispersion laser diffraction at 3.0 Bar PP) in the blending vessel (15 mL glass vial) and subjected to whirlimixing for 60 s. Lactose additions were made geometrically, followed by whirlimixing after each addition, such that the mass of the blend doubled, up to the final blend mass. Blend homogeneity samples were removed (10 x 12.5 mg) as well as a further sample (approx. 75 mg) for ad hoc analysis. Two ceramic balls (diameter approx. 10 mm) were then added to the vessel and placed in a Turbula blender for 40 min at 62 rpm.

5.4.2 BLEND HOMOGENEITY

5.4.2.1 PRE-BLENDS

To assess the homogeneity of the pre-blends, approximately 2 mg of blend was accurately weighed and dissolved in mobile phase (prepared as described in Section 3.4.1.1) with the aid of sonication prior to being made to final volume (10 mL). Drug recovery was assessed by HPLC analysis (as described in Section 3.4.1.1) using freshly prepared mixed standard calibration curves in the range 20 – 400 $\mu g.mL^{-1}$. To assess homogeneity, the theoretical concentration of SX and FP in each sample was calculated from the sample mass, compared to the detected concentration, and expressed as a percentage recovery (PR, %). The blend was considered homogenous when the CV of the PR values of the samples (n = 6) was less than 10 %. The SX and FP content was calculated by converting the detected drug concentration into a drug mass, which was then expressed as a proportion of the weighed sample mass (in $\mu g.mg^{-1}$) for each content uniformity sample. The mean drug content of the samples was then used to calculate the detected SX:FP ratio.

5.4.2.2 DRY POWDER INHALER BLENDS

The content uniformity of the DPI blends was assessed at two time points. The first was after geometric mixing of the powders i.e. prior to tumbling (n = 10) and the second was following tumbling in the Turbula blender (n = 6). Samples were prepared by accurately weighing 12.5 mg of blend and dissolving in 20 mL mobile phase (see Section 3.4.1.1) for SX and FP in the ratio 1:1, and 10 mL for the ratios 1:8, 8:1, 1:0 and 0:1 with the aid of sonication for approx. 10 min until the powder dissolved. The samples were syringe filtered (0.20 µm pore size filter unit), to remove any un-dissolved lactose particles prior to analysis. Drug recovery was assessed by HPLC (see Section 3.4.1.1.) using freshly prepared mixed standard calibration curves in the range 0.5 - 50 $\mu g.mL^{-1}$. The % CV of

the PR values and the detected drug ratios were calculated as described in Section 3.4.3 at both time points. The blend was considered homogenous when the % CV of the PR values at time point two was < 10 %.

5.4.3 SCANNING ELECTRON MICROSCOPY

SEM imaging to view the morphology of the pre-blends and DPI blends was undertaken as described in Chapter 2, Section 2.4.2, using an FEI Quanta 200F field emission SEM however high vacuum mode was employed and the microscope was operated at 3.5 kV.

5.4.4 WORK OF COHESION AND ADHESION

Surface energy analysis of CL was conducted using an IGC Surface Energy Analyser as described in Chapter 3, Section 3.4.8, and the dispersive, specific and total surface energy distributions were determined. The work of cohesion and work of adhesion between the different powders was calculated according to Equation 2.11.

5.4.5 NEXT GENERATION IMPACTOR ANALYSIS

5.4.5.1 SERETIDE DRY POWDER INHALER PRODUCTS

NGI analysis was conducted as described in Chapter 3, Section 3.4.6 with the following modifications. The flow rate through the NGI was adjusted to 67 ± 5 % $L.min^{-1}$ and 90 ± 5 % $L.min^{-1}$ corresponding to pressure drops across the device of approximately 2 and 4 kPa, respectively. These flow rates were determined using a dose uniformity sampling apparatus (DUSA). The DUSA was attached to a vacuum pump, and a critical flow controller TPK was used to set the pressure drop required. The inhaler was attached to the DUSA, the vacuum pump switched on, and the flow rate measured using a flow meter. For each NGI analysis, the vacuum pump was switched on for 3.6 s and 2.7 s, respectively, for the two flow rates in order to correspond to 4 L of air being drawn through the NGI. To quantify the amount of drug depositing, the throat and pre-separator were rinsed with 50 mL and 100 mL of mobile phase (Section 3.4.1.1) respectively. The samples were sonicated (approx. 5 min and 20 min, respectively) prior to being made up to final volume; the pre-separator sample was filtered (syringe filter unit, 0.20 µm pore size) to remove un-dissolved lactose as necessary prior to quantification. The stages were rinsed with 10 mL and 5 mL mobile phase for stages 1

– 5 and 6 – 8, respectively, with the aid of sonication (approx. 1 min per plate). Three batches of SA100 and SA500 were tested at each flow rate (10 actuations per run, n = 3), and are subsequently referred to as B1 – 3 as shown in Table 5.2.

Table 5.2 Batch characteristics of the Seretide Accuhalers tested in the study.

Identifier	Batch Number	Expiry Date (month.year)
Seretide Accuhaler 100 (SA100)		
Batch 1 (B1)	R174041	10.2006
Batch 2 (B2)	R564583	04.2013
Batch 3 (B3)	0241-1	01.2014
Seretide Accuhaler 500 (SA500)		
Batch 1 (B1)	R177573	11.2006
Batch 2 (B2)	R572744	07.2013
Batch 3 (B3)	1413-2-1	12.2013

5.4.5.2 PRE-BLENDS

NGI analysis of the pre-blends (n = 3) was conducted as described in Chapter 3, Section 3.4.6 using a flow rate of 60 $L.min^{-1}$ ± 5 % (corresponding to a pressure drop of 1.4 kPa) for 4 s. The Monodose inhaler device was used as previously except in this instance a capsule fill weight of 10.0 ± 1.0 mg was employed and a single capsule was actuated per NGI analysis. The device, capsules, throat and pre-separator were rinsed with 50 mL, 20 mL, 50 mL and 100 mL of mobile phase (Section 3.4.1.1), respectively, with the aid of sonication (approx. 5 min) prior to being made up to final volume. The stages were rinsed with 10 mL and 5 mL of mobile phase for stages 1 – 5 and 6 – 8, respectively, with sonication (approx. 1 min per plate).

5.4.5.3 DRY POWDER INHALER BLENDS

NGI analysis of the DPI blends was carried out as described in Chapter 3, Section 3.4.6, using a flow rate of 60 $L.min^{-1}$ ± 5 % for 4 s and a Monodose inhaler device, with the following modifications. The capsule fill weight was 12.5 ± 0.5 mg and the number of capsules actuated was six for the SX-only (1:0) and the FP-only (0:1) DPIs, and fifteen capsules for the 1:8, 1:1 and 8:1 DPIs. For the DPIs with SX:FP ratios 1:0 and 0:1, the device, capsules, throat and pre-separator were rinsed with 50 mL, 20 mL, 50 mL and 100 mL of mobile phase (Section 3.4.1.1), respectively, with sonication (approx. 5 min; 10 min for the pre-separator sample) prior to being made up to final volume. Stages 1 –

5 were rinsed with 5 mL and stages 6 - 8 with 2.5 mL of mobile phase, with the aid of sonication (approx. 1 min and 30 s, respectively). For the DPIs containing SX:FP in the ratio 1:8. 1:1 and 8:1, due to the larger number of capsules employed, 50 mL mobile phase was used to recover the drug remaining in the capsules; the pre-separator sample was also sonicated for 20 min, after which the sample was filtered (syringe filter, 0.20 µm pore size) if undissolved lactose was visible. For the 1:8 and 8:1 DPIs, rinse solutions from the stages were pooled to ensure that the deposited drug was detectable using the HPLC method described (Section 3.4.1.1). The protocol adopted was as follows: stage 1 was rinsed with 5 mL mobile phase with sonication (1 min), stage 2 was rinsed with 2.5 mL mobile phase with sonication (30 s). For stage 3, rinsing was with 2.5 mL mobile phase followed by sonication (30 s). The sample was then transferred into stage 4, to which a further 2.5 mL of mobile phase was added and sonicated (30 s) to form a single sample for stages 3 – 4. This process was repeated for stages 5 – 6 and stages 7 – 8. Each NGI run therefore consisted of samples corresponding to drug deposition in the device, capsules, throat, pre-separator, stage 1, stage 2, stages 3 – 4, stages 5 – 6, and stages 7 – 8.

5.4.5.4 QUANTIFICATION BY HIGH PERFORMANCE LIQUID CHROMATOGRAPHY

The quantification of drug recovery for the NGI samples was using the HPLC method described in Chapter 3, Section 3.4.1.1. For the SA100 and SA500, B1, freshly prepared calibration curves were pooled (n = 5) in the range 0.5 – 25 µg.mL^{-1} for SX and 0.5 - 50 µg.mL^{-1} for FP. For the remaining batches, new calibration curves were prepared on the day of sample analysis. For the pre-blends, fresh calibration curves were pooled (n = 5) in the range 0.5 – 50 µg.mL^{-1} (or 20 – 400 µg.mL^{-1} for individual samples outside this range). For the DPI blends, calibration curves were prepared on the day in the range 0.1 – 50 µg.mL^{-1} (standards below 0.5 µg.mL^{-1} were prepared by dilution of the lowest standard) and 20 – 100 µg.mL^{-1} where necessary, and the range of standards used was selected based on the samples.

5.4.6 DISPERSIBILITY ASSESSMENT BY LASER DIFFRACTION

5.4.6.1 SYMPATEC HELOS/RODOS

De-agglomeration analysis was conducted using the Sympatec HELOS/RODOS and protruding aspiration tube as described in Chapter 2, Section 2.4.4. The D_{v50} particle

size data were normalised using the D_H/D_x approach and empirically modelled using Equation 2.8. The SA100 (B3, BN. 0241-1) and SA500 (B3, BN. 1412-2-1) inhalers were opened by hand and the contents of the blister strip transferred into glass vials and stored in a desiccator until required. Particle size measurements for the DPI blends and SA inhalers were made at primary pressures (PPs) in the range 0.2 – 5.0 Bar (n = 1) with the following modifications. The C_{opt} to trigger the start of the measurement was reduced to ≥ 0.5 %. In order to remove the influence of coarse particles in the calculation of the PSD to allow changes in the fine particle PSD as a function of primary pressure to be deduced, a forced stability of '9' was applied. This removed data corresponding to particles larger than 40 µm, providing insight into the de-agglomeration behaviour of the fine fraction. At each PP, the D_{v10}, D_{v50}, D_{v90} and VMD were recorded.

5.4.6.2 SYMPATEC INHALER 2000

Particle size measurements were made using the Sympatec INHALER 2000 for the SA100 (B1, BN. R174041) and SA500 (B1, BN. R177573) products. An empty Accuhaler device was first used to determine the instrument pressure drop required to achieve the flow rates of interest i.e. 67 $L.min^{-1}$ ± 5 % and 90 $L.min^{-1}$ ± 5 %. The R3 lens was used (0.5 – 175 µm), timebase 1 ms, and trigger conditions of C_{opt} ≥ 0.1 % to start a measurement and C_{opt} ≤ 0.2 % for 4 s (or 4 s real time) to end a measurement. A reference was taken; the inhaler was primed and then held firmly in place at the inlet prior to initiating the measurement using the instrument software (WINDOX 5.0, Sympatec GmbH, Clausthal-Zellerfeld, Germany). In order to determine the change in the fine fraction (FF) during the measurement, the time slice feature was used, with the particle size data being recorded by the instrument every 250 ms over a 4 s period. If 16 time slice measurements were not generated, which would correspond to a total measurement duration of 4 s, the measurement was repeated (n = 3 - 4). The PSD was calculated using Fraunhofer theory. The cumulative distribution was used to monitor the change in the percentage of particles < 5 µm and < 15 µm during the 4 s measurement. The area under the curve (AUC) over the 4 s period was calculated in Origin Pro 8 using the 'Integrate Multiple Peaks' function. The AUC was divided into eight sections covering 0.50 s segments of the measurement period (except for 0.25 – 0.50 s, for which a 0.25 s segment was used), using a constant y baseline (i.e. y = 0). The total AUC was calculated by summing the AUC values derived from each of the eight sections.

5.5 RESULTS

5.5.1 SERETIDE DRY POWDER INHALER PRODUCTS

5.5.1.1 NEXT GENERATION IMPACTOR ANALYSIS

5.5.1.1.1 BATCH EFFECTS

In order to determine batch-to-batch consistency prior to probing the effect of product strength and flow rate on aerosolisation behaviour, the reproducibility of three batches of SA100 and SA500 in terms of their aerodynamic deposition profile was assessed. The European Medicines Agency (EMEA) guidance for demonstrating bioequivalence states that inhalation products should show no greater than ± 15 % variability with regards to the individual stage deposition, or four justified grouped stages, which incorporate the fine particle mass and the upper stages of the impactor (EMEA, 2009). The BP (2012) further stipulates that products should show no greater than 15 % deviation in their dosage uniformity. In order to account for variability in the recovered doses between NGI analyses, the amounts of drug depositing on the stages (per actuation) were normalised to the recovered dose (Equation 5.1).

Equation 5.1 $$Amount\ per\ Actuation = \frac{Mass\ deposited\ on\ the\ stages / Total\ recovered\ dose}{Number\ of\ actuations}$$

Figure 5.1 and Figure 5.2 show the amount of SX and FP deposited, normalised to the recovered dose, for the grouped stages as follows: throat and pre-separator, stages 1 – 2, stage 3 and stages 4 – 7. In the majority of instances the deposition profiles were within the ± 15 % variability limits indicated by the EMEA. On a few occasions the deposition was within ± 20 %, indicated by an unfilled star in Figure 5.1 and Figure 5.2 (i.e. FP, SA500, stage 4 – 7, 60 and 90 $L.min^{-1}$; SX, SA500, stage 3, 90 $L.min^{-1}$). A limit of 20 % was recommended when assessing the accuracy and precision of dose delivery for a number of inhaler devices, including DPIs (Prime et al., 1999). Three grouped stages remained outside the ± 20 % limit, however, the magnitude of these deviations was considered to be small (indicated by a filled star in Figure 5.1 and Figure 5.2). Therefore, although the SA products did not fully align with the EMEA guidance on variability, they were considered equivalent for the purposes of this study.

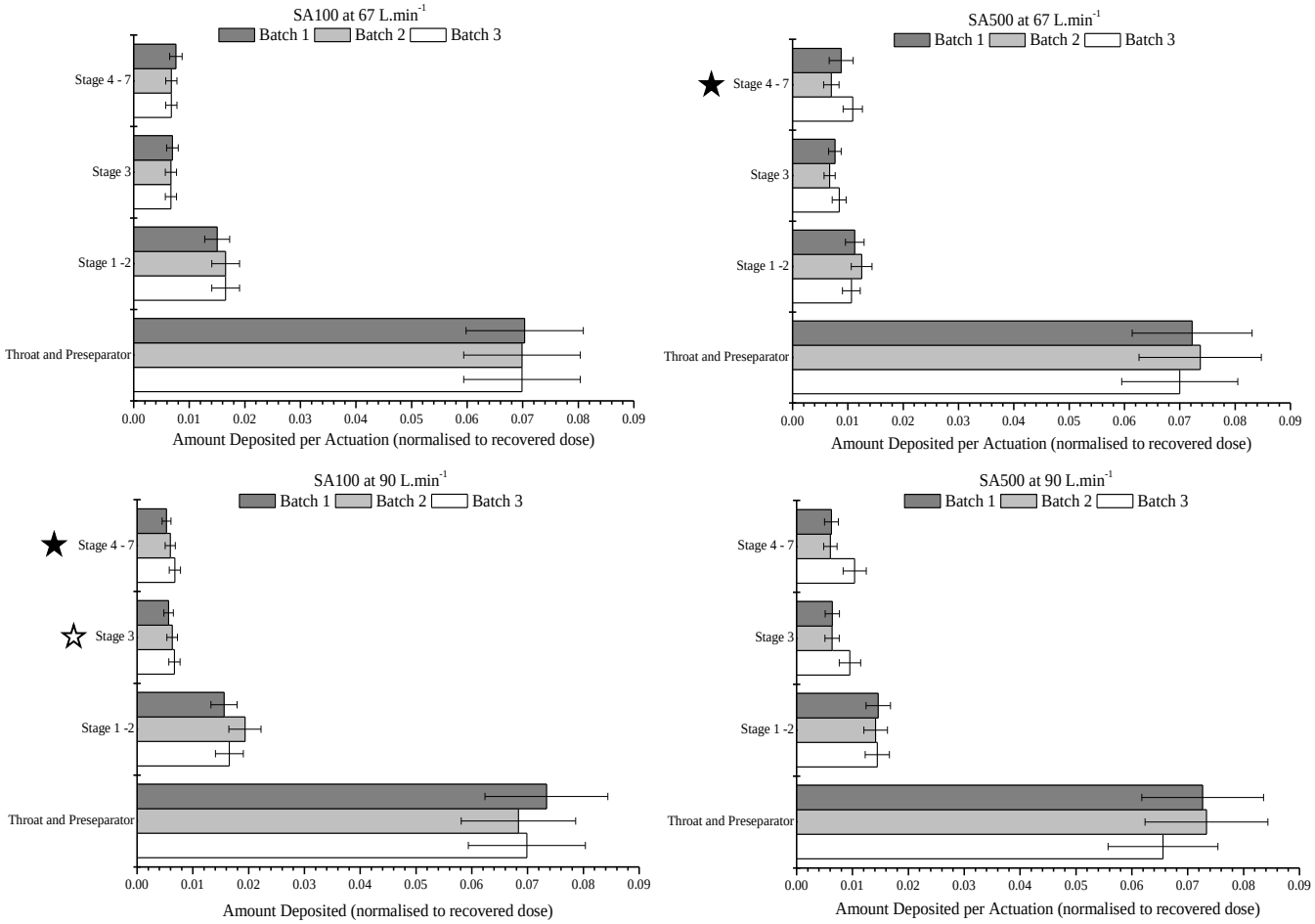

Figure 5.1 The amount of salmeterol xinafoate (SX) deposited per actuation, normalised to the total recovered dose, in the Next Generation Impactor for three batches of Seretide Accuhaler 100 (SA100) and 500 (SA500) aerosolised at 67 and 90 L.min^{-1} (n = 3 per batch, values are within the range mean ± 15 % deviation, except ☆ where the deviation was ± 20 % and ★ where the deviation exceeded ± 20 %).

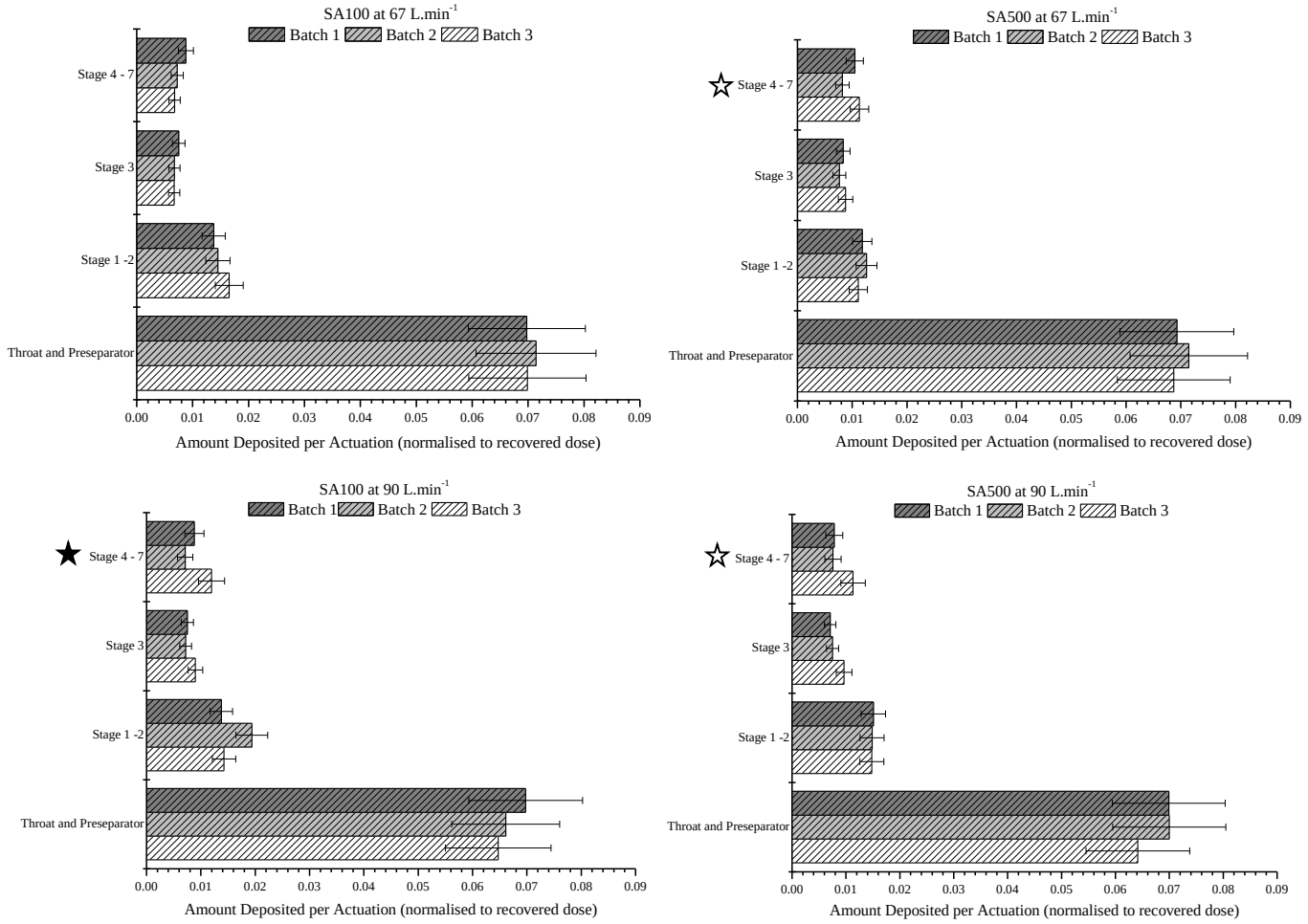

Figure 5.2 The amount of fluticasone propionate (FP) deposited per actuation, normalised to the total recovered dose, in the Next Generation Impactor for three batches of Seretide Accuhaler 100 (SA100) and 500 (SA500) aerosolised at 67 and 90 L.min^{-1} (n = 3 per batch, values are within the range mean ± 15 % deviation, except ☆ where the deviation was ± 20 % and ★ where the deviation exceeded ± 20 %).

5.5.1.1.2 STRENGTH AND FLOW RATE EFFECTS

A summary of the recovery, FPF (% ED), FPM, MMAD, and GSD of the SA100 and SA500 batches are shown in Table 5.3 and Table 5.4. In order to ascertain the effect of product strength and flow rate on aerosolisation performance, the data from the three batches were pooled according to the product strength i.e. SA100 (n = 9) and SA500 (n = 9) for SX and FP. A two-way ANOVA was then employed *post-hoc* to determine the statistical effects ($p < 0.05$, using GraphPad Prism 5) of product strength and flow rate on the aerodynamic deposition profile.

For SX, there was no change in the FPF or FPM with either product strength or flow rate (interaction term $p > 0.05$ for both). This indicates good reproducibility of the delivered dose regardless of flow rate or the amount of FP in the inhaler formulation. There was however a change in the MMAD (interaction term $p > 0.05$) with flow rate only, in which for both the SA100 and SA500 inhaler an increase in the MMAD occurred at higher flow rates. Although the MMAD was smaller for the SA500 than the SA100 at both flow rates, this difference was not significant ($p > 0.05$).

For FP, the FPF was also unaffected between flow rates or product strength (interaction term $p > 0.05$); the FPM (interaction term $p > 0.05$), however, increased significantly which is not unexpected as the higher strength product contains a greater proportion of FP. A change in the MMAD was also observed for FP (interaction term $p > 0.05$). The MMAD from the higher strength product was smaller than the lower strength product at both flow rates ($p < 0.05$). An increase in the MMAD of FP was also seen at higher flow rates for each product strength but this was not significant.

Table 5.3 The recovery (% of the actuated dose), fine particle fraction (FPF; % < 5 µm), fine particle mass (FPM) per actuation (< 5 µm), mass median aerodynamic diameter (MMAD) and geometric standard deviation (GSD) of salmeterol xinafoate (SX) from Seretide Accuhaler 100 (SA100) and 500 (SA500) inhalers aerosolised into the Next Generation Impactor at airflow rates of 67 and 90 L.min^{-1} (mean ± SD, n = 3 – 4).

Inhaler	**Flow Rate (L.min^{-1})**	**Batch**	**Date of Experiment (month.year)**	**Recovery (%)**	**FPF (% ED)**	**FPM (µg)**	**MMAD (µm)**	**GSD**
SA100	67	B1	06.2011	83.1 ± 2.26	17.4 ± 1.29	10.5 ± 1.03	4.21 ± 0.14	2.15 ± 0.06
	67	B2	10.2012	88.9 ± 1.68	16.0 ± 0.62	10.3 ± 0.50	4.70 ± 0.16	2.23 ± 0.04
	67	B3	10.2012	91.2 ± 1.50	23.6 ±1.21	15.6 ± 0.95	3.38 ± 0.18	2.19 ± 0.02
				Mean of n = 9 NGI runs	**19.0 ± 3.60**	**12.1 ± 2.69**	**4.10 ± 0.60**	**2.19 ± 0.05**
	90	B1	06.2011	79.3 ± 5.40	14.9 ± 1.72	8.59 ± 1.56	4.43 ± 0.36	2.33 ± 0.01
	90	B2	10.2012	88.0 ± 4.36	14.6 ± 0.34	9.30 ± 0.31	5.44 ± 0.12	2.36 ± 0.03
	90	B3	10.2012	102 ± 2.03	23.8 ± 1.16	13.2 ± 8.82	3.68 ± 0.11	2.15 ± 0.04
				Mean of n = 9 NGI runs	**17.8 ± 4.65**	**11.8 ± 4.42**	**4.52 ± 0.79**	**2.28 ± 0.10**
SA500	67	B1	06.2011	75.6 ± 3.20	18.4 ± 1.24	9.84 ± 0.84	3.69 ± 0.12	2.09 ± 0.03
	67	B2	10.2012	95.0 ± 0.95	15.6 ± 0.28	8.06 ± 5.38	4.18 ± 0.04	2.14 ± 0.02
	67	B3	10.2012	93.9 ± 7.07	21.1 ± 1.45	14.3 ± 0.95	3.46 ± 0.03	1.99 ± 0.03
				Mean of n = 9 NGI runs	**18.4 ± 2.57**	**11.6 ± 2.16**	**3.78 ± 0.32**	**2.07 ± 0.07**
	90	B1	06.2011	74.4 ± 1.72	16.9 ± 1.13	9.11 ± 0.82	3.95 ± 0.12	2.20 ± 0.03
	90	B2	10.2012	96.0 ± 3.25	14.3 ± 0.34	9.92 ± 0.33	4.66 ± 0.24	2.17 ± 0.13
	90	B3	10.2012	101 ± 5.27	22.0 ± 1.25	16.1 ± 1.08	3.90 ± 0.10	2.02 ± 0.03
				Mean of n = 9 NGI runs	**17.7 ± 3.50**	**11.7 ± 3.40**	**4.17 ± 0.11**	**2.13 ± 0.11**

Table 5.4 The recovery (% of the actuated dose), fine particle fraction (FPF; % < 5 µm), fine particle mass (FPM) per actuation (< 5 µm), mass median aerodynamic diameter (MMAD) and geometric standard deviation (GSD) of fluticasone propionate (FP) from Seretide Accuhaler 100 (SA100) and 500 (SA500) inhalers aerosolised into the Next Generation Impactor at airflow rates of 67 and 90 L.min^{-1} (mean ± SD, n = 3 – 4).

Inhaler	**Flow Rate (L.min^{-1})**	**Batch**	**Date of Experiment (month.year)**	**Recovery (%)**	**FPF (% ED)**	**FPM (µg)**	**MMAD (µm)**	**GSD**
SA100	67	B1	06.2011	94.7 ± 3.04	18.5 ± 0.98	17.6 ± 0.42	4.00 ± 0.11	2.17 ± 0.07
	67	B2	10.2012	105 ± 4.14	16.2 ± 0.63	17.1 ± 1.00	4.36 ± 0.02	2.22 ± 0.16
	67	B3	10.2012	115 ± 12.0	18.4 ± 1.35	21.3 ± 3.20	3.77 ± 0.51	2.17 ± 0.20
			Mean of n = 9 NGI runs	**17.7 ± 1.43**	**18.6 ± 2.64**	**4.04 ± 0.37**	**2.19 ± 2.64**	
	90	B1	06.2011	94.9 ± 7.88	16.4 ± 1.60	15.6 ± 2.56	4.23 ± 0.27	2.23 ± 0.04
	90	B2	10.2012	89.7 ± 9.73	16.9 ± 1.51	15.1 ± 0.68	5.01 ± 0.12	2.36 ± 0.04
	90	B3	10.2012	114 ± 8.02	23.4 ± 1.38	20.0 ± 13.3	3.70 ± 0.10	2.05 ± 0.03
			Mean of n = 9 NGI runs	**18.9 ± 3.59**	**19.1 ± 5.81**	**4.31 ± 0.59**	**2.21 ± 0.14**	
SA500	67	B1	06.2011	88.7 ± 1.42	20.8 ± 1.49	92.3 ± 5.69	3.61 ± 0.10	2.02 ± 0.06
	67	B2	10.2012	93.3 ± 5.47	18.0 ± 0.76	62.7 ± 41.8	3.94 ± 0.04	2.06 ± 0.05
	67	B3	10.2012	96.7 ± 11.7	22.1 ± 2.17	106 ± 6.43	3.43 ± 0.05	2.00 ± 0.02
			Mean of n = 9 NGI runs	**20.3 ± 2.30**	**94.0 ± 10.8**	**3.66 ± 0.23**	**2.03 ± 0.05**	
	90	B1	06.2011	86.5 ± 1.48	19.6 ± 0.98	84.7 ± 4.38	3.68 ± 0.08	2.21 ± 0.03
	90	B2	10.2012	90.2 ± 1.99	17.3 ± 0.24	77.9 ± 1.69	4.32 ± 0.18	2.16 ± 0.03
	90	B3	10.2012	96.0 ± 9.92	23.4 ± 2.19	112 ± 2.74	3.76 ± 0.04	2.08 ± 0.03
			Mean of n = 9 NGI runs	**20.1 ± 2.92**	**91.4 ± 15.6**	**3.92 ± 0.32**	**2.15 ± 0.06**	

5.5.1.1.3 SALMETEROL XINAFOATE:FLUTICASONE PROPIONATE RATIO

The deviation from the nominal SX:FP ratio in the deposited mass across the NGI of the Seretide Accuhalers is shown in Figure 5.3. A deviation value greater than 0.0 would indicate more SX in the deposited mass, and a value smaller than 0.0 would indicate more FP in the deposited mass, compared to the nominal ratio. The SA100 inhalers showed a greater deviation than the SA500 inhalers in the SX:FP ratio of the deposited masses. However, for both inhaler strengths, there was proved to be negligible difference in the magnitude of the deviations according to the flow rate.

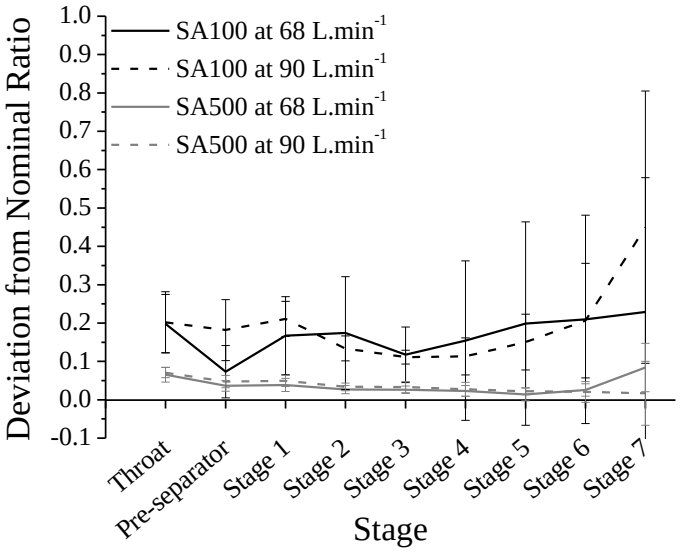

Figure 5.3 Deviation in the salmeterol xinafoate:fluticasone propionate (SX:FP) ratio of the deposited mass across the Next Generation Impactor for the Seretide Accuhaler 100 (SA100) and 500 (SA500) at 68 L.min^{-1} and 90 L.min^{-1} (mean ± SD, n = 3 – 4).

5.5.1.2 DE-AGGLOMERATION ANALYSIS BY SYMPATEC HELOS/RODOS

The particle size data (i.e. D_{v50} values) for the SA100 (B3, BN. 0241-1) and SA500 (B3, BN. 1412-2-1) were empirically modelled as described in Chapter 2. Although the data showed excellent linearity and DA_{max} close to 1, the DA_{50} of the SA100 product was -0.04 Bar (Table 5.5). The DA_{50} of the SA500 was 0.60 Bar. The CPP, a measure of powder cohesivity, of the SA100 product was 1.2 Bar. For the SA500 inhaler the particle size, in terms of the D_{v50}, remained consistent when pressures of 1.2 – 1.5 Bar, 3.0 – 3.5 Bar, and 4.5 – 5.0 Bar were employed. Examination of the particle size-primary pressure profile suggested that the plateau was likely to be in the range 3.0 – 3.5 Bar, therefore 3.0 Bar was assigned as the CPP.

Table 5.5 The R^2, primary pressure for 50 % de-agglomeration (DA_{50}) and maximum degree of de-agglomeration (DA_{max}) of Seretide Accuhaler 100 (SA100) and 500 (SA500) dry powder inhaler products by dry dispersion laser diffraction analysis.

Sample	Batch	R^2	DA_{max}	DA_{50} (Bar)	CPP (Bar)
SA100	0241-1	0.9951	1.06	-0.04	1.2
SA500	1413-2-1	0.9869	1.10	0.60	3.0*

*Particle size consistent for 2 increases in PP only within the pressure ranges 1.2 – 1.5 Bar, 3.0 – 3.5 Bar and 4.5 – 5.0 Bar. Examination of the particle size-primary pressure profile suggested that 3.0 – 3.5 Bar represented the plateau region and 3.0 Bar the CPP value.

5.5.1.3 DE-AGGLOMERATION ANALYSIS BY SYMPATEC INHALER

5.5.1.3.1 PRODUCT STRENGTH

The C_{opt}, fine fraction (FF; % < 5 µm) and intermediate fraction (IF; % < 15 µm) of the Seretide Accuhalers at 67 $L.min^{-1}$ ± 5 % over a typical 4 s inhalation was measured using the Sympatec INHALER (Figure 5.4 and Figure 5.5, respectively). For both the SA100 (B1, BN. R174041) and SA500 (B1; BN. R177573), the peak emission of fines was recorded after 0.5 s. The fraction then reduced and remained constant from 1.75 s onwards. During the first 1.75 s of the measurement, the higher strength SA500 product produced a higher fine (AUC = 11.1 ± 6.07 $\%.s^{-1}$) and intermediate (AUC = 25.6 ± 13.6 $\%.s^{-1}$) fraction compared to the SA100 (AUC = 8.49 ± 1.99 $\%.s^{-1}$ and 19.7 ± 5.23 $\%.s^{-1}$, respectively). The FF peak maximum (11.1 ± 2.73 % and 14.0 ± 6.63 %, respectively) and total AUC (11.5 ± 4.14 $\%.s^{-1}$ and 14.7 ± 8.83 $\%.s^{-1}$, respectively) were higher for the SA500 compared to the SA100. However, when expressed as a cumulative AUC undersize distribution, the curves for the two products overlapped. Furthermore, the C_{opt} traces over the 4 s period were almost identical (Figure 5.4). The C_{opt} can provide an indication of the relative amount of powder emitted by the inhaler over the measurement time, therefore indicating similar emissions between the inhaler strengths. It is therefore likely that a higher fine particle content in the higher strength product resulted in the larger AUC values, rather than a greater efficiency in fine particle generation.

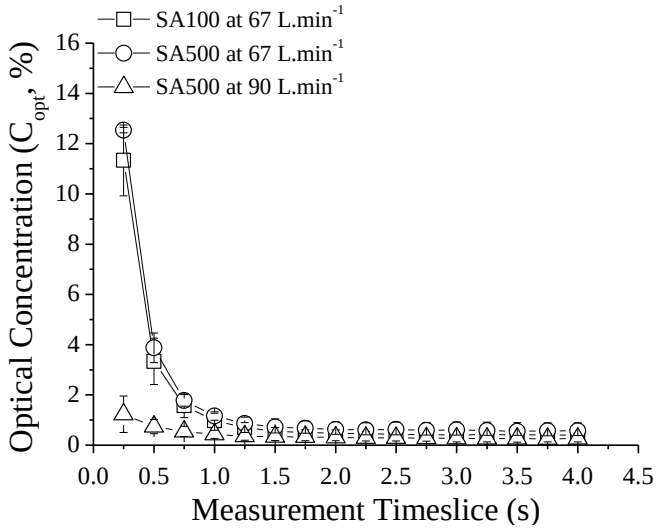

Figure 5.4 The optical concentration (C_{opt}) of the Seretide Accuhaler 100 (SA100) and 500 (SA500) operated at airflow rates of 67 and 90 L.min^{-1} (mean ± SD, *n* = 3).

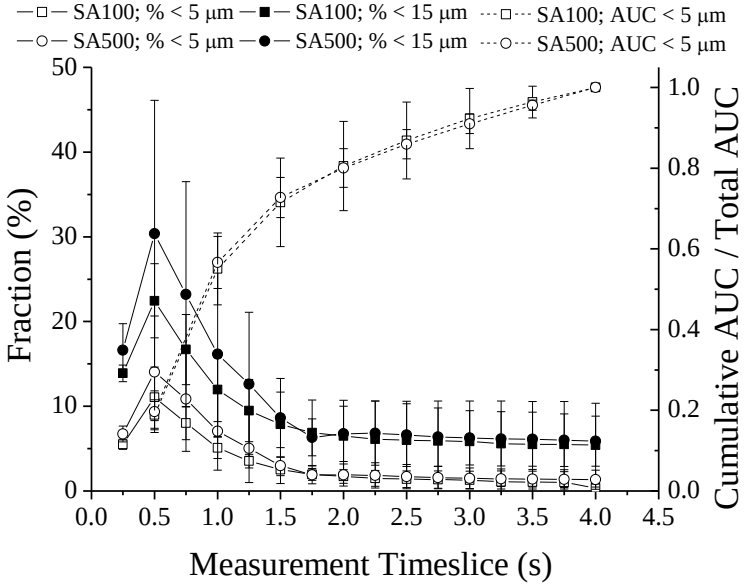

Figure 5.5 The fine fraction (% < 5 µm) and intermediate fraction (% < 15 µm) and the cumulative area under the curve (AUC; normalised to the total AUC) of the fine fraction only, of the Seretide Accuhaler 100 (SA100) and 500 (SA500) operated at an airflow rate of 67 L.min^{-1} over a 4 s measurement, split into 250 ms timeslices, following sizing in the Sympatec INHALER (mean ± SD, *n* = 3).

5.5.1.3.2 FLOW RATE

The influence of flow rate on the fine and intermediate fraction of the SA500 (B1, BN. R177573) is shown in Figure 5.6. Whereas at 67 L.min^{-1} the fraction of fines detected peaked at 0.5 s, this did not occur at 90 L.min^{-1}. The highest fraction was found to be present at the first measurement point (i.e. 0.25 s) and this was subsequently reduced to a plateau value after 1.75 s. At the higher flow rate, the contents of the inhaler may have therefore emptied quicker, corresponding to the lower C_{opt} values observed at the higher

flow rate (Figure 5.4). The AUC at 90 L.min^{-1} was smaller than at 67 L.min^{-1} for the fine fraction only (AUC = 8.51 ± 8.83 %.s^{-1} and 14.7 ± 8.83 %.s^{-1}, respectively). Despite this, when expressed as the cumulative AUC undersize distribution, the reduction in the AUC was apparent suggesting that de-agglomeration efficiency may have worsened.

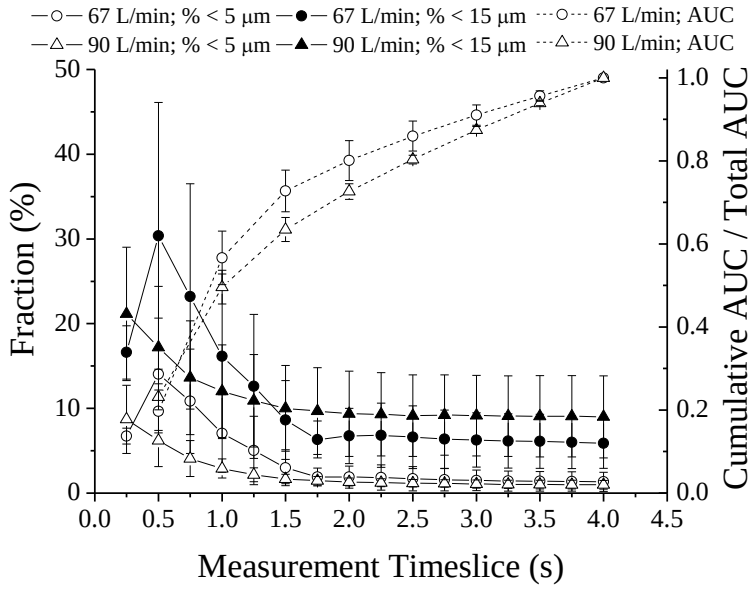

Figure 5.6 The fine fraction (% < 5 µm) and intermediate fraction (% < 15 µm) and the cumulative area under the curve (AUC; normalised to the total AUC) of the fine fraction only, of the Seretide Accuhaler 500 (SA500) over a 4 s measurement, split into 250 ms timeslices, following sizing in the Sympatec INHALER (mean ± SD, n = 3 - 4) operated at two flow rates (67 and 90 L.min^{-1}).

5.5.2 MANUFACTURED DRY POWDER INHALER BLENDS

5.5.2.1 BLEND HOMOGENEITY OF PRE-BLENDS

The blend homogeneity and drug content of SX:FP pre-blends used to prepared the DPI blends is summarised in Table 5.6. In all instances the CV of n = 6 samples was < 10 %.

Table 5.6 Blend homogeneity expressed as the % coefficient of variance (% CV), drug content (mean ± SD) and detected drug ratio of salmeterol xinafoate (SX) and fluticasone propionate (FP) in fine particle blends (n = 6).

SX:FP ratio	Homogeneity (% CV)		Drug Content (µg.mg^{-1})		Detected
	SX	FP	SX	FP	Drug Ratio
1:8	3.93	1.39	100.0 ± 3.53	909.9 ± 16.2	1.0:9.1
1:1	4.59	6.22	512.9 ± 22.6	492.3 ± 29.2	1.0:1.0
8:1	2.68	7.07	879.0 ± 22.4	109.6 ± 7.41	8.0:1.0

5.5.2.2 BLEND HOMOGENEITY OF DRY POWDER INHALER BLENDS

The homogeneity and drug content of the DPI blends is shown in Table 5.7. Homogeneity was assessed at two time points, prior to and post-tumbling. Prior to tumbling the homogeneity was very poor. Following tumbling, the homogeneity improved. Apart from the 1:1 blend, in all instances the CV was less than 4 %. The 1:1 blend had the poorest homogeneity for both SX and FP at 7.40 and 6.07 %, respectively.

Table 5.7 Blend homogeneity expressed as the % coefficient of variance (% CV), drug content (mean ± SD) and detected drug ratio of unfractionated salmeterol xinafoate (SX) and fluticasone propionate (FP) carrier based dry powder inhaler (DPI) blends prior to (n = 10) and post tumbling (n = 6).

Blend	**Homogeneity (% CV)**		**Drug Content (µg.mg^{-1})**		**Detected Drug Ratio**
Pre-tumbling	**SX**	**FP**	**SX**	**FP**	
SX:FP 1:8	32.1	24.8			
SX:FP 1:1	33.0	20.5			
SX:FP 8:1	19.5	74.0			
Post-tumbling	**SX**	**FP**	**SX**	**FP**	
SX:FP 0:1	n.a.	1.42	n.a.	13.6 ± 0.20	n.a.
SX:FP 1:8	2.45	3.57	1.39 ± 0.04	12.0 ± 0.41	1.0:8.7
SX:FP 1:1	7.40	6.07	6.53 ± 0.47	6.68 ± 0.44	1.0:1.0
SX:FP 8:1	3.78	2.59	12.3 ± 0.45	1.44 ± 0.04	8.6:1.0
SX:FP 1:0	1.83	n.a.	12.7 ± 0.23	n.a.	n.a.

5.5.3 SCANNING ELECTRON MICROSCOPY

5.5.3.1 PRE-BLENDS

The SEM images of the pre-blends containing micronised (i.e. unfractionated) SX and FP particles are shown in Figure 5.7. Each blend consisted of agglomerates. The blend containing SX and FP in the ratio 8:1 formed agglomerates predominantly containing flat SX particles, and the 1:8 blend had predominantly more rounded FP particles. The agglomerates in the 1:1 blend appeared to be mixed, with particle morphology characteristic of each drug (SEM images of micronised SX and FP are shown again for reference in Figure 5.8 and Figure 5.9).

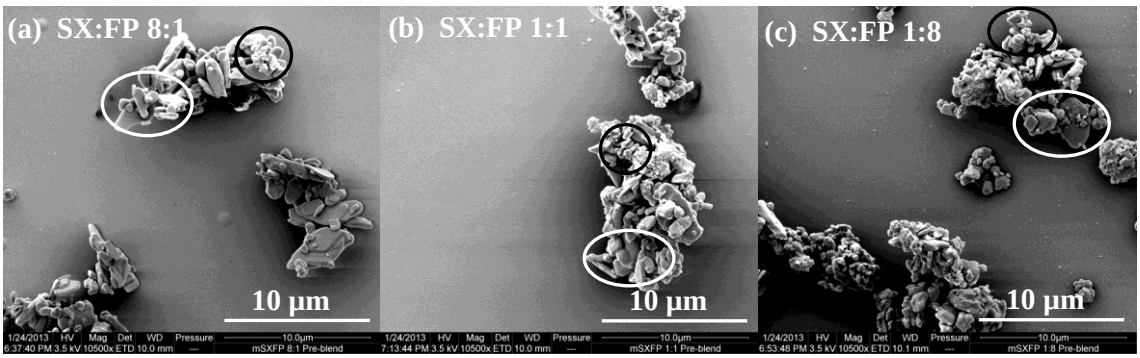

Figure 5.7 Scanning electron microscopy images of pre-blends containing salmeterol xinafoate (SX) and fluticasone propionate (FP) in the SX:FP ratio (a) 8:1, (b) 1:1 and (c) 1:8 at x 10500 magnification. Mixed SXFP agglomerates are present. Examples of flat, plate-like SX particles are circled in white and smaller, rounded FP particles are circled in black within mixed agglomerates.

5.5.3.2 DRY POWDER INHALER BLENDS

Figure 5.8, Figure 5.9, and Figure 5.10 show the SEM images of the 1.38 % DPI blends. In all instances individual drug particles were observed on the surface of the lactose carrier particles, as well as smaller drug-only agglomerates, again either on the surface of the carrier or free standing in the blend. The SX-only and FP-only blends could be distinguished by the shape of the drug particles; SX was flat and plate-like, whereas FP was more rounded in morphology. The blend containing SX and FP in the ratio 8:1 contained predominantly flatter SX particles, and the 1:8 ratio blend had an abundance of more rounded FP particles. The 1:1 blend did not have a predominance of either drug particle shape. Based on particle shape, in the combination blends, some drug agglomerates appeared to consist of both SX and FP.

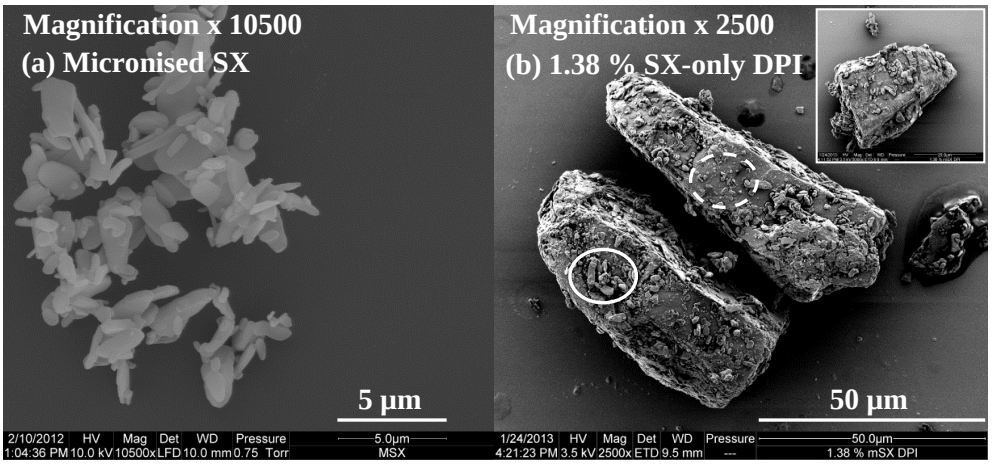

Figure 5.8 Scanning electron microscopy images of (a) micronised salmeterol xinafoate (SX) (taken from Chapter 4, Figure 4.4) and (b) 1.38 % w/w SX-only dry powder inhaler (DPI) blend. Drug agglomerates are circled with solid lines and individual drug particles are circled with dashed lines. The inset image is at x 10500 magnification.

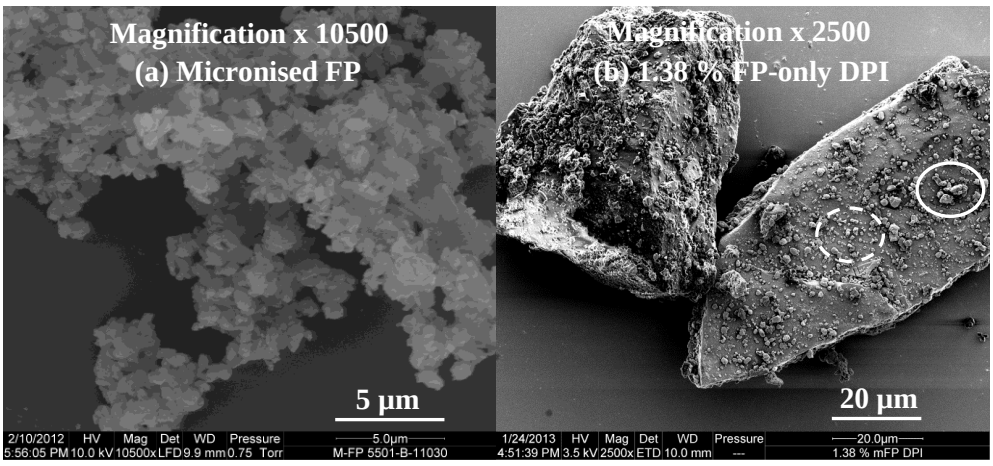

Figure 5.9 Scanning electron microscopy images of (a) micronised fluticasone propionate (FP) (taken from Chapter 4, Figure 4.4) and (b) 1.38 % w/w FP-only dry powder inhaler (DPI) blend. Drug agglomerates are circled with solid lines and individual drug particles are circled with dashed lines.

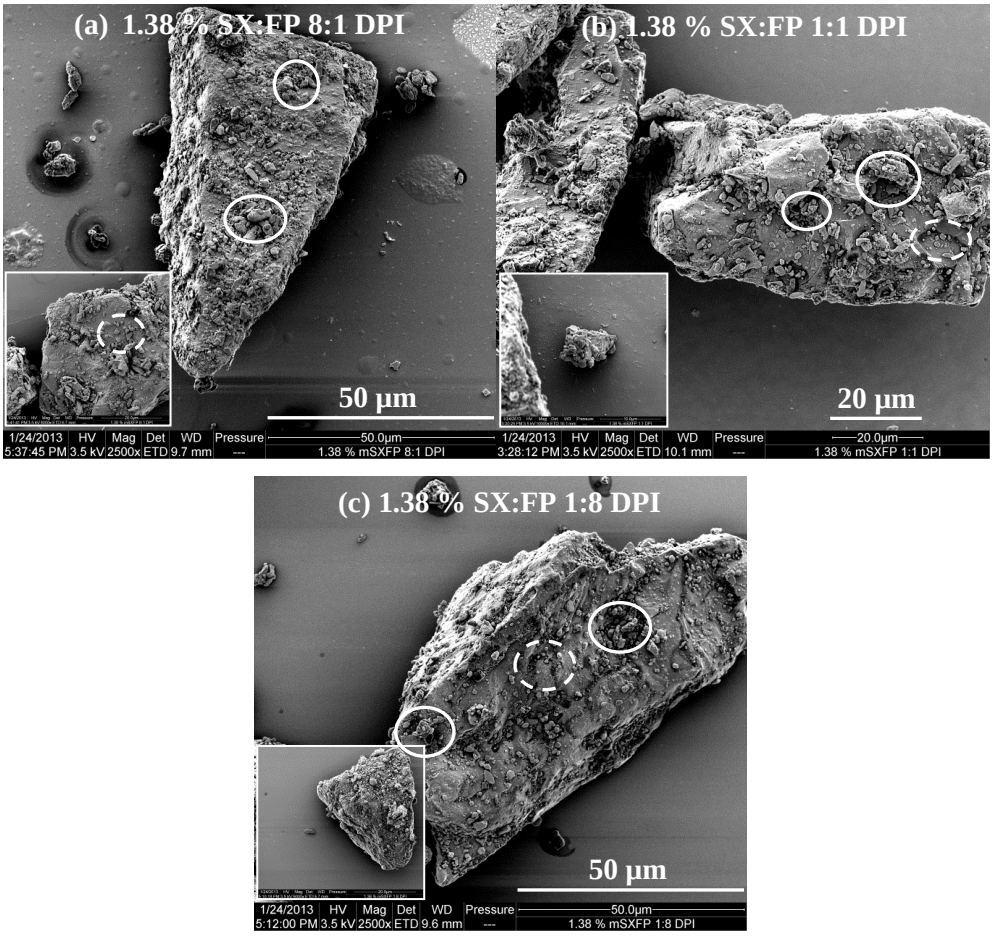

Figure 5.10 Scanning electron microscopy images of the dry powder inhaler (DPI) blends containing 1.38 % w/w salmeterol xinafoate (SX) and fluticasone propionate (FP) in the SX:FP ratio (a) 8:1, (b) 1:1 and (c) 1:8 at x 2500 magnification. Examples of drug agglomerates are circled with solid lines and individual particles are circled with dashed lines; inset images are at x 5000 magnification except SX:FP 1:1 x 10000 magnification.

5.5.4 WORK OF COHESION AND ADHESION

The work of cohesion between SX, FP and CL, and the work of adhesion between each component is shown in Figure 5.11. The values were calculated from the surface energy distributions of each drug determined by IGC, and represent the total surface energy (i.e. arising from both specific and dispersive interactions). Differences in the work of cohesion/adhesion occurred, revealing a different tendency for interaction. The work of adhesion for SX-FP was higher than the work of cohesion of SX, but lower than the work of cohesion of FP. Furthermore FP showed a stronger interaction with CL than SX with CL. Despite the larger particle size of CL relative to the drugs, CL was found to display the highest work of cohesion.

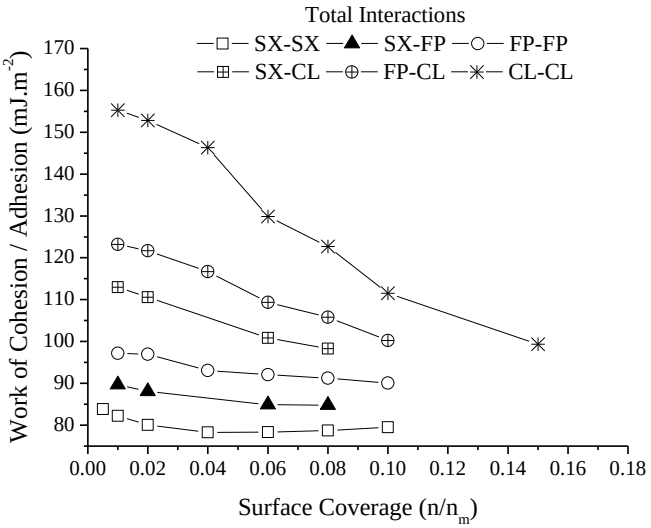

Figure 5.11 The work of cohesion and work of adhesion of salmeterol xinafoate (SX), fluticasone propionate (FP) and coarse lactose (CL) determined from the total surface energy distributions of the powders obtained by finite dilution inverse gas chromatography.

5.5.5 DISPERSIBILITY ASSESSMENT BY CASCADE IMPACTION

5.5.5.1 DRUG RATIO EFFECTS ON THE AEROSOLISATION OF PRE-BLENDS

Different aerosolisation behaviours were seen for micronised (i.e. unfractionated) SX and FP depending on whether delivery was alone or in combination into the NGI. Differences also appeared to depend on the drug ratio. For SX there was a reduction in the FPF when delivered in combination (Figure 5.12). The reduction in the FPF RD and ED was not significant except at the SX:FP ratio 1.0:9.1, in which it reduced by almost half that of SX alone ($p < 0.05$, Kruskal Wallis ANOVA with Dunn's post-test, GraphPad Prism 5). Furthermore, the MMAD of SX increased when aerosolised in

combination with FP (Table 5.8). The largest MMAD occurred in the blend containing the largest amount of FP ($p < 0.05$ at SX:FP 1.0:9.1 only, compared to SX alone). For FP, the small reduction in the FPF (RD or ED, Figure 5.13) was not significant ($p < 0.05$) and there was no change in the MMAD ($p > 0.05$, Table 5.8). The emission of neither drug was changed when aerosolised in combination ($p > 0.05$).

Table 5.8 The recovery (% of the actuated dose), mass median aerodynamic diameter (MMAD) and geometric standard deviation (GSD) of salmeterol xinafoate (SX) and fluticasone propionate (FP) aerosolised into the Next Generation Impactor from fine particle blends with different SX:FP ratios (mean ± SD, $n = 3$).

SX:FP Ratio	Recovery (%)	MMAD (μm)	GSD
Salmeterol xinafoate			
1.0:0.0	77.8 ± 6.47	2.66 ± 0.08	1.80 ± 0.02
8.0:1.0	92.6 ± 4.04	3.14 ± 0.22	1.86 ± 0.05
1.0:1.0	94.0 ± 2.80	3.51 ± 0.11	1.79 ± 0.03
1.0:9.1	101 ± 5.94	3.81 ± 0.09	1.80 ± 0.02
Fluticasone propionate			
0.0:1.0	78.0 ± 3.08	4.06 ± 0.25	2.00 ± 0.06
1.0:9.1	83.7 ± 3.67	3.81 ± 0.12	1.99 ± 0.04
1.0:1.0	91.5 ± 0.84	3.70 ± 0.09	2.00 ± 0.04
8.0:1.0	87.6 ± 11.9	3.58 ± 0.34	2.15 ± 0.16

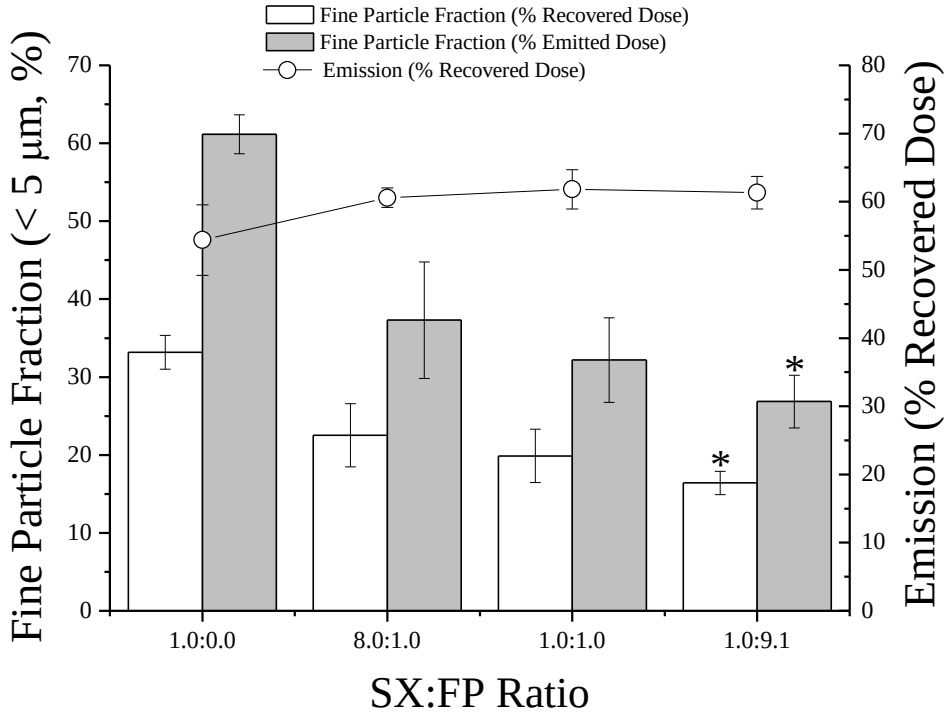

Figure 5.12 The fine particle fraction (FPF < 5 µm, expressed as a percentage of the emitted dose, ED, and recovered dose, RD) and emission (% RD) of salmeterol xinafoate (SX) in fine particle blends co-formulated with fluticasone propionate (FP) at different SX:FP ratios (mean ± SD, *n* = 3); * = $p < 0.05$ for co-formulation vs. SX alone by Kruskal Wallis with Dunn's post-test.

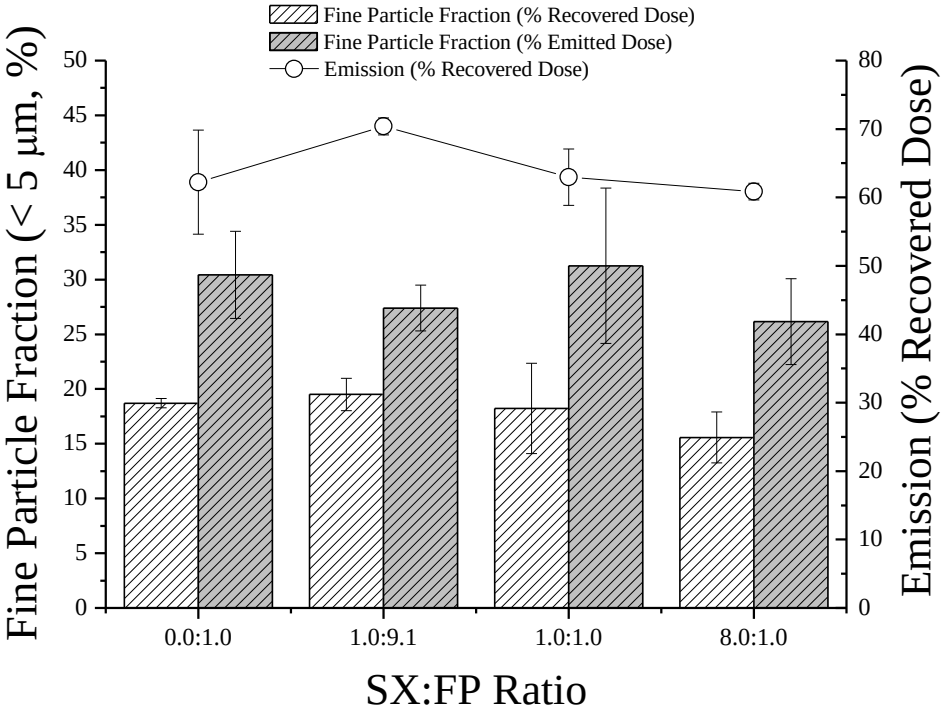

Figure 5.13 The fine particle fraction (FPF < 5 µm, expressed as a percentage of the emitted dose, ED, and recovered dose, RD) and emission (% RD) of fluticasone propionate (FP) in fine particle blends co-formulated with salmeterol xinafoate (SX) at different SX:FP ratios (mean ± SD, *n* = 3); * = $p < 0.05$ for co-formulation vs. FP alone by Kruskal Wallis with Dunn's post-test.

5.5.5.2 DRUG RATIO EFFECTS ON THE AEROSOLISATION OF DRY POWDER INHALER BLENDS

When aerosolised in combination from DPI blends, no difference in the aerosolisation behaviour of SX and FP was observed compared to single drug delivery. Considering SX, when aerosolised in combination at any SX:FP ratio, there was no significant difference in the FPF RD, FPF ED, emission or MMAD ($p > 0.05$, Kruskal Wallis ANOVA with Dunn's post-test) compared to the SX-only DPI (Figure 5.14, Table 5.9). However, for internal group comparisons between combination blends only, higher FPFs (both ED and RD) of SX were obtained from the 8.6:1.0 ratio compared to the 1.0:8.7 ratio, suggesting that the particles may be interacting (Figure 5.14). For FP, there were no significant differences between any of the parameters when comparing FP alone with FP in combination at all SX:FP ratios (Figure 5.15).

Table 5.9 The recovery (% of the actuated dose), mass median aerodynamic diameter (MMAD), and geometric standard deviation (GSD) of salmeterol xinafoate (SX) and fluticasone propionate (FP) from dry powder inhaler (DPI) blends with a 1.38 % w/w drug content composed of varying SX:FP drug ratios aerosolised into the Next Generation Impactor (mean ± SD, $n = 3$).

SX:FP Ratio	Recovery (%)	MMAD (µm)	GSD
Salmeterol xinafoate			
1.0:0.0	108 ± 6.01	3.08 ± 0.03	2.07 ± 0.11
8.6:1.0	92.7 ± 4.23	2.92 ± 0.11	2.09 ± 0.05
1.0:1.0	91.6 ± 8.94	2.97 ± 0.12	2.75 ± 0.18
1.0:8.7	102 ± 9.89	3.03 ± 0.15	2.28 ± 0.12
Fluticasone propionate			
0.0:1.0	94.0 ± 2.13	4.22 ± 0.07	2.01 ± 0.77
1.0:8.7	92.0 ± 4.10	4.09 ± 0.09	2.18 ± 0.03
1.0:1.0	83.0 ± 2.90	3.80 ± 0.25	2.15 ± 0.07
8.6:1.0	104 ± 20.6	3.69 ± 0.11	2.26 ± 0.03

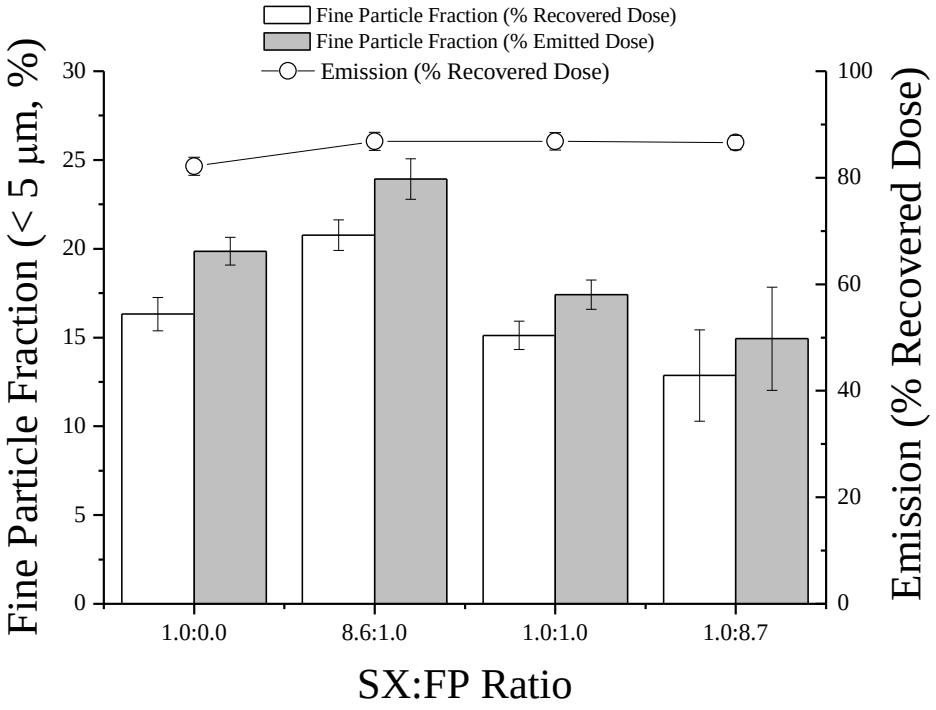

Figure 5.14 The fine particle fraction (FPF < 5 µm, expressed as a percentage of the emitted dose, ED, and recovered dose, RD) and emission (% RD) of salmeterol xinafoate (SX) from 1.38 % w/w total drug content dry powder inhaler blends containing SX and FP in different SX:FP ratios (1:0, 8.6:1.0, 1.0:1.0 and 1.0:8.7) assessed by Next Generation Impactor analysis (mean ± SD, *n* = 3).

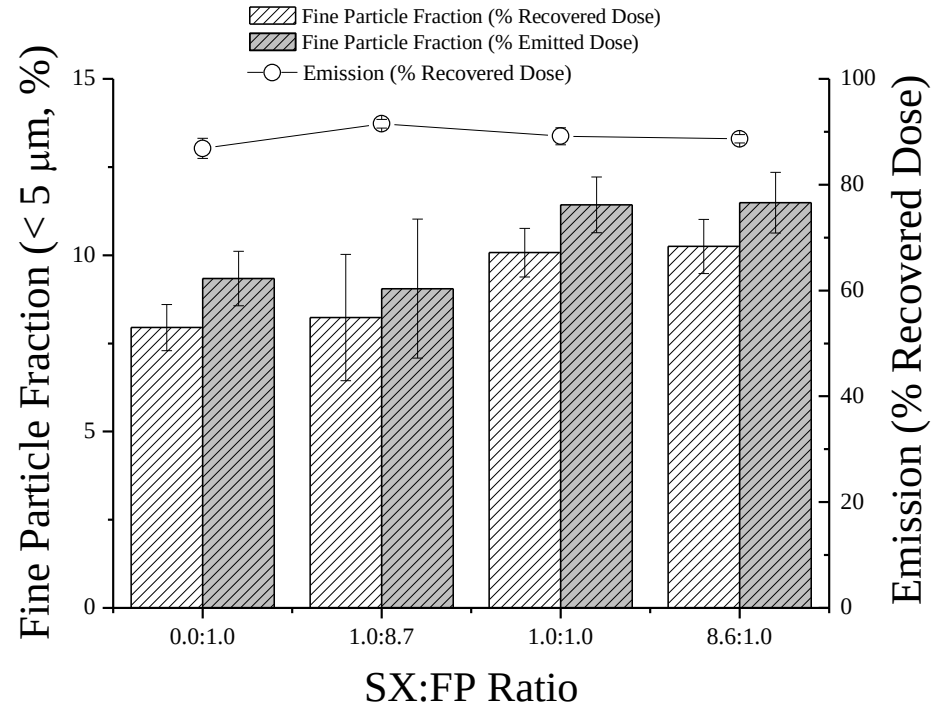

Figure 5.15 The fine particle fraction (FPF < 5 µm, expressed as a percentage of the emitted dose, ED, and recovered dose, RD) and emission (% RD) of fluticasone propionate from 1.38 % w/w total drug content dry powder inhaler blends containing SX and FP in different SX:FP ratios (0.0:1.0, 1.0:8.7, 1.0:1.0 and 8.6:1.0) assessed by Next Generation Impactor analysis (mean ± SD, *n* = 3).

Figure 5.16 shows the SX:FP ratios of the deposited masses across the NGI for the pre-blends and DPI blends. Considering the device, capsules, throat and pre-separator, across all the blends the greatest deviation in the ratio occurred in the capsules, in which there was greater SX retention than FP retention when compared to the nominal values. Differences between the deviations in the ratios were seen between the blend compositions and blend types. For pre-blends and DPIs, the greatest deviation occurred as the amount of SX in the blend increased. Whereas for the SX:FP 1:8 pre-blend there was negligible deviation from 1:8 in terms of deposition across the NGI stages, for the 1:1 blend deviations occurred beyond stage 3, and for the 8:1 ratio deviations occurred beyond stage 2; greater amounts of SX deposited on these stages relative to the nominal amount in the blend. When formulated as DPI blends the magnitude of the deviations increased. Furthermore, for the stages corresponding to the larger aerodynamic particle sizes (i.e. stages 1 – 2), there was a shift towards greater FP deposition relative to the nominal blend ratio in the DPI containing SX and FP in the ratio 8:1.

5.5.6 DISPERSIBILITY OF DRY POWDER INHALER BLENDS BY DRY DISPERSION LASER DIFFRACTION

The R^2, DA_{50} and DA_{max} of the DPI blends are shown in Table 5.10. In all instances the linearity of the modelled data was good ($R^2 > 0.94$) and the DA_{max} was < 1.20. Higher DA_{50} values are associated with poorer ease of de-agglomeration, therefore the data indicated that an FP-only DPI blend has a greater propensity for de-agglomeration than an SX-only DPI blend. Relative to these values, the SX:FP 8:1 DPI had the poorest de-agglomeration of all the blends and the SX:FP 1:1 DPI dispersed with intermediate efficiency. The SX:FP 1:8 DPI had comparable dispersibility to the FP-only DPI blend.

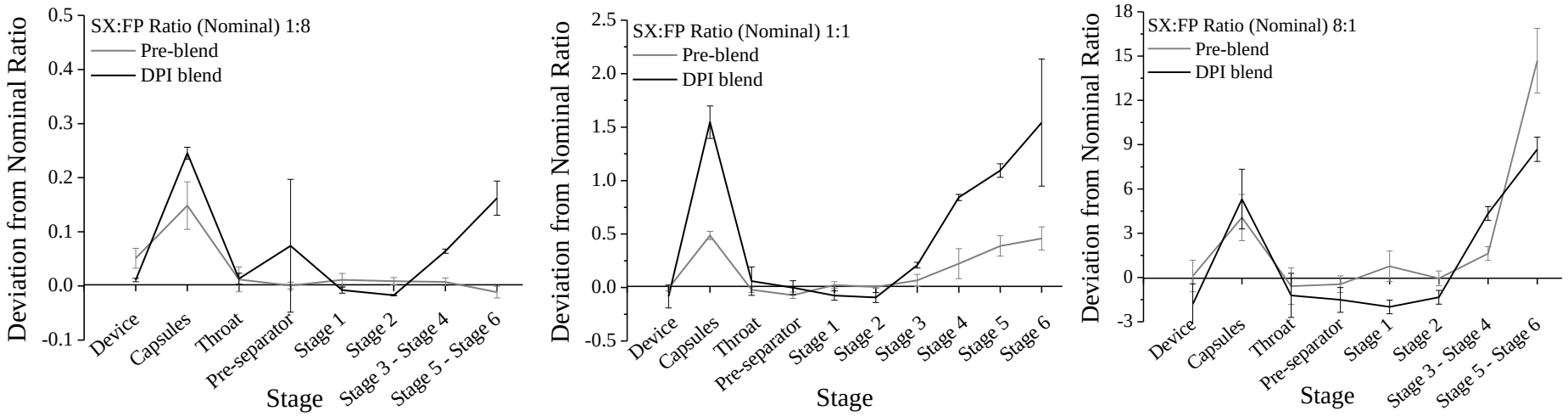

Figure 5.16 The deviation in the salmeterol xinafoate :fluticasone propionate (SX:FP) ratio of the deposited mass in the Next Generation Impactor for pre-blends and dry powder inhaler blends containing SX and FP in the nominal ratios 1:8, 1:1 and 8:1 (mean ± SD, n = 3).

It was not possible to deduce a CPP for the SX-only and SX:FP 8:1 ratio DPI (Table 5.10). For these blends, the measured size reduced with increasing PP, but did not remain at a constant value for three (or even two) consecutive increases in pressure. For the 1:1, 1:8 and FP-only blends, a gradual increase in the CPP was observed, coinciding with a higher FP content, and indicating less efficient de-agglomeration to primary particles, particularly of the most cohesive particles in the blend. This was corroborrated by the trend in the CPP of the Seretide Accuhalers, in that a higher FP content blend had higher bulk cohesivity.. The FP-only blend showed consistancy in the measured size in the PP range 0.2 – 1.5 Bar (5 PPs), 2.5 – 3.0 Bar (2 PPs), and 4.0 – 4.5 Bar (2 PPs). Upon inspection of the particle size-primary pressure profile, it was deduced that the latter range most closely resembled the plateau region in the pressure range studied and thus the CPP was asigned as 4.0 Bar. Considering both the DA_{50} and CPP values, this indicated a greater heterogeniety in agglomerate strengths/inter-particulate forces with increasing FP content in the blend.

Table 5.10 The R^2, primary pressure for 50 % de-agglomeration (DA_{50}), and maximum degree of de-agglomeration (DA_{max}) of carrier based dry powder inhaler blends containing 1.38 % w/w drug comprising SX and FP in varying SX:FP ratios assessed by dry dispersion laser diffraction analysis.

SX:FP Ratio	**R^2**	**DA_{max}**	**DA_{50} (Bar)**	**CPP (Bar)**
1.0:0.0	0.9378	1.13	1.01	-
8.6:1.0	0.9385	1.13	1.36	-
1.0:1.0	0.9856	1.06	0.66	3.0
1.0:8.7	0.9897	1.02	0.46	3.5
0.0:1.0	0.9879	1.01	0.41	4.0

5.6 DISCUSSION AND CONCLUSIONS

Combination DPIs are complex systems and contain multiple components. This includes the drug, carrier particle and in some cases a ternary agent. Understanding the physicochemical interactions between the particles, and the resultant aerosolisation performance, can aid in the optimisation of DPI characteristics for maximum therapeutic effect. The combination product Seretide®/Advair®, manufactured by GlaxoSmithKline, was introduced to the market in 2002, having received product approval in November 1999 (Hickey, 2013). The inhalers contains 50 µg SX and either 100, 250 or 500 µg FP (BNF, 2013). The aerodynamic deposition profiles of SX and FP from SA inhalers measured in the current study (Table 5.3 and Table 5.4) were generally in good agreement with those reported in the literature, as summarised in Table 5.11. These studies utilised a range of cascade impactors; only Taki et al. (2011) report the aerodynamic deposition profiles of SA100 and SA500 in the NGI. In a separate study Taki et al. (2010) determined the deposition profiles of the inhalers using different impactors (i.e. the ACI, MSLI and NGI), and although showing broadly similar trends, significant differences in the PSD was observed. It would therefore not be appropriate to make direct comparisons between the data reported in the literature. For this reason, the influence of product strength and flow rate on SX and FP aerosolisation were investigated in this study.

5.6.1 DISPERSION BEHAVIOUR OF THE SERETIDE ACCUHALER

Prior to probing the influence of product strength and flow rate on aerosolisation performance, it was necessary to establish equivalence between different batches of inhalers. This would ensure that any differences observed were not attributable to inter-batch variability. The BP (2012) stipulates that when assessing the uniformity of the delivered dose from a multi-dose inhaler, it is not sufficient to test a single inhaler, and inter- (and intra-) inhaler dose uniformity must be taken into account. Three batches of the SA100 and SA500 strength inhaler were therefore tested, each having different expiry dates. Batch 1 for both strength of inhaler was tested outside of its expiry date (Table 5.2). Under ambient conditions, the inhalers have shown good reproducibility in fine particle delivery. Following storage at 25 ^{o}C and 30 % RH for 3 months, Borgström et al. (2005a) reported no change in the FPF of SX or FP (19 and 20 %, respectively) from an SA100 product. Only storage under hot and humid conditions (40 ^{o}C, 75 % RH for 3 months) resulted in a reduction in the FPF (Borgström et al., 2005a).

Table 5.11 A summary of the aerodynamic deposition profiles of Seretide Accuhaler products reported in the literature in terms of the fine particle dose or mass (FPD or FPM), fine particle fraction (FPF) and mass median aerodynamic diameter (MMAD).

Product	**Impactor**	**Flow Rate (L.min^{-1})**	**Parameter**	**Results**		**Reference**
				Salmeterol xinafoate	**Fluticasone propionate**	
SA100	MSLI	60	FPD[1] (% < 5 µm of label dose)	21	22	Borgström et al. (2005a)
SA500	ACI	Electronic Lung to simulate realistic inhalation profiles	FPD[2] (% < 5.8 µm of label dose) MMAD (µm)	18.4 ± 4.4 3.54 ± 0.47	20.4 ± 4.8 3.57 ± 0.48	Tarsin et al. (2006)
SA250*	ACI	60	FPM[3] (µg per dose, 0.8 – 6.2 µm)	12.8	66.2	Daley-Yates et al. (2009)
SA100	NGI	60	FPF[4] (% < 5 µm) MMAD (µm)	19.33 ± 0.81 4.08 ± 0.04	17.99 ± 0.75 4.50 ± 0.08	Taki et al. (2011)
SA500	NGI	60	FPF[4] (% < 5 µm) MMAD (µm)	20.18 ± 1.09 3.46 ± 0.08	21.34 ± 0.99 3.60 ± 0.05	
SA100	NGI	30 / Q$^{\#}$	FPF[5] (% < 5 µm) MMAD (µm)	8.50 ± 0.19 / 23.98 ± 0.97 6.81 ± 0.03 / 3.71 ± 0.63	10.70 ± 0.27 / 22.53 ± 0.88 6.39 ± 0.06 / 4.16 ± 0.07	Taki et al. (2010)
SA100	MSLI	30 / Q$^{\#}$	FPF[5] (% < 5 µm) MMAD (µm)	11.92 ± 0.47 / 12.23 ± 0.40 6.12 ± 0.40 / 4.50 ± 0.12	14.22 ± 0.71 / 21.54 ± 0.36 5.62 ± 0.41 / 4.08 ± 0.15	
SA100	ACI	30 / Q$^{\#}$	FPF[5] (% < 5 µm) MMAD (µm)	10.66 ± 0.64 / 20.01 ± 1.27 5.21 ± 0.15 / 3.13 ± 0.12	14.68 ± 1.01 / 21.17 ± 1.18 4.81 ± 0.13 / 2.97 ± 0.01	
SA500	NGI	30 / Q$^{\#}$	FPF[5] (% < 5 µm) MMAD (µm)	13.34 ± 0.03 / 25.12 ± 1.27 4.96 ± 0.16 / 3.23 ± 0.05	16.14 ± 0.52 / 26.44 ± 1.14 4.78 ± 0.13 / 3.30 ± 0.04	
SA500	ACI	30 / Q$^{\#}$	FPF[5] (% < 5 µm) MMAD (µm)	16.00 ± 0.02 / 17.35 ± 1.13 4.15 ± 0.09 / 3.05 ± 0.12	18.25 ± 0.63 / 22.53 ± 1.30 4.20 ± 0.05 / 3.07 ± 0.06	
SA500	MSLI	30 / Q$^{\#}$	FPF[5] (% < 5 µm) MMAD (µm)	15.58 ± 0.51 / 18.19 ± 1.63 4.05 ± 0.12 / 3.78 ± 0.13	21.61 ± 0.42 / 23.22 ± 0.67 3.87 ± 0.17 / 3.43 ± 0.02	

*SA250 not tested in the current study. # flow rate corresponding to a pressure drop of 4 kPa across the device (approx. 70 L.min^{-1}). [1]mass of drug < 5 µm as a percentage of label claim, mean of n = 3. [2]mass of drug < 5.8 µm as a percentage of label claim, mean ± SD of n = 20. [3]mass of drug 0.8 – 6.2 µm, mean of n = 4. [4]percentage of drug < 5 µm, mean ± SD of n = 4, [5]percentage of drug < 5 µm of the total recovered dose, mean ± SD of n = 4.

To assess equivalence between the batches, the EMEA guidance for bioequivalence was adopted. The guidance requires deposition across the upper and lower stages of the impactor to be considered, comprising both lung and non-lung deposition sites, and with a suggested acceptable level of variation of ± 15 % (EMEA, 2009). For the analysis, the amount deposited was normalised to the recovered dose (Section 5.5.1.1.1). The reasons for this were two-fold, firstly to account for differences in the recovered doses between NGI experiments (Table 5.3 and Table 5.4) and secondly, due to the design of the Accuhaler device, it was not possible to determine the amount of drug that was retained in the device/foil strip without dismantling the device. Therefore it was only possible to determine the emitted dose and not the total recovered dose, which would include drug retention in the device, for each NGI experiment. The percentage of stages showing equivalence ranged from 83.3 – 100 % for SX and 91.7 – 100 % for FP. Despite 100 % equivalence not being found in all instances, for the purpose of this study the batches were considered equivalent. The data for the batches were therefore pooled according to product strength and flow rate prior to statistical analysis.

Considering the aerosolisation characteristics of the SA products, the FPF of SX and FP was unchanged between product strengths and flow rates ($p > 0.05$) indicating consistent fine particle delivery. This finding is corroborated by Taki et al. (2010) where only small changes in the FPF between these product strengths was observed. Differences, although small, were also reported between flow rates in the latter study, when a higher flow rate was found to improve the FPF of both drugs in the NGI. The Diskus/Accuhaler device is generally considered to show minimal flow rate dependence, and has demonstrated consistent performance across different inhalation profiles (Bisgaard et al., 1998; Tarsin et al., 2006). To probe co-association, the SX:FP ratio of the deposited masses through the NGI were compared to the nominal values for the inhalers. Where the ratio of SX and FP deposition matched that of the formulation, this could be considered as a possible marker for co-association of the particles. For both inhaler strengths, the flow rate had only minor effects on the SX:FP ratio depositing on each stage. However, the SA500 inhaler not only showed a smaller magnitude in the deviation from the nominal ratio compared to the SA100, but the ratio also closely matched the nominal ratio. The ability to match the ratio of deposition to that in the formulation may therefore depend on the amount of SX and FP in the formulation.

Both SX and FP also displayed differences in MMAD. For SX, at both flow rates the SA500 inhaler produced a smaller MMAD than the SA100 inhaler, but the difference was not significant ($p > 0.05$). For both the SA100 and SA500, the MMAD values of SX at 90 $L.min^{-1}$ were larger than at 67 $L.min^{-1}$, and this change was significant ($p < 0.05$). For FP, the trends were the same but the statistics were the converse i.e. a larger MMAD occurred at 90 $L.min^{-1}$ compared to 67 $L.min^{-1}$ but the difference was not significant ($p > 0.05$). However, the smaller MMAD from the SA500 compared to SA100 inhaler at both flow rates was found to be significant ($p < 0.05$). These changes in the MMAD suggested a level of interaction between SX and FP in these formulations. For both drugs a higher FP content was beneficial in terms of reducing the MMAD, a finding also reported by Taki et al. (2011). The larger MMAD at the higher flow rate demonstrated that there is an inter-play between formulation properties, flow rate and inhaler design on the dispersion of inhalable powders (Chew and Chan, 1999; Chew et al., 2000). Despite higher flow rates increasing turbulence and the number and intensity of particle impactions in an inhaler device, higher inhaler exit velocities are associated with higher deposition in the throat of the impactor for the Aerolizer. It has been suggested therefore that for maximal overall inhaler performance, an optimal flow rate will exist, which will be specific to the device and cohesivity of the drug (Coates et al., 2005).

Laser diffraction particle sizing in the dry state was used to probe further the aerosolisation behaviours of the SA inhalers. Particle size-primary pressure curves were generated using the Sympatec HELOS/RODOS to determine the dispersibility of the bulk powder. Following empirical modelling, the SA100 inhaler had a DA_{50} of 0.60 Bar. Despite good linearity and DA_{max} values, the DA_{50} of the SA500 inhaler was -0.04 Bar. This arose due to the negative intercept of the linearised data and the relatively small change in the D_{v50} across the dispersing pressures (i.e. D_{v50} at 0.2 Bar = 12.72 µm and D_{v50} at 5.0 Bar = 8.84 µm). It was not possible to assign a CPP for the SA500 using the criteria in Chapter 2; instead three regions were identified in which the particle size remained constant for two consecutive PP increases. Following a visual assessment of the curve, a CPP of 3.0 Bar was assigned. This was higher than the CPP of SA100 (CPP = 1.2 Bar) indicating that the SA500 was a more cohesive powder. Although providing some useful information, the technique may therefore be less suitable for powder mixtures containing particles with a wide range of particle sizes compared to fine particle mixtures, which would contain smaller particles and narrower overall PSDs in

the bulk blend. However, clearly more work is required using a wider range of DPI formulations.

The Sympatec INHALER provided insight into the emptying kinetics of the powders from within the inhaler device. The particle size of the formulations was recorded over 4 s and the fine and intermediate fraction was monitored. At 67 $L.min^{-1}$ there was no difference in the onset of the peak maximum of the fractions between the SA100 and SA500 inhalers. To provide a quantitative measure of emptying, the area under the curve (AUC) was calculated. Cumulative AUC curves indicated identical emptying of the inhaler formulations at this flow rate (Figure 5.5). The fine and intermediate fractions were higher from the SA500 inhaler than from the SA100, whereas when aerosolised into the NGI the FPFs were similar for SX or higher for FP from the SA500 ($p > 0.05$). The C_{opt}, a measure of the relative amount of powder emitted, was identical between the inhalers (Figure 5.4) therefore higher fine/intermediate fractions may have arisen from better bulk dispersibility and a higher fine particle content for the SA500, as the inhalers contain the respective amount of drug per 12.5 mg of formulation containing the lactose carrier (GSK, 2011). Differences were also observed for the SA500 inhaler between flow rates. At the higher flow rate, the peak maximum occurred earlier and there was a reduction in the emptying efficiency of the inhaler (Figure 5.6). NGI analysis revealed similar or lower FPFs (for SX and FP, respectively, $p > 0.05$) and larger MMADs at 90 $L.min^{-1}$ compared to 68 $L.min^{-1}$, further suggesting that the de-agglomeration efficiency may be altered. A comparison of the C_{opt} between flow rates also revealed that less powder was emitted at 90 $L.min^{-1}$, or alternatively it is possible that some of the powder emptying process may have been missed during the sizing measurement due to very rapid emptying of the inhaler.

5.6.2 DISPERSION BEHAVIOUR OF SALMETEROL XINAFOATE AND FLUTICASONE PROPIONATE IN CO-FORMULATED PRE-BLENDS AND DRY POWDER INHALER BLENDS

In order to probe the origin of potential SX-FP interactions which may have led to the differing MMAD values between the different SA inhaler strengths, a series of DPI blends were prepared. It is necessary to control as many variables as possible in the design of such studies, such that the influence of individual factors can be determined (Taki, 2008a). For example, in Diskus formulations the size of the lactose carrier can

range from 50 – 150 µm (Borgström et al., 2005b), and the grade of the lactose, and concentration of lactose fines, are not known (Taki et al., 2011). By matching the blends in terms of their manufacturing methodology, storage history and drug content, differences in aerosolisation behaviour could then be attributed to particulate interactions (Taki, 2008a). Despite extensive research relating to DPI performance, there has been little focus on the aerosolisation efficiency of combination formulations in relation to drug ratios (Jetmalani et al., 2012). SX-FP pre-blends of varying drug ratios were therefore prepared, and showed adequate homogeneity. In all instances the % CV was less than 10. This value was higher than that typically used for DPI formulations; however, SX and FP have previously demonstrated poor mixing/homogeneity requiring the accepted limit of homogeneity for small scale low shear mixing to be increased to 7 – 10 % (Louey et al., 2004b; Murnane et al., 2009). For FP, the homogeneity became poorer as the SX content of the blend increased (from 1.39 %, 6.22 % to 7.07 % CV at nominal SX:FP ratios of 1:8, 1:1 and 8:1, respectively), whereas the homogeneity of SX was less than 5 % CV across the different ratios. When viewed by SEM, the pre-blends formed mixed agglomerates. Based on the particle shape, it was possible to identify agglomerates consisting of both SX and FP, and the proportion of SX/FP particles in the agglomerates reflected the composition of the pre-blend. Poorer FP homogeneity may therefore have arisen due to segregation as highly cohesive FP particles can form strong, FP-only agglomerates during blending, particularly at high FP concentrations (Sebti et al., 2007; Le et al., 2012b; Le et al., 2012d). During blending, highly cohesive particles require high shear forces to initially disrupt drug-drug interactions and promote mixing. However, where particle properties within a mixture differ for example in size, density or surface characteristics, and when subjected to the progressive formation and disruption of drug agglomerates during processing such as Turbula blending, particle de-mixing can occur leading to poor homogeneity (Sebti et al., 2007).

When aerosolised into the NGI, the composition of the pre-blend affected the aerosolisation performance of the drugs. For SX, although the emission was unchanged, the FPF (ED and RD) reduced and the MMAD increased with increasing FP content; this effect was significant only at the highest FP content. For FP, conversely, there was no change in the emission, FPF (ED or RD) or MMAD in the presence of SX, and regardless of the SX content. Mixed agglomerates viewed by SEM are formed randomly upon mixing dependent upon the composition and strength of the powder mix and on

the balance of cohesive and adhesive forces within the blend (Jetmalani et al., 2012). Both SX and FP tend to adhere to each other but a higher SX adhesivity towards FP compared to that of FP to SX suggested that SX would be more likely to interact with and thus demonstrate altered dispersibility when in combination with FP. Furthermore, an SX-rich blend demonstrated better bulk dispersibility (DA_{50} = 0.20 Bar) compared to an FP-rich blend (DA_{50} = 0.87 Bar) as shown by the results presented in Section 3.5.4. The dominance of weaker adhesive SX-FP interactions compared to stronger cohesive FP-FP interactions in an SX-rich and FP-rich blend, respectively, would have led to better dispersion of the bulk SX-rich blend.

As a measure of co-association, the SX:FP ratios of the deposited masses upon the successive stages of the NGI were compared to the nominal ratios of the blends. For all the pre-blends, a large deviation in the ratio was observed after aerosolisation of the powders from the capsules, potentially due to high SX adhesion to the capsule walls. Across the NGI stages 1 - 6, the SX:FP 1:8 blend showed negligible deviation in the ratio suggesting that the particles could be co-associated during aerosolisation and thus deposited in these proportions across the NGI. For the SX:FP 1:1 and 8:1 blend, the ratio was maintained on stages 1 – 3 and 1 – 2, respectively. Beyond these stages, the amount of SX depositing relative to FP was greater than the nominal ratio. For these blends, it is likely that a proportion of the particles were not co-associated during aerosolisation and therefore the smaller (D_{v50} = 1.42 ± 0.08 µm, MMAD = 2.7 ± 0.1 µm; Chapter 4) and more dispersible SX particles (DA_{50} = 1.45 Bar, work of cohesion = 83.8 – 79.5 $mJ.m^{-2}$) were able to travel further into the NGI compared to the larger, less dispersible FP particles (D_{v50} = 2.94 ± 1.22 µm, MMAD = 4.1 ± 0.3 µm, DA_{50} = 1.75 Bar, work of cohesion = 90.1 – 97.2 $mJ.m^{-2}$). Furthermore, it was only when the SX:FP ratio of the deposited masses matched the nominal ratio (i.e. 1:8) in which the dispersibility of SX became worse compared to that of SX alone, suggesting co-association may be playing in role in altering the dispersion behaviour of SX when co-formulated with FP.

When preparing DPI blends from the SX:FP pre-blends, a fixed drug content of 1.38 % w/w was selected. DPI blends containing SX or FP have been prepared with drug concentrations in the range 0.58 – 5 % (e.g. Shekunov et al., 2003; Islam et al., 2004; Tong et al., 2006; Das et al., 2009a, Das et al., 2009b; Murnane et al., 2009) whereas combination SX:FP formulations have contained 1.6 % and 5 % total drug (Taki, 2008;

Pitchayajittipong et al., 2009; Kubavat et al., 2012). The SA 50/100 strength inhaler contains 72.5 µg SX (equivalent to 50 µg salmeterol base) and 100 µg FP per 12.5 mg pre-metered dose. Therefore, in keeping with this composition, a drug content of 1.38 % and capsule fill weight of 12.5 mg was selected for the study.

In order to follow the process of SX-FP interaction, blend homogeneity was assessed prior to and post-tumbling in a Turbula mixer. Prior to tumbling the homogeneity was extremely poor, ranging from 19.5 – 74.0 % CV. The low level energy input from the whirlimixer was insufficient to disrupt SX-SX, FP-FP, SX-FP and CL-CL interactions and promote mixing between the particle types to obtain a homogenously mixed carrier-based blend, despite the adequate homogeneity of the pre-blends. CL was found to have a high, heterogeneous, surface energy (γ_D = 46.2 – 65.3 $mJ.m^{-2}$) which corresponded with a high, heterogeneous, work of cohesion (Figure 5.11). The surface energy and heterogeneity of lactose can vary depending on the grade (e.g. 40 – 48 $mJ.m^{-2}$, Ho et al., 2010), processing (e.g. 42 – 53 $mJ.m^{-2}$ at infinite dilution, Thielmann et al., 2007) and pseudo-polymorphic form (e.g. 36 – 46 $mJ.m^{-2}$ at infinite dilution, Traini et al., 2008), and this may influence the mixing and segregation rate during blending (Saleem et al., 2008). Where formulations contain a low concentration of a cohesive drug blended with a coarse excipient, for optimal homogeneity, 'powerful' shear mixers are required and approaches such as increasing the mixing speed (in rpm) can improve homogeneity by increasing the forces associated with particle collisions and enabling cohesive interactions to be overcome (Sebti et al., 2007; Le et al., 2012c). Post-tumbling, the % CV values reduced dramatically to 2.45 – 7.40 % CV. Therefore the combination of additional shear forces in the Turbula mixer and the propensity for SX-CL and FP-CL adhesive interactions, led to the formation of relatively homogeneously mixed blends. This finding was confirmed by SEM imaging, where predominantly individual drug particles and drug agglomerates distributed over the surface of lactose particles were observed (Figure 5.8, Figure 5.9 and Figure 5.10).

Differences in the bulk powder dispersibility of the combination DPI blends were found. Considering the single-drug DPIs, a paradoxical effect in terms of the DA_{50} and FPF was seen, for which the bulk dispersibility of the FP-only blend was better (DA_{50} = 0.40 Bar) than the SX-only blend (DA_{50} = 1.01 Bar), despite FP producing a lower FPF when aerosolised into the NGI (FPF ED 9.3 ± 0.77 % and 19.9 ± 0.78 % for FP and SX,

respectively). When considering the absolute particle sizes (with forced stability 9), the D_{v50} ranged from 16.3 – 26.3 µm for the FP-only blend compared to 8.5 – 25.5 µm for the SX-only blend. Therefore, although the bulk powder dispersibility was better, stronger inter-particulate interactions between the individual particles within agglomerates resulted in larger measured particle sizes compared to the SX-only blend. Furthermore, a high CPP of 4.0 Bar for the FP-only blend indicated that the powder was highly cohesive and that the most tightly associated agglomerates within the powder bulk had strong inter-particulate forces. Although it was not possible to determine a CPP value for the SX-only DPI, the magnitude of FP-CL and FP-FP interactions were higher than SX-CL and SX-SX interactions as determined by IGC, thus supporting the proposal that the interactive forces between particles in the FP blend were stronger. When in combination, as the FP content of the DPI blend increased, the DA_{50} reduced from 1.36 Bar to 0.66 Bar and 0.46 Bar, approaching that of the FP-only DPI (DA_{50} = 0.41 Bar). It was not possible to determine a CPP value for the SX-only or SX:FP 8:1 DPI. However, the CPP increased for the SX:FP 1:1, 1:8 and 0:1 ratio DPIs from 3.0, 3.5 to 4.0 Bar indicating increasingly cohesive powders and greater heterogeneity in agglomerate strengths. The rank order in the magnitude of particle interactions deduced from surface energy analysis was: FP-CL > SX-CL > FP-FP > FP-SX > SX-SX according to the work of cohesion and adhesion. Therefore, the overall magnitude of the interactive forces in an FP-rich blend were likely to be greater than those in an SX-rich blend.

When aerosolised into the NGI, the emission, FPF (ED or RD) and MMAD of SX and FP from a DPI blend were not affected by the DPI containing either a single drug or a co-formulation. Examining the effect of drug ratio on aerosolisation, by internal group analysis of the combination blends only, a similar trend to the pre-blend behaviour was observed. Hence, FP was unaffected by the presence of SX in terms of any of the calculated parameters. For SX, the emission did not change between ratios, indicating that SX was detached from the carrier with equal efficiency regardless of the SX:FP ratio, and that similar amounts of SX entered the stages of the impactor below the pre-separator (Podczeck, 1998). However, the FPF (ED and RD) of SX was lower in the nominal SX:FP ratio 1:8 compared to the ratio 8:1 ($p < 0.05$), and the MMAD was larger ($p > 0.05$). If fine particle agglomerates are able to detach from the carrier intact, although the emission may be high, the FPF may be low due to poor dispersion of tightly associated agglomerates (Podczeck, 1998). Agglomerates consisting

predominantly of FP in the SX:FP ratio 1:8 may therefore have been more difficult to disperse than agglomerates containing smaller proportions of FP in the SX:FP ratio 8:1 upon the release of agglomerates from the carrier. The interactive forces were in the following rank in terms of their magnitude: FP-FP > SX-FP > SX-SX, and FP-rich fine particle blends had a higher DA_{50} values than SX-rich fine particle blends (Table 3.6). The deposition of agglomerates rather than dispersed individual particles in the NGI would also have had a more detrimental effect on the FPF of SX than FP due to the former's inherently smaller particle size.

5.6.3 CONCLUSIONS

In conclusion, this study has probed the co-association of SX and FP in combination formulations. The FPF of SX and FP from Seretide Accuhalers was found to be consistent regardless of the inhaler strength or flow rate tested using NGI analysis. However, differences in the MMAD and SX:FP ratio of the deposited masses between the product strengths suggested that the two component drugs may undergo some physicochemical interaction which alters the deposition profiles of the drugs. When formulated as pre-blends, the presence of FP was detrimental to the dispersibility of SX but not the converse, and this effect was further dependent on the SX:FP ratio. When formulated as DPIs, co-formulation did not alter the dispersion of either drug compared to single drug delivery, however, intergroup analysis of the combination ratios only found an FP concentration-dependent worsening in the dispersibility of SX from these formulations in the NGI. Analysis of the SX:FP ratios through the impactor revealed that FP-rich (i.e. SX:FP 1:8) blends showed the smallest deviation in the SX:FP ratio of the deposited mass compared to the nominal value, and had a detrimental effect on the dispersibility of SX from the blend. Furthermore, the deviation increased in the presence of a carrier for all the formulations. The occurrence of co-association between SX and FP, as represented by the deviation from the nominal ratios where no deviation would indicate particle co-association, may therefore be influenced by the formulation in terms of the SX:FP ratio and the presence of a carrier.

6 ENGINEERING DRUG PARTICLE DISPERSION, DEPOSITION AND DISSOLUTION IN COMBINATION DRY POWDER INHALER FORMULATIONS- THE INFLUENCE OF PARTICLE PROPERTIES

6.1 INTRODUCTION

The development of dry powder inhaler technology towards optimal performance has taken two routes, the design of novel devices with enhanced efficiency, and the improvement of existing powder formulations. Although sophisticated device designs such as active dispersion are possible, they are complex and costly. A more favourable option is therefore to optimise the formulation for use with simple, user-friendly devices (Chow et al., 2007). Engineering approaches can therefore involve either advancing the formulation or the particle manufacturing process in order to attain critical features in the particles. The aim of particle engineering can be to improve stability, increase dispersibility, achieve controlled release or increase drug permeability or bioavailability (Weers et al., 2010).

The engineering of combination formulations for dry powder delivery has taken a number of routes. These include the production of combination particles containing both of the constituent drugs in a single particle either through controlled crystallisation (e.g. Westmeier and Steckel, 2008; Pitchayajittipong et al., 2009), co-spray drying (e.g. Corrigan et al., 2006; Tajber et al., 2009a; Tajber et al., 2009b; Kumon et al., 2010; Traini et al., 2012) or inducing the agglomeration of drug nanoparticles (El-Gendy et al., 2011). To date, combination particles have demonstrated similar aerosolisation to micronised drug blends following aerosolisation from DPIs, however, not only is the physical and chemical stability of these novel particles not yet known, obtaining scale up and regulatory acceptance of new particle engineering technologies will remain a challenge (Weers et al., 2010). In combination formulations consisting of physically mixed particles, re-crystallisation to yield particles with defined surface properties has been used to investigate the implications of interfacial chemistry on drug aerosolisation (Kubavat et al., 2012), and the effect of drug ratio has been studied in carrier free blends (Jetmalani et al., 2012). The inclusion of drug particles with different aerodynamic particle sizes has also been shown to influence dispersion when formulated in combination blends (Taki, 2008a).

In Chapter 4, the intra-batch variability in the particle properties of micronised powders was demonstrated through the isolation of aerodynamic size fractions. These properties were found to have implications for the aerosolisation of salmeterol xinafoate (SX) and fluticasone propionate (FP) sub-populations. In Chapter 5, the SX:FP ratio was found to

influence the aerosolisation of SX but not FP in pre-blends prepared from bulk, unfractioned drug particles, however, upon formulation with a lactose carrier, co-formulation did not alter the aerosolisation of either drug particle type compared to single drug delivery. Studies have shown that when aerodynamic size fractions are formulated as carrier-based blends, the aerosolisation behaviour of the drug particles is affected, in both single drug and co-formulated blends. However, the potential reasons for the changes in dispersion behaviour were not studied (Taki, 2008). In this chapter, the variability in SX and FP particle properties within bulk micronised powders will be exploited in an attempt to engineer aerosolisation performance without the need for complex particle engineering technologies. Such an approach may also provide insight into the properties that may be favourable for the dispersion of micronised particles when formulated in combination, in addition to identifying the key properties which could be monitored in order to direct formulation engineering for a quality by design approach to DPI development and manufacture.

Following deposition in the lungs, drug particles that are not cleared by innate mechanisms such as mucocillary clearance or phagocytosis must be in solution in order to elicit their local (and/or systemic) effects. Particles therefore need to undergo dissolution and cellular uptake/absorption across the epithelium in order to reach their site of action (Davies and Feddah, 2003; Bur et al., 2010). Although the small particle size of deposited particles would be expected to facilitate high dissolution rates due to a large surface area to weight ratio, poor water solubility is often a rate limiting step (Davies and Feddah, 2003). Furthermore, the small volumes of aqueous fluid (approximately 10 – 20 mL/100 m^2) can further hinder dissolution (May et al., 2012). The lung is a complex organ, and the thickness of the fluid lining varies according to the site; it can be 20 µm in the upper airways, compared to 0.1 - 10 µm or less in the lower airways i.e. bronchioles and alveoli. In these latter airways the layer can be extremely thin or even absent (Pryor, 1992). Therefore depending on the site of deposition, a micronised particle may only have a proportion of its diameter immersed in the liquid layer (Bur et al., 2010). The composition of the fluid also varies across the lungs. In the conducting airways of the upper respiratory tract, the fluid is composed of two phases/layers. A viscous gel phase which is the mucus blanket and removes particles, cells and cell debris by mucociliary clearance. Below the gel layer is a less viscous sol phase, referred to as the periciliary sol that facilitates efficient cilia beating and the movement of the mucus blanket to the mouth (Gehr et al., 1993; Widdicombe, 2002). In

the respiratory bronchioles, the mucus-secreting cells are absent therefore there is no mucus blanket, but the cilia and periciliary sol is present (Widdicombe, 2002). The alveolar lining fluid comprises an aqueous subphase which is covered by a film of pulmonary surfactant; the surfactant prevents collapse of the alveoli by reducing the air-liquid interfacial tension, (Bastacky et al., 1995), and may play a role in the wetting and translocation of deposited particles into the aqueous layer (Gehr et al., 1993). Although the alveolar lining layer is very thin, it can also vary in depth (few hundredths to several micrometres in the rat lung, Bastacky et al., 1995). The microenvironment in which the particle is exposed within the lung will therefore further determine the dissolution and availability of the inhaled particle for therapeutic action.

Using *in vitro* approaches, it has been demonstrated that particle dissolution of inhaled corticosteroids in a limited volume of aqueous fluid differs not only depending on drug solubility, but also particle size, aerosol mass and formulation. The potential to engineer particles for their dissolution behaviour therefore warrants further investigation (Arora et al., 2010). The effect of particle size has been demonstrated; aerodynamic size fractions of hydrocortisone, salbutamol sulphate and budesonide have shown faster dissolution rates as the particle size reduced (Cartier et al, 2008; Son and McConville, 2009; Arora et al., 2010), as have nanoparticles compared to nanoparticle agglomerates and micronised particles of budesonide and fluticasone, attributed to the higher surface areas of the non-agglomerated nanoparticles (El-Gendy et al., 2009; El-Gendy et al., 2011). In addition to differences, although small, between the particle sizes of fractionated SX particles isolated in Chapter 4, more dramatic differences in their bulk and surface disorder were observed, presenting a potential opportunity to engineer SX dissolution. Amorphous particles demonstrate improved solubility (e.g. Sakagami et al., 2001) and faster dissolution than crystalline particles (e.g. Pilcer et al., 2013). Changes in the dispersive and specific surface energy of the particles, relating to changes in the surface chemistry of the exposed crystal facet, can also alter the wettability of the particles (e.g. Heng et al., 2006a).

Combination formulation of DPIs, and the potential for mixed drug agglomerates, may further alter the dissolution rate of one or both drugs. This may be through modifications in agglomerate structure altering the exposure of drug surfaces to dissolution media and/or the proportion of dispersed particles, or changes to the MMAD altering the site of deposition in the lungs. For example, co-delivery from a Seretide

Accuhaler reduced SX deposition on stage 5 of the NGI compared to the Serevent Accuhaler (Taki et al., 2011). If *in vivo* this corresponded to a change in SX deposition site to an area with a different lining layer volume/composition, there may be alterations in the dissolution profile of the drug. Although research in this area is beginning (e.g. Haghi et al., 2013) there is limited understanding on the implications of co-formulation on the dissolution and cell layer transport of drugs in combination, and the potential to engineer the dissolution of one or both drugs in the formulation.

6.2 AIM AND OBJECTIVES

The aim of this study was to investigate the ability to engineer particle aerosolisation performance and/or dissolution by controlling particle properties. The objectives were to:

a) Measure the aerosol PSD of SX and FP in pre-blends (1:1 ratio) compared to SX alone or FP alone to determine the influence of particle physicochemical properties as follows:
    a. Crystallised particles,
    b. Aerodynamically size fractionated particles.

b) Investigate the ability to engineer SX aerosolisability in DPI formulations using crystallised and/or fractionated particles.

c) Determine the dissolution profile of micronised SX particles following dry powder aerosolisation using dissolution media containing methanol and water in varying compositions.

d) Determine how the dissolution profile of aerodynamically fractionated SX particles (from Stage 4 and Stage 5) and re-crystallised particles is altered compared to micronised (unfractionated) SX particles.

e) Determine how the dissolution profile of micronised SX changes following co-delivery with micronised FP particles.

6.3 MATERIALS

The materials and equipment used in Chapter 6, not listed in Section 2.3, 3.3, 4.3 and 5.3, are shown in Table 6.1.

Table 6.1 Suppliers of materials and equipment (Chapter 6).

Material / Equipment	**Supplier**
Transwells® (6.5 mm diameter, 0.4 µm pore size, tissue culture treated, polyester membrane, polystyrene plates)	Costar®, Corning Incorporated, Corning, USA (supplied by Sigma-Aldrich Company Ltd, UK)
Shaker Plate	Orbital Model R100 Rotatest Shaker, Luckham Ltd, UK
Centrifuge	Biofuge Pico, Heraeus (supplied by Jencons-PLS, UK)

6.4 METHODS

6.4.1 BLEND PREPARATION AND HOMOGENEITY

Engineered pre-blends and DPI blends were prepared as described in Chapter 5, Section 5.4.1. All co-formulations were prepared with an SX:FP ratio of 1:1, and all DPI blends had a total drug content of 1.38 % w/w. Fine particle blends were prepared using stage fractionated particles i.e. Stage 4 and Stage 5 for SX and Stage 3 and Stage 4 for FP, and re-crystallised SX and FP particles, which were prepared and tested for their individual dispersion behaviours in Chapter 4. This enabled the effects of co-formulation to be compared to that of single drug aerosolisation for each particle type (Figure 4.11 and Table 4.9), and therefore identify whether inter-particulate interactions can be engineered by controlling the physicochemical properties of the particles. DPI blends were prepared in order to investigate the ability to engineer SX aerosolisation. Firstly, the ability to engineer aerosolisation from single drug formulations was investigated using DPIs containing unfractionated, crystallised, Stage 4 and Stage 5 SX only. DPIs were prepared containing crystallised SX (CSX) and crystallised FP (CFP), and Stage 4 SX and Stage 3 FP in combination to further determine the influence of particle properties on SX aerosolisation in co-formulation. A summary of the blends prepared is shown in Table 6.2. The homogeneity of the blends was assessed as

described in Chapter 5, Section 5.4.2. Quantification of homogeneity samples was according to the HPLC method detailed in Chapter 3, Section 3.4.1.1. Freshly prepared mixed calibration curves were prepared in the range 20 – 400 µg.mL^{-1} and 0.5 - 50 µg.mL^{-1} for quantification of homogeneity samples for pre-blends and DPI blends, respectively.

Table 6.2 A summary of the pre-blends and dry powder inhaler (DPI) blends prepared and tested in Chapter 6, and the engineered particles (prepared and tested in Chapter 4) employed in the study.

	Salmeterol xinafoate	Fluticasone propionate	Drug Ratio
Engineered particles	Crystallised	n.a.	1:0
	Stage 4	n.a.	1:0
	Stage 5	n.a.	1:0
	n.a.	Crystallised	0:1
	n.a.	Stage 3	0:1
	n.a.	Stage 4	0:1
Fine particle blends	Crystallised	Crystallised	1:1
	Stage 4	Stage 3	1:1
	Stage 4	Stage 4	1:1
	Stage 5	Stage 3	1:1
	Stage 5	Stage 4	1:1
DPI blends	Crystallised	n.a.	1:0
	Crystallised	Crystallised	1:1
	Stage 4	n.a.	1:0
	Stage 4	Stage 3	1:1
	Stage 5	n.a.	1:0

n.a = not applicable.

6.4.2 NEXT GENERATION IMPACTOR ANALYSIS

NGI analysis of the fine particle blends and DPI blends was as described in Chapter 5, Section 5.4.5. Powder blend was filled into size 3 gelatin capsules and aerosolised using a Monodose inhaler device at 60 L.min^{-1} (ΔP = 1.4 kPa) for 4 s. Capsule fill weights were 10.0 ± 1.0 mg and 12.5 ± 0.5 mg for pre-blends and DPI blends, respectively. One, six and fifteen capsules were actuated per NGI experiment for pre-blends, single drug DPI blends, and combination DPI blends, respectively. Quantification of NGI samples was undertaken using the HPLC method described in Chapter 3, Section 3.4.1.1, using

freshly prepared mixed calibration curves in the range 0.5 – 50 µg.mL^{-1} (20 – 400 µg.mL^{-1} for individual samples outside this range), either pooled for fine particle blends (n = 5) or prepared on the day for DPI blends. For the latter, dilutions of the lowest standard were undertaken to lower the LOQ; the calibration range was selected based on the concentration of the samples, and was typically 0.1 – 25 µg.mL^{-1}.

6.4.3 DISPERSIBILITY BY DRY DISPERSION LASER DIFFRACTION

The bulk dispersibility of the DPI blends was assessed by Sympatec HELOS/RODOS laser diffraction with protruding aspiration tube and rotary feeder, as described in Chapter 5, Section 5.4.6.1.

6.4.4 WORK OF COHESION AND ADHESION

The surface energy distributions of bulk micronised (i.e. unfractionated), crystallised and stage-fractionated SX and FP particles and CL from Chapters 4 and 5 were used to calculate the work of cohesion and adhesion between the different particle types according to Equation 2.11.

6.4.5 SOLUBILITY DETERMINATION

The solubility of SX was determined in methanol, water, and methanol-water mixtures in the ratios 75:25, 50:50 and 25:75. Solvent mixtures were prepared by measuring the required volume of solvent in a measuring cylinder, transferring into a Duran bottle, and gently shaking. A visible excess of SX was added to a 1.5 mL centrifuge tube and 1 mL of solvent was added. The tube was sealed and placed on a plate shaker set at speed control setting 3 at room temperature. After 24 h the samples were removed and visually checked for saturation. Following centrifugation at 10,000 rpm for 5 min, 0.5 mL of supernatant was diluted as necessary with the respective methanol-water mixture (1 in 10, 1 in 100 or 1 in 200) and analysed by HPLC according to the method in Chapter 3, Section 3.4.1.1.

6.4.6 AERODYNAMIC DEPOSITION USING THE TWIN STAGE IMPINGER

SX particles were aerodynamically deposited onto Transwell inserts using the TSI as described by Grainger et al. (2009) with the following modifications. The TSI was assembled as described in the BP (2012), and shown in Figure 6.1. A Transwell filter was wetted with 100 µL of the solvent mixture and attached to the end of the connecting tube. Parafilm was wrapped around the base of the tube to ensure a tight fit, the Transwell was checked for horizontal alignment and that the air ports were not occluded. 7 mL of the solvent mixture was added to the upper chamber only. The TSI was connected to a vacuum pump, and a flow meter attached to the throat using a tightly fitting mouthpiece. The vacuum pump was switched on and the airflow adjusted to 60 $L.min^{-1}$ ± 5 % using the flow meter. Size 3 gelatin capsules were filled with 12.5 ± 0.5 mg of DPI blend, transferred into the Monodose inhaler device, and the side buttons depressed to pierce the capsule. The flow meter was replaced with the inhaler and the vacuum pump was switched on for 5 s. Three capsules were actuated per experiment for single drug DPI formulations, and six capsules were actuated for the combination DPI formulations to ensure that an equivalent mass of SX was aerosolised into the TSI for each experiment.

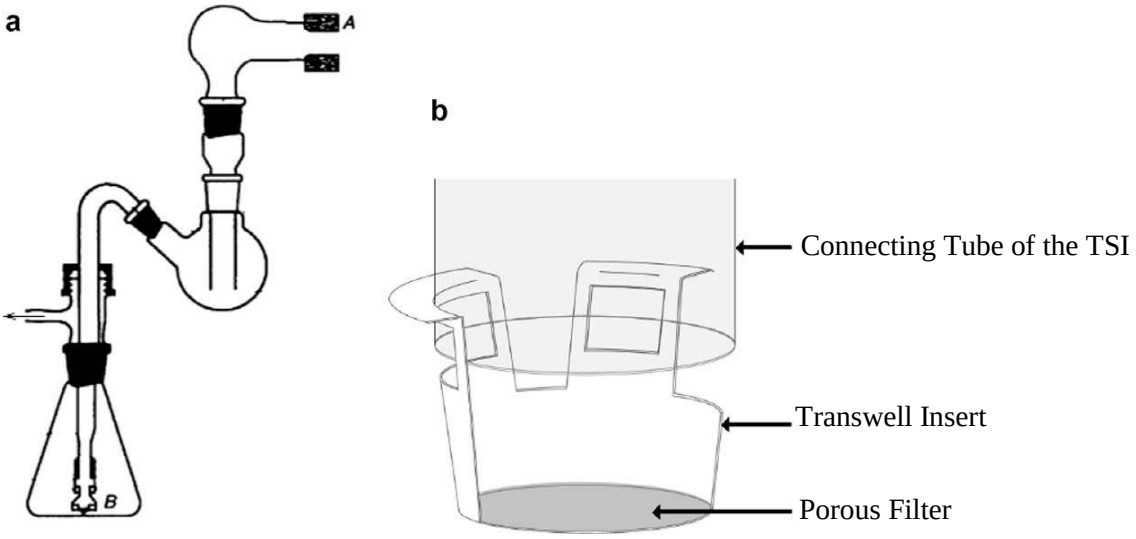

Figure 6.1 (a) The assembled Twin Stage Impinger (TSI); the Monodose inhaler was attached at position A and following actuation particles travel and deposit by inertial impaction onto the porous filter of a Transwell insert which is attached at position B. (b) The Transwell insert attached to the end of the connecting tube. Image taken from Grainger et al. (2009).

6.4.7 DISSOLUTION PROFILE

Following aerodynamic deposition of the particles, the TSI was dismantled. The Transwell was carefully removed from the connecting tube and placed in the well of a baseplate containing 600 µL of solvent mixture. 100 µL of solvent mixture was added to the apical chamber of the Transwell and the lid was replaced. At pre-defined time points, the Transwell was moved into an adjacent well containing 600 µL of fresh solvent mixture, and a sample was removed from the preceding well for HPLC analysis. For dissolution profiling of unfractionated SX in the various methanol-water mixtures, the time points were 5, 15, 30, 60, 120, 180, 240, 300, 360 and 420 min. For the engineered particles (i.e. CSX, Stage 4 SX and Stage 5 SX), and the co-formulation (unfractionated SX:FP, 1:1), the intervals were 30, 60, 120, 240 and 360 min. Sample recovery at the final time point, i.e. 480 min, differed between the solvent mixture compositions. For the 50:50 methanol:water composition, at the final time point, the solvent in the apical and basolateral chamber was removed and transferred into a 5 mL volumetric flask such that the solvent from the two chambers was combined. The chambers were washed by adding 100 µL and 600 µL of the solvent mixture to the apical and basolateral chamber, respectively, three times and transferring it into the volumetric flask. The sample was made to volume and analysed by HPLC. Due to very low detected concentrations for this sample due to the high dilution factor, for the 75:25 solvent composition, solvent in the apical and basolateral chamber was removed and transferred into a small glass vial. A 1 mL graduated glass pipette was used to determine the volume of the sample, which was then analysed by HPLC. The wash was conducted as above and analysed separately by HPLC. For the 25:75 solvent composition sampling was as for the 75:25 composition except 600 – 1000 µL of methanol was added to the fluid removed from the apical and basolateral chambers to aid SX dissolution whilst trying to maintain as low a sample volume as possible. The wash was conducted as above except using methanol instead of the solvent mixture. The samples were sonicated (approx. 5 min) prior to analysis by HPLC. Dissolution experiments were conducted in triplicate.

6.4.7.1 CONSTRUCTION OF DISSOLUTION PROFILE CURVES

To construct the dissolution profile curves, the detected concentration at each sampling time point, including at the final time point, was used to calculate the mass of SX that had dissolved at each time point. The masses were summed to determine the total mass of SX that had dissolved during the experiment. To account for differences in the

deposited mass between experiments, the amount of SX dissolved at each time point was expressed as a percentage of the total amount of SX that had dissolved during the course of the experiment, and plotted to generate a cumulative dissolution profile curve.

6.4.7.1.1 SIMILARITY FACTOR

To determine whether there were differences between the dissolution profiles, a similarity factor (f2) was calculated. The f2 value is a measure of the similarity of two dissolution curves in terms of the percentage of drug that dissolved. The value is calculated according to Equation 6.1, where N is the number of time points, R_t is the mean percentage of drug dissolved in the reference sample at a specific time point, and T_t is the mean percentage of drug dissolved in the test sample at a specific time point. When the f2 value is ≥ 50, the dissolution curves are considered to be similar (FDA, 2000).

Equation 6.1 $$f2 = 50.log\left\{\left[1 + \left(\frac{1}{N}\right)\sum_{t=1}^{t=N}(R_t + T_t)^2\right]^{-0.5}.100\right\}$$

6.4.8 RECOVERY VALIDATION

A 100 µg.mL^{-1} stock solution of SX in methanol:water 75:25 was prepared by accurately weighing 5 mg of SX and dissolving in 50 mL solvent mixture with initial sonication (approx. 10 min). The sample was then made to final volume. Dilutions of the stock solution were made (1 in 2 and 1 in 5) to prepare 50 µg.mL^{-1} and 20 µg.mL^{-1} SX solutions, respectively. A Transwell insert was placed in the well of a baseplate containing 600 µL of the 75:25 solvent mixture. 100 µL of solution, containing either 10 µg, 5 µg or 2 µg of SX, was added to the apical chamber (n = 3) and the lid replaced. After 8 h, the solvent from the apical and basolateral chambers was removed and the volume determined as described in Section 6.4.7. The chambers were washed three times with 75:25 methanol-water mixture (100 µL and 600 µL per wash for the apical and basolateral chamber, respectively) and the samples analysed by HPLC.

In order to determine SX recovery, the stock and standard solutions were analysed by HPLC to determine the amount of SX that was present in the 100 µL of solution which had been placed in the apical chamber of the Transwell insert for each experiment. The

total amount of SX recovered was calculated by summing the mass of SX in the basolateral and apical chamber sample, and in the washing. This was then expressed as a percentage of the amount of SX in 100 µL of the stock/standard solution used in the experiment, and represented the recovery.

6.5 RESULTS

6.5.1 BLEND HOMOGENEITY OF ENGINEERED FINE PARTICLE BLENDS

Overall the homogeneity of the aerodynamically fractionated particles was superior to the crystallised (Table 6.3) and micronised pre-blends (Table 5.6). The crystallised particles had the poorest homogeneity; following tumbling the % CV of CSX and CFP was 14.1 and 13.9 %, respectively, and was much higher than that which is typically accepted for DPI formulations, although in this instance the blends did not contain a coarse carrier. The blend was tumbled a second time (62 rpm, 40 min) which reduced the % CV to 10.6 and 7.0 %, respectively, and the particles were deemed adequately mixed for the purposes of this study.

Table 6.3 Blend homogeneity, expressed as the % coefficient of variance (% CV), drug content (mean ± SD) and detected drug ratio of salmeterol xinafoate (SX) and fluticasone propionate (FP) in co-formulated fine particle blends in the SX:FP ratio 1:1 (n = 6).

SX:FP ratio	Homogeneity (% CV)		Drug Content (μg.mg^{-1})		Detected
	SX	FP	SX	FP	Drug Ratio
Crystallised particles					
SX:FP*	10.6	7.00	517.9 ± 52.1	473.2 ± 31.6	1.0:0.9
Fractionated particles					
Stage 4 SX:Stage 3 FP	1.08	2.02	507.1 ± 6.18	485.9 ± 9.76	1.0:1.0
Stage 4SX:Stage 4 FP	2.61	1.42	513.7 ± 13.5	455.6 ± 116	1.0:0.9
Stage 5 SX:Stage 3 FP	2.37	3.39	518.1 ± 12.7	479.7 ± 15.8	1.0:0.9
Stage 5 SX:Stage 4 FP	1.86	1.01	508.2 ± 10.3	485.4 ± 6.95	1.0:1.0

*The blend was tumbled twice at 62 rpm for 40 min to improve homogeneity.

6.5.2 PARTICLE TYPE EFFECTS IN FINE PARTICLE BLENDS

6.5.2.1 UNFRACTIONATED AND CRYSTALLISED POWDERS

The aerodynamic deposition of crystallised SX and FP alone and in combination is shown in Figure 6.2 and Table 6.4. When aerosolised in combination, unfractionated SX and FP showed a non-significant reduction and no change in the FPF (RD and ED), respectively, as shown in Chapter 5 (Figure 5.12, Figure 5.13, and Table 5.8). However, for crystallised particles, the FPF of SX was reduced significantly ($p < 0.05$) and for FP increased significantly ($p < 0.05$, two sample t-test, OriginPro 8) when in combination.

The emission also changed, and was lower for CSX when combined with CFP ($p < 0.05$) but increased for FP crystals ($p < 0.05$) when combined with CSX. Changes were also observed in the MMAD, increasing in combination for CSX ($p < 0.05$) whilst reducing for CFP ($p < 0.05$) when in combination.

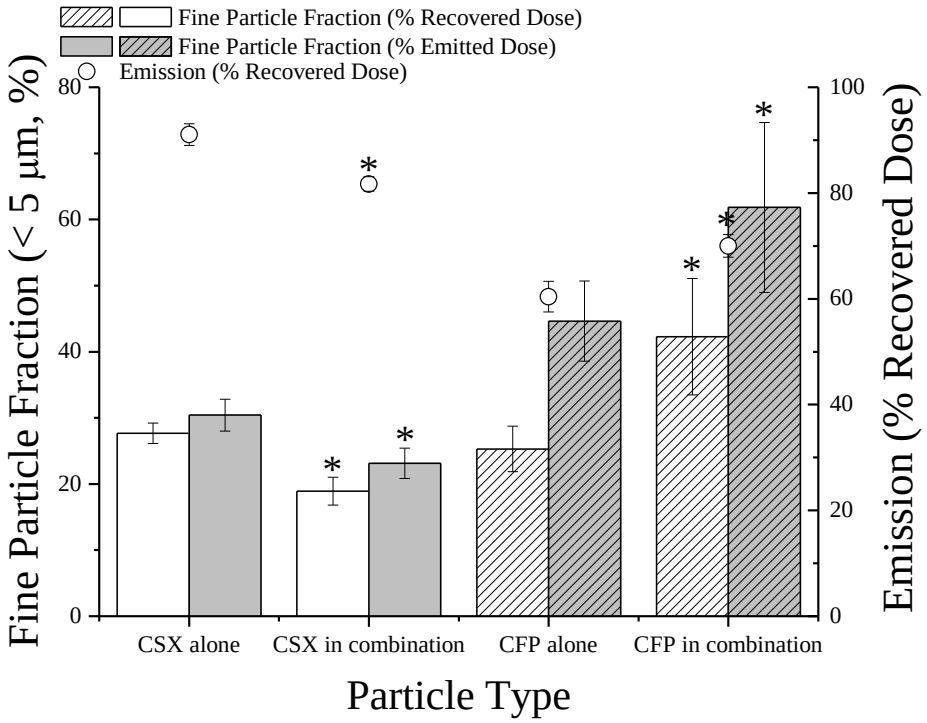

Figure 6.2 The fine particle fraction (FPF < 5 µm, expressed as a percentage of the emitted dose, ED, and recovered dose, RD) and emission (% RD) of crystallised salmeterol xinafoate (CSX) and crystallised fluticasone propionate (CFP) aerosolised alone and in combination (1:1) into the Next Generation Impactor (mean ± SD, $n = 3$); * = $p < 0.05$ using an un-paired t-test.

Table 6.4 The recovery (% of the actuated dose), mass median aerodynamic diameter (MMAD) and geometric standard deviation (GSD) of crystallised salmeterol xinafoate and fluticasone propionate aerosolised alone and in combination into the Next Generation Impactor (mean ± SD, $n = 3$).

SX:FP Ratio	Recovery (%)	MMAD (µm)	GSD
Salmeterol xinafoate			
1.0:0.0	87.1 ± 1.25	3.50 ± 0.24	2.07 ± 0.01
1.0:0.9	94.1 ± 2.59	4.09 ± 0.20	1.93 ± 0.05
Fluticasone propionate			
0.0:1.0	89.5 ± 1.98	4.12 ± 0.22	2.02 ± 0.05
1.0:0.9	93.1 ± 11.7	3.24 ± 0.17	1.87 ± 0.05

6.5.2.2 FRACTIONATED POWDERS

The aerodynamically fractionated particles demonstrated a change in their aerosolisation depending on whether the particles were aerosolised alone or in combination. The ratios of the mean FPF RD and ED of SX or FP between single and co-delivery are shown in Figure 6.3 and Figure 6.4; the standard deviations were obtained using propagation of errors (Lindberg, 2000). A ratio of 1.0 would indicate no difference in the FPF, ratios > 1.0 indicated a lower FPF, and ratios < 1.0 indicated a higher FPF when in combination compared to drug aerosolised alone. Stage 4 SX particles exhibited an improvement in their emission when combined with Stage 3 FP particles ($p < 0.05$, two sample t test) but not with Stage 4 FP particles ($p > 0.05$). Stage 5 SX exhibited improved emission regardless of FP particle type ($p < 0.05$ for Stage 3 and 4 FP). For Stage 4 SX, despite the improved emissions, the FPF was lower when combined with Stage 3 and Stage 4 FP particles ($p < 0.05$, Figure 6.3); the FPF reduced the most when in combination with Stage 3 FP. Stage 5 SX did not show a difference in the FPF when in combination with either FP particle type ($p > 0.05$). For both Stage 4 and Stage 5 SX the MMAD increased ($p < 0.05$, Table 6.4), regardless of FP particle type.

For both FP types, there was no change in emission when in combination with either Stage 4 or Stage 5 SX particles compared to single drug delivery ($p > 0.05$, Figure 6.4). For Stage 3 FP, the FPF RD was reduced in combination blends regardless of SX particle type ($p < 0.05$), despite no change in the MMAD of Stage 3 FP ($p > 0.05$, Table 6.4). Although FP retention in the device and capsules was unchanged in co-formulation compared to single drug delivery (40.5 ± 3.44 % RD for Stage 3 FP alone, 40.2 ± 4.21 % RD and 44.4 ± 0.54 % RD for combined delivery with Stage 4 and Stage 5 SX, respectively) overall the non-sizable fraction i.e. deposition of Stage 3 FP in the device, capsules, throat and pre-separator increased. This is because in combination there was greater Stage 3 FP deposition in the throat and pre-separator (33.9 ± 4.93 % RD and 33.3 ± 5.37 % RD when combined with Stage 4 and Stage 5 SX, respectively), compared to single drug delivery (12.4 ± 0.93 % RD).

For Stage 4 FP particles there was also a lower FPF RD when combined with both Stage 4 and Stage 5 SX ($p < 0.05$), corresponding with a higher non-sizable fraction

when in combination (65.4 ± 1.00 % RD and 73.1 ± 2.32 % RD, respectively) compared to Stage 4 FP aerosolised alone (56.3 ± 0.42 % RD) despite similar device and capsule retention. The MMAD did not change when in combination with Stage 5 SX but was smaller in the presence of Stage 4 SX. Therefore, although when in combination with Stage 5 SX there was a greater reduction in the sizable fraction of FP (i.e. deposition on the stages) compared to in combination with Stage 4 SX, in the latter the aerodynamic particle size of the deposited FP particles was smaller.

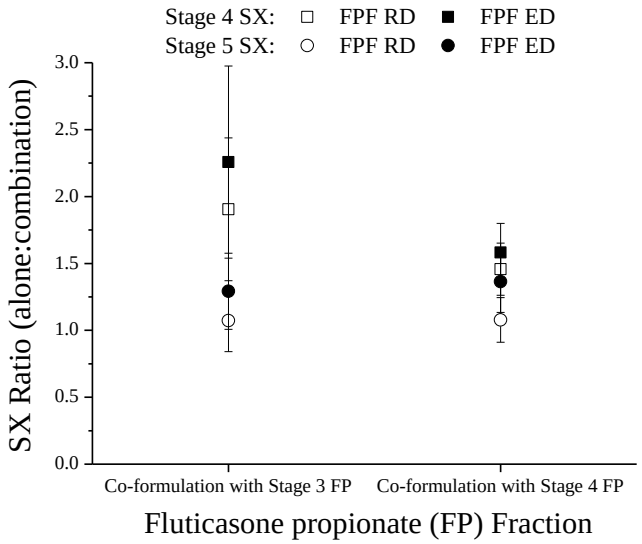

Figure 6.3 The fine particle fraction (% of the emitted dose, ED and recovered dose, RD) of salmeterol xinafoate (SX) expressed as a ratio of drug alone versus drug co-formulated with fluticasone propionate (FP) for fractionated SX (i.e. Stage 4 and Stage 5). Ratios > 1.0 indicate a poorer FPF.

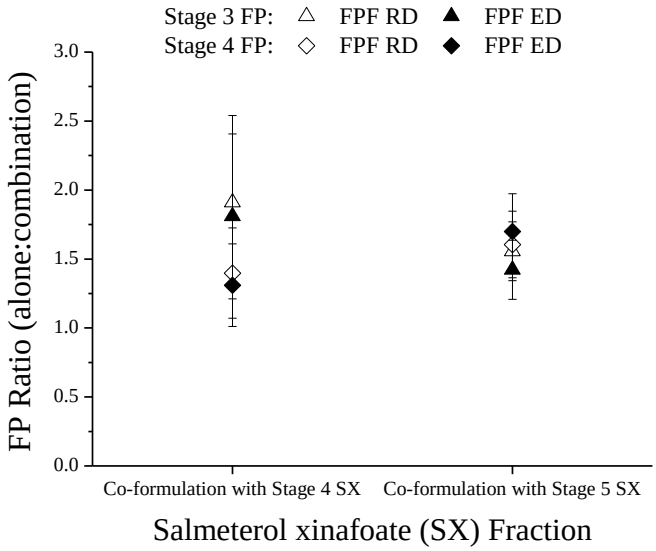

Figure 6.4 The fine particle fraction (% of the emitted dose, ED and recovered dose, RD) of fluticasone propionate (FP) expressed as a ratio of drug alone versus drug co-formulated with salmeterol xinafoate (SX) for fractionated FP (i.e. Stage 3 and Stage 4). Ratios > 1.0 indicate a poorer FPF.

Table 6.5 The recovery (% of the actuated dose), fine particle fraction (FPF < 5 µm, expressed as a percentage of the emitted dose, ED), mass median aerodynamic diameter (MMAD) and geometric standard deviation (GSD) of fractionated salmeterol xinafoate (SX) and fluticasone propionate (FP) when aerosolised alone and in combination into the Next Generation Impactor (mean ± SD, *n* = 3).

Sample	Recovery (%)	Emission (% RD)	FPF (% ED)	MMAD (µm)	GSD
Salmeterol xinafoate					
SXS4- alone	78.9 ± 6.70	47.3 ± 3.93	71.3 ± 5.96	2.47 ± 0.11	1.75 ± 0.02
SXS4- FPS3	91.4 ± 0.36	56.5 ± 2.13	31.6 ± 9.68	3.61 ± 0.19	1.76 ± 0.05
SXS4- FPS4	90.3 ± 0.65	51.5 ± 1.81	45.1 ± 4.93	3.45 ± 0.07	1.70 ± 0.03
SXS5- alone	71.5 ± 2.62	44.8 ± 2.59	45.9 ± 2.86	2.67 ± 0.06	1.98 ± 0.02
SXS5- FPS3	87.7 ± 3.31	54.1 ± 1.90	35.6 ± 7.50	3.28 ± 0.14	1.81 ± 0.04
SXS5- FPS4	91.8 ± 1.69	56.9 ± 2.09	33.7 ± 5.32	3.24 ± 0.10	1.79 ± 0.02
Fluticasone propionate					
FPS3- alone	78.6 ± 3.50	59.6 ± 3.44	52.2 ± 2.08	3.74 ± 0.05	1.94 ± 0.02
FPS3- SXS4	88.7 ± 1.44	59.6 ± 2.14	28.8 ± 9.46	3.75 ± 0.24	2.02 ± 0.05
FPS3- SXS5	83.1 ± 3.12	58.4 ± 2.16	36.7 ± 7.59	3.50 ± 0.15	1.95 ± 0.04
FPS4- alone	77.7 ± 1.70	58.7 ± 3.58	53.3 ± 3.37	3.50 ± 0.12	1.89 ± 0.02
FPS4- SXS4	92.3 ± 3.19	54.4 ± 1.81	40.7 ± 6.15	3.46 ± 0.08	1.91 ± 0.04
FPS4- SXS5	86.6 ± 1.81	60.2 ± 1.03	31.4 ± 4.65	3.31 ± 0.11	1.92 ± 0.03

6.5.3 ENGINEERING SALMETEROL XINAFOATE AEROSOLISATION

Having observed in Chapter 5 that SX and FP co-formulation, in the presence of a lactose carrier, mitigated against the reduction in SX dispersibility that occurred in the respective combination SX:FP pre-blends, the ability to engineer SX aerosolisation in DPI formulations by using SX particles with distinct physicochemical properties was investigated.

6.5.3.1 BLEND HOMOGENEITY OF DRY POWDER INHALER BLENDS

The homogeneity of the SX-only and combination DPI blends prior to and post-tumbling, and detected drug contents, are shown in Table 6.6. Prior to tumbling the homogeneity was poor, however, following tumbling all the blends demonstrated adequate homogeneity with CV values less than 6 % .

Table 6.6 Blend homogeneity expressed as the % coefficient of variance (% CV), detected drug content (mean ± SD) and detected drug ratio of fractionated and crystallised salmeterol xinafoate (SX) co-formulated with fluticasone propionate (FP) in carrier based dry powder inhaler blends prior to (n = 10) and post tumbling (n = 6).

Blend	**Homogeneity (% CV)**		**Drug Content (μg.mg^{-1})**		**Detected Drug Ratio**
Pre-tumbling	**SX**	**FP**	**SX**	**FP**	
Stage 4 SX:Stage 3 FP	46.2	41.6			
CSX:CFP	28.8	18.2			
Post-tumbling	**SX**	**FP**	**SX**	**FP**	
Stage 5 SX- alone	5.44	n.a.	12.5 ± 0.64	n.a.	n.a.
Stage 4 SX- alone	1.13	n.a.	12.3 ± 0.16	n.a.	n.a.
Stage 4 SX:Stage 3FP	3.75	1.94	6.67 ± 0.24	6.98 ± 0.13	1.0:1.0
CSX- alone	2.75	n.a.	13.6 ± 0.37	n.a.	n.a.
CSX:CFP	4.69	4.48	6.84 ± 0.30	6.84 ± 0.22	1.0:1.0

n.a. = not applicable.

6.5.3.2 DE-AGGLOMERATION ANALYSIS BY LASER DIFFRACTION

The de-agglomeration parameters for the engineered DPI blends from dry dispersion laser diffraction are shown in Table 6.7. In all instances the R^2 was ≥ 0.99 and the DA_{max} was 1.0 ± 0.1 indicating an adequate fit of the data following empirical modelling. Considering the single drug formulations, the rank in terms of improving dispersibility (assigned according to the magnitude of the DA_{50}) was: Stage 5 SX = Crystallised SX < Stage 4 SX; there was negligible difference in the DA_{50} between Stage 5 and crystallised particles. Considering the co-formulations, the bulk dispersibility of both the fractionated and crystallised DPI blends improved compared to the respective single drug formulation, such that an improvement in powder entrainability and de-agglomeration efficiency would be likely. The latter, however, would also depend on the cohesivity of the powder, represented by the CPP. As indicated in the table, on some occasions the particle size did not remain constant for 3 consecutive increases in PP for determination of the CPP using the criteria assigned in Chapter 2 therefore two consistent PPs were used instead. The CPP had the following rank order for the single drug formulations with regards to increasing cohesivity, according to the magnitude of the CPP: Crystallised SX < Stage 5 SX < Stage 4 SX. Upon co-formulation, whereas the CPP of the fractionated blend did not change, the CPP increased for the blend prepared from crystallised particles. A high CPP represents a proportion of particles within the bulk powder which disperse poorly and thus require

high dispersal forces for de-agglomeration. Therefore, despite a low DA_{50}, a high CPP may be detrimental to the overall de-agglomeration efficiency of the bulk powder due to a proportion of tightly agglomerated, poorly dispersible particles.

Table 6.7 The R^2, primary pressure for 50 % de-agglomeration (DA_{50}) and maximum degree of de-agglomeration (DA_{max}) of 1.38 % w/w dry powder inhaler formulations containing crystallised or stage fractionated salmeterol xinafoate (SX) alone or in combination with fluticasone propionate. Stage 4 SX was co-formulated with stage 3 FP, and crystallised SX was co-formulated with crystallised FP.

DPI Formulation	R^2	DA_{max}	DA_{50} (Bar)	CPP (Bar)
Stage 4 SX – alone	0.9922	1.11	0.48	3.0
Stage 4 SX:Stage 3 FP	0.9939	1.03	0.39	3.0
Stage 5 SX – alone	0.9863	1.12	0.61	3.5*
Crystallised SX – alone	0.9888	1.10	0.62	1.2 / 2.5*
Crystallised SX:Crystallised FP	0.9937	1.04	0.35	3.0

*The particle size remained consistent for two consecutive increases in PP only in plateau region.

6.5.3.3 DISPERSIBILITY ASSESSMENT BY CASCADE IMPACTION

The aerodynamic deposition of the SX particles when formulated with a lactose carrier either alone or in the presence of FP (in a 1:1 ratio) are shown in Figure 6.5 and Table 6.8. Comparing between the different SX particle physicochemical properties, there was no change in the FPF (RD or ED), emission, MMAD or FPM of crystallised, Stage 4 or Stage 5 SX compared to the micronised (i.e. unfractionated) SX ($p > 0.05$, Kruskal-Wallis test with Dunn's post-test). There were however differences between the latter three particle types. Crystallised SX had a lower FPF (RD and ED) compared to Stage 4 SX ($p < 0.05$), and a larger MMAD compared to Stage 5 SX ($p < 0.05$).

Differences between single and co-delivery were observed for crystallised and fractionated SX. For CSX, there was an increase in the emission and FPF ED in combination ($p < 0.05$ unpaired t-test), but no change in the FPF RD or MMAD compared to single drug delivery. These changes were the converse to those observed in the pre-blends, indicating that an altered balance in particulate interactions in the presence of lactose may have affected SX dispersibility. For Stage 4 SX, there was an increase in emission and a reduction in FPF ED following co-delivery with Stage 3 FP from a carrier-based blend suggesting changes to the de-agglomeration behaviour occurred. These changes were similar to those observed in the fine particle blends i.e.

there was an increase in emission and a reduction in the FPF ED for Stage 4 SX when in combination with Stage 3 FP in the absence of a carrier. In the DPI combination formulation there was no change in the MMAD or FPF RD of Stage 4 SX compared to single delivery, however, in the pre-blend the FPF RD was lower and MMAD larger compared to single drug delivery. Therefore, upon co-formulation of the particles in a carrier based blend, the detrimental effects on Stage 4 SX dispersion as a result of combined delivery were less severe compared to in a carrier free blend.

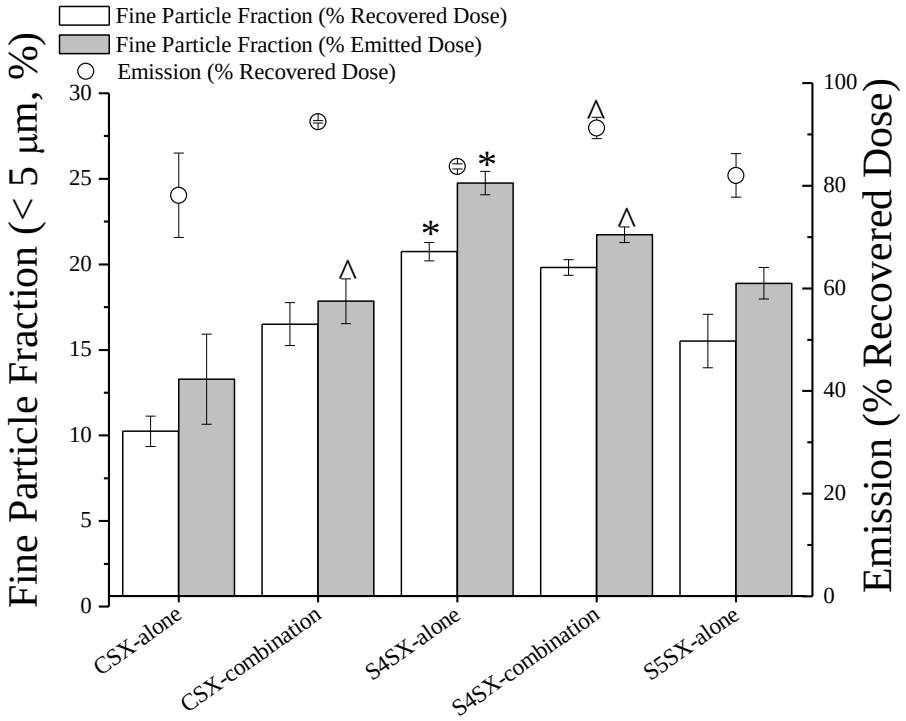

Figure 6.5 The fine particle fraction (FPF < 5 µm, expressed as a percentage of the emitted dose, ED, and recovered dose, RD) and emission (% RD) of 1.38 % w/w crystallised, stage 4 and stage 5 salmeterol xinafoate (CSX, S4SX and S5SX, respectively) formulated with a lactose carrier alone and in combination with fluticasone propionate (FP; in the SX:FP ratio 1:1) assessed by Next Generation Impactor analysis (mean ± SD, *n* = 3). CSX was combined with CFP, and S4SX combined with S3FP. For comparison between single drug and co-delivery, ^ = $p < 0.05$ by unpaired t-test; for comparison between particle types, * = $p < 0.05$ vs. CSX only by Kruskal-Wallis test with Dunn's post-test.

Table 6.8 The recovery (% of the actuated dose), mass median aerodynamic diameter (MMAD) and geometric standard deviation (GSD) of 1.38% w/w crystallised, Stage 4 and Stage 5 salmeterol xinafoate (CSX, S4SX and S5SX, respectively) formulated with a lactose carrier in the absence and presence of fluticasone propionate (FP; in the SX:FP ratio 1:1). CSX was co-formulated with CFP, and S4SX was co-formulated with S3FP (mean ± SD, n = 3).

SX Particle Type	Recovery (%)	MMAD (μm)	GSD
CSX-alone	111 ± 21.4	4.34 ± 0.42	2.21 ± 0.10
CSX-combination	93.0 ± 0.51	3.86 ± 0.14	2.20 ± 0.05
S4SX-alone	91.1 ± 1.9 7	2.69 ± 0.04	2.11 ± 0.04
S4SX-combination with S3FP	91.7 ± 2.37	2.85 ± 0.09	2.17 ± 0.06
S5SX-alone	89.7 ± 0.81	2.56 ± 0.07	2.43 ± 0.10

6.5.4 WORK OF COHESION AND ADHESION

Figure 6.6 shows the work of cohesion and adhesion of the various SX and FP particles and CL. The values were calculated from the total surface energy distributions obtained from IGC at finite dilution (generated in Chapter 4 and 5), and therefore take into account dispersive and specific interactions. Overall, the magnitude of FP-FP cohesive interactions was larger than SX-SX cohesive interactions across all of the particle types. Generally the crystallised particles of SX and FP had a lower work of cohesion than the fractionated particles. Considering the cohesivity of SX, the work of cohesion between Stage 5 SX particles was higher than between Stage 4 SX particles, and they also exhibited regions on the particle surface with very high cohesive strength. For FP, conversely, there was negligible difference in the work of cohesion between Stage 3 and Stage 4 particles. Considering the adhesivity, all the particles (i.e. both SX and FP) demonstrated drug-CL adhesive interactions that were larger in magnitude than the corresponding drug-drug cohesive interactions. Across the engineered particles, the magnitude of SX-CL interactions was smaller than FP-CL interactions. Differences were also observed between the adhesivity of SX and FP towards each other. The work of adhesion between Stage 4 SX particles and fractionated FP particles was lower than the work of adhesion between Stage 5 SX and fractionated FP particles. At low surface coverages, the adhesivity of Stage 5 SX was greater than Stage 4 SX towards fractionated FP, but this diminished as the surface coverage of the probes increased. This indicated that the Stage 5 SX powder exhibited some very high surface energy regions which would dictate the inter-particulate interactions in the blends and potentially form strong interactions with any FP particles present.

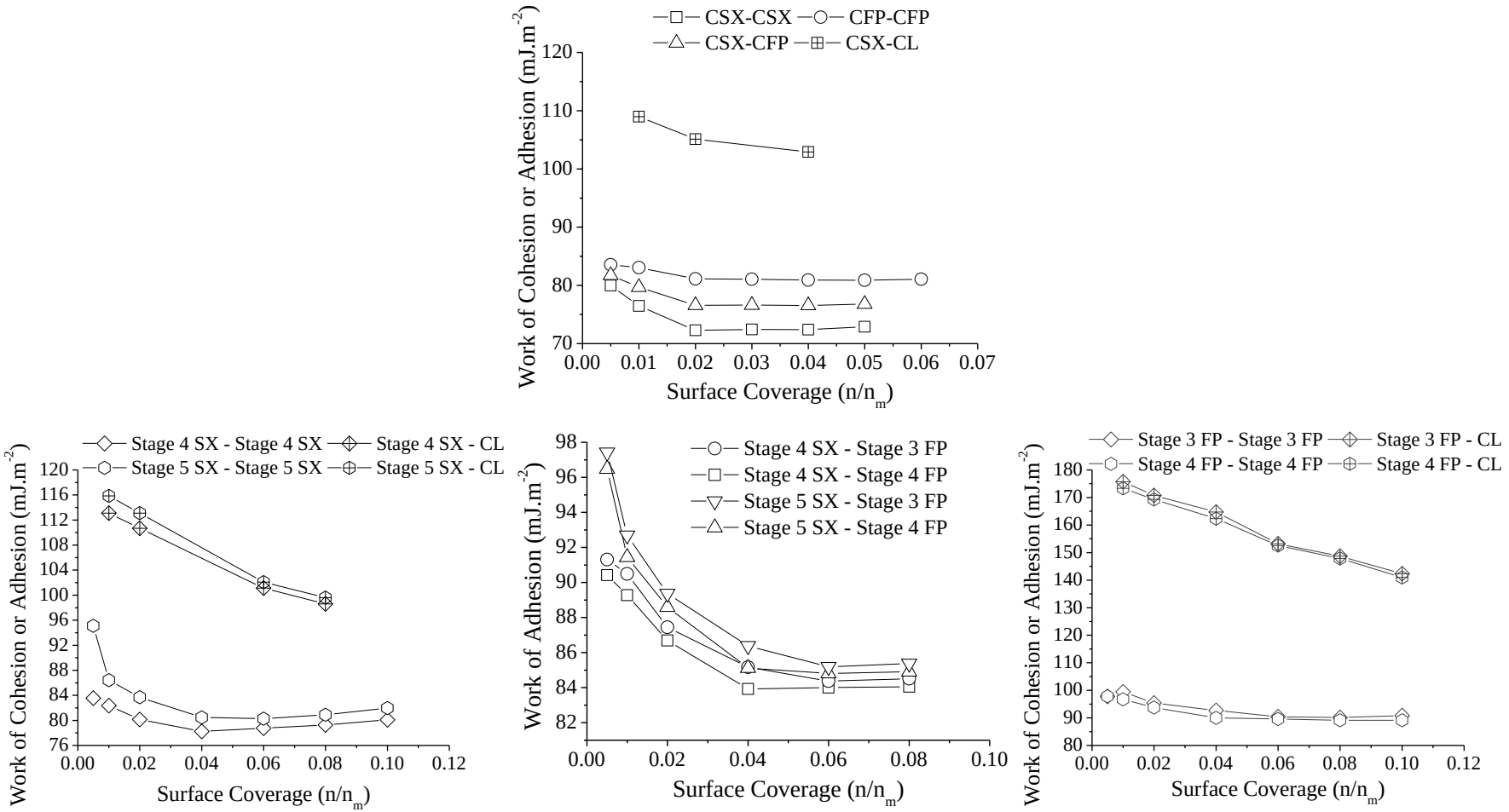

Figure 6.6 The work of cohesion and work of adhesion between crystallised and stage fractionated salmeterol xinafoate (SX) and fluticasone propionate (FP) powders, and coarse lactose (CL), determined from the total surface energy distributions obtained from inverse gas chromatography at finite dilution. Please note the different axes between the plots.

6.5.5 SALMETEROL XINAFOATE SOLUBILITY

The solubility of SX in various methanol and water systems is shown in Table 6.9. The solubility of SX reduced as the amount of water in the system increased.

Table 6.9 The solubility of salmeterol xinafoate (SX) in water and methanol systems determined at room temperature (mean ± SD, n = 3).

Methanol to Water Ratio	Solubility ($mg.mL^{-1}$)
100:0	35.4 ± 2.72
75:25	7.81 ± 1.25
50:50	1.21 ± 0.13
25:75	0.19 ± 0.00
0:100	0.04 ± 0.01

6.5.6 DRUG RECOVERY FROM DISSOLUTION MEDIA

The amount of SX recovered from the Transwell insert (including the well of the baseplate) following the application of a known amount of SX in solution is shown in Table 6.10. The percentage recovered varied from 75.8 to 92.2 %; the recovery therefore increased with greater amounts of SX added to the insert. It is therefore likely that there were sites of loss due to SX adsorption onto the plastic of the insert/well. Upon reaching a threshold amount of SX, above the saturable level of adsorption, SX recovery from the Transwell became higher and closer to 100 %.

Table 6.10 The amount (in µg) and percentage of salmeterol xinafoate (SX) recovered following the application of known amounts of SX onto a Transwell insert in a methanol-water mixture with composition 75:25 methanol:water (mean ± SD, n = 3).

Amount of SX (µg)	Amount Recovered (µg)	Percentage Recovered (%)
9.94	9.16 ± 0.58	92.2 ± 5.87
4.97	4.31 ± 0.11	86.6 ± 2.30
1.99	1.51 ± 0.15	75.8 ± 7.42

6.5.7 DISSOLUTION PROFILE OF SALMETEROL XINAFOATE

The dissolution profile of micronised SX in methanol:water mixtures is shown in Figure 6.7. The amount of SX actuated into the TSI, along with the amount deposited on the Transwell insert are shown in Table 6.11. The amount of SX depositing on the insert

was comparable between the solvent compositions. SX dissolution appeared to alter depending on the solvent composition; the dissolution rate was fastest in the methanol to water ratio 75:25, and slowest in the ratio 25:75. The similarity factors indicated that the dissolution curves were different between solvent compositions. Compared to the 25:75 composition, the f2 values were 32 and 25 for the 50:50 and 75:25 compositions, respectively. Considering the latter two compositions, the profiles were also dissimilar with an f2 value of 47.

In some instances, the detected concentration of the samples was at or below the LOQ of the calibration curve (circled in Figure 6.7) and in most instances at the final time point (480 min) and/or wash. In the case of the 75:25 and 50:50 compositions, this indicated that dissolution was likely to be complete from 360 min onwards, and for the 50:50 composition, that dissolution was negligible before 5 min. For the 25:75 composition, the low detected concentrations at 5, 15 and 30 min again indicated little dissolution occurring initially, and that dissolution slowed beyond 300 min. The amount of SX dissolved in the dissolution media at these latter time points indicated that saturation had not occurred; i.e. at 300 min the total amount of SX was 4.12 ± 1.47 µg, and at 360 min it was 7.00 ± 2.12 µg and 8.08 ± 3.10 µg for the 25:75, 50:50 and 75:25 methanol-water compositions, respectively. For each methanol-water composition there was also a high degree of variability between repeat experiments. The variability was particularly high for the 25:75 methanol:water composition.

Table 6.11 The amount of salmeterol xinafoate actuated into the Twin Stage Impinger, and the amount deposited on the Transwell insert, in dissolution experiments utilising methanol-water dissolution media in the ratio 75:25, 50:50 and 25:75 (mean ± SD, n = 3).

Solvent System (Methanol:Water)	**Amount Actuated (µg)**	**Amount Deposited (µg)**	**Percentage Deposited (%)**
75:25	477.8 ± 4.63	8.74 ± 3.35	1.83 ± 0.71
50:50	475.9 ± 3.90	8.32 ± 3.20	1.75 ± 0.68
25:75	473.6 ± 2.92	9.96 ± 5.22	2.11 ± 1.11

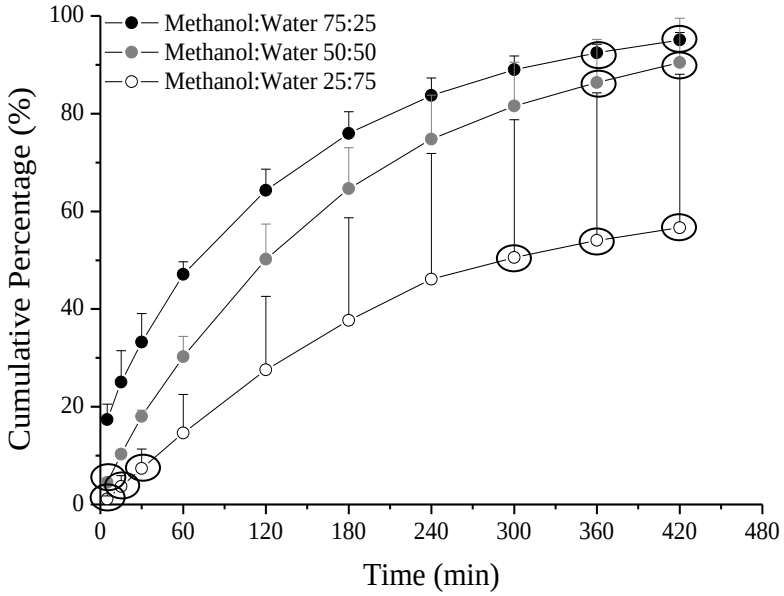

Figure 6.7 The dissolution profile of micronised salmeterol xinafoate (SX) in methanol:water mixtures (75:25, 50:50, 25:75) expressed as the cumulative amount of SX dissolved over 480 min (mean ± SD, n = 3). Circled data points were on or below the limit of quantification of the calibration curve on at least one occasion.

6.5.8 EFFECT OF PARTICLE PROPERTIES AND CO-FORMULATION ON THE DISSOLUTION PROFILE OF SALMETEROL XINAFOATE

The dissolution profile of the varying SX particle types, as well as the micronised (i.e. unfractionated) SX:FP co-formulation is shown in Figure 6.8. The amount of SX actuated into the TSI and the amount deposited on the Transwell insert are shown in Table 6.12. The dissolution media was methanol and water in the ratio 25:75. This composition was selected to ensure that differences in the dissolution profiles of the particles would not be masked by high drug solubility in the dissolution media (El-Gendy et al., 2011). Using this media, there remained a high degree of variability between repeat experiments. The data for the micronised (i.e. unfractionated) SX is a repetition of the data presented in Figure 6.7, which is included for comparison. Compared to unfractionated SX, there was no change in the dissolution profile of crystallised, Stage 4 or Stage 5 SX as indicated by the f2 values, which were 67, 66 and 58, respectively. There was also no change is the dissolution profile when comparing between any of the particle types; in all instances the f2 value was ≥ 50. In co-formulation, the dissolution rate of unfractionated SX appeared to increase compared to single drug delivery, and was corroborated by an f2 value of 40.

Table 6.12 The amount of salmeterol xinafoate (SX) actuated into the Twin Stage Impinger, and the amount deposited on the Transwell insert from dry powder inhaler formulations using methanol:water 25:75 as the dissolution media (mean ± SD, *n* = 3 except Stage 5 SX, *n* =2).

Formulation	**Amount Actuated (µg)**	**Amount Deposited (µg)**	**Percentage Deposited (%)**
Micronised SX co-formulation	462.2 ± 45.2	4.67 ± 0.93	1.01 ± 0.22
Crystallised SX	513.6 ± 2.61	6.19 ± 1.77	1.20 ± 0.34
Stage 4 SX	472.2 ± 20.5	8.53 ± 1.48	1.78 ± 0.38
Stage 5 SX	464.0 ± 3.47	4.49 ± 0.02	0.96 ± 0.01

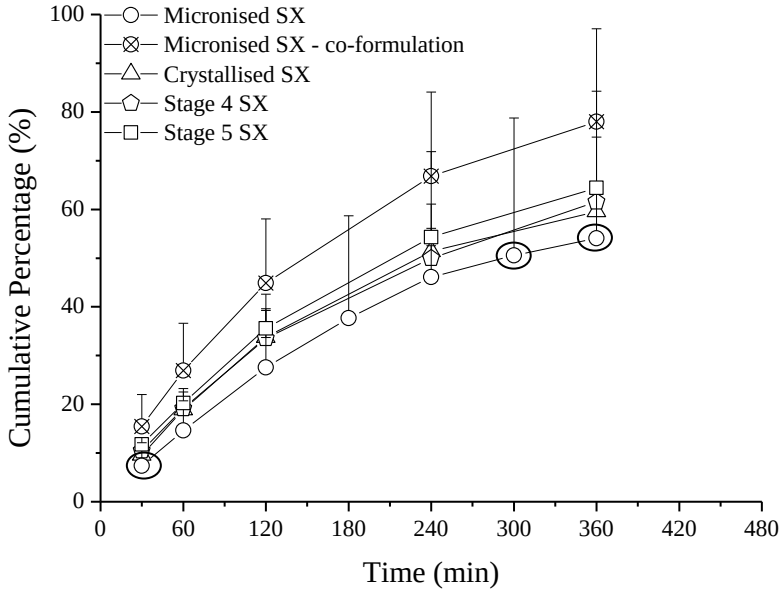

Figure 6.8 The dissolution profile of micronised, stage 4, stage 5 and crystallised salmeterol xinafoate (SX) in methanol and water (25:75), and micronised (i.e. unfractionated) SX when in combination with fluticasone propionate, expressed as the cumulative amount of SX dissolved over 480 min (mean ± SD, *n* = 3 except stage 5 SX, *n* = 2). Circled data points were on or below the limit of quantification of the calibration curve on at least one occasion.

6.6 DISCUSSION AND CONCLUSIONS

The ability to engineer the aerosolisation performance of drug particles from combination inhalers would enable these complex formulations to be designed for optimal drug dispersion and deposition at the target sites in the lungs. The additional component in these formulations presents the opportunity for drug agglomerates consisting of one or both drugs, as well as the carrier particles. It was postulated that by understanding the agglomeration behaviour in drug-drug pre-blends prior to formulating with a carrier, it may be possible to manipulate the deposition profiles of the drugs when blended as representative DPI formulations. Specifically, by controlling the physicochemical properties of the component particles (i.e. size, crystalinity, surface energy and initial cohesive agglomeration tendency), it would be possible to direct the formulation behaviour of combination DPI formulations.

6.6.1 ENGINEERING DRUG PARTICLE DISPERSION BEHAVIOUR USING RE-CRYSTALLISED DRUG POWDERS

The drug pre-blends had adequate homogeneity. The crystallised blend had the poorest homogeneity with CV values of 10.6 and 7.00 % for SX and FP, respectively. This is typical for crystallised particles in which smoother particle surfaces have lower interactive forces, and there are greater drug losses during handling, storage and mixing (Kaialy et al., 2012). When aerosolised into the NGI, co-formulation had different effects on each drug. Co-formulation was detrimental to the emission and FPF (ED and RD) of CSX, and resulted in an increase in the MMAD. Conversely, for CFP there was an increase in the emission and FPF (RD and ED) and reduction in the MMAD when aerosolised in combination. The work of cohesion and adhesion, derived from the surface energy of the particles, was lower in magnitude compared to the micronised particles, but the relative cohesivity and adhesivity of the particles was the same i.e. the magnitude of CSX-CFP adhesive interactions was greater than CSX-CSX cohesive interactions and smaller than CFP-CFP cohesive interactions (Figure 6.6). In combination carrier-based formulations, the performance of FP (in terms of the FPF) was optimal when FP particles were less adhesive towards SX particles and more cohesive towards itself (Kubavat et al., 2012). The work of cohesion/adhesion distributions were used to calculate the cohesion:adhesion (C:A) ratios based on the cohesive adhesive balance principle (Kubavat et al., 2012); at each surface coverage the

ratio between the work of cohesion and work of adhesion was calculated, a value > 1.00 would indicate a cohesive led system whereas a value < 1.00 would indicate an adhesive led system. For both micronised (i.e. unfractionated) particles and crystallised particles, the overall balance of interactions was dominated by cohesive interactions i.e. C:A > 1.0. The micronised particles were marginally more cohesive and thus less adhesive (1.08 – 1.10) than crystallised (1.02 – 1.06) FP particles, despite no change in FP dispersion following co-formulation in micronised pre-blends but improved dispersion in crystallised pre-blends. There were, however, other differences in the properties of the particles which may have contributed to the aerosolisation behaviours. A distinctive change in particle shape occurred for CFP and particles were elongated and needle-like after crystallisation. Carrier particles exhibiting this morphology have fewer drug-carrier contact points, less stable contact, and experience lower press-on forces during mixing (Kaialy et al., 2012). CFP particles exhibiting this morphology may therefore also exhibit weaker agglomeration with other fine particles in the pre-blend due to these structural factors and thus may promote their dispersion. Particles of this shape are also able to remain airborne for longer compared to particles of the same geometric size but different morphology (Kaialy et al., 2012). Therefore, CFP agglomerates as well as any CFP-CSX agglomerates that may have formed during mixing would be easier to disperse, and the released CFP particles would have a high propensity to remain airborne. Dry dispersion laser diffraction analysis also revealed that CFP was more dispersible than MFP; the DA_{50} was lower, indicating that 50 % of the CFP particles dispersed at a lower dispersing pressure than the MFP particles. The CFP particles were also less cohesive than the micronised particles when assessed by IGC. CFP particles would therefore be more easily entrained, and due to lower cohesive interactions require lower dispersion forces for complete de-agglomeration.

For SX, higher FPFs have been obtained in carrier-based formulations when there is a higher adhesive tendency between SX and FP particles compared to SX cohesivity (Kubavat et al., 2012). The plate-like, highly crystalline, smooth surfaces of crystallised SX particles are known to exhibit low surface energy (Rehman et al., 2003), and this was observed in the current study (Chapter 4, Figure 4.10). Both crystallised and micronised SX were more adhesive to FP than cohesive to itself, and the crystallised SX particles had a marginally higher cohesive tendency relative to the adhesive tendency towards FP (0.94 – 0.98) compared to micronised SX (0.91 – 0.93). Dry dispersion laser diffraction analysis also revealed than CSX was more dispersible than MSX, and IGC

revealed lower cohesive interactions between CSX particles compared to MSX particles. This highlighted the interplay between bulk powder and particulate properties in determining aerosolisation behaviour. Although the large particle size and lower magnitude in the cohesive strength of CSX particles compared to MSX resulted in good flow and low device/capsule retention (9.0 ± 2.07 % RD), CSX deposition was high in the throat and pre-separator (51.0 ± 4.54 % RD) due to the deposition of both CSX agglomerates and large, de-agglomerated CSX particles. In the CSX-CFP pre-blend, CSX deposition in the throat and pre-separator was comparably high (51.3 ± 1.21 % RD), and there was a doubling in device/capsule retention (18.3 ± 1.37 % RD) compared to that of CSX alone. The combination pre-blend therefore contained agglomerated CSX particles which exhibited poorer flow and were less dispersible than in the pure CSX powder, due to stronger CSX-CFP interactions compared to CSX-CSX interactions in the powders.

6.6.2 ENGINEERING DRUG PARTICLE DISPERSION BEHAVIOUR USING SIZE-FRACTIONATED DRUG POWDERS

Pre-blends containing aerodynamically fractionated particles also showed good blend homogeneity with CV values less than 3.5 %. Significant changes to the aerosolisation behaviour were seen following co-formulation, and appeared to be influenced by the particle type. For Stage 4 SX, when in combination with either Stage 3 or Stage 4 FP, there was a lower FPF and a bigger MMAD. The magnitude of the reduction of the FPF depended on the size of the FP particle; when combined with the larger Stage 3 FP there was a bigger reduction in the FPF and increase in the MMAD. Despite this, there was an increase in SX emission when in combination with Stage 3 FP but no change when in combination with Stage 4 FP. Stage 4 SX particles were more adhesive towards FP than cohesive, but there was little change in the relative SX adhesivity depending on the FP particle type (Figure 6.6). Improved flowability of larger S4SX-S3FP agglomerates (S3FP; liquid dispersion D_{v50} 2.14 ± 0.18 µm) compared to S4SX-S4FP agglomerates (S4FP; D_{v50} 1.91 ± 0.09 µm) may have contributed towards the reduction in device/capsule retention and increase in the emitted dose through improved flow properties (Shariare et al., 2011). However, incomplete dispersion of the larger S4SX-S3FP agglomerates compared to the smaller S4SX-S4FP agglomerates, both of which would have experienced similar intra-agglomerate forces (based on the work of cohesion and adhesion of the particles), would have resulted in a greater reduction in the

FPF and increase in MMAD due to greater deposition occurring in the throat, pre-separator and stages relating to larger aerodynamic particle sizes (stage 1 – 3) for S4SX-S3FP compared to S4SX-S4FP (48.5 ± 4.40 % and 41.2 ± 2.08 % RD, respectively).

Conversely, for Stage 5 SX particles there was no change in the FPF when combined with Stage 3 or Stage 4 FP particles. There was however an increase in the MMAD and higher emission following co-formulation with either FP particle type. Stage 5 SX particles also showed an adhesive tendency for FP, and there was marginally higher adhesivity towards Stage 3 FP compared to Stage 4 FP. Unlike Stage 4 SX, there was no difference in the magnitude of the changes in the aerosolisation parameters depending on the FP particle. Overall the aerosolisation parameters of Stage 5 SX particles were affected to a lesser extent by co-formulation compared to Stage 4 SX particles. Despite having a smaller geometric particle size (D_{v50} 1.12 ± 0.04 µm and 1.51 ± 0.06 µm, for Stage 5 SX and Stage 4 SX, respectively), Stage 5 SX particles had a higher agglomeration tendency as demonstrated by dry dispersion particle sizing. The D_{v50} at 0.2 Bar was 7.64 µm and 23.06 µm for Stage 4 and Stage 5 SX, respectively. Coupled with the higher cohesivity of Stage 5 particles (in terms of the overall magnitude of the forces of cohesion and relative magnitude of the forces of adhesion towards FP), there may have been less pronounced changes in aerosolisation behaviour when in combination with FP due to a lower propensity for interaction/disruption of SX agglomerates by FP particles, as demonstrated by the non-sizable fractions obtained in the NGI. Due to the high agglomeration tendency of Stage 5 SX, the non-sizable fraction was high (75.3 ± 1.83 % RD). However, when co-formulated with Stage 3 or Stage 4 FP the non-sizable fraction did not change (74.9 ± 3.84 % RD and 75.3 ± 2.46 % RD, respectively). For Stage 4 SX, the non-sizable fraction was lower (62.3 ± 4.98 % RD), however, upon co-formulation with Stage 3 or Stage 4 FP there was an increase in the non-sizable fraction (75.5 ± 5.21 % RD and 69.3 ± 3.32 % RD, respectively), indicating disruptions/alterations to the agglomeration of the blend, particularly in terms of the proportion of large, poorly dispersible agglomerates.

In the case of FP fractions, unlike the behaviour observed with SX, neither Stage 3 nor Stage 4 FP demonstrated changes in emission when in combination with either Stage 4 or Stage 5 SX but the FPF was observed to decrease. Whereas for Stage 3 FP a bigger reduction in the FPF occurred when in combination with the larger Stage 4 SX particles, for Stage 4 FP a bigger reduction occurred with the smaller Stage 5 SX particles. There

was no change in the MMAD, except for Stage 4 FP in combination with Stage 4 SX, in which the MMAD was smaller than for FP alone ($p < 0.05$). The overall consistency in the MMAD between the blends, while changes in the FPF were observed, indicates that this parameter cannot alone be used to predict drug aerosolisation behaviour. Were this a carrier-based system, it would indicate similar drug particle agglomeration and differences in the adhesive rather than cohesive interactions for the drug in the formulation (Kaialy et al., 2012). Of the co-formulations, FP deposition in the throat and pre-separator was lowest from the S4FP-S4SX pre-blend (21.9 ± 2.19 % RD) compared to the other combinations (33.3 ± 5.37 % RD to 33.9 ± 4.93 % RD); FP deposition in the throat and pre-separator was 16.7 ± 0.77 % RD and 12.4 ± 0.14 % RD for Stage 4 and Stage 3 FP, when aerosolised alone, respectively. In the absence of a carrier, deposition in the throat and pre-separator represents the deposition of large, undispersed drug agglomerates. In all the carrier-free co-formulations, there was therefore a higher proportion of large, difficult to disperse agglomerates compared to single drug delivery, demonstrated by the high throat and pre-separator deposition. For the S4FP-S4SX pre-blend however there was a smaller proportion of these agglomerates compared to the other combination pre-blends and thus an increase in the sizable fraction. Although this did not increase the FPF of Stage 4 FP relative to single drug delivery, there was a shift in the aerodynamic particle size of the deposited sizable fraction towards a smaller particle size. All the co-formulations are therefore likely to have experienced a change in their powder structure, in terms of the agglomeration state, compared to the single drug powder fractions.

Fractionated FP particles, similar to bulk micronised (i.e. unfractionated) particles, were more cohesively balanced than adhesive to SX. The magnitude of the cohesive FP-FP interaction, and its heterogeneity, did not differ dramatically between the unfractionated, Stage 3 and Stage 4 FP particles. However, it was only in blends containing fractionated SX and FP particles in which the aerosolisation of FP changed and the FPF was lower compared to single drug delivery, and the reasons for this were unclear. Both SX and FP showed heterogeneity in their surface energy distributions and therefore work of cohesion. In pre-blends containing unfractionated particles, SX may therefore have only been able to disrupt the more weakly associated FP agglomerates, and thus did not impact the overall dispersibility of FP from the pre-blend. However, when formulated with Stage 5 SX, for example, which had much higher surface energy and thus magnitude of interactive forces, SX particles may have been able to disrupt

even the most cohesive FP-FP agglomerates within the pre-blend, and thus the consequence was a reduction in the dispersibility of the FP particles. Stage 4 SX particles conversely had a similar magnitude in the cohesive/adhesive forces compared to unfractionated SX, and therefore would also only have been able to disrupt the more weakly associated FP agglomerates. Therefore, it is also important to consider the differences in the fractionated FP particles compared to the unfractionated FP particles.

Agglomerate strength is determined not only by the work of cohesion/adhesion between the component particles, but also the particle size and packing fraction (Kendall and Stainton, 2001). Stage-fractionated FP was more dispersible than the unfractionated FP particles (DA_{50} = 0.85 Bar, 1.50 Bar and 1.72 Bar, respectively, for Stage 3, Stage 4 and unfractionated FP, respectively, Chapter 4, Table 4.8), potentially arising due to changes in packing fraction, agglomerate and/or powder structure. More dispersible FP agglomerates would therefore have been more favourable for promoting SX interactions with FP during blending. This may have contributed towards the superior homogeneity of the fractionated pre-blends compared to the unfractionated pre-blends (Chapter 5, Table 5.6), however, a consequence of this as observed in the study was a detrimental effect on the dispersion of FP from the blend. Although low shear Turbula mixing is able to generate homogenously mixed blends containing FP (Le et al., 2012b), and was demonstrated in the current work, there may also still remain drug agglomerates comprising very cohesive particles within the final blend. Therefore, using optimal amounts of mixing aids (e.g. silica-gel beads) or high hear mixers it has been shown to enable further improvement in homogeneity due to disruption of these highly cohesive agglomerates (Sebti et al., 2007; Le et al., 2012b). In fractionated pre-blends, a combination of highly cohesive FP agglomerates and SX-FP mixed agglomerates present within the powder structure which hindered FP dispersion may have dictated the poor aerosolisation of FP. Furthermore, SX-FP adhesive interactions may have altered following blending, as the balance of cohesive and adhesive interactions has been shown to be sensitive to processing conditions for FP (Kubavat et al., 2012). Blending/handling of these particle sub-populations may therefore also have unfavourably altered the balance of interactions with regards to FP dispersion. The blending process itself, including use of the low shear Turbula mixer, can induce changes in particle properties such as amorphisation of particle surfaces and even altered particle morphology, with plate-like SX showing plastic deformation to near spherical particles and FP fragmenting to needle-like particles, although occurring

following much longer mixing times (420 min for SX, 780 min for FP) compared to those in the current study (Grasmeijer et al., 2013).

The trends in aerosolisation performance observed for the aerodynamically fractionated particles differed to those seen for the micronised (i.e. unfractionated) particles following co-formulation. Although overall the aerosolisation behaviour of the unfractionated SX and FP particles did not change when formulated as combination pre-blends in a 1:1 ratio ($p > 0.05$), there existed a proportion of particles within the bulk powder for which aerosolisation efficiency was compromised when in combination, as demonstrated by the pre-blends prepared from size-fractionated powders. Furthermore, the extent of the change in aerosolisation performance depended on the specific fractions that were co-formulated. When considering the aerosolisation performance of combination inhalers, it is therefore too simplistic an approach to consider the behaviour of the bulk micronised particles, as powder sub-populations demonstrate different aerosol behaviours. It is the behaviour of these sub-populations which may contribute towards inter-batch variability between the aerosol performance of inhaled powders/formulations despite apparent similarity between measured bulk properties such as surface energy, AFM force measurements, and particle size analysis. To fully understand both inter- and intra-batch variability in powder aerosolisation performance and the consequences for the final inhaler product, it may therefore be necessary to undertake thorough physicochemical analysis using sufficiently sensitive techniques to enable the variability in particle properties, including those arising due to damage upon micronisation, within a bulk powder to be assessed.

6.6.3 ENGINEERING SALMETEROL XINAFOATE DISPERSION BEHAVIOUR; THE INFLUENCE OF DRUG PARTICLE PROPERTIES IN CARRIER BASED BLENDS

In Chapter 5 it was observed that when unfractionated SX and FP particles were co-formulated in the presence of a lactose carrier the detrimental effects on SX dispersibility that occurred in the respective combination SX:FP pre-blends were no longer present. In both Chapter 3 and Chapter 5, unfractionated SX appeared to be more sensitive to changes in aerosolisation due to the presence of the FP powder compared to FP in the presence of the SX powder. Therefore, the ability to engineer SX aerosolisation in carrier-based DPI formulations was investigated by using SX particles

with distinct physicochemical properties generated in Chapter 4. The aerosolisation behaviour of the unformulated SX particles was found to not be representative of the aerosolisation of 'engineered' SX when formulated with a lactose carrier. Whereas significant differences were observed in the emission, FPF (ED and RD) and MMAD of micronised (i.e. unfractionated) SX particles and crystallised, Stage 4 and Stage 5 SX when aerosolised into the NGI in the absence of a carrier (as described in Chapter 4), when formulated with a lactose carrier, the engineered SX particles exhibited no change in any of the aerosolisation parameters compared to micronised (i.e. unfractionated) SX particles. Changes in the bulk dispersibility determined from laser diffraction however were apparent for the single drug DPI blends. In all instances the blends showed better bulk dispersibility than the micronised (i.e. unfractionated) SX DPI blend (DA_{50} = 1.01 Bar), indicating a change in powder structure and agglomeration occurred.

Considering the fractionated particles, Stage 4 and Stage 5 SX produced the same FPF ($p > 0.05$, although there was a non-significant reduction) and emission when formulated as a DPI. Similar FPFs may arise in two situations. Firstly, when there is lack of saturation of active binding sites on the carrier such that adhesive forces between the drug and carrier dominate any differences in drug properties (e.g. cohesivity, agglomeration state) in determining the FPF (Murnane et al., 2009). Assessment of the SEM images of the DPI blends containing 1.38 % w/w unfractionated SX particles revealed large areas of the carrier surface with no drug associated (Chapter 5, Figure 5.9). Similar FPFs may also arise from similar SX agglomeration within the blends, such that de-agglomeration efficiency in the turbulent air stream is not enhanced by larger agglomerate masses and/or sizes (Murnane et al., 2009). Similar agglomeration would also lead to similar press-on forces during blending, which occur as a drug is loaded onto a carrier surface; highly agglomerated particles experience stronger press-on forces due to a larger area of contact between the individual particles, and this results in lower levels of drug detachment from a carrier (Selvam and Smyth, 2011). Despite the similarities in the FPF and emission, bulk blend dispersibility measurements indicated that the Stage 5 SX DPI was less dispersible (DA_{50} = 0.61 Bar), marginally more cohesive (CPP = 3.5 Bar) and showed greater heterogeneity in agglomeration than the Stage 4 SX DPI (DA_{50} = 0.48 Bar, CPP = 3.0 Bar), indicating different bulk powder structures. The improvement in powder flow as a result of inclusion of a carrier resulted in equivalent emissions in the NGI despite different SX physicochemical properties. The non-significant reduction in the FPF of Stage 5 SX compared to Stage 4 SX may

have arisen from the marginally higher S5SX-CL adhesion compared to SXS4-CL adhesion, and lower detachment and dispersibility of the smaller, more cohesive Stage 5 particles.

Stage 5 SX particles also exhibited a non-significant smaller MMAD ($p > 0.05$) compared to Stage 4 SX and a significantly smaller MMAD than crystallised SX ($p < 0.05$) following aerosolisation from a DPI blend, which may have arisen due to the inherently smaller geometric particle size of this sample. The effect of particle size on aerosolisation in the literature has been variable. For example, when formulated as binary drug-lactose blends, smaller SX particles (in terms of geometric and aerodynamic particle size, comprising fractions of the same powder) had lower FPFs in the NGI (Taki, 2008a). Smaller salbutamol particles have generated similar emissions, higher FPFs, FPMs and smaller MMADs compared to larger drug particles (Adams et al., 2012); whereas larger SS particles (aerosolised without a carrier) have generated higher emissions (Shariare et al., 2011). Mannitol particles prepared by jet-milling or spray drying with D_{v50} values in the range 1 – 10 µm, had optimal FPFs when the D_{v50} was 2 – 5 µm (Louey et al., 2004a). The effect of particle size (and thus mass) on detachment from a carrier has also been shown to be less critical with increasing inhaler device de-agglomeration efficiency (Dickhoff et al., 2002). The factors responsible for changes in the dispersion of powder aerosols therefore arise from a complex inter-play of the particle size of the drug, particle properties, airflow and inhaler design (Chew and Chan, 1999; Chew et al., 2000) and relate to the specific set of conditions employed in the particular study. The bulk powder properties, which are determined by the component particles, also influence dispersiblity (i.e. DA_{50}), in addition to the heterogeneity in the dispersion behaviours of sub-populations of particles within the bulk (i.e. contrasting DA_{50} and CPP parameters).

Stage 4 SX particles produced had a higher FPF than crystallised SX particles when formulated as single drug DPIs ($p < 0.05$), but the emission and MMAD were the same ($p > 0.05$). Stage 4 SX also had a lower DA_{50} and thus was more dispersible than CSX. The bulk dispersibility of the crystallised and Stage 5 SX DPI blends was equivalent (DA_{50} 0.62 Bar and 0.61 Bar, respectively), as were the aerosolisation parameters (excluding the MMAD) following NGI analysis. The CSX DPI was marginally less cohesive (CPP = 2.5 Bar) than the Stage 4 (CPP = 3.0 Bar) and Stage 5 (CPP = 3.5 Bar) SX DPI blends, and this rank was in agreement with the cohesivity of the component

SX particles determined from surface energy measurements (Figure 6.6). When formulated with a lactose carrier, CSX has shown equivalent FPFs to micronised particles despite having a larger particle size and PSD, and demonstrated no difference in throat deposition (Murnane et al., 2009). The lower FPF of CSX observed in the current study compared to Stage 4 SX resulted from a larger non-sizable fraction (i.e. SX retention in the device, capsules, throat and pre-separator) for the crystallised particles (82.1 ± 0.18 % RD) compared to the Stage 4 SX particles (74.0 ± 0.35 % RD). Despite a smaller crystal particle size in the current work compared to that of Murnane et al. (2009) (D_{v50} = 4.93 ± 0.37 µm and 6.59 ± 0.31 µm, respectively), a higher drug content in the blends (1.38 % w/w and 0.58 % w/w, respectively) would result in a blend in which cohesive interactions play a more dominant role. CSX agglomeration would show favourable competition over CSX-CL adhesion at higher drug contents, such there would be a larger proportion of drug agglomerates, as well as agglomerates with larger diameters (Murnane et al., 2009). The component particles of the agglomerates would also be larger for crystallised compared to Stage 4 particles. Therefore undispersed CSX agglomerates, in addition to any dispersed CSX particles, due to their large particle size, would both deposit on NGI stages corresponding to larger aerodynamic particle sizes resulting in an increase in the non-sizable fraction.

When formulated as a combination DPI, CSX exhibited an increase in emission and FPF RD, and no change in MMAD, when combined with CFP. These changes were in direct contrast to those observed for CSX formulated with CFP in a pre-blend. Furthermore, the bulk dispersibility improved when in combination (DA_{50} = 0.35 Bar compared to 0.62 Bar for the CSX-only DPI) and there was an increase in cohesivity. The reasons for this change in aerosolisation behaviour were a little unclear. During blending, drug agglomeration on a carrier surface occurs due to press on i.e. inertial and frictional forces resulting from carrier particle collisions and relative displacements (De Boer et al., 2004). During the first 0.5 min, drug particles/agglomerates reside in carrier surface irregularities. As mixing time increases, they redistribute over the entire carrier surface, and there is the generation of further drug agglomerates (Grasmeijer et al., 2013). De Boer et al. (2004) suggest that there are two types of drug agglomerates: 'natural' agglomerates in the starting material which are not disrupted during mixing or inhalation, even after removal from the carrier, and newly formed agglomerates on the carrier surface. These latter agglomerates are weaker and disperse under relatively weak de-agglomeration forces (De Boer et al., 2004). Blending would therefore result in

restructuring of the CSX or CSX:CFP pre-blend starting material such that there would be a proportion of more weakly associated agglomerates.

In the combination blend, due to the higher adhesive rather than cohesive tendency of CSX towards CFP, the newly formed weaker agglomerates may comprise mixed CSX-CFP agglomerates. In this instance, these mixed agglomerates may have altered properties such as size, shape and packing fraction compared to CSX-CSX agglomerates that may have been favourable for de-agglomeration. If, for example, the mixed agglomerates were larger than the single drug agglomerates, larger diameters and thus larger detachment masses would increase the ratio of the removal force to the adhesive force, further increasing the chance of agglomerate removal (De Boer et al., 2004). Dry dispersion laser diffraction provided evidence for agglomerate re-structuring between the crystallised DPI blends; in combination blends the DA_{50} was lower but the CPP higher than the single drug, CSX-only blend (Table 6.7). The low DA_{50} represented a fraction of the powder which dispersed well at low dispersion forces thus comprising weakly held agglomerates, however, the high CPP indicated that there remained a fraction of powder within the bulk comprising strongly-associated agglomerates which required much higher dispersion forces for de-agglomeration. Despite this, there was no change between SX aerosolisation for single drug and co-formulated DPIs prepared with micronised (i.e. unfractionated) particles which are also likely to have undergone a degree of agglomerate re-structuring. This further indicates that the properties and aerosolisation of mixed agglomerates in a combination DPI may differ post-blending, and that the fundamental agglomerate properties depend on the particle type in the formulation.

When formulated as combination pre-blends, changes to the dispersibility of fractionated SX were dependent on the SX and FP particle type included in the blend. The biggest change in SX dispersion, in terms of the emission, FPF ED/RD and MMAD occurred when Stage 4 SX was combined with Stage 3 FP (Figure 6.3, Figure 6.4 and Table 6.5). This combination was therefore selected to investigate the ability to engineer SX aerosolisation using fractionated particles in combination DPI blends. Stage 4 SX had a higher emission but a lower FPF ED in combination with Stage 3 FP, and no change in the MMAD or FPF RD, when formulated as a carrier-based DPI blend. The trends seen in the NGI aerosolisation were similar to those observed in the pre-blend. Although blending with a carrier was unable to overcome the detrimental effect on the

FPF ED upon co-formulation, the emission improved, and unlike in the pre-blend, the FPF RD and MMAD did not change between the single drug and combination DPI blends, suggesting that despite worsening dispersibility with combination delivery, the changes were less severe. These findings were in contrast to those of Taki (2008a), in which upon co-formulation of aerodynamic size fractions of SX and FP, there was no change in the FPF of SX particles. When assessed by laser diffraction, there was no change in the bulk cohesivity of the powder blend (i.e. CPP = 3.0 Bar) but an increase in the dispersibility from DA_{50} = 0.48 Bar for the single drug DPI compared to DA_{50} = 0.39 Bar for the combination DPI. This difference also highlighted an increase in the heterogeneity in agglomerate strengths within the powder bulk as the dispersing pressure required to achieve 50 % de-agglomeration (i.e. DA_{50}) was lower despite the dispersing pressure for 100 % de-agglomeration (i.e. CPP) remaining the same. Therefore, the lower DA_{50} may have been more favourable for powder entrainment into the airstream as it represented a population of more dispersible agglomerates within the blend. However, there still remained a proportion of tightly associated agglomerates that did not disperse well, and these ultimately dictated the FPF. These strongly associated agglomerates may have been the 'natural' agglomerates which pre-existed in the powder/blend prior to formulating with lactose, as explained above. Strong inter-particulate interactions between Stage 4 SX and Stage 3 FP particles (work of adhesion = 84.5 – 91.3 $mJ.m^{-2}$) and high S4SX-S4SX cohesion (80.5 – 83.1 $mJ.m^{-2}$) may have limited the disruption of 'natural' agglomerates in the powder during blending with a carrier. However, due to the greater heterogeneity in the work of adhesion compared to the work of cohesion of Stage 4 SX, newly formed drug agglomerates in the combination blend comprising one or both drugs would be like ly to show a wider range in agglomerate strengths compared to S4SX-only agglomerates in the single drug blend.

6.6.4 THE INFLUENCE OF DRUG PARTICLE PROPERTIES AND CO-FORMULATION ON SALMETEROL XINAFOATE DISSOLUTION

Following deposition, aerosolised drug particles must undergo dissolution in the fluid lining of the lungs in order to become available for therapeutic action. Dissolution involves the transfer of molecules or ions from the solid state into a solution. The rate of dissolution of solid particles is dependent on the surface area available for contact with the dissolution media, and is therefore affected by the particle size and degree of agglomeration (Aulton, 2002). The physicochemical properties of the drug are therefore

anticipated to dictate the rate of dissolution and subsequent absorption, metabolism and elimination of inhaled drugs (Davies and Feddah, 2003). Despite the small particle size of inhaled drugs, poor solubility is often a rate limiting step in the dissolution process (Davies and Feddah, 2003). The solubility values determined for SX showed slight variation to those reported in the literature. SX is known to be practically insoluble in water but soluble in methyl alcohol (Martindale, 2013). The aqueous solubility was lower than reported values of 61.70 $\mu g.mL^{-1}$ (Tong et al., 2001) and ~ 70 $\mu g.mL^{-1}$ (am Ende, 2011) however the high solubility in methanol was comparable to the literature (~ 40 $mg.mL^{-1}$, am Ende, 2011). Differences between solubility values may arise from the relative proportions of the SX polymorph present, in which metastable SX-II has higher aqueous solubility than the more stable SX-I polymorph (Tong et al., 2001). Alternatively, the 24 h period may not have been long enough to achieve equilibrium in water, compared to the 72 h period employed by Tong et al. (2001), or there may have been differences in the sensitivity of the analytical method used. The degree of mechanical stress imparted as a result of manufacturing and processing may also alter between batches of powders and can alter solubility, for example, subjecting SX to different mixing times resulted in an increase in the apparent solubility potentially arising from amorphisation of the initially crystalline particles (Grasmeijer et al., 2013).

The dissolution rate of micronised (i.e. unfractionated) SX when formulated with a lactose carrier appeared to be dependent on the composition of the dissolution media. The use of different dissolution media enabled the influence of SX solubility on the dissolution rate to be determined. The composition of the airway lining fluid changes according to the site in the lungs (Gehr et al., 1993; Bastacky et al., 1995; Widdicombe, 2002); if particle/formulation engineering changed the deposition site of the drug particles, a change in drug solubility in the fluid may occur. For example the presence of surfactant in the fluid can increase dissolution by improving wettability and reducing the agglomeration of particles in the media (Son and McConville, 2009), and may therefore dictate dissolution rates. SX solubility was found to be sensitive to changes in the amount of methanol and water in the media, and reduced with the rank: 75:25 > 50:50 > 25:75 for the different methanol:water compositions. This corresponded with a reduction in dissolution rate of SX and was corroborated by f2 values that were less than 50 between all the dissolution media compositions. High standard deviations (SD) were also observed between repeat experiments, particularly for the 25:75 composition. High SD values have been reported for the Franz diffusion cell method which similar to

the Transwell system mimics the diffusion controlled air-liquid interface of the lung (May et al., 2012). High variability was attributed to poor, or lack of, particle wetting due to the experimental set-up, and which would also arise from poor solubility of the drug in the media. There may also have been a degree of solvent evaporation and losses during the experiment and sampling steps. Variability in agglomerate sizes and/or the PSD < 5 μm, as well as non-uniform drug loading due to irregular powder deposition, are also factors which may be responsible for high variability between dissolution experiments (Son and McConville, 2009; May et al., 2012).

There was no difference in the dissolution rate of unfractionated SX compared to crystallised, Stage 4 and Stage 5 particles, as indicated by f2 values ≥ 50. There was also no change in the dissolution rate between any of the latter engineered particle types (f2 values ≥ 50), despite there being differences in the aerodynamic deposition profiles of crystallised SX and the SX fractions in the NGI, and differences in the bulk dispersibility, of the DPI blends. The larger MMAD ($p < 0.05$) of CSX compared to Stage 5 SX (arising in part due to the larger geometric D_{v50} of CSX), and lower FPF ($p < 0.05$) and DA_{50} compared to Stage 4 SX would suggest that the dispersion of CSX particles was poorer than that of the fractions. Different deposition patterns, in terms of different agglomerate sizes and particle/agglomerate size distributions, may have occurred between the samples following aerosolisation into the TSI. Any deposited agglomerates would need to first undergo dispersion to individual particles prior to dissolution. The rate of dissolution may therefore be limited either by the disintegration/dispersion of the deposited agglomerates in the media and/or the properties of the individual particles once they are dispersed in the media. Microscopy would therefore be required to determine the deposited state (i.e. as particles/agglomerates and the PSD) of the formulations on the Transwell insert. For example, the most cohesive Stage 5 SX particles may have deposited predominantly as agglomerates when compared to Stage 4 or crystallised SX. However, upon adequate wetting and liberation of the particles into the dissolution media, the smaller particle size (i.e. D_{v50} following complete dispersion) and higher surface area of Stage 5 SX, and higher disorder (in terms of both bulk and surface disorder, as observed in Chapter 4) of the particles may have demonstrated higher solubility and thus promoted faster dissolution, such that overall there was no alteration in dissolution rate between the particle types. In the literature, stage fractionated hydrocortisone, salbutamol sulphate and budesonide have shown faster dissolution rates as particle size reduced, and was

attributed to the larger exposed surface area per unit mass of deposited drug for smaller particles (Cartier et al., 2008; Son and McConville, 2009; Arora et al., 2010). Significant differences in the initial release rates of budesonide have also been observed between stage fractions of different sizes (Son et al., 2010). Despite differences in the geometric D_{v50} of CSX, Stage 4 and Stage 5 SX, this did not appear to alter the dissolution rate of the particles, potentially due to the deposition of powder agglomerates rather than individual particles on the Transwell insert, which would require microscopy for confirmation.

A lack of more pronounced differences between the particles may have arisen from experimental factors. For example, drug loading has been shown to affect dissolution rate. Higher drug loadings slow dissolution, and have the biggest impact on large particles and more hydrophobic drugs (Son and McConville, 2009; Arora et al., 2010; Son et al., 2010). Highly agglomerated drug particles have also shown slower dissolution rates due to large agglomerate sizes and high packing fractions which limit the exposure of particle surfaces to the dissolution medium (Kale et al., 2009). There was a high level of variability between repeat experiments, and the methodological parameters may not have been fully optimal. SX recovery from the insert following application of known amounts of SX in solution varied from 75.8 ± 7.42 % to 92.2 ± 5.87 % for 2 µg and 10 µg of SX, respectively, suggesting there may be SX adsorption and/or sampling errors, particularly at low drug concentrations. At a number of sampling time points, including the final time point and wash, the detected concentration was at or below the LOQ of the calibration curve. Dissolution studies, particularly when attempting to match as closely as possible the likely *in vivo* dosing, require more sensitive analytical techniques such as HPLC-MS in order to enable quantification of small amounts of drug. Despite these limitations, following co-formulation there appeared to be an increase in the dissolution rate and total cumulative amount dissolved for micronised (i.e. unfractionated) SX compared to the single drug DPI formulation, and this was confirmed by an f2 value ≤ 50. A greater adhesive (rather than cohesive) tendency for SX towards FP may have resulted in modifications in agglomerate structures such that SX was exposed to a greater extent to the dissolution media. Adhesive interactions between SX and FP may have disrupted SX-only agglomerates held together by SX-SX interactions that were weaker than both SX-FP and FP-FP interactions, and therefore increased the surface area available for SX dissolution. Due to the heterogeneity in surface energy and therefore the work of

cohesion and adhesion, FP may have interrupted even the most cohesive SX agglomerates and thus exposed SX particles with higher degrees of disorder and therefore wettability to the dissolution media.

6.6.5 CONCLUSIONS

In this study, an attempt was made to engineer the aerosolisation performance of combination DPI formulations by controlling the physicochemical properties of physically mixed drug particles. In the absence of a carrier, fractionated particles exhibited different aerosolisation behaviours in co-formulation compared with the unformulated fractionated powders. Furthermore, the changes that occurred were specific to the fractions that were blended together. Generally, the co-formulation of fractions in a 1:1 ratio was detrimental to the aerosolisation performance of SX and FP particles, whereas no change in aerosolisation behaviour occurred for co-formulated unfractionated particles as described in Chapter 5. Fractionated particles were therefore able to modify the dispersion behaviour of SX and FP in combination pre-blends, and indicated that within a bulk micronised powder there would be populations of particles for which aerosolisation would be affected to a different extent. The aerosolisation behaviour of the unformulated engineered SX particles and formulated combination pre-blends, however, was not fully representative of SX aerosolisation when formulated as carrier-based DPI blends. Upon assessment of SX dissolution following aerodynamic deposition from a DPI formulation, whereas SX particle properties were found to have no effect on the dissolution profile, co-formulation of unfractionated particles seemed to increase the dissolution rate of SX. Combination delivery may therefore have benefits in terms of the dissolution profile of SX, warranting further investigation into the cause of the improvement. Further studies would also benefit from generating dissolution profiles in media more representative of the *in vivo* environment, and using particle/formulation engineering to attempt to further improve the dissolution profile of SX in co-formulation.

7 GENERAL DISCUSSION

Fixed dose combination dry powder inhaler (DPI) formulations containing inhaled corticosteroids (ICs) and long-acting bronchodilators (LABAs) are now in routine use for the treatment of lung diseases. Since the introduction of the Seretide®/Advair® Diskus and Symbicort® Turbohaler, the number of combination inhalers commercially available has steadily increased. A pharmacological synergistic effect between ICs and LABAs has been suggested to occur, however, whether this occurs in reality remains a controversial area for research and discussion. Nevertheless and regardless of any possible synergism, the two classes of drugs will have at least a complementary effect in managing disease due to their different modes of action: the IC administered to control airway inflammation and the LABA to treat smooth muscle dysfunction (Nelson et al., 2003). The inhalation of two drugs from a single inhaler device may also simplify medication regimens, improve compliance (Taki et al., 2011a) and therefore provide greater patient acceptability. There is also the potential for physicochemical interactions to occur between the component particles, which may lead to altered aerosolisation of one or both drugs in the formulation.

LABAs currently formulated in combination inhalers include salmeterol xinafoate (SX) and formoterol fumarate, and the ICs budesonide, beclometasone dipropionate and fluticasone propionate (FP) (Tamm et al., 2012). In the current work, SX and FP were studied as representative drugs in order to determine the influence of particle physicochemical properties and inter-particulate interactions on powder dispersion upon co-formulation. Studies have suggested that combination delivery of SX and FP from DPI formulations may alter the aerosolisation and deposition patterns of the drugs (Taki et al., 2010; Taki et al., 2011). Significant differences in the stage deposition of the commercial single active and combination formulations led the authors to conclude that separate and combined delivery may not be pharmaceutically equivalent (Taki et al., 2011). A cause of this non-equivalence may arise from particle co-association within the formulation thus altering the dispersion and deposition profile of the drugs. Interactions between SX and FP have been identified upon aerosolisation in pMDI and DPI formulations (Theophilus et al., 2006; New et al., 2008; Rogueda et al., 2011) which may increase the likelihood of the drugs depositing at the same location in the lungs simultaneously. Whereas an interactive affinity has been identified between SX and FP powders (Young et al., 2004a; Vernall et al., 2012) which may promote co-agglomeration of the particles, this interaction will also depend on particle properties such as the surface inter-facial chemistry, which has recently been shown to alter the

balance of cohesive and adhesive forces in a combination formulation (Kubavat et al., 2012).

Inhalation powders are traditionally produced by micronisation which is well known to induce changes in particle properties which are difficult to control; these include the generation of a wide PSD (Steckel et al., 2003a; Steckel et al., 2003b), increased amorphous content (Brodka-Pfeiffer et al., 2003; Gaisford et al., 2010), and higher surface energy (Feeley et al., 1998; Gamble et al., 2012). This can result in a heterogeneous powder, which may exhibit sub-populations of particles with distinct microstructure, and different propensities for particulate interactions when formulated (e.g. with a carrier or particles of a second drug type). Whereas batch-to-batch variation in powder properties have been identified and characterised (e.g. Ticehurst et al., 1994; Feeley et al., 1998; Le et al., 2012) the characterisation of intra-batch variability and the subsequent consequences for aerosolisation behaviour have not been extensively investigated, and the particular implications for complex combination formulations have not been widely considered. Despite the growing option of the use of particle engineering as a means of producing respirable particles, the batch production of micronised drug powders is likely to be of prime importance to inhalation formulation over the coming years. There remains merit therefore in understanding the implications of co-formulation on the deposition patterns of physically mixed micronised particles. In particular, there is merit in identifying the particle properties in powder batches that contribute towards the heterogeneity of interactions with co-formulated drug, carrier and ternary particles. By understanding and characterising drug agglomeration behaviour, there may be the potential to modify aerosolisation in combination formulations without the need for alternative particle production methodologies. In order to address these issues, a systematic study was undertaken in order to ascertain the influence of co-formulation and intra-batch variability of SX and FP particles on their aerosolisation behaviour in powder formulations. An in-depth analysis of the physicochemical and agglomeration properties of the bulk powders and their intra-batch variability would allow for a fundamental understanding of the consequences of co-formulation to be achieved.

Prior to determining the aerosol performance of a combination, or indeed any type of DPI formulation, it is important to gain an understanding of the inherent dispersibility of the bulk drug powders. This information provides an indication of fundamental

powder behaviour and can aid the formulation process in terms of selecting the most appropriate excipients or device technology to achieve efficient drug dispersion. The techniques currently available for this purpose exhibit drawbacks which include complex methodologies, the requirement for a large quantity of material, and the need for specialist equipment. A data analysis technique was therefore developed in the current study to characterise the inherent dispersibility of fine particle powders using dry dispersion laser diffraction and an airflow titration approach. Unlike previous applications in which the analysis was mainly qualitative (e.g. Adi et al., 2008) or involved the powder being actuated from an inhaler device (e.g. Adi et al., 2006, Adi et al., 2008; Behara et al., 2011b), the developed analysis technique generated two parameters which described the dispersion and de-agglomeration behaviour of the bulk powder from a static bed, such that the natural powder structure was subjected to minimal disturbance.

A series of eight individual inhaled powdered drugs/excipients were screened and found to have different dispersion behaviours that could be linked to differences in powder structure and heterogeneity in particle properties. These dispersion characteristics would aid in dictating the formulation approaches and inhaler device technology that would be required to achieve efficient de-agglomeration of individual particles during delivery. For example, salbutamol base (SB) and tofimilast (Tof) dispersed readily (DA_{50} = 0.25 and 0.28 Bar, respectively) and required relatively low dispersal forces to achieve 50 % powder de-agglomeration. A higher CPP for Tof compared to SB (3.0 and 1.0 Bar, respectively) indicated a heterogeneous population of agglomerates within the bulk powder for Tof. Therefore, higher dispersal forces are required in order to achieve complete dispersion of this powder, as is also the case for the most tightly associated agglomerates. Both SX and FP dispersered poorly in their natural state (DA_{50} = 1.45 and 1.15 Bar, respectively) and had high bulk cohesivity (CPP = 3.5 and 3.0 Bar, respectively). These powders would require formulation/device approaches that would lower the bulk cohesivity of the powder (e.g. particle engineering or inclusion of a carrier) and/or provide high forces for dispersion (e.g. devices which generate high turbulence and numbers of impactions). Further characterisation of the latter powders revealed that FP had a larger particle size than SX (D_{v50} = 2.81 ± 0.03 µm and 2.05 ± 0.12 µm, respectively) and different morphology; FP particles appeared rounder compared to the flatter, more plate-like SX. FP was also found to have a higher and more heterogeneous surface energy than SX, which corresponded to a higher work of

cohesion for FP than SX. When aerosolised into the NGI, FP displayed a higher emission but was found to exhibit both a lower FPF and larger MMAD than SX. These observations confirmed the inherent cohesive and agglomerative behaviour of the SX and FP particles. However, differences in the agglomeration state, agglomeration tendencies and agglomerate strength would affect the particle interactions between SX and FP when co-formulated.

The higher emission for FP than SX may derive from the highly cohesive nature of FP agglomerates that display good flowability and entrainment (Steckel et al., 2003b), but for which de-agglomeration is poor at low airflow rates. This leads to low FPFs (Steckel et al., 2003b; Louey et al., 2004) and high MMADs, as confirmed in the present study. Micronised SX (Adi et al., 2008) aerosolised in the absence of a carrier also demonstrated low FPFs. Unlike FP, this was predominantly due to low emissions for SX that may arise due to a high adhesive tendency of SX towards the device and capsule (Adi et al., 2008). Despite a lower emission for SX, more dispersible SX agglomerates resulted in a higher FPF ED (and lower MMAD) than FP. These findings were corroborated by surface energy analysis, which indicated that SX-SX cohesive interactions were weaker than FP-FP cohesive interactions, and thus it would be expected that lower dispersal forces would be required to overcome cohesive SX interactions between the particles. A lower DA_{50} and CPP value for SX compared to FP (following tumbling of the powders) also supported better SX dispersibility compared to that of FP. Analogous to there always being a size distribution within any powder sample, there will inevitably be a distribution of agglomerate strengths within the bulk of a powder structure (Das et al., 2012). This was exemplified by the surface energy distributions and differences in the magnitude of the DA_{50} and CPP values of the SX and FP powders. Although both showed a degree of heterogeneity, this was greater for FP than SX, whereby poor dispersion of the most cohesive agglomerates may also have contributed towards the lower FPF values observed for FP than SX. It is therefore important to understand both the inherent behaviour and the heterogeneity of agglomeration behaviour of drug powders in order to control formulation behaviour when micronised drug particles are blended with further particles. Such blends include carrier containing formulations and co-formulated drug particles in combination formulations.

Upon aerosolisation into the NGI, FP deposition was generally not affected by combined formulation in carrier-free blends, but a reduction in the MMAD suggested some minor benefit in co-formulation. SX conversely showed worsening dispersibility in the presence of FP. The MMAD of SX increased as the amount of FP in the blend increased, and the FPF was significantly lower at the highest SX:FP ratio employed compared to single drug delivery. In the absence of a carrier, interactive forces would arise from the cohesivity and adhesivity of the drug particles. To the author's knowledge, this was the first investigation of the dispersion modifying effects of SX and FP at various ratios in the absence of a carrier. Such investigations for SS and BDP particles formulated in combination in the absence of a carrier indicated that while for both drugs the emission was altered by co-formulation, only BDP exhibited a change in its FPF compared to BDP alone, despite both drugs being relatively more adhesive towards each other than cohesive (Jetmalani et al., 2012). Using the surface energy distributions to derive the work of cohesion and adhesion of the powders, the adhesive SX-FP interactions were found to be lower than cohesive FP-FP interactions but higher than SX-SX interactions. Therefore, it was postulated that SX de-agglomeration would be affected by co-formulation with FP to a greater extent than FP de-agglomeration by co-formulation with SX. The weaker SX-SX interactions would be more easily disrupted than stronger FP-FP interactions in the respective powders upon co-formulation. This balance of interactions differed to those reported previously. For example, using the atomic force microscope (AFM), SX-FP adhesive interactions were reported to be larger than the cohesive interactions of both drugs (Young et al., 2004a). In another study also using AFM, SX was found to have stronger cohesive interactions than adhesive interactions towards FP, whereas FP formed stronger interactions with SX than FP cohesive interactions (Vernall et al., 2012). These differences may arise due to different batches of powder being tested, which may also have been subjected to different processing histories. For example, it has been reported that the cohesive-adhesive properties of FP towards SX varied as a result of different interfacial chemistries which arose with increasing numbers of passes through a micronisier (Kubavat et al., 2012). Furthermore, the use of AFM, which is a single particle technique, may have been unable reveal the heterogeneity in particle properties which, as demonstrated in the current work, are present within the bulk of a powder.

The micronisation process itself, and any secondary processing, therefore has the potential to alter the balance of interactive forces not only between different batches of

powder, but also within a single batch of powder. The interactive nature of the particles in a blend can also lead to a change in powder structure (Jetmalani et al., 2012), and this was exemplified by the changes in bulk dispersibility of the combination particle mixtures determined by laser diffraction analysis, compared to the dispersibilities of the single drug entities. As the proportion of FP in the blend increased, the dispersibility worsened, as demonstrated by the DA_{50} values (i.e. the dispersing pressure required to achieve 50 % de-agglomeration). The DA_{50} values gradually increased according to increasing proportions of FP from 0.20 Bar for the highest SX content blend to 0.89 Bar for the highest FP content blend. The powders also became more cohesive. The CPP values (i.e. the dispersing pressure required to achieve 100 % de-agglomeration) were 1.00 – 1.20 Bar for the SX-rich blends compared to 1.20 – 1.70 Bar for the FP-rich blends. This also represented a change in agglomerate heterogeneity. A reduction in the magnitude of the difference between the DA_{50} and CPP values was observed as the amount of FP in the blend increased, indicating less variable agglomerate strengths within the bulk powder. The structure of powder mixtures will comprise of a range of agglomerates including mixed and single component agglomerates with differing dispersibilities (Behara et al., 2011a). Mixed SX-FP agglomerates, SX-only and FP-only agglomerates would therefore be present in varying proportions within the mixtures, some of which would be poorly dispersible (and represented by a high CPP). Higher FP content blends therefore consisted of larger proportions of poorly dispersible agglomerates, demonstrated by higher CPPs, compared to high SX content blends, and less variability in agglomerate strengths as the DA_{50} values were also higher for these blends.

The intra-batch variability of the powders was characterised quantitatively using a recently developed fractionating technique in which cascade impaction is used to isolate aerodynamic size fractions of bulk powders (Taki et al., 2011b). Both SX and FP powders were found to comprise sub-populations of particles with distinct properties. Of particular importance was the identification of a sub-population of SX particles with higher bulk and surface disorder and a reduction in dispersibility compared to the bulk, unfractionated powder. Conversely for FP, sub-populations were identified with comparable disorder to the bulk powder but improved dispersibility. Micronisation is well known to generate particles with heterogeneity in their properties (Steckel et al., 2003a; Steckel et al., 2003b) but to date this has not been fully quantified. Studies have however shown that powders may respond differently to processing pressures and that

this will affect the aersolisation performance between batches; differences might therefore also be expected within batches due to the unequal pressures experienced by the particles during manufacturing (Marek et al., 2011). Such a finding was identified within bulk SX and FP powders and hence this may also be a consequence for all powders subjected to micronisation. Not only may this affect the variability of DPI performance, but may also have implications for drug aerosolisation when formulated with a carrier either alone or in combination with a second drug.

Prior to probing the implications of intra-batch variability on drug aerosolisation, single drug and combination DPI blends were prepared using the bulk (i.e. unfractionated) powders. The FP-only DPI was found to be more dispersible than the SX-only DPI according to laser diffraction de-agglomeration analysis. When aerosolised into the NGI, despite FP being found to have a higher emission, the FPF ED and RD were lower and the MMAD larger than SX. This indicated that the FP-only DPI blend contained higher proportions of drug agglomerates that were more poorly dispersible than those in the SX-only DPI blend, and it was this that dictated the poorer fine particle delivery of FP. Comparing the aerosolisation behaviour of SX:FP pre-blends before and after blending with a coarse carrier, it was found that when formulated with a carrier, the detrimental effects on SX dispersion upon co-formulation was no longer manifest, and there proved to be no change in the dispersion of FP, across the three SX:FP ratios employed. These findings were in contrast to those of the commercial carrier-based Seretide Accuhaler formulations reported in the literature. In the latter study, SX caused a small but significant increase in the aerosolisation of FP, generating higher FPFs in co-formulation, whereas SX was found to have a smaller FPF from the combination in comparison to the single drug product (Taki et al., 2011). The results presented in the current study suggest that by pre-mixing SX and FP particles prior to blending with the carrier, it may be possible to negate changes in dispersion behaviour (in terms of the emission, FPF and MMAD) that may occur upon co-formulation of the drug particles at different SX:FP ratios. When internal group analysis of the combination DPI blends only was effected, to ascertain whether there were differences in aerosolisation performance between the co-formulated blends only, no change in FP dispersion was again demonstrated. This therefore, was in keeping with the previous observations derived from aerosolising fine particle blends and pre-blends. However, for SX, despite there being no change in the emission, the FPF RD and ED were lower when SX was present in the 1:8 SX:FP ratio compared to the 8:1 ratio ($p < 0.05$, Kruskal Wallis

ANOVA with Dunns post-test). Therefore, although SX entrainment may have been similar between the ratios, the agglomerate properties of the drug particles may have differed, resulting in different efficiencies for de-agglomeration. It therefore may be possible to modify the aerosolisation performance of SX from combination blends by altering the SX:FP ratio.

The dispersibility of the combination DPI blends, according to the DA_{50} from laser diffraction analysis, was also found to alter; becoming worse as the amount of SX in the blend increased. This trend was opposite to that observed in the fine particle blends in which the bulk dispersibility (i.e. DA_{50}) of the bulk powder improved with increasing SX content. There also seemed to be a shift towards greater heterogeneity in agglomerate strengths in the DPI blends containing increasing amounts of SX. This could be attributable to changes in powder structure and the balance of inter-particulate interactions within the blend. The dispersion of carrier blends to produce individual particles would be dictated by the ease in which drug particles/agglomerates are liberated from the surface of the carrier, as well as to how efficiently and effectively they disperse once released. This is in contrast to fine particle blends, when dispersibility will only be dictated by the dissociation of drug agglomerates. Therefore, in addition to interactions between SX and FP particles, interactions with the lactose particles in the formulation would also contribute towards the aerosolisation behaviour of the drugs. This would be affected by the specific physicochemical properties of the drug particles, as well as the carrier or any ternary agent particles that may be present in the formulation. These properties may differ between and even within batches of powders, and hence warrant thorough characterisation in order to fully determine the effects of co-formulation on powder systems of interest.

FPF and MMAD values only represent two metrics of formulation performance that might be predictive of *in vivo* deposition. One aim of this thesis was to investigate whether co-association of particles occurs within combination DPI blends. It was found that an heterogeneity of agglomerate strengths and structures is present in bulk micronised materials and therefore it is likely that the degree of mixing of two drugs in mixed agglomerates would also be heterogeneous. As a measure of co-association, the SX:FP ratio of the deposited masses across the NGI were calculated for both the co-formulated pre-blends and DPI blends. In the absence of a carrier, the SX:FP ratio of the deposited mass was maintained in the throat, pre-separator and on stages 1 – 6 of

the NGI when the nominal SX:FP ratio was 1:8. There were deviations in the ratio of the deposited mass for blends containing SX:FP in the proportion 1:1 and 8:1 beyond stage 3 and stage 2 of the impactor, respectively. In the presence of a carrier, the magnitude of the deviations increased further. Physically mixed combination formulations have demonstrated deposition profiles in which different amounts of each drug were deposited on the impactor stages. These have included salbutamol base and beclometasone dipropionate (Traini et al., 2012) and SX and FP combinations (Pitchayajittipong et al., 2009), and has been overcome by the formulation of combination particles where it was possible to achieve uniformity of the ratio of deposition of the respective drugs on each impactor stage (e.g. Westmeier and Steckel., 2008; Pitchayajittipong et al., 2009; Kumon et al., 2010; Traini et al., 2012). The current study suggests that the deposition patterns, in terms of the drug ratio on the impactor stages, may also be influenced by the drug ratio of the formulation and the formulation type (i.e. carrier-based vs. carrier-free formulation). It has also recently been reported that following aerosolisation of the Seretide Accuhaler 50/250 into the NGI, approximately 45 – 50 % of the particles depositing on stage 3 of the impactor were free standing, and that a much smaller proportion were agglomerated, either with fine lactose or drug particles (Vernall et al., 2012). The change in the ratios of the deposited masses observed in the current study may therefore be due to changes in the aerosolisation behaviour which do not arise due to association between the particles (which may cause them to deposit as mixed agglomerates), and therefore warrants further investigation.

Inhaled powders have been shown to contain a distribution of powder strengths within the bulk which have different propensities for de-agglomeration, resulting from a distribution in particle properties such as particle size, density and surface energy (Das et al., 2012). In order to investigate the heterogeneity of agglomeration state of micronised particles in DPI blends, fractionated sub-populations were investigated in isolation and in co-formulated blends, with and without a lactose carrier. When formulated in combination in the absence of a carrier, the fractions displayed changes in their dispersibility when compared to the individual drug fractions. Furthermore, the trends were different to those seen for the unfractionated powders, and the magnitude of the changes varied depending on the specific combination of particles employed.

An improvement in the emission of Stage 5 SX upon co-formulation with either Stage 3 or Stage 4 FP powders was observed, and also improvement in the emission of Stage 4 SX upon co-formulation with Stage 3 FP powder. A smaller MMAD for Stage 4 FP co-formulated with Stage 4 SX also resulted. Although, in the majority of instances, the emission, FPF and MMAD of the drug fractions were either worsened or did not change upon co-formulation. Therefore, it was not possible to optimise (i.e. improve) aerosolisation performance using the specific combination of fractions employed. There were also differences in the SX:FP ratios of the deposited masses in the NGI. The magnitude of the deviation from the nominal ratio (present in the powder mixtures) was small and comparable for all the blends when considering the deposition on the throat, pre-separator and stages 1 - 4 of the impactor. From stage 5 onwards, however, whereas the Stage 4 SX:Stage 4 FP blend displayed negligible deviation in the ratio of the deposited mass from the nominal ratio, the magnitude of the deviation appeared to increase with the following rank order: Stage 4 SX:Stage 3 FP < Stage 5 SX:Stage 4 FP < Stage 5 SX:Stage 3 FP. The most striking outcome of this study was therefore that within the bulk powder there were populations of particles that responded differently to co-formulation. These different responses of the powder sub-populations may contribute towards batch to batch variability in inhaler performance, and even result in sub-optimal drug delivery. For example, whereas unfractionated FP exhibited no change in its emission, FPF or MMAD upon co-formulation in a 1:1 ratio, Stage 3 and Stage 4 FP samples both exhibited a significant reduction in the FPF upon co-formulation with either Stage 4 or Stage 5 SX. If a bulk FP powder batch contained large proportions of these Stage 3 or 4 particles, it may be the case that upon co-formulation with SX the aerosolisation performance of FP would be dramatically different (and possibly poorer) than an FP powder containing fewer of the particle agglomerates produced by blending powders within these size ranges.

As a comparator, the aerosolisation of co-formulated SX and FP crystals was compared to single drug delivery of the recrystallised powders. Unlike the unfractionated or fractionated FP powders, co-formulation improved the dispersion of crystallised FP (CFP) beyond that of CFP alone. Conversely for crystallised SX (CSX), the dispersion worsened upon co-formulation. Further optimisation of the properties (such as size and size distribution) of the recrystallised particles may therefore provide the most promising route in which to improve the aerosolisation efficiency of combination formulations. Furthermore, when the crystals were formulated with a carrier, the effects

of co-formulation on CSX particles were opposite to those of the pre-blend; the emission and FPF ED improved, and the intrinsic dispersibility of the bulk powder improved. Where concomitant deposition of multiple actives across the different regions of the lung (as appears would be likely for engineered combination particles, Pitchayajittipong et al., 2009) may not be favourable, physically mixed recrystallised particles may provide a means of generating high fine particle delivery in complex combination formulations whilst maintaining individual deposition profiles for the drugs in the formulation.

In order to further elucidate the particulate factors that affected SX drug dispersion, single drug DPIs containing crystallised, Stage 4 or Stage 5 SX particles were prepared and aerosolised into the NGI. Compared to the DPI prepared from the unfractionated powder, the aerosolisation behaviour of SX in the NGI (in terms of the emission, MMAD and FPF) was unchanged for these blends. There were subtle differences between the aerosolisation of the latter blends, in which use of the crystallised SX sample produced a lower FPF and larger MMAD than Stage 4 and Stage 5 SX, respectively. The presence of the carrier therefore offset the different SX physicochemical properties which resulted in different aerosolisation behaviours when the powders were aerosolised into the NGI in the absence of a carrier. There were however differences in the values of the DA_{50}, CPP and the relative magnitude of the values following dry dispersion laser diffraction. Therefore, although there were changes in the bulk dispersibility and agglomerate heterogeneity between the blends, this was insufficient to alter SX dispersion in the NGI in this instance. By developing optimal formulation and delivery systems, it may therefore be possible to exploit the differences in the bulk dispersibility of the powder blends to engineer the aerosolisation performance of SX particles for improved dispersion.

When co-formulated with Stage 3 FP in a DPI blend, Stage 4 SX exhibited changes in dispersion compared to the single drug Stage 4 SX containing DPI. These changes were comparable to those observed between the aerosolisation of the Stage 4 SX powder alone and from the Stage 4 SX:Stage 3 FP pre-blend. SX emission increased and the FPF was lower in combination compared to the Stage 4 SX-only DPI. An improvement in the bulk dispersibility of the combination DPI blend was also observed compared to the single drug DPI. Therefore, for the co-formulated fractions, formulating with a carrier was unable to mitigate changes in SX dispersibility as occurred for the

unfractionated SX powders upon co-formulation. Furthermore, a comparison of the aersolisation performance of SX in a DPI containing unfractionated SX co-formulated with unfractionated FP, and Stage 4 SX co-formulated with Stage 3 FP indicated that SX from the latter formulation generated a higher emission, FPF RD and FPF ED ($p < 0.05$, unpaired t test), compared to the unfractionated SX. Similar to the behaviour observed in the pre-blends, this indicated that bulk micronised drug particles may demonstrate a distribution in aerosolisation performance upon co-formulation in DPI blends, arising from intra-batch variation in powder properties, which may contribute towards variability in DPI performance.

Considering the dissolution of SX particles, when formulated as single drug DPIs, there were no differences in dissolution depending on SX particle properties, despite pronounced differences being observed previously for stage fractions of hydrocortisone, salbutamol sulphate and budesonide (Cartier et al., 2008; Son and McConville, 2009; Arora et al., 2010). However, when co-formulated with FP, the dissolution of unfractionated SX increased compared to the dissolution of SX from the single drug formulation. The ability to increase dissolution rate, which can be a rate limiting step in determining the availability of inhaled drugs, may therefore be an important finding. Upon co-formulation, the MMAD, FPF, and emission of SX did not differ ($p > 0.05$) compared to the single drug DPI when aerosolised into the NGI. There was however a change in the bulk dispersibility of the blends, suggesting that there may have been differences in the agglomeration and agglomerate properties (e.g. strength and structure). A lower DA_{50} for the combination blend indicated the presence of more dispersible agglomerates. Drug particles landing on the Transwell insert for dissolution testing would be detached from the carrier, and SEM imaging of the pre-blends and DPI blends indicated the presence of mixed SX-FP drug agglomerates. A change in agglomerate structure may therefore have altered the exposure of SX to the dissolution media, increased exposure of the more disordered regions on the particle surface, or disrupted the most damaged, and most cohesive, agglomerated SX particles, thus enhancing SX dissolution. Studies to elucidate the causes of the increased dissolution are required, as well as further investigations into the ability to modify the dissolution rate of SX following combination delivery using particle/formulation engineering approaches.

7.1 FUTURE WORK

A continuation of the project designed to build on the findings reported in this thesis could therefore progress along two linked thematic pathways. The bulk powder dispersibility, particulate and agglomeration properties (dictated by factors such as particle size, morphology, surface energy, crystalline content and powder structure) and powder heterogeneity were found to influence drug dispersion from combination formulations. Therefore, further investigations into the ability to engineer SX and FP dispersion in physically mixed formulations could be undertaken. This could involve use of the Raman microscope since this would allow particle association to be identified and traced during the manufacturing and aerosolisation process. Examination of Raman spectra and images of drug powders during blending (in co-formulation, both with and without a carrier), and prior to and post-aerosolisation could be carried out. This would enable identification of whether co-association, if it does indeed occur, exhibits a dynamic nature and therefore changes during the formulation and/or dispersion process. It would also provide insight into the role of the carrier in mitigating the dispersion modifying effects that occurred in drug pre-blends. The development of a quantitative analysis technique would also allow SX:FP ratios to be determined and related back to chemical analysis from cascade impactor testing, to determine whether the composition of the deposited masses reflected association between the particles and hence provide a novel tool to assess combination formulations. As described above it has been found that combination pre-blends containing different aerodynamic size fractions of SX and FP with distinct properties exhibited different aerosolisation compared to single drug delivery. It would therefore be of interest to investigate different SX:FP ratios, inhaler devices, flow rates and formulations in terms of, for example, carrier properties and fines content, as a means of further engineering the deposition profiles of the drugs, in particular using Raman microscopy. Alternative drugs and drug combinations could also be tested to determine if the findings of the current study are generic across combination formulations or whether they are drug-specific. A second theme could involve further investigation of the biopharmaceutics of the drugs, and evaluation of the dissolution and cell layer transport of SX and FP upon co-formulation. Having observed that SX dissolution may be altered by co-formulation, SX dissolution experiments can be designed that provide a more realistic comparison with the *in vivo* environment, for example, using simulated lung fluids and undertaking the experiments at a temperature and humidity representative of the lungs. Analysis can also be extended to include FP. It

has recently been shown that co-delivery of SX and FP may have implications on drug transport across an epithelial cell layer, particularly for FP (Haghi et al., 2013). The influence of intra-batch variability and particle properties, represented by the aerodynamic size fractions, on the epithelial cell layer transport could be assessed. The implications of co-formulation of these engineered particles, in addition to bulk (i.e. unfractionated) particles could also be assessed, as a means to optimise the dissolution and transport profiles of the drugs.

7.2 OVERALL SUMMARY OF FINDINGS

The work detailed in this thesis has made a number of key contributions towards the area of respiratory drug delivery. A de-agglomeration analysis using laser diffraction was developed which will provide a tool for inhalation scientists to rapidly screen fine particles and powder mixtures for their inherent powder dispersibility. Eight inhaled powders were found to demonstrate different dispersion behaviours, which would aid in selecting the formulation and device approaches necessary to achieve efficient dispersion. Upon co-formulation in carrier-free blends, SX was affected by co-formulation to a greater extent than FP, which was generally unaffected. SX dispersion became worse, particularly when blended with large amounts of FP, and was attributed to a greater adhesive tendency of SX for FP compared to FP for SX. The drug powders were also found to display intra-batch variability: powder sub-populations had distinct physicochemical and dispersibility properties and thus different agglomeration behaviours which may have consequences for aerosolisation performance upon formulation with a carrier, ternary agent, or a second drug particle type. However, when the bulk (i.e. unfractionated) powders were formulated with a carrier, there was no change in SX or FP dispersion between single drug and co-delivery, at various SX:FP ratios. This was despite differences in SX dispersion occurring between the co-formulated pre-blends (which were subsequently blended with the lactose carrier) and the individual drug powders. It was therefore possible to mitigate drug ratio effects on drug dispersion by formulating the drug powders with a carrier. The practical implications of intra-batch powder variability were demonstrated further upon co-formulation in the absence of a carrier, in which SX and FP fractions responded differently to co-formulation compared to the unfractionated powders, and depending on the specific combination of fractions blended together. Furthermore, when

formulated as carrier-based DPIs, the response to co-formulation of stage fractionated SX differed to that of the unfractionated SX. The different responses to co-formulation within a bulk powder indicated an additional source of variability in DPI performance, and demonstrated that both bulk and particulate factors influence the aerosolisation behaviour of combination DPI formulations.

REFERENCES

Adams, W.P., Lee, S.L., Plourde, R., Lionberger, R.A., Bertha, C.M., Doub, W.H., Bovet, J.M., Hickey, A.J., 2012. Effects of device and formulation on in vitro performance of dry powder inhalers. AAPS Journal 14, 400-409.

Adi, H., Larson, I., Chiou, H., Young, P., Traini, D., Stewart, P., 2006. Agglomerate strength and dispersion of salmeterol xinafoate from powder mixtures for inhalation. Pharmaceutical Research 23, 2556-2565.

Adi, H., Larson, I., Chiou, H., Young, P., Traini, D., Stewart, P., 2008a. Role of agglomeration in the dispersion of salmeterol xinafoate from mixtures for inhalation with differing drug to fine lactose ratios. Journal of Pharmaceutical Sciences 97, 3140-3152.

Adi, H., Traini, D., Chan, H.K., Young, P.M., 2008b. The influence of drug morphology on the aerosolisation efficiency of dry powder inhaler formulations. Journal of Pharmaceutical Sciences 97, 2780-2788.

Adi, H., Young, P.M., Traini, D., 2012. Co-deposition of a triple therapy drug formulation for the treatment of chronic obstructive pulmonary disease using solution-based pressurised metered dose inhalers. Journal of Pharmacy and Pharmacology 64, 1245-1253.

Adi, S., Adi, H., Chan, H.K., Finlay, W.H., Tong, Z., Yang, R., Yu, A., 2011. Agglomerate strength and dispersion of pharmaceutical powders. Journal of Aerosol Science 42, 285-294.

Akabane, H., Murata, M., Kubota, M., Takashima, E., Tanaka, H., Inagaki, N., Horiba, M., Nagai, H., 2006. Effects of salmeterol xinafoate and fluticasone propionate on immunological activation of human cultured mast cells. Allergology International 55, 387-393.

am Ende, D.J. (Ed), 2011. Chemical Engineering in the Pharmaceutical Industry: R&D to Manufacturing. John Wiley & Sons, Inc. New Jersey, USA.

Anderson, P.J., 2005. History of aerosol therapy: Liquid nebulization to MDIs to DPIs. Respiratory Care 50, 1139-1149.

Arora, D., Shah, K.A., Halquist, M.S., Sakagami, M., 2010. In vitro aqueous fluid-capacity-limited dissolution testing of respirable aerosol drug particles generated from inhaler products. Pharmaceutical Research 27, 786-795.

ATS/ERS Task Force 2004. Standards for the Diagnosis and Management of Patients with COPD [Internet], Version 1.2, American Thoracic Society / European Respiratory Society Task Force. American Thoracic Society, New York, USA. [Updated 8 September 2008] Available from http://www.thoracic.org/go/copd.

Aubier, M., Pieters, W.R., Schlösser, N.J.J., Steinmetz, K.O., 1999. Salmeterol/fluticasone propionate (50/500 μg) in combination in a Diskus® inhaler (Seretide®) is effective and safe in the treatment of steroid-dependent asthma. Respiratory Medicine 93, 876-884.

Aulton, M.E., 2002. Pharmaceutics: The Science of Dosage Form Design (Second Edition). Churchill Livingstone.

Azioune, A., Chehimi, M.M., Miksa, B., Basinska, T., Slomkowski, S., 2002. Hydrophobic protein-polypyrrole interactions: The role of van der Waals and Lewis acid-base forces as determined by contact angle measurements. Langmuir 18, 1150-1156.

BP 2012. British Pharmacopoeia, Aerodynamic Assessment of Fine Particles - Fine Particle Dose and Particle Size Distribution, Appendix XII C. British Pharmacopeia Commision, The Stationary Office, London, UK.

Barnes, P.J., 2002. Scientific rationale for inhaled combination therapy with long-acting β2-agonists and corticosteroids. European Respiratory Journal 19, 182-191.

Bastacky, J., Lee, C.Y.C., Goerke, J., Koushafar, H., Yager, D., Kenaga, L., Speed, T.P., Chen, Y., Clements, J.A., 1995. Alveolar lining layer is thin and continuous: Low-temperature scanning electron microscopy of rat lung. Journal of Applied Physiology 79, 1615-1628.

Bateman, E.D., Britton, M., Carrillo, J., Almeida, J., Wixon, C., 1998. Salmeterol/fluticasone combination inhaler. A new, effective and well tolerated treatment for asthma. Clinical Drug Investigation 16, 193-201.

Begat, P., Morton, D.A.V., Staniforth, J.N., Price, R., 2004a. The cohesive-adhesive balances in dry powder inhaler formulations I: Direct quantification by atomic force microscopy. Pharmaceutical Research 21, 1591-1597.

Begat, P., Morton, D.A.V., Staniforth, J.N., Price, R., 2004b. The cohesive-adhesive balances in dry powder inhaler formulations II: Influence on fine particle delivery characteristics. Pharmaceutical Research 21, 1826-1833.

Behara, S.R.B., Kippax, P., McIntosh, M.P., Morton, D.A.V., Larson, I., Stewart, P., 2011a. Structural influence of cohesive mixtures of salbutamol sulphate and lactose on aerosolisation and de-agglomeration behaviour under dynamic conditions. European Journal of Pharmaceutical Sciences 42, 210-219.

Behara, S.R.B., Larson, I., Kippax, P., Morton, D.A.V., Stewart, P., 2011b. An approach to characterising the cohesive behaviour of powders using a flow titration aerosolisation based methodology. Chemical Engineering Science 66, 1640-1648.

Behara, S.R.B., Larson, I., Kippax, P., Stewart, P., Morton, D.A.V., 2012. Insight into pressure drop dependent efficiencies of dry powder inhalers. European Journal of Pharmaceutical Sciences 46, 142-148.

Bell, J.H., Hartley, P.S., Cox, J.S., 1971. Dry powder aerosols. I. A new powder inhalation device. Journal of Pharmaceutical Sciences 60, 1559-1564.

Berthold, C., Klein, R., Lühmann, J., Nickel, K.G., 2000. Characterization of fibres and fibre collectives with common laser diffractometers. Particle and Particle Systems Characterization 17, 113-116.

Bisgaard, H., Klug, B., Sumby, B.S., Burnell, P.K.P., 1998. Fine particle mass from the Diskus inhaler and Turbuhaler inhaler in children with asthma. European Respiratory Journal 11, 1111-1115.

BNF 2013. British National Formulary 66, September 2013. BMJ Group and Pharmaceutical Press, London, UK.

Borgström, L., Bisgaard, H., O'Callaghan, C., Pedersen, S., 2002. Dry Powder Inhalers, In Lenfant, C., Bisgaard, H., O'Callaghan, C., Smaldone, G.C. (Eds) Drug Delivery to the Lungs, Lung Biology in Health and Disease. Volume 162, Marcel Dekker, Inc., New York, USA.

Borgström, L., Asking, L., Lipniunas, P., 2005a. An in vivo and in vitro comparison of two powder inhalers following storage at hot/humid conditions. Journal of Aerosol Medicine: Deposition, Clearance, and Effects in the Lung 18, 304-310.

Borgström, L., Asking, L., Thorsson, L., 2005b. Idealhalers or realhalers? A comparison of Diskus and Turbuhaler. International Journal of Clinical Practice 59, 1488-1495.

Brodka-Pfeiffer, K., Häusler, H., Graß, P., Langguth, P., 2003a. Conditioning Following Powder Micronization: Influence on Particle Growth of Salbutamol Sulfate. Drug Development and Industrial Pharmacy 29, 1077-1084.

Brodka-Pfeiffer, K., Langguth, P., Graß, P., Häusler, H., 2003b. Influence of mechanical activation on the physical stability of salbutamol sulphate. European Journal of Pharmaceutics and Biopharmaceutics 56, 393-400.

BTS/SIGN, 2008 (revised 2012). British Guideline on the Management of Asthma- A National Clinical Guideline. British Thoracic Society and Scottish Intercollegiate Guidelines Network, May 2008, revised January 2012, ISBN 978 1 905813 28 5.

Bunker, M., Davies, M., Roberts, C., 2005. Towards screening of inhalation formulations: Measuring interactions with atomic force microscopy. Expert Opinion on Drug Delivery 2, 613-624.

Bur, M., Huwer, H., Muys, L., Lehr, C.M., 2010. Drug transport across pulmonary epithelial cell monolayers: Effects of particle size, apical liquid volume, and deposition technique. Journal of Aerosol Medicine and Pulmonary Drug Delivery 23, 119-127.

Burnell, P.K.P., Malton, A., Reavill, K., Ball, M.H.E., 1998. Design, validation and initial testing of the Electronic Lung® device. Journal of Aerosol Science 29, 1011-1025.

Busse, W., Koenig, S.M., Oppenheimer, J., Sahn, S.A., Yancey, S.W., Reilly, D., Edwards, L.D., Dorinsky, P.M., 2003. Steroid-sparing effects of fluticasone propionate 100 μg and salmeterol 50 μg administered twice daily in a single product in patients previously controlled with fluticasone propionate 250 μg administered twice daily. Journal of Allergy and Clinical Immunology 111, 57-65.

Buttini, F., Colombo, P., Wenger, M.P.E., Mesquida, P., Marriott, C., Jones, S.A., 2008. Back to basics: The development of a simple, homogenous, two-component dry-powder inhaler formulation for the delivery of budesonide using miscible vinyl polymers. Journal of Pharmaceutical Sciences 97, 1257-1267.

Calvert, G., Ghadiri, M., Tweedie, R., 2009. Aerodynamic dispersion of cohesive powders: A review of understanding and technology. Advanced Powder Technology 20, 4-16.

Caramori, G., Ito, K., Papi, A., Adcock, I.M., 2006. Interactions between long-acting β2-agonists and glucocorticoids. Drug Discovery Today: Therapeutic Strategies 3, 261-268.

Cartier, R., Egen M., Kruger, M., 2008. In vitro system to assess the size-dependent dissolution profile of inhalable aerosols. Drug Delivery to the Lungs 19, Edinburgh, Scotland, UK.

Chapman, K.R., 1999. Salmeterol and fluticasone propionate (50/250 μg) administered via combination Diskus inhaler: As effective as when given via separate Diskus inhalers. Canadian Respiratory Journal 6, 45-51.

Chew, N.Y.K., Bagster, D.F., Chan, H.K., 2000. Effect of particle size, air flow and inhaler device on the aerosolisation of disodium cromoglycate powders. International Journal of Pharmaceutics 206, 75-83.

Chew, N.Y.K., Chan, H.K., 1999. Influence of particle size, air flow, and inhaler device on the dispersion of mannitol powders as aerosols. Pharmaceutical Research 16, 1098-1103.

Chow, A.H.L., Tong, H.H.Y., Chattopadhyay, P., Shekunov, B.Y., 2007. Particle engineering for pulmonary drug delivery. Pharmaceutical Research 24, 411-437.

Cline, D., Dalby, R., 2002. Predicting the quality of powders for inhalation from surface energy and area. Pharmaceutical Research 19, 1274-1277.

Coates, M.S., Chan, H.K., Fletcher, D.F., Raper, J.A., 2005. Influence of air flow on the performance of a dry powder inhaler using computational and experimental analyses. Pharmaceutical Research 22, 1445-1453.

Coates, M.S., Fletcher, D.F., Chan, H.K., Raper, J.A., 2005. The role of capsule on the performance of a dry powder inhaler using computational and experimental analyses. Pharmaceutical Research 22, 923-932.

Cornish-Bowden, A., 2004. Fundamentals of Enzyme Kinetics, 3rd Edition. Portland Press Ltd., London, UK.

Corrigan, D.O., Corrigan, O.I., Healy, A.M., 2006. Physicochemical and in vitro deposition properties of salbutamol sulphate/ipratropium bromide and salbutamol sulphate/excipient spray dried mixtures for use in dry powder inhalers. International Journal of Pharmaceutics 322, 22-30.

Crowder, T.M., 2005. Highly reproducible powder aerosolisation for lung delivery using powder-specific electromechanical vibration. Expert Opinion on Drug Delivery 2, 579-585.

Daley-Yates, P.T., Parkins, D.A., Thomas, M.J., Gillett, B., House, K.W., Ortega, H.G., 2009. Pharmacokinetic, pharmacodynamic, efficacy, and safety data from two randomized, double-blind studies in patients with asthma and an in vitro study comparing two dry-powder inhalers delivering a combination of salmeterol 50 μg and fluticasone propionate 250 μg: Implications for establishing bioequivalence of inhaled products. Clinical Therapeutics 31, 370-385.

Das, S., Larson, I., Young, P., Stewart, P., 2009a. Agglomerate properties and dispersibility changes of salmeterol xinafoate from powders for inhalation after storage at high relative humidity. European Journal of Pharmaceutical Sciences 37, 442-450.

Das, S., Larson, I., Young, P., Stewart, P., 2009b. Influence of storage relative humidity on the dispersion of salmeterol xinafoate powders for inhalation. Journal of Pharmaceutical Sciences 98, 1015-1027.

Das, S.C., Behara, S.R.B., Bulitta, J.B., Morton, D.A.V., Larson, I., Stewart, P.J., 2012. Powder strength distributions for understanding de-Agglomeration of lactose powders. Pharmaceutical Research 29, 2926-2935.

Das, S.C., Larson, I., Morton, D.A.V., Stewart, P.J., 2011a. Determination of the polar and total surface energy distributions of particulates by inverse gas chromatography. Langmuir 27, 521-523.

Das, S.C., Stewart, P.J., 2012. Characterising surface energy of pharmaceutical powders by inverse gas chromatography at finite dilution. Journal of Pharmacy and Pharmacology 64, 1337-1348.

Das, S.C., Zhou, Q., Morton, D.A.V., Larson, I., Stewart, P.J., 2011b. Use of surface energy distributions by inverse gas chromatography to understand mechanofusion processing and functionality of lactose coated with magnesium stearate. European Journal of Pharmaceutical Sciences 43, 325-333.

Davies, N.M., Feddah, M.R., 2003. A novel method for assessing dissolution of aerosol inhaler products. International Journal of Pharmaceutics 255, 175-187.

De Boer, A.H., Gjaltema, D., Hagedoorn, P., Frijlink, H.W., 2002a. Characterization of inhalation aerosols: A critical evaluation of cascade impactor analysis and laser diffraction technique. International Journal of Pharmaceutics 249, 219-231.

De Boer, A.H., Gjaltema, D., Hagedoorn, P., Schaller, M., Witt, W., Frijlink, H.W., 2002b. Design and application of a new modular adapter for laser diffraction characterization of inhalation aerosols. International Journal of Pharmaceutics 249, 233-245.

De Boer, A.H., Hagedoorn, P., Gjaltema, D., Goede, J., Frijlink, H.W., 2003. Air classifier technology (ACT) in dry powder inhalation: Part 1. Introduction of a novel force distribution concept (FDC) explaining the performance of a basic air classifier on adhesive mixtures. International Journal of Pharmaceutics 260, 187-200.

De Boer, A.H., Hagedoorn, P., Gjaltema, D., Lambregts, D., Irngartinger, M., Frijlink, H.W., 2004. The mode of drug particle detachment from carrier crystals in an air classifier-based inhaler. Pharmaceutical Research 21, 2167-2174.

Della Volpe, C., Siboni, S., 1997. Some reflections on acid-base solid surface free energy theories. Journal of Colloid and Interface Science 195, 121-136.

Dickhoff, B.H.J., Ellison, M.J.H., De Boer, A.H., Frijlink, H.W., 2002. The effect of budesonide particle mass on drug particle detachment from carrier crystals in adhesive mixtures during inhalation. European Journal of Pharmaceutics and Biopharmaceutics 54, 245-248.

Dolovich, M., 1993. Lung dose, distribution, and clinical response to therapeutic aerosols. Aerosol Science and Technology 18, 230-240.

Dong, S., Brendlé, M., Donnet, J.B., 1989. Study of solid surface polarity by inverse gas chromatography at infinite dilution. Chromatographia 28, 469-472.

Donovan, M.J., Smyth, H.D.C., 2010. Influence of size and surface roughness of large lactose carrier particles in dry powder inhaler formulations. International Journal of Pharmaceutics 402, 1-9.

Dorris, G.M., Gray, D.G., 1980. Adsorption of n-alkanes at zero surface coverage on cellulose paper and wood fibers. Journal of Colloid and Interface Science 77, 353-362.

Dransfield, M.T., Bailey, W.C., 2004. Fluticasone propionate/salmeterol for the treatment of chronic-obstructive pulmonary disease. Expert Opinion on Pharmacotherapy 5, 1815-1826.

Edwards, D.A., Hanes, J., Caponetti, G., Hrkach, J., Ben-Jebria, A., Eskew, M.L., Mintzes, J., Deaver, D., Lotan, N., Langer, R., 1997. Large porous particles for pulmonary drug delivery. Science 276, 1868-1871.

El-Gendy, N., Gorman, E.M., Munson, E.J., Berkland, C., 2009. Budesonide nanoparticle agglomerates as dry powder aerosols with rapid dissolution. Journal of Pharmaceutical Sciences 98, 2731-2746.

El-Gendy, N., Pornputtapitak, W., Berkland, C., 2011. Nanoparticle agglomerates of fluticasone propionate in combination with albuterol sulfate as dry powder aerosols. European Journal of Pharmaceutical Sciences 44, 522-533.

EMEA, 2009. Guideline on the Requirements for Clinical Documentation for Orally Inhaled Products (OIP) including the Requirements for Demonstration of Therapeutic Equivalence Between Two Inhaled Products for use in the Treatment of Asthma and Chronic Obstructive Pulmomary Disease (COPD) in adults and for use in the Treatment of Asthma in children and adolescents. Committee for Medicinal Products for Human Use (CHMP), European Medicines Agency (EMEA).

FDA, 2000. Guidance for Industry: Waiver of in vivo bioavailability and bioequivalence studies for immediate release solid oral dosage forms based on a Biopharmaceutics Classification System. Food Drug Administration Center for Drugs Evaluation Research (FDA) Maryland, USA.

FDA, 2010. Drug Safety Communication: New safety requirements for long-acting inhaled asthma medications called Long-Acting Beta Agonists (LABAs). U.S. Food and Drug Administration (FDA) Safety Announcement [02-18-2010]

Feddah, M.R., Brown, K.F., Gipps, E.M., Davies, N.M., 2000. In-vitro characterisation of metered dose inhaler versus dry powder inhaler glucocorticoid products: influence of inspiratory flow rates. Journal of pharmacy & pharmaceutical sciences [electronic resource] : a publication of the Canadian Society for Pharmaceutical Sciences, Societe canadienne des sciences pharmaceutiques 3, 318-324.

Feeley, J.C., York, P., Sumby, B.S., Dicks, H., 1998. Determination of surface properties and flow characteristics of salbutamol sulphate, before and after micronisation. International Journal of Pharmaceutics 172, 89-96.

Fleming, F.S., 2007. Microdose Technologies, Flexible, smart and low cost: The microdose DPI, a true platform inhaler. ONdrugDELIVERY, Pulmonary Drug Delivery: New perspectives on inhalers and inhalables, 26-30.

Freeman, R., 2007. Measuring the flow properties of consolidated, conditioned and aerated powders - A comparative study using a powder rheometer and a rotational shear cell. Powder Technology 174, 25-33.

Frijlink, H.W., De Boer, A.H., 2004. Dry powder inhalers for pulmonary drug delivery. Expert Opinion on Drug Delivery 1, 67-86.

Gaisford, S., Dennison, M., Tawfik, M., Jones, M.D., 2010. Following mechanical activation of salbutamol sulphate during ball-milling with isothermal calorimetry. International Journal of Pharmaceutics 393, 74-78.

Gamble, J.F., Leane, M., Olusanmi, D., Tobyn, M., Šupuk, E., Khoo, J., Naderi, M., 2012. Surface energy analysis as a tool to probe the surface energy characteristics of micronized materials - A comparison with inverse gas chromatography. International Journal of Pharmaceutics 422, 238-244.

Gehr, P., Bachofen, M., Weibel, E.R., 1978. The normal human lung: ultrastructure and morphometric estimation of diffusion capacity. Respiration Physiology 32, 121-140.

Gehr, P., Geiser, M., Hof, V.I., Schurch, S., Waber, U., Baumann, M., 1993. Surfactant and inhaled particles in the conducting airways: Structural, stereological, and biophysical aspects. Microscopy Research and Technique 26, 423-436.

Ghoroi, C., Han, X., To, D., Jallo, L., Gurumurthy, L., Davé, R.N., 2013. Dispersion of fine and ultrafine powders through surface modification and rapid expansion. Chemical Engineering Science 85, 11-24.

GINA, 2012. Global Strategy for Asthma Management and Prevention. Global Initiative for Asthma (GINA). Available from http://ginaasthma.org/.

GSK, 2011. Prescribing Information (Advair Diskus 100/50, 250/50, 500/50). Available from http://us.gsk.com/products/assets/us_advair.pdf.

GOLD, 2013. Global Strategy for the Diagnosis, Management and Prevention of Chronic Obstructive Pulmonary Disease. Global Initiative for Chronic Obstructive Pulmonary Disease (GOLD). Available from http://www.goldcopd.org/.

Gonda, I., 2000. The ascent of pulmonary drug delivery. Journal of Pharmaceutical Sciences 89, 940-945.

Grainger, C.I., Greenwell, L.L., Martin, G.P., Forbes, B., 2009. The permeability of large molecular weight solutes following particle delivery to air-interfaced cells that model the respiratory mucosa. European Journal of Pharmaceutics and Biopharmaceutics 71, 318-324.

Grasmeijer, F., Hagedoorn, P., Frijlink, H.W., de Boer, H.A., 2013. Mixing Time Effects on the Dispersion Performance of Adhesive Mixtures for Inhalation. PLoS ONE 8, 1 - 18.

Hagedorn, C., Kässner, F., Banik, N., Ntampakas, P., Fielder, K., 2013. Influence of salmeterol/fluticasone via single versus separate inhalers on exacerbations in severe/very severe COPD. Respiratory Medicine 107, 542-549.

Haghi, M., Traini, D., Postma, D.S., Bebawy, M., Young, P.M., 2013. Mediated Fluticasone Uptake Across Calu-3 Cells by Salmeterol as Combination Powder Inhaler. Respirology, DOI: 10.1111/resp.12146

Han, X., Jallo, L., To, D., Ghoroi, C., Davé, R., 2013. Passivation of high-surface-energy sites of milled ibuprofen crystals via dry coating for reduced cohesion and improved flowability. Journal of Pharmaceutical Sciences 102, 2282-2296.

Harding, S.M., 1990. The human pharmacology of fluticasone propionate. Respiratory Medicine 84, 25-29.

Harper, N.J., Gray, S., De Groot, J., Parker, J.M., Sadrzadeh, N., Schuler, C., Schumacher, J.D., Seshadri, S., Smith, A.E., Steeno, G.S., Stevenson, C.L., Taniere, R.,

Wang, M., Bennett, D.B., 2007. The design and performance of the Exubera® pulmonary insulin delivery system. Diabetes Technology and Therapeutics 9, S-16-S-27.

Healthcare Commission, 2006. Clearing the air; A national study of chronic obstructive pulmonary disease. © 2006 Commission for Healthcare Audit and Inspection.

Heng, J.Y.Y., Bismarck, A., Lee, A.F., Wilson, K., Williams, D.R., 2006a. Anisotropic surface energetics and wettability of macroscopic form I paracetamol crystals. Langmuir 22, 2760-2769.

Heng, J.Y.Y., Thielmann, F., Williams, D.R., 2006b. The effects of milling on the surface properties of form I paracetamol crystals. Pharmaceutical Research 23, 1918-1927.

Hersey, J.A., 1975. Ordered mixing: A new concept in powder mixing practice. Powder Technology 11, 41-44.

Hickey, A.J., 2013. Back to the future: Inhaled drug products. Journal of Pharmaceutical Sciences 102, 1165-1172.

Hickey, A.J., Mansour, H.M., Telko, M.J., Xu, Z., Smyth, H.D.C., Mulder, T., McLean, R., Langridge, J., Papadopoulos, D., 2007. Physical characterization of component particles included in dry powder inhalers. I. Strategy review and static characteristics. Journal of Pharmaceutical Sciences 96, 1282-1301.

Ho, R., Muresan, A.S., Hebbink, G.A., Heng, J.Y.Y., 2010. Influence of fines on the surface energy heterogeneity of lactose for pulmonary drug delivery. International Journal of Pharmaceutics 388, 88-94.

Hoe, S., Traini, D., Chan, H.K., Young, P.M., 2009. The influence of flow rate on the aerosol deposition profile and electrostatic charge of single and combination metered dose inhalers. Pharmaceutical Research 26, 2639-2646.

Holzner, P.M., Müller, B.W., 1997. Effect of air flow and acceleration on particle size of dry powder aerosols determined by time-of-flight aerosol beam spectrometry. Particulate Science and Technology 15, 187-202.

Islam, N., Cleary, M.J., 2012. Developing an efficient and reliable dry powder inhaler for pulmonary drug delivery - A review for multidisciplinary researchers. Medical Engineering and Physics 34, 409-427.

Islam, N., Stewart, P., Larson, I., Hartley, P., 2004. Lactose surface modification by decantation: Are drug-fine lactose ratios the key to better dispersion of salmeterol xinafoate from lactose-interactive mixtures? Pharmaceutical Research 21, 492-499.

ISO 13320-1 (1999). Particle Size Analysis - Laser Diffraction Methods - Part 1: General Principles. International Organisation for Standardisation (ISO), ISO 13320-1:1999(E).

Jarjour, N.N., Wilson, S.J., Koenig, S.M., Laviolette, M., Moore, W.C., Davis, W.B., Doherty, D.E., Hamid, Q., Israel, E., Kavuru, M.S., Ramsdell, J.W., Tashkin, D.P., Reilly, D.S., Yancey, S.W., Edwards, L.D., Stauffer, J.L., Dorinsky, P.M., Djukanovic, R., 2006. Control of airway inflammation maintained at a lower steroid dose with 100/50 μg of fluticasone propionate/salmeterol. Journal of Allergy and Clinical Immunology 118, 44-52.

Jetmalani, K., Young, P.M., Smith, T., Stewart, P., Traini, D., 2012. Micronized drug powders in binary mixtures and the effect of physical properties on aerosolization from combination drug dry powder inhalers. Drug Development and Industrial Pharmacy 38, 1504-1511.

Johnson, M., 1998. Development of fluticasone propionate and comparison with other inhaled corticosteroids. Journal of Allergy and Clinical Immunology 101, S434-S439.

Johnson, M., 2004. Interactions between corticosteroids and beta2-agonists in asthma and chronic obstructive pulmonary disease. Proceedings of the American Thoracic Society 1, 200-206.

Johnson, M., Butchers, P.R., Coleman, R.A., Nials, A.T., Strong, P., Sumner, M.J., Vardey, C.J., Whelan, C.J., 1993. The pharmacology of salmeterol. Life Sciences 52, 2131-2143.

Jones, M.D., Harris, H., Hooton, J.C., Shur, J., King, G.S., Mathoulin, C.A., Nichol, K., Smith, T.L., Dawson, M.L., Ferrie, A.R., Price, R., 2008a. An investigation into the relationship between carrier-based dry powder inhalation performance and formulation cohesive-adhesive force balances. European Journal of Pharmaceutics and Biopharmaceutics 69, 496-507.

Jones, M.D., Hooton, J.C., Dawson, M.L., Ferrie, A.R., Price, R., 2008b. An investigation into the dispersion mechanisms of ternary dry powder inhaler formulations by the quantification of interparticulate forces. Pharmaceutical Research 25, 337-348.

Jones, M.D., Price, R., 2006. The influence of fine excipient particles on the performance of carrier-based dry powder inhalation formulations. Pharmaceutical Research 23, 1665-1674.

Jones, M.D., Young, P., Traini, D., 2012. The use of inverse gas chromatography for the study of lactose and pharmaceutical materials used in dry powder inhalers. Advanced Drug Delivery Reviews 64, 285-293.

Kaialy, W., Alhalaweh, A., Velaga, S.P., Nokhodchi, A., 2011. Effect of carrier particle shape on dry powder inhaler performance. International Journal of Pharmaceutics 421, 12-23.

Kaialy, W., Larhrib, H., Ticehurst, M., Nokhodchi, A., 2012. Influence of batch cooling crystallization on mannitol physical properties and drug dispersion from dry powder inhalers. Crystal Growth and Design 12, 3006-3017.

Kale, K., Hapgood, K., Stewart, P., 2009. Drug agglomeration and dissolution - What is the influence of powder mixing? European Journal of Pharmaceutics and Biopharmaceutics 72, 156-164.

Kavuru, M., Melamed, J., Gross, G., Laforce, C., House, K., Prillaman, B., Baitinger, L., Woodring, A., Shah, T., 2000. Salmeterol and fluticasone propionate combined in a new powder inhalation device for the treatment of asthma: A randomized, double-blind, placebo-controlled trial. Journal of Allergy and Clinical Immunology 105, 1108-1116.

Kaye, R.S., Purewal, T.S., Alpar, H.O., 2009. Simultaneously Manufactured Nano-In-Micro (SIMANIM) particles for dry-powder modified-release delivery of antibodies. Journal of Pharmaceutical Sciences 98, 4055-4068.

Kendall, K., Stainton, C., 2001. Adhesion and aggregation of fine particles. Powder Technology 121, 223-229.

Kim, D., Glaum, M., Lockey, R., 2009. Evaluation of combination long-acting β-2 agonists and inhaled glucocorticosteroids for treatment of asthma. Expert Opinion on Drug Metabolism and Toxicology 5, 933-940.

Kinnunen, H., Shur J., Hebbink, G., Muresan, A.S., Price, R., 2010. Effect of lactose fines on fluidization properties and in vitro performance of Handihaler, Drug Delivery to the Lungs 21, Edinburgh, Scotland, UK.

Kubavat, H.A., Shur, J., Ruecroft, G., Hipkiss, D., Price, R., 2012. Investigation into the influence of primary crystallization conditions on the mechanical properties and secondary processing behaviour of fluticasone propionate for carrier based dry powder inhaler formulations. Pharmaceutical Research 29, 994-1006.

Kumon, M., Kwok, P.C.L., Adi, H., Heng, D., Chan, H.K., 2010. Can low-dose combination products for inhalation be formulated in single crystalline particles? European Journal of Pharmaceutical Sciences 40, 16-24.

Kurkela, J.A., Brown, D.P., Raula, J., Kauppinen, E.I., 2008. New apparatus for studying powder deagglomeration. Powder Technology 180, 164-171.

Labiris, N.R., Dolovich, M.B., 2003a. Pulmonary drug delivery. Part I: Physiological factors affecting therapeutic effectiveness of aerosolized medications. British Journal of Clinical Pharmacology 56, 588-599.

Labiris, N.R., Dolovich, M.B., 2003b. Pulmonary drug delivery. Part II: The role of inhalant delivery devices and drug formulations in therapeutic effectiveness of aerosolized medications. British Journal of Clinical Pharmacology 56, 600-612.

Larhrib, H., Martin, G.P., Marriott, C., Prime, D., 2003. The influence of carrier and drug morphology on drug delivery from dry powder formulations. International Journal of Pharmaceutics 257, 283-296.

Lass, J.S., Sant, A., Knoch, M., 2006. New advances in aerosolised drug delivery: Vibrating membrane nebuliser technology. Expert Opinion on Drug Delivery 3, 693-702.

Le, V.N.P., Bierend, H., Robins, E., Steckel, H., Flament, M.P., 2012a. Influence of the lactose grade within dry powder formulations of fluticasone propionate and terbutaline sulphate. International Journal of Pharmaceutics 422, 75-82.

Le, V.N.P., Robins, E., Flament, M.P., 2010. Air permeability of powder: A potential tool for Dry Powder Inhaler formulation development. European Journal of Pharmaceutics and Biopharmaceutics 76, 464-469.

Le, V.N.P., Robins, E., Flament, M.P., 2012b. Agglomerate behaviour of fluticasone propionate within dry powder inhaler formulations. European Journal of Pharmaceutics and Biopharmaceutics 80, 596-603.

Le, V.N.P., Thi, T.H.H., Robins, E., Flament, M.P., 2012c. Dry powder inhalers: Study of the parameters influencing adhesion and dispersion of fluticasone propionate. AAPS PharmSciTech 13, 477-484.

Le, V.N.P., Thi, T.H.H., Robins, E., Flament, M.P., 2012d. In vitro evaluation of powders for inhalation: The effect of drug concentration on particle detachment. International Journal of Pharmaceutics 424, 44-49.

Leach, C.L., Davidson, P.J., Boudreau, R.J., 1998. Improved airway targeting with the CFC-free HFA-beclomethasone metered- dose inhaler compared with CFC-beclomethasone. European Respiratory Journal 12, 1346-1353.

Leschonski, K., Rüthele, S., Menzel, U., 1984. A Special Feeder for Diffraction Pattern Analysis of Dry Powders. Particle & Particle Systems Characterization 1, 161-166.

Lewis, D., 2007. Metered-dose inhalers: Actuators old and new. Expert Opinion on Drug Delivery 4, 235-245.

Lindberg, V., 2000. Uncertainties and error propagation. Manual on Uncertainties, Graphing and the Vernier Caliper, Part I. Rochester Institute of Technology, New York, USA.(http://www. rit. edu/uphysics/uncertinities/Uncertinitiespart2. html# addsub).

Liu, X., Jin, L., Upham, J.W., Roberts, M.S., 2013. The development of models for the evaluation of pulmonary drug disposition. Expert Opinion on Drug Metabolism and Toxicology 9, 487-505.

Lofdahl, C.G., 1990. Basic pharmacology of new long-acting sympathomimetics. Lung 168, 18-21.

Louey, M.D., Stewart, P.J., 2002. Particle interactions involved in aerosol dispersion of ternary interactive mixtures. Pharmaceutical Research 19, 1524-1531.

Louey, M.D., Van Oort, M., Hickey, A.J., 2004a. Aerosol dispersion of respirable particles in narrow size distributions produced by jet-milling and spray-drying techniques. Pharmaceutical Research 21, 1200-1206.

Louey, M.D., Van Oort, M., Hickey, A.J., 2004b. Aerosol dispersion of respirable particles in narrow size distributions using drug-alone and lactose-blend formulations. Pharmaceutical Research 21, 1207-1213.

Louey, M.D., Van Oort, M., Hickey, A.J., 2006. Standardized entrainment tubes for the evaluation of pharmaceutical dry powder dispersion. Journal of Aerosol Science 37, 1520-1531.

Lucas, P., Anderson, K., Potter, U.J., Staniforth, J.N., 1999. Enhancement of small particle size dry powder aerosol formulations using an ultra low density additive. Pharmaceutical Research 16, 1643-1647.

Lucas, P., Anderson, K., Staniforth, J.N., 1998. Protein deposition from dry powder inhalers: Fine particle multiplets as performance modifiers. Pharmaceutical Research 15, 562-569.

Malcolmson, R.J., Embleton, J.K., 1998. Dry powder formulations for pulmonary delivery. Pharmaceutical Science and Technology Today 1, 394-398.

Marek, S.R., Donovan, M.J., Smyth, H.D.C., 2011. Effects of mild processing pressures on the performance of dry powder inhaler formulations for inhalation therapy (1): Budesonide and lactose. European Journal of Pharmaceutics and Biopharmaceutics 78, 97-106.

Marriott, C., MacRitchie, H.B., Zeng, X.M., Martin, G.P., 2006. Development of a laser diffraction method for the determination of the particle size of aerosolised powder formulations. International Journal of Pharmaceutics 326, 39-49.

Martin, G.P., Marriott, C., Zeng, X.M., 2007. Influence of realistic inspiratory flow profiles on fine particle fractions of dry powder aerosol formulations. Pharmaceutical Research 24, 361-369.

Martindale, 2013. Martindale: The Complete Drug Reference. Edited by Sweetman, S., 37th Edition. Electronic version, Pharmaceutical Press, London.

Martonen, T.B., 1993. Mathematical model for the selective deposition of inhaled pharmaceuticals. Journal of Pharmaceutical Sciences 82, 1191-1199.

May, S., Jensen, B., Wolkenhauer, M., Schneider, M., Lehr, C.M., 2012. Dissolution techniques for in vitro testing of dry powders for inhalation. Pharmaceutical Research 29, 2157-2166.

Michael, Y., Chowdhry, B.Z., Ashurst, I.C., Snowden, M.J., Davies-Cutting, C., Gray, S., 2000. The physico-chemical properties of salmeterol and fluticasone propionate in different solvent environments. International Journal of Pharmaceutics 200, 279-288.

Michael, Y., Snowden, M.J., Chowdhry, B.Z., Ashurst, I.C., Davies-Cutting, C.J., Riley, T., 2001. Characterisation of the aggregation behaviour in a salmeterol and fluticasone propionate inhalation aerosol system. International Journal of Pharmaceutics 221, 165-174.

Murnane, D., 2007. The crystallisation and characterisation of particles for the delivery of inhaled drugs. PhD Thesis, King's College London UK.

Murnane, D., Marriott, C., Martin, G.P., 2008a. Comparison of salmeterol xinafoate microparticle production by conventional and novel antisolvent crystallization. European Journal of Pharmaceutics and Biopharmaceutics 69, 94-105.

Murnane, D., Marriott, C., Martin, G.P., 2008b. Crystallization and crystallinity of fluticasone propionate. Crystal Growth and Design 8, 2753-2764.

Murnane, D., Marriott, C., Martin, G.P., 2008c. Developing an environmentally benign process for the production of microparticles: Amphiphilic crystallization. European Journal of Pharmaceutics and Biopharmaceutics 69, 72-82.

Murnane, D., Marriott, C., Martin, G.P., 2008d. Polymorphic control of inhalation microparticles prepared by crystallization. International Journal of Pharmaceutics 361, 141-149.

Murnane, D., Martin, G.P., Marriott, C., 2006. Validation of a reverse-phase high performance liquid chromatographic method for concurrent assay of a weak base (salmeterol xinafoate) and a pharmacologically active steroid (fluticasone propionate). Journal of Pharmaceutical and Biomedical Analysis 40, 1149-1154.

Murnane, D., Martin, G.P., Marriott, C., 2009. Dry powder formulations for inhalation of fluticasone propionate and salmeterol xinafoate microcrystals. Journal of Pharmaceutical Sciences 98, 503-515.

Nelson, H., Kemp, J.P., Bieler, S., Vaughan, L.M., Hill, M.R., 1999. Comparative efficacy and safety of albuterol sulfate spiros inhaler and albuterol metered-dose inhaler in asthma. Chest 115, 329-335.

Nelson, H.S., Chapman, K.R., Pyke, S.D., Johnson, M., Pritchard, J.N., 2003. Enhanced synergy between fluticasone propionate and salmeterol inhaled from a single inhaler versus separate inhalers. Journal of Allergy and Clinical Immunology 112, 29-36.

New, A., Prime, D., Zomer, S., Elder, D., Donovan, R., Freney, E., 2008. Detection and assessment of co-association in inhalable drug particles using aerosol time-of-flight mass spectrometry. Rapid Communications in Mass Spectrometry 22, 3873-3882.

Newell, H.E., Buckton, G., 2004. Inverse gas chromatography: Investigating whether the technique preferentially probes high energy sites for mixtures of crystalline and amorphous lactose. Pharmaceutical Research 21, 1440-1444.

Newell, H.E., Buckton, G., Butler, D.A., Thielmann, F., Williams, D.R., 2001. The use of inverse phase gas chromatography to measure the surface energy of crystalline, amorphous, and recently milled lactose. Pharmaceutical Research 18, 662-666.

Newman, S.P., Agnew, J.E., Pavia, D., Clarke, S.W., 1982. Inhaled aerosols: Lung deposition and clinical applications. Clinical Physics and Physiological Measurement 3, 1-20.

Nguyen, T.T., Rambanapasi, C., de Boer, A.H., Frijlink, H.W., Ven, P.M.V.D., de Vries, J., Busscher, H.J., Maarschalk, K.V.V., 2010. A centrifuge method to measure particle cohesion forces to substrate surfaces: The use of a force distribution concept for data interpretation. International Journal of Pharmaceutics 393, 88-95.

NHLBI, 2007. National Asthma Education and Prevention Program Expert Panel Report 3: Guidelines for the Diagnosis and Management of Asthma. National Heart Blood and Lung Institute, U.S. Department of Health and Human Services, National Institutes of Health.

NICE, 2010. Chronic obstructive pulmonary disease, Management of chronic obstructive disease in adults in primary and secondary care. NICE Clinical Guideline 101. National Institute for Health and Care Excellence, London, UK.

Ong, H.X., Traini, D., Cipolla, D., Gonda, I., Bebawy, M., Agus, H., Young, P.M., 2012. Liposomal nanoparticles control the uptake of ciprofloxacin across respiratory epithelia. Pharmaceutical Research 29, 3335-3346.

Ooi, J., Traini, D., Hoe, S., Wong, W., Young, P.M., 2011. Does carrier size matter? A fundamental study of drug aerosolisation from carrier based dry powder inhalation systems. International Journal of Pharmaceutics 413, 1-9.

Pang, L., Knox, A.J., 2000. Synergistic inhibition by β2-agonists and corticosteroids on tumor necrosis factor-α-induced interleukin-8 release from cultured human airway smooth-muscle cells. American Journal of Respiratory Cell and Molecular Biology 23, 79-85.

Perkins, M.C., Bunker, M., James, J., Rigby-Singleton, S., Ledru, J., Madden-Smith, C., Luk, S., Patel, N., Roberts, C.J., 2009. Towards the understanding and prediction of material changes during micronisation using atomic force microscopy. European Journal of Pharmaceutical Sciences 38, 1-8.

Pilcer, G., Rosière, R., Traina, K., Sebti, T., Vanderbist, F., Amighi, K., 2013. New co-spray-dried tobramycin nanoparticles-clarithromycin inhaled powder systems for lung infection therapy in cystic fibrosis patients. Journal of Pharmaceutical Sciences 102, 1836-1846.

Pilcer, G., Wauthoz, N., Amighi, K., 2012. Lactose characteristics and the generation of the aerosol. Advanced Drug Delivery Reviews 64, 233-256.

Pitchayajittipong, C., Shur, J., Price, R., 2009. Engineering of crystalline combination inhalation particles of a long-acting β2-agonist and a corticosteroid. Pharmaceutical Research 26, 2657-2666.

Podczeck, F., 1998. The relationship between physical properties of lactose monohydrate and the aerodynamic behaviour of adhered drug particles. International Journal of Pharmaceutics 160, 119-130.

Podczeck, F., Newton, J.M., James, M.B., 1994. Assessment of adhesion and autoadhesion forces between particles and surfaces: I. The investigation of autoadhesion phenomena of salmeterol xinafoate and lactose monohydrate particles using compacted powder surfaces. Journal of Adhesion Science and Technology 8, 1459-1472.

Podczeck, F., Newton, J.M., James, M.B., 1996. The adhesion force of micronized Salmeterol Xinafoate particles to pharmaceutically relevant surface materials. Journal of Physics D: Applied Physics 29, 1878-1884.

Price, R., 2011. Crystals, particles and powder. APS Inhalation Conference, University of Bath, Bath, UK.

Prime, D., Grant, A.C., Slater, A.L., Woodhouse, R.N., 1999. A critical comparison of the dose delivery characteristics of four alternative inhalation devices delivering salbutamol: Pressurized metered dose inhaler, Diskus inhaler, Diskhaler inhaler, and Turbuhaler inhaler. Journal of Aerosol Medicine: Deposition, Clearance, and Effects in the Lung 12, 75-84.

Pryor, W.A., 1992. How far does ozone penetrate into the pulmonary air/tissue boundary before it reacts? Free Radical Biology and Medicine 12, 83-88.

Rawle, A. F., 1993. The basic principles of particle size analysis. Application no. MRK038, Malvern Instruments, UK (available from www.malvern.co.uk)

Rehman, M., Kippax, P., York, P., 2003. Particle engineering for improved dispersion in dry powder inhalers. Pharmaceutical Technology Europe 15, 34-37+39.

Riley, T., Christopher, D., Arp, J., Casazza, A., Colombani, A., Cooper, A., Dey, M., Maas, J., Mitchell, J., Reiners, M., Sigari, N., Tougas, T., Lyapustina, S., 2012. Challenges with developing in vitro dissolution tests for orally inhaled products (OIPs). AAPS PharmSciTech 13, 978-989.

Rogueda, P.G.A., Price, R., Smith, T., Young, P.M., Traini, D., 2011. Particle synergy and aerosol performance in non-aqueous liquid of two combinations metered dose inhalation formulations: An AFM and Raman investigation. Journal of Colloid and Interface Science 361, 649-655.

Röthele, S.I., Kesten, U., Lake,A, 1990. The Application of the Sympatec Laser Diffraction System in the Range of 0.1 µm to 2.6 mm, INPARTECH 1990 London, UK.

Sakagami, M., Sakon, K., Kinoshita, W., Makino, Y., 2001. Enhanced pulmonary absorption following aerosol administration of mucoadhesive powder microspheres. Journal of Controlled Release 77, 117-129.

Salama, R.O., Traini, D., Chan, H.K., Sung, A., Ammit, A.J., Young, P.M., 2009. Preparation and evaluation of controlled release microparticles for respiratory protein therapy. Journal of Pharmaceutical Sciences 98, 2709-2717.

Salama, R.O., Traini, D., Chan, H.K., Young, P.M., 2008. Preparation and characterisation of controlled release co-spray dried drug-polymer microparticles for inhalation 2: Evaluation of in vitro release profiling methodologies for controlled release respiratory aerosols. European Journal of Pharmaceutics and Biopharmaceutics 70, 145-152.

Saleem, I., Smyth, H., Telko, M., 2008. Prediction of dry powder inhaler formulation performance from surface energetics and blending dynamics. Drug Development and Industrial Pharmacy 34, 1002-1010.

Scheuch, G., Kohlhaeufl, M.J., Brand, P., Siekmeier, R., 2006. Clinical perspectives on pulmonary systemic and macromolecular delivery. Advanced Drug Delivery Reviews 58, 996-1008.

Schultz, J., Lavielle, L., Martin, C., 1987. Role of the interface on carbon fibre/epoxy composites.

Schulz, H., 1998. Mechanisms and factors affecting intrapulmonary particle deposition: Implications for efficient inhalation therapies. Pharmaceutical Science and Technology Today 1, 336-344.

Sebti, T., Vanderbist, F., Amighi, K., 2007. Evaluation of the content homogeneity and dispersion properties of fluticasone DPI compositions. Journal of Drug Delivery Science and Technology 17, 223-229.

Selvam, P., Smyth, H.D.C., 2011. Effect of press-on forces on drug adhesion in dry powder inhaler formulations. Journal of Adhesion Science and Technology 25, 1659-1670.

Shariare, M.H., De Matas, M., York, P., 2011. Effect of crystallisation conditions and feedstock morphology on the aerosolization performance of micronised salbutamol sulphate. International Journal of Pharmaceutics 415, 62-72.

Shaw, R.J., Greening, A.P., Barnes, N., Honour, J.W., Parker, C., 1994. Pharmacology of fluticasone propionate. Respiratory Medicine 88, 5-8.

Shekunov, B.Y., Feeley, J.C., Chow, A.H.L., Tong, H.H.Y., York, P., 2003. Aerosolisation behaviour of micronised and supercritically-processed powders. Journal of Aerosol Science 34, 553-568.

Sherwood, L., 2001. Human Physiology From Cells to Systems. Brooks/Cole Thomson Learning, California, USA.

Shur, J., Harris, H., Jones, M.D., Kaerger, J.S., Price, R., 2008. The role of fines in the modification of the fluidization and dispersion mechanism within dry powder inhaler formulations. Pharmaceutical Research 25, 1631-1640.

Smyth, H.D.C., 2003. The influence of formulation variables on the performance of alternative propellant-driven metered dose inhalers. Advanced Drug Delivery Reviews 55, 807-828.

Son, Y.J., Horng, M., Copley, M., McConville, J.T., 2010. Optimization of an in vitro dissolution test method for inhalation formulations. Dissolution Technologies 17, 6-13.

Son, Y.J., McConville, J.T., 2009. Development of a standardized dissolution test method for inhaled pharmaceutical formulations. International Journal of Pharmaceutics 382, 15-22.

Steckel, H., Brandes, H.G., 2004. A novel spray-drying technique to produce low density particles for pulmonary delivery. International Journal of Pharmaceutics 278, 187-195.

Steckel, H., Markefka, P., TeWierik, H., Kammelar, R., 2006. Effect of milling and sieving on functionality of dry powder inhalation products. International Journal of Pharmaceutics 309, 51-59.

Steckel, H., Rasenack, N., Müller, B.W., 2003a. In-situ-micronization of disodium cromoglycate for pulmonary delivery. European Journal of Pharmaceutics and Biopharmaceutics 55, 173-180.

Steckel, H., Rasenack, N., Villax, P., Müller, B.W., 2003b. In vitro characterization of jet-milled and in-situ-micronized fluticasone-17-propionate. International Journal of Pharmaceutics 258, 65-75.

Steele, D.F., Young, P.M., Price, R., Smith, T., Edge, S., Lewis, D., 2004. The potential use of Raman mapping to investigate in vitro deposition of combination pressurized metered-dose inhalers. AAPS Journal 6, 1-4.

Stempel, D.A., Stoloff, S.W., Rosenzweig, J.R.C., Stanford, R.H., Ryskina, K.L., Legorreta, A.P., 2005. Adherence to asthma controller medication regimens. Respiratory Medicine 99, 1263-1267.

Stoloff, S.W., Stempel, M.A., Meyer, J., Stanford, R.H., Carranza Rosenzweig, J.R., 2004. Improved refill persistence with fluticasone propionate and salmeterol in a single inhaler compared with other controller therapies. Journal of Allergy and Clinical Immunology 113, 245-251.

Tajber, L., Corrigan, D.O., Corrigan, O.I., Healy, A.M., 2009a. Spray drying of budesonide, formoterol fumarate and their composites-I. Physicochemical characterisation. International Journal of Pharmaceutics 367, 79-85.

Tajber, L., Corrigan, O.I., Healy, A.M., 2009b. Spray drying of budesonide, formoterol fumarate and their composites-II. Statistical factorial design and in vitro deposition properties. International Journal of Pharmaceutics 367, 86-96.

Taki, M., 2008. The deposition of drugs from combination dry powder inhaler formulations. PhD Thesis, King's College London, London, UK.

Taki, M., Ahmed, S., Marriott, C., Zeng, X.M., Martin, G.P., 2011. The 'stage-by-stage' deposition of drugs from commercial single-active and combination dry powder inhaler formulations. European Journal of Pharmaceutical Sciences 43, 225-235.

Taki, M., Esmaeili, F., Martin, G.P., 2011a. The scientific basis and challenges of combination inhaled products. Journal of Drug Delivery Science and Technology 21, 293-300.

Taki, M., Marriott, C., Zeng, X.M., Martin, G.P., 2010. Aerodynamic deposition of combination dry powder inhaler formulations in vitro: A comparison of three impactors. International Journal of Pharmaceutics 388, 40-51.

Taki, M., Marriott, C., Zeng, X.M., Martin, G.P., 2011b. The production of 'aerodynamically equivalent' drug and excipient inhalable powders using a novel fractionation technique. European Journal of Pharmaceutics and Biopharmaceutics 77, 283-296.

Taki, M., Marriott, C., Zeng, X.M., Martin, G.P., 2008a. The Aerodynamic Deposition of Drugs from Combination DPI Formulations: The Influence of Particle Size and Drug-Drug Interactions. Drug Delivery to the Lungs 19, Edinburgh, Scotland, UK.

Tamm, M., Richards, D.H., Beghé, B., Fabbri, L., 2012. Inhaled corticosteroid and long-acting β2-agonist pharmacological profiles: effective asthma therapy in practice. Respiratory Medicine 106, Supplement 1, S9-S19.

Tang, S., 2008. An investigation into the limits of analysis of amorphism in pharmaceutical powders using a variety of different techniques including a novel application of DMA. PhD Thesis, King's College London, UK.

Tarsin, W.Y., Pearson, S.B., Assi, K.H., Chrystyn, H., 2006. Emitted dose estimates from Seretide (R) Diskus (R) and Symbicort (R) Turbuhaler (R) following inhalation by severe asthmatics. International Journal of Pharmaceutics 316, 131-137.

Tee, S.K., Marriott, C., Zeng, X.M., Martin, G.P., 2000. The use of different sugars as fine and coarse carriers for aerosolised salbutamol sulphate. International Journal of Pharmaceutics 208, 111-123.

Telko, M.J., Hickey, A.J., 2005. Dry powder inhaler formulation. Respiratory Care 50, 1209-1227.

Theophilus, A., Moore, A., Prime, D., Rossomanno, S., Whitcher, B., Chrystyn, H., 2006. Co-deposition of salmeterol and fluticasone propionate by a combination inhaler. International Journal of Pharmaceutics 313, 14-22.

Thielmann, F., 2004. Introduction into the characterisation of porous materials by inverse gas chromatography. Journal of Chromatography A 1037, 115-123.

Thielmann, F., Burnett, D.J., Heng, J.Y.Y., 2007. Determination of the surface energy distributions of different processed lactose. Drug Development and Industrial Pharmacy 33, 1240-1253.

Ticehurst, M.D., Rowe, R.C., York, P., 1994. Determination of the surface properties of two batches of salbutamol sulphate by inverse gas chromatography. International Journal of Pharmaceutics 111, 241-249.

Ticehurst, M., A. Basford, P., I. Dallman, C., M. Lukas, T., V. Marshall, P., Nichols, G., Smith, D., 2000. Characterisation of the influence of micronisation on the crystallinity and physical stability of revatropate hydrobromide. International Journal of Pharmaceutics 193, 247-259.

Tobyn, M., Staniforth, J.N., Morton, D., Harmer, Q., Newton, M.E., 2004. Active and intelligent inhaler device development. International Journal of Pharmaceutics 277, 31-37.

Tong, H.H.Y., Shekunov, B.Y., York, P., Chow, A.H.L., 2001. Characterization of two polymorphs of salmeterol xinafoate crystallized from supercritical fluids. Pharmaceutical Research 18, 852-858.

Tong, H.H.Y., Shekunov, B.Y., York, P., Chow, A.H.L., 2002. Influence of polymorphism on the surface energetics of salmeterol xinafoate crystallized from supercritical fluids. Pharmaceutical Research 19, 640-648.

Tong, H.H.Y., Shekunov, B.Y., York, P., Chow, A.H.L., 2003. Thermal analysis of trace levels of polymorphic impurity in salmeterol xinafoate samples. Pharmaceutical Research 20, 1423-1429.

Tong, H.H.Y., Shekunov, B.Y., York, P., Chow, A.H.L., 2006. Predicting the aerosol performance of dry powder inhalation formulations by interparticulate interaction analysis using inverse gas chromatography. Journal of Pharmaceutical Sciences 95, 228-233.

Traini, D., Adi, H., Valet, O.K., Young, P.M., 2012. Preparation and evaluation of single and co-engineered combination inhalation carrier formulations for the treatment of asthma. Journal of Pharmaceutical Sciences 101, 4267-4276.

Traini, D., Young, P.M., Thielmann, F., Acharya, M., 2008. The influence of lactose pseudopolymorphic form on salbutamol sulfate-lactose interactions in DPI formulations. Drug Development and Industrial Pharmacy 34, 992-1001.

Tsukada, M., Irie, R., Yonemochi, Y., Noda, R., Kamiya, H., Watanabe, W., Kauppinen, E.I., 2004. Adhesion force measurement of a DPI size pharmaceutical particle by colloid probe atomic force microscopy. Powder Technology 141, 262-269.

Tuley, R., Shrimpton, J., Jones, M.D., Price, R., Palmer, M., Prime, D., 2008. Experimental observations of dry powder inhaler dose fluidisation. International Journal of Pharmaceutics 358, 238-247.

Ungaro, F., d'Emmanuele di Villa Bianca, R., Giovino, C., Miro, A., Sorrentino, R., Quaglia, F., La Rotonda, M.I., 2009. Insulin-loaded PLGA/cyclodextrin large porous particles with improved aerosolization properties: In vivo deposition and hypoglycaemic activity after delivery to rat lungs. Journal of Controlled Release 135, 25-34.

Usmani, O.S., Biddiscombe, M.F., Barnes, P.J., 2005. Regional lung deposition and bronchodilator response as a function of β2-agonist particle size. American Journal of Respiratory and Critical Care Medicine 172, 1497-1504.

Vernall, C., Olkhovyk, O., Priore. R.J., Price, R., Shur, J., 2012. Investigation of the microstructure of combination dry powder inhaler formulations by atomic force microscopy and Raman Imaging. Respiratory Drug Delivery Proceedings, pp. 793-797, Arizona, USA.

Voelkel, A., Strzemiecka, B., Adamska, K., Milczewska, K., 2009. Inverse gas chromatography as a source of physiochemical data. Journal of Chromatography A 1216, 1551-1566.

Voss, A., Finlay, W.H., 2002. Deagglomeration of dry powder pharmaceutical aerosols. International Journal of Pharmaceutics 248, 39-50.

Ward, G.H., Schultz, R.K., 1995. Process-induced crystallinity changes in albuterol sulfate and its effect on powder physical stability. Pharmaceutical Research 12, 773-779.

Watts, A.B., McConville, J.T., Williams Iii, R.O., 2008. Current therapies and technological advances in aqueous aerosol drug delivery. Drug Development and Industrial Pharmacy 34, 913-922.

Weers, J.G., Bell, J., Chan, H.K., Cipolla, D., Dunbar, C., Hickey, A.J., Smith, I.J., 2010. Pulmonary formulations: What remains to be done? Journal of Aerosol Medicine and Pulmonary Drug Delivery 23, S5-S23.

Weibel, E.R., Gomez, D.M., 1962. Architecture of the human lung. Science 137, 577-585.

Westmeier, R., Steckel, H., 2008. Combination particles containing salmeterol xinafoate and fluticasone propionate: Formulation and aerodynamic assessment. Journal of Pharmaceutical Sciences 97, 2299-2310.

WHO, 2011. Asthma Factsheet. World Health Organisation, Factsheet N^{o} 307, May 2011.

WHO, 2012. Chronic Obstructive Pulmonary Disease (COPD) Factsheet. Factsheet N^{o} 315, November 2012.

Widdicombe, J.H., 2002. Regulation of the depth and composition of airway surface liquid. Journal of Anatomy 201, 313-318.

Wong, W., Fletcher, D.F., Traini, D., Chan, H.K., Crapper, J., Young, P.M., 2011. Particle aerosolisation and break-up in dry powder inhalers: Evaluation and modelling of impaction effects for agglomerated systems. Journal of Pharmaceutical Sciences 100, 2744-2754.

www.sympatec.com/EN/LaserDiffraction/RODOS.html, accessed 27.08.13.

Xu, Z., Mansour, H.M., Mulder, T., McLean, R., Langridge, J., Hickey, A.J., 2010a. Dry powder aerosols generated by standardized entrainment tubes from drug blends with lactose monohydrate: 2. Ipratropium bromide monohydrate and fluticasone propionate. Journal of Pharmaceutical Sciences 99, 3415-3429.

Xu, Z., Mansour, H.M., Mulder, T., McLean, R., Langridge, J., Hickey, A.J., 2010b. Heterogeneous particle deaggregation and its implication for therapeutic aerosol performance. Journal of Pharmaceutical Sciences 99, 3442-3461.

Ylä-Mäihäniemi, P.P., Heng, J.Y.Y., Thielmann, F., Williams, D.R., 2008. Inverse gas chromatographic method for measuring the dispersive surface energy distribution for particulates. Langmuir 24, 9551-9557.

Young, P.M., Chan, H.K., Chiou, H., Edge, S., Tee, T.H.S., Traini, D., 2007. The influence of mechanical processing of dry powder inhaler carriers on drug aerosolization performance. Journal of Pharmaceutical Sciences 96, 1331-1341.

Young, P.M., Price, R., Tobyn, M.J., Buttrum, M., Dey, F., 2003. Effect of Humidity on Aerosolization of Micronized Drugs. Drug Development and Industrial Pharmacy 29, 959-966.

Young, P.M., Price, R., Tobyn, M.J., Buttrum, M., Dey, F., 2004. The Influence of Relative Humidity on the Cohesion Properties of Micronized Drugs Used in Inhalation Therapy. Journal of Pharmaceutical Sciences 93, 753-761.

Young, P.M., Wood, O., Ooi, J., Traini, D., 2011. The influence of drug loading on formulation structure and aerosol performance in carrier based dry powder inhalers. International Journal of Pharmaceutics 416, 129-135.

Young, P., Price, R., Jones, S., Billings, M.P., 2004a. Investigation into drug and excipient interaction in dry powder combination products. Respiratory Drug Delivery IX Proceedings, pp. 749-751, California, USA.

Zeng, X.M., Pandhal, K.H., Martin, G.P., 2000. The influence of lactose carrier on the content homogeneity and dispersibility of beclomethasone dipropionate from dry powder aerosols. International Journal of Pharmaceutics 197, 41-52.

Zeng, X.M., Martin, G.P., Marriott, C., 2001. Particulate Interactions in Dry Powder Formulations for Inhalation. 1st Edition, Taylor & Francis, London, UK.

Zeng, X.M., Martin, G.P., Tee, S.K., Marriott, C., 1998. The role of fine particle lactose on the dispersion and deaggregation of salbutamol sulphate in an air stream in vitro. International Journal of Pharmaceutics 176, 99-110.

Zhou, Q.T., Armstrong, B., Larson, I., Stewart, P.J., Morton, D.A.V., 2010a. Understanding the influence of powder flowability, fluidization and de-agglomeration characteristics on the aerosolization of pharmaceutical model powders. European Journal of Pharmaceutical Sciences 40, 412-421.

Zhou, Q.T., Qu, L., Larson, I., Stewart, P.J., Morton, D.A.V., 2010b. Improving aerosolization of drug powders by reducing powder intrinsic cohesion via a mechanical dry coating approach. International Journal of Pharmaceutics 394, 50-59.